

AD-A049 264

FOREIGN TECHNOLOGY DIV WRIGHT-PATTERSON AFB OHIO
DEFORMED ALUMINUM ALLOY METALLOGRAPHY. (U)
AUG 77

F/G 11/6

UNCLASSIFIED

FTD-ID(RS)T-0577-77

NL

1 OF 5
AD
A049 264



AD-A049264

FTD-ID(RS)T-0577-77

①

FOREIGN TECHNOLOGY DIVISION



DEFORMED ALUMINUM ALLOY METALLOGRAPHY



DDC
RECEIVED
3 FEB 1978
E

Approved for public release;
distribution unlimited.



EDITED TRANSLATION

FTD-ID(RS)T-0577-77

3 August 1977

MICROFICHE NR: *FD-77-C-000992*

DEFORMED ALUMINUM ALLOY METALLOGRAPHY

English pages: 387

Source: DEFORMED ALUMINUM ALLOY METALLOGRAPHY,
1975, China, PP 1-224

Country of origin: China

Translated by: LINGUISTICS SYSTEMS, INC.

F33657-76-D-0389

Jerry K. Chung and H. P. Lee

Requester: FTD/PDRR

Approved for public release; distribution unlimited.

THIS TRANSLATION IS A RENDITION OF THE ORIGINAL FOREIGN TEXT WITHOUT ANY ANALYTICAL OR EDITORIAL COMMENT. STATEMENTS OR THEORIES ADVOCATED OR IMPLIED ARE THOSE OF THE SOURCE AND DO NOT NECESSARILY REFLECT THE POSITION OR OPINION OF THE FOREIGN TECHNOLOGY DIVISION.

PREPARED BY:

TRANSLATION DIVISION
FOREIGN TECHNOLOGY DIVISION
WP-AFB, OHIO.

FTD -ID(RS)T-0577-77

Date 3 Aug 19 77

Quotations of Chairman Mao

The crucial force that directs all our undertakings is the Chinese Communist Party.

The theoretical foundation that guides our thoughts is the principles of Marx and Lenin.

Man must not fail to draw inferences from experience, but constantly seeks to engage himself in discovery, invention, and progress.

We must essay to break away from conventions, and to adopt as much advanced technology as possible, so as to build our country into a strong socialist nation within not too long a period in history.

China should commit herself to giving sizable contributions to the well-being of mankind.

DEFORMED ALUMINIUM ALLOY METALLOGRAPHY

Edited by the Metallography Editorial Board

Metallurgical Industry Press
1975

Deformed Aluminium Alloy Metallography
Edited by the Metallography Editorial Board

*

Published by Metallurgical Industry Press
Distributed by New China Bookstore, Peking
Printed by Foreign Language Printing Factory
of the Metallurgical Industry Press

*

787 x 1092 1/16	14 plates	265 thousand words
1st Edition...August, 1975	1st Printing...August, 1975	
Number of Books Printed 00,001~10,000		
United Book Number : 15062·3155	Price(4th Class)\$5.30	

PREFACE

Under the direction of Chairman Mao in the Proletariat Revolution since the Liberation, the aluminium alloy industry of our country has made enormous progress, from non-existence to existence, from small scale to large scale. Quantity and variety of products increase steadily, while quality witnesses continuous improvement. This industry has produced its due effects in the construction of the civilian economy and the national defense industry.

In accordance with the teachings of our great leader Chairman Mao, "not to fail to draw inferences from experience", we have edited, for the need of the rapidly developing metallurgical industry, the book "Deformed Aluminium Alloy Metallography". It is intended to serve as a reference source for those who are working in the production, application, scientific research, teaching, and other related areas of deformed aluminium alloys.

This book places emphasis on the introduction of the phase formations and special features of eight principal alloy systems (including pure aluminium) of deformed aluminium alloys, the effects of various working methods (e.g. extrusion, **rolling**, forging, cold-drawing, etc.) on the alloy structures, **and the peculiarities and regularities** of alloy structures under various kinds of heat treatments (e.g. homogenization, annealing, quenching, ageing, etc.). Diagrams and accompanying explanations are generally included for the illustration of typical cases.

In the course of editing this book, we received plenty

of support and help from Chen-Yang Metal Research Institute, Peking Steel Research Institute, Shanghai Material Research Institute, Peking Aerospace Academy, Peking Steel Academy, Northeastern Institute of Technology, Mid-South Mineralogy Academy, Shanghai Traffic University, and other fraternal factories, schools and units. To them we would like to express our deep appreciation.

Owing to our limited knowledge, this book may contain many errors and shortcomings. We sincerely welcome any criticism and correction from the readers.

Metallography Editorial Board

June, 1974

CONTENT

General Discussion.....	9
I Classification of Alloys.....	9
II Constitution of Alloys and Formation of Alloy Phases.....	10
III Structures of Cast and Wrought Products under Various Conditions.....	17
1. Structures of Ingots Made by Semi-Continuous Casting (Watercooled).....	17
2. Structures of Alloys under Various Working Conditions.....	25
(1) Structures of Alloys under Hot Rolling.....	25
(2) Structures of Alloys under Hot Extrusion.....	28
(3) Structures of Alloys under Forging.....	31
(4) Structures of Alloys under Cold Rolling, Cold Drawing, and Cold Spinning.....	37
3. Structures of Cast and Wrought Products under Heat Treatments.....	38
(1) Structures of Ingots under Homogenization.....	38
(2) Structures of Products under Recovery and Recrystallization.....	39
(3) Structures of Alloys under Annealing.....	44
(4) Structures of Alloys under Quenching and Ageing.....	46

Chapter One	Industrial-Pure Aluminium.....	54
Section 1	Impurities Contents and Phase Formation.....	54
Section 2	Properties under Heat Treatments.....	61
Section 3	Structures of Cast Ingots and Processed Products.....	65
Chapter Two	Aluminium-Magnesium Alloys.....	90
Section 1	Chemical Composition and Phase Formation.....	90
Section 2	Properties under Heat Treatments.....	93
Section 3	Structures of Cast Ingots and Processed Products.....	100
Chapter Three	Aluminium-Manganese Alloys.....	120
Section 1	Chemical Composition and Phase Formation.....	120
Section 2	Properties under Heat Treatments.....	126
Section 3	Structures of Ingots and Processed Products.....	133
Chapter Four	Aluminium-Copper-Magnesium Alloys.....	151
Section 1	Chemical Composition and Phase Formation.....	151
Section 2	Properties under Heat Treatments.....	157
Section 3	Structures of Ingots and Processed Products.....	162
Chapter Five	Aluminium-Magnesium-Silicon- Copper Alloys.....	202
Section 1	Chemical Composition and Phase Formation.....	202
Section 2	Properties under Heat Treatments.....	208
Section 3	Structures of Cast Ingots and Processed Products.....	212
Chapter Six	Aluminium-Zinc-Magnesium-Copper Alloys.....	262

Section 1	Chemical Composition and Phase Formation.....	262
Section 2	Properties under Heat Treatments.....	265
Section 3	Structures of Cast Ingots and Processed Products.....	269
Chapter Seven	Aluminium-Copper-Magnesium-Iron-Nickel Alloys.....	301
Section 1	Chemical Composition and Phase Formation.....	301
Section 2	Properties under Heat Treatments.....	307
Section 3	Structures of Cast Ingot and Processed Products.....	310
Chapter Eight	Aluminium-Copper-Manganese Alloys.....	337
Section 1	Chemical Composition and Phase Formation.....	337
Section 2	Properties under Heat Treatments.....	341
Section 3	Structures of Cast Ingots and Processed Products.....	348
Appendixes		
Table 1	Chemical Composition of Deformed Aluminium Alloys.....	369
Table 2	Crystalline Structures of Principal Deformed Aluminium Alloy Phases and Their Features Before and After Etching.....	375
Table 3	Mechanical Properties of Some Deformed Aluminium Alloy Products.....	384
Table 4	Designation of Aluminium Alloy Products.....	386
Table 5	Symbols for Various Tempers of Aluminium Alloy Products.....	387

General Discussion

Following the rapid development in the construction of our country based on socialism, products of aluminium and its alloys, available in sheets, ribbons, foils, tubes, rods, structural shapes, wires, and forgings, find increasingly wide applications in machine production, transportation, electrical appliances, aviation, shipbuilding, chemical engineering, and other civilian sectors.

Structures and properties of products made from aluminium and its alloys are dependent on the following three factors : alloy compositions, deformation methods, and production techniques. Therefore, the investigation of structural features of products made from aluminium and its alloys under various conditions is essential to the improvement of product quality, to the refinement of production techniques, and to the proper choice of material in applications.

I Classification of Alloys

Alloys are usually classified according to one of the following 3 schemes : Their properties under heat treatments, their alloy compositions, or their properties in regard to their utilizations. Deformed aluminium alloys produced in this country are classified according to the last scheme into industrial-pure aluminium, stainless aluminium, hard aluminium, ultra-hard aluminium, and forged aluminium. All except industrial-pure aluminium are alloys formed by the combination of aluminium with other principal elements. Stainless aluminium includes the alloys aluminium-manganese and aluminium-

magnesium. Hard aluminium includes the alloys aluminium-copper-magnesium and aluminium-copper-manganese. Ultra-hard aluminium includes the alloy aluminium-zinc-magnesium-copper. Forged aluminium includes the alloys aluminium-magnesium-silicon-copper and aluminium-copper-magnesium-iron-nickel. All except industrial-pure aluminium and stainless aluminium can be hardened by means of heat treatments. The chemical compositions of these alloys are listed in Table 1 in the Appendixes. Designation for different variety specifications and symbols for different tempers of aluminium alloy products are listed in Table 4 and Table 5 respectively in the Appendixes.

Since the alloys LY6 and LY2 in the aluminium-copper-magnesium-iron-nickel and aluminium-copper-manganese alloy systems are capable of enduring high temperature, they are also known as refractory aluminium alloys.

In this metallography, we use the classification according to alloy compositions.

II Constitution of Alloys and Formation of Alloy Phases

Aluminium combines with lesser amounts of the commonly used alloy elements such as zinc, magnesium, copper, lithium, manganese, nickel, or iron by means of eutectic reactions; with chromium or titanium by means of peritectic reactions; and with lead by means of monotectic reactions. Zinc, magnesium, copper, and lithium have the highest solid solubilities in aluminium, followed by manganese, silicon, nickel, titanium, chromium, and iron. Lead is the least soluble in aluminium.

Because of the appreciable changes in solubilities with temperature of the alloy elements such as copper, lithium, and silicon, and of the alloy phases such as Mg_2Si , $MgZn_2$, and $S(CuMgAl_2)$, the alloys can be hardened considerably after quenching and ageing.

In some alloys, the amounts of iron and silicon can be varied controllably as impurities. They combine with aluminium to form $FeAl_3$, $\alpha(FeSi_3Al_{12})$, and $\beta(Fe_2Si_2Al_9)$. They can also combine with elements such as manganese to form more complex compounds like $(FeMn)Al_6$, Mn_3SiAl_{12} , Cu_2FeAl_7 , and $(FeMnSi)Al_6$. $(FeMn)Al_6$ is a solid solution formed by either Fe dissolving into $MnAl_6$, or Mn dissolving into $FeAl_3$. $(FeMnSi)Al_6$ is a solid solution formed by Fe dissolving into Mn_3SiAl_{12} . Since these compounds only dissolve slightly or not at all in $\alpha(Al)$, they hardly participate, if at all, in the process of age-hardening.

In summary, the phases associated with the impurities in the alloys do not favor age-hardening. However, if their special properties are properly utilized, they can be employed to improve other properties of the alloys. For example, when $Fe/Si \geq 2$, there is a sizable amount of $FeAl_3$ phase in a piece of industrial-pure aluminium, making the alloy more resistant to high temperature and corrosion. By adjusting the contents of iron and silicon, or by adding other elements, one can avoid the deterioration of alloy malleability and machinability caused by the coarse and flake-shaped $\beta(Fe_2Si_2Al_9)$ or $(FeMn)Al_6$ through the formation of bone-shaped $\alpha(FeSi_3Al_{12})$ or $(FeMnSi)Al_6$.

Elements that are soluble in Al such as Mn, Cr, and Zr, can increase the alloy recrystallization temperature. They

do not precipitate easily under slow-cooling, but only after subsequent heating. This phenomenon is called **Tempering Decomposition**. The distribution of these dot-like precipitates, **which** are compounds of Al with Mn or Cr, has very important influence on the properties of the alloys **They are the principal** phases during the dispersion hardening of some alloys.

Titanium, a modifier for certain alloys, can help to **reduce grain sizes**, thereby guaranteeing good technical and mechanical properties for the alloys.

Among the deformed Al alloys **hardenable by heat treatments**, those based on the Al-Cu-Mg, Al-Mg-Si, and Al-Mg-Zn systems are most extensively used. The structures of their phases are rather complex. The basic understanding of the distributions of **phase zones in the equilibrium diagrams** near the Al-rich end for these alloy systems will be very essential to the analysis of the alloy phase structures and to the **choice of procedures for heat treatments**.

From the equilibrium diagram of Al-Cu-Mg (Figure 1), this alloy system can form the $S(CuMgAl_2)$ and $T(CuMg_4Al_6)$ phases aside from the $CuAl_2$ and Mg_2Al_3 phases. At $506.5^\circ C$, the ternary eutectic reaction occurs: $L \rightleftharpoons \alpha(Al) + CuAl_2 + S(CuMgAl_2)$, with 33.1%Cu and 6.25%Mg by weight. At this temperature, the maximum solubilities of Cu and Mg in $\alpha(Al)$ are 4.1% and 1.7% respectively. At $518^\circ C$, the liquid that contains 24.5%Cu and 10.5%Mg undergoes the binary eutectic reaction: $L \rightleftharpoons \alpha(Al) + S(CuMgAl_2)$, where the solid solubilities of Cu and Mg in $\alpha(Al)$ are both 2.9%. Commercially available hard Al is composed of the above mixtures in the binary and ternary phase zones. The strength of the alloy is greatest when it is in the ternary phase zone and is close to the binary phase zone. Alloys in

the binary phase zone has very good ability in enduring high temperature.

From the equilibrium diagram of Al-Mg-Si (Figure 2), there is a binary pseudoeutectic section $\alpha(\text{Al}) + \text{Mg}_2\text{Si}$ which is composed of 8.25%Mg and 4.75%Si at 595°C, with solid solubilities of Mg and Si in $\alpha(\text{Al})$ being 1.17% and 0.68% respectively. There is a ternary eutectic system on each side of this section : $\alpha(\text{Al})\text{-Mg}_2\text{Si-Si}$ near the Si side, and $\alpha(\text{Al})\text{-Mg}_2\text{Al}_3\text{-Mg}_2\text{Si}$ near the Mg side. The strength of the alloy is greatest (after heat treatment) when its composition is in the $\alpha(\text{Al})\text{-Mg}_2\text{Si-Si}$ phase zone. Accordingly, the composition of Al-Mg-Si used in the industry is such that the solubilities in $\alpha(\text{Al})$ are greatest at the above ternary eutectic temperature, and is at the same time restricted to the vicinity of the binary pseudoeutectic section.

In the Al-Mg-Zn system, there exist the Mg_2Al_3 , MgZn_2 , and $\text{Mg}_3\text{Zn}_3\text{Al}_2$ phases. From the equilibrium diagram of Al-Mg-Zn (Figure 3), there are two binary eutectic reactions. One of them produces $\alpha(\text{Al})\text{-MgZn}_2$, with 11.5%Mg and 61%Zn at 475°C. The maximum solubilities of Mg and Zn in $\alpha(\text{Al})$ are 2.65% and 14.25% respectively. The other one occurs at 489°C : $\text{L} \rightleftharpoons \alpha(\text{Al}) + \text{Mg}_3\text{Zn}_3\text{Al}_2$, with 17%Mg and 45%Zn. The maximum solubilities of Mg and Zn at this eutectic temperature are 4.2% and 11.4% respectively. At 530°C, there occurs also a binary pseudo-peritectic reaction : $\text{L} + \text{MgZn}_2 \rightleftharpoons \text{Mg}_3\text{Zn}_3\text{Al}_2$. Commercially available ultra-hard Al has its composition in between or near the above two binary eutectic sections.

In order to improve the machinability and corrosion resistivity of Al-Mg-Zn alloys, copper is usually added. Hence, ultra-hard Al is an alloy based on the Al-Mg-Zn-Cu system, so

that copper-containing phases also appear in the alloy (Figure 4). (For details, see Chapter Six on the analysis of Al-Mg-Zn alloy phases.)

Among the eight existing alloy systems, the most common phases include $\alpha(\text{Al})$, Si, Mg_2Al_3 , MnAl_4 , MnAl_6 , TiAl_3 , CuAl_2 , FeAl_3 , Mg_2Si , MgZn_2 , $\alpha(\text{FeSi}_3\text{Al}_{12})$, $\beta(\text{Fe}_2\text{Si}_2\text{Al}_9)$, $(\text{FeMn})\text{Al}_6$, $\text{Mn}_3\text{SiAl}_{12}$, $\text{S}(\text{CuMgAl}_2)$, FeNiAl_9 , Cu_2FeAl_7 , Cu_3NiAl_6 , $\text{T}(\text{CuMnAl}_{12})$, $\text{T}(\text{Mg}_2\text{Zn}_3\text{Al}_2)$, $\text{W}(\text{Cu}_4\text{Mg}_5\text{Si}_4\text{Al}_x)$, and $(\text{FeMnSi})\text{Al}_6$. In addition, there also exist CrAl_7 , $(\text{MnCr})\text{Al}_6$, and AlCuMnSi , as well as ZrAl_3 in Zr-containing alloys. $(\text{Cr}_x\text{FeMnSi})\text{Al}_6$ is also found in ultra-hard Al made by means of semi-continuous casting when the contents of Mn, Cr, and Ti are sufficiently high.

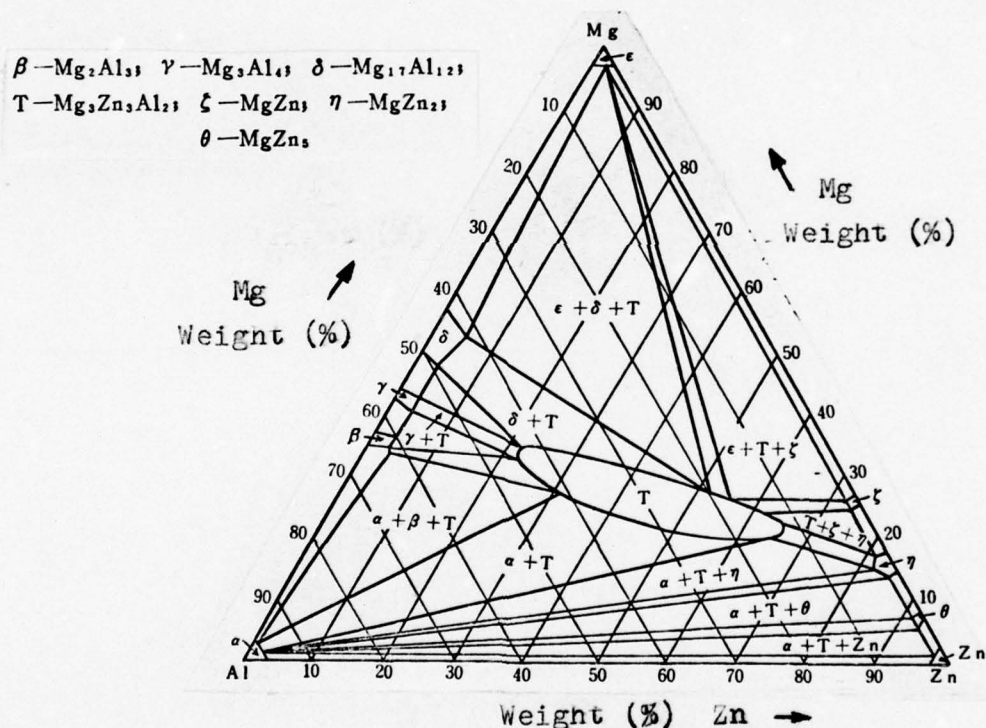


Figure 3. Distribution of Solid-State Phase Zones of Al-Zn-Mg Alloy System at Room Temperature

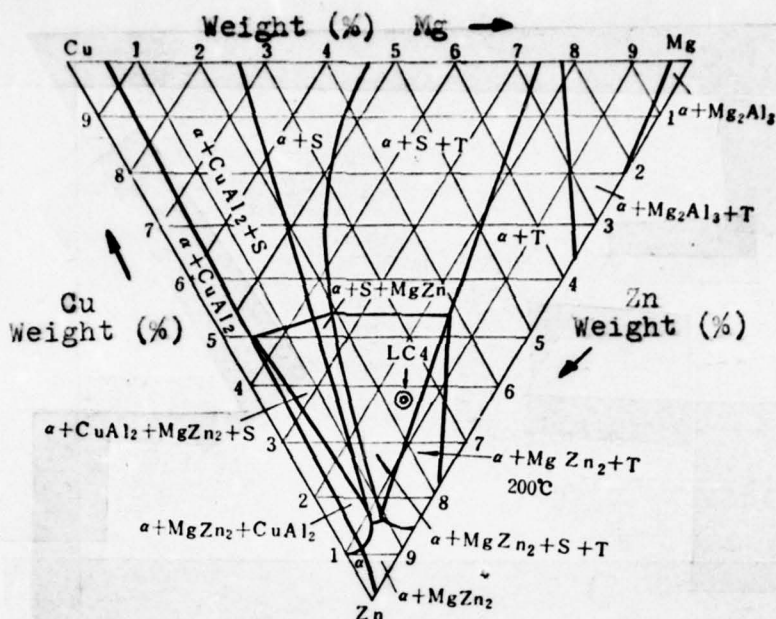


Figure 4 Distribution of Phase Zones of Al-Zn-Cu in the 90% Al Plane at 200°C

Of the phases mentioned above, excluding Si, MnAl_4 , MnAl_6 , TiAl_3 , ZrAl_3 , and Mg_2Si , which are insoluble in Al (Mg_2Si is also insoluble in both Mg and Si), all binary phases have varying degrees of solubilities in Al and their respective components. For ternary and quaternary compounds, all except $\text{S}(\text{CuMgAl}_2)$ have varying degrees of solubilities in their respective components. In particular, $\text{T}(\text{Mg}_3\text{Zn}_3\text{Al}_2)$ has the widest range, while that of $\text{W}(\text{Cu}_4\text{Mg}_5\text{Si}_4\text{Al}_x)$ is rather restricted, and $\text{S}(\text{CuMgAl}_2)$ has almost none at all.

In the production of deformed Al alloys, the formations of the above phases are dependent on the rates of crystallization during casting, chemical compositions of the alloys, heat treatment techniques, and working methods. The various kinds of compounds introduced in this book are identified by means

of metallographic analysis and microstructure-probing by electrons. The alloy specimens are prepared by a specified set of melting and casting techniques and heat treatment methods. Figure 5 exhibits the features of different compounds under slow-rate crystallization. The crystalline structures of these compounds and the effects of various etching reagents on them are listed in Table 2 in the Appendices. The analyses of the different industrial alloy systems are given in Chapter One through Chapter Eight.

III Structures of Cast and Wrought Products under Various Conditions

1. Structures of Ingots Made by Semi-Continuous Casting (Watercooled)

Because of the rapid rate of cooling during the process of semi-continuous casting of deformed aluminium alloys, the ingot structures are often those of non-equilibrium eutectic systems and other metastable phases, which can be illustrated by means of Figure 6. For example, for an alloy containing 4% Cu, it will completely solidify at point b if it proceeds in accordance with equilibrium crystallization. Between points b and d, the alloy is a homogeneous single-phase solid solution of $\alpha(\text{Al})$. When the temperature drops below point d, the $\alpha(\text{Al})$ solid solution decomposes, from which particles of CuAl_2 are precipitated. Under the drastic cooling condition in the process of semi-continuous casting, the crystallization rate becomes so rapid during the solidification of the alloy that conditions for equilibrium crystallization are destroyed. Now, the composition of $\alpha(\text{Al})$ in the alloy will not obey the solidus line in the equilibrium diagram, but will obey the flat dashed line in Figure 6. Accordingly, the 4% Cu alloy cannot

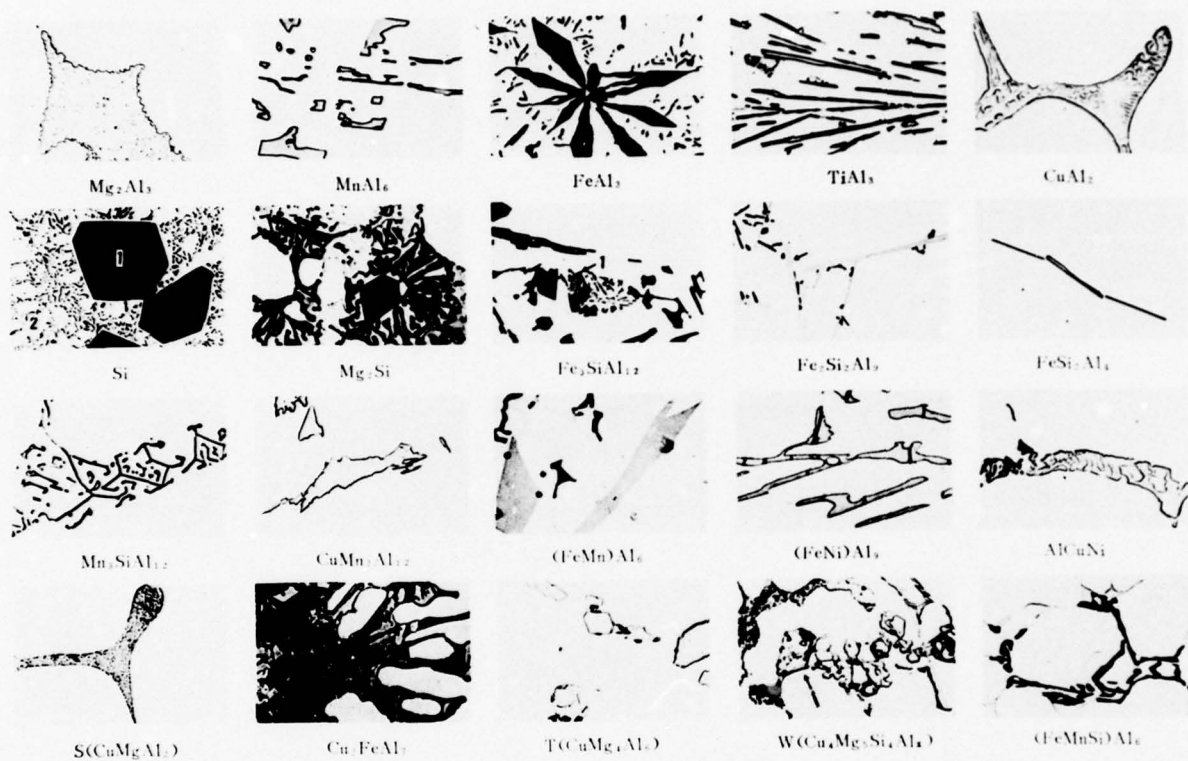


Figure 5. Principal Phases of Deformed Aluminium Alloys

solidify completely until it cools to point c. It is evident then that there is a considerable amount of liquid solidifying into eutectic structures at the eutectic temperature. These secondary eutectic structures are distributed on the arms of the dendrites and on the grain boundaries. They are few in number, and often appear as **segregated eutectic** structures. That is to say, the $\alpha(\text{Al})$ participating in the eutectic reaction joins with the $\alpha(\text{Al})$ matrix, so that the compounds comprising the eutectic structures appear isolated. Under the optical microscope, the appearance of the cross-section of a sample with dendritic structure resembles that of a net, so this structure is often called the dendritic network. It is apparent that the inside of each cell of the net is made of $\alpha(\text{Al})$, and the **narrow strips** between the cells are made of non-equilibrium eutectic structures. Figure 6a shows the equilibrium structure; Figure 6b shows the non-equilibrium structure.

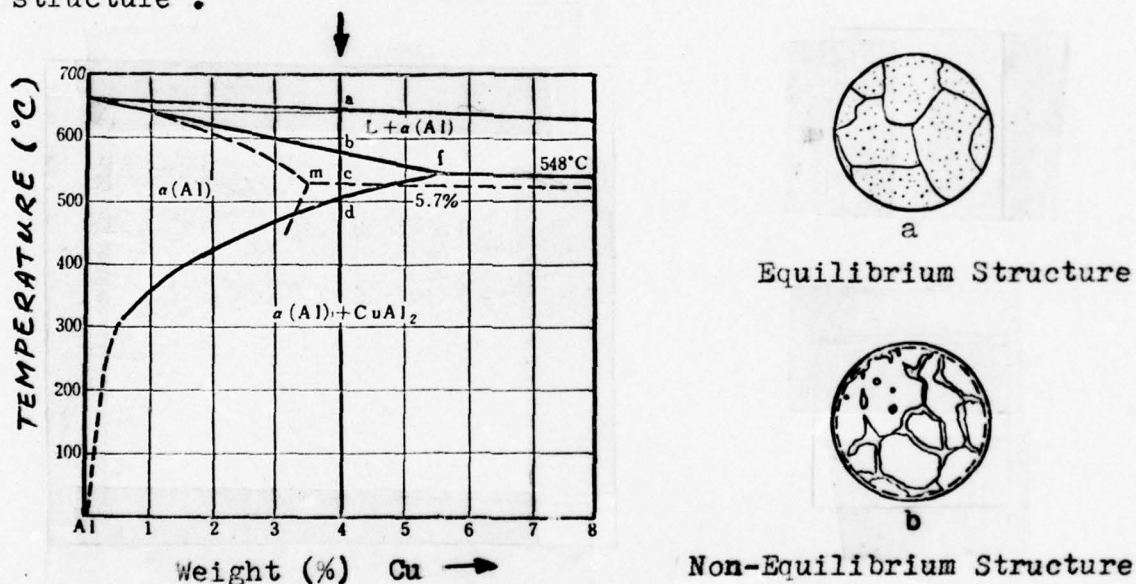


Figure 6 Structures of Alloy under Equilibrium and Non-Equilibrium Conditions

As a result of selective crystallization during casting, alloy elements are not distributed uniformly within the arms of each dendrite, whence preferential precipitation occurs, exhibiting wave-form structures (Figure II-2a in Chapter Three). The way in which preferential precipitation is manifested is related to that of the alloys which behave in accordance with the equilibrium diagram. In eutectic alloys, the contents of alloy elements are lowest in the central regions of the dendrites and increase gradually to the sides. For peritectic alloys, the situation is just the opposite to that of the eutectic alloys.

During the rapid cooling of some alloys, the formations of certain compounds do not proceed in accordance with equilibrium conditions, and metastable structures are formed. For example, in the case of Al-9.7%Mn alloy, MnAl_6 is formed under equilibrium conditions at room temperature; but under rapid crystallization, the structures formed are layers of MnAl_4 surrounded by MnAl_6 , because the peritectic reaction $\text{L} + \text{MnAl}_4 \rightleftharpoons \text{MnAl}_6$ is not carried out into completion (Figure 7).

The microstructure of the ingot is a dendritic network. For example, Figure 8A shows the structure of an LY12 alloy ingot made by semi-continuous casting, which has this form. The structures at the grain boundaries appear to be the same as those at the dendritic boundaries. In order to distinguish between them, the sample has to be anodized and then observed under polarized light. Each grain will show up as a region of uniform light intensity (Figure 8B).

The size of each cell of the dendritic network of an ingot and the width separating two adjacent cells are not uniform. Figure 9 shows the structure of an LD2 $\phi 272\text{mm}$

round alloy ingot under low power and high power microscope. At the place where the preferentially precipitated structures are found at the edge of the ingot, the size of the cells of the dendritic network is small and the separations between the cells are rather thick. In the next layer, the so-called peripheral fine-grain region, the size of the cells of the dendritic network is large and the separations between the cells are sparse. In the middle region of the ingot, the cells of the dendritic network are smaller and more non-uniform than those in the previous layer, and the separations between the cells are thick. In the central region, the cells have irregular sizes, but are generally smaller than those



Figure 7 Layer Structure of MnAl_4 Surrounded by MnAl_6 in Al-Mn Alloy

Alloy	Al-9.7%Mn
Condition	As cast
Etching Reagent	10% NaOH Aqueous Solution
Structural Features	1 -- MnAl_6 2 -- MnAl_4

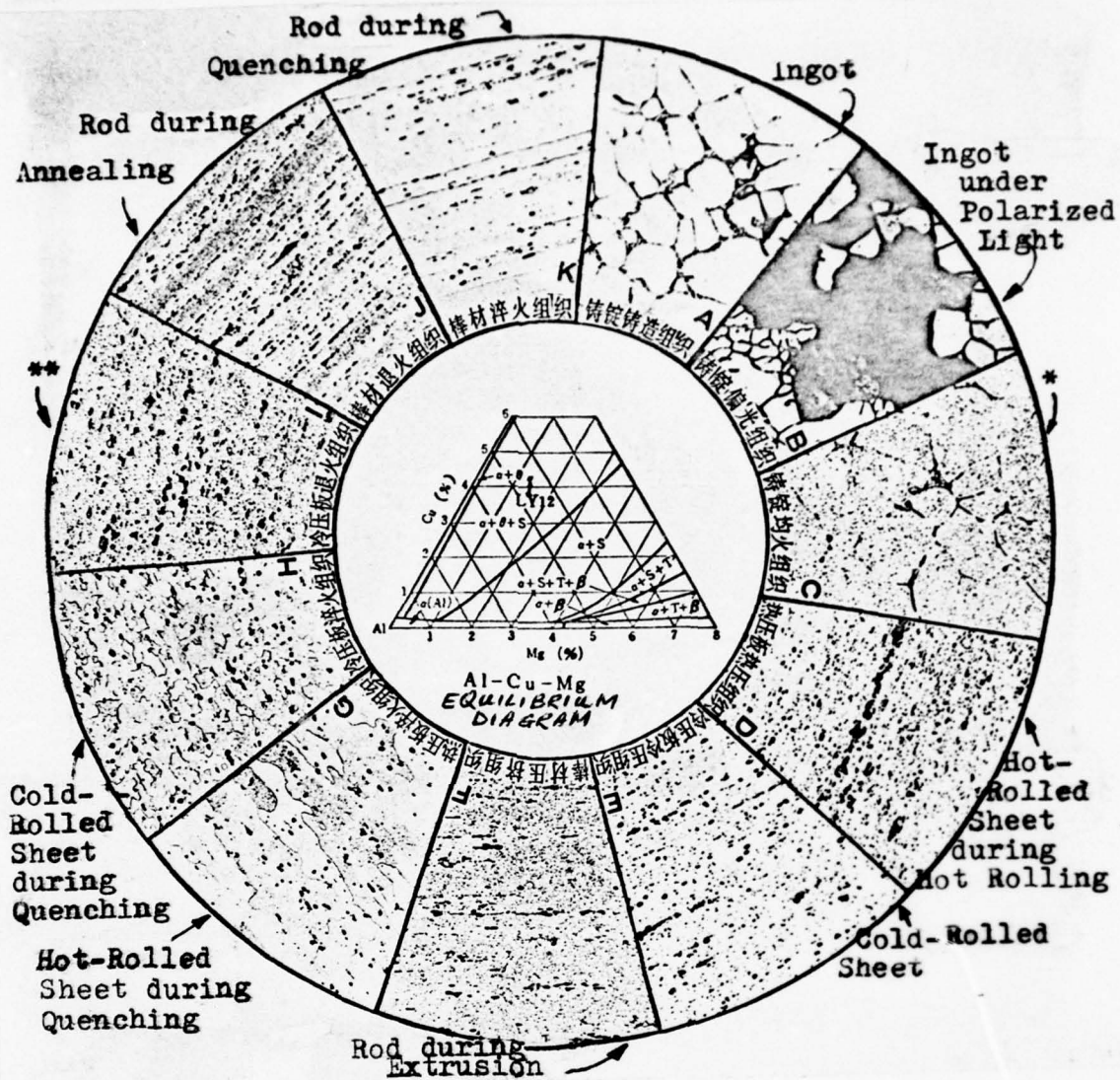


Figure 8 Effects of Various Methods of Deformation and Heat Treatment on the Alloy Structure of LY12

*C -- Ingot under homogenization

**I -- Cold-Rolled sheet after annealing

in the peripheral fine-grain region. We have studied a sample of the $\phi 272\text{mm}$ LY12 alloy ingot and determined the size of the cells of each region mentioned above. The results are listed in Table 1.

Table 1 Average Sizes of Cells of the Dendritic Network in Various Regions of the Ingot

Diameter of Ingot (millimeter)	Average Size of Dendritic Network Cells (Microns)			
	Preferential Precipitation Region	Peripheral Fine -Grain Region	Middle Region	Central Region
272	6	26	7	9

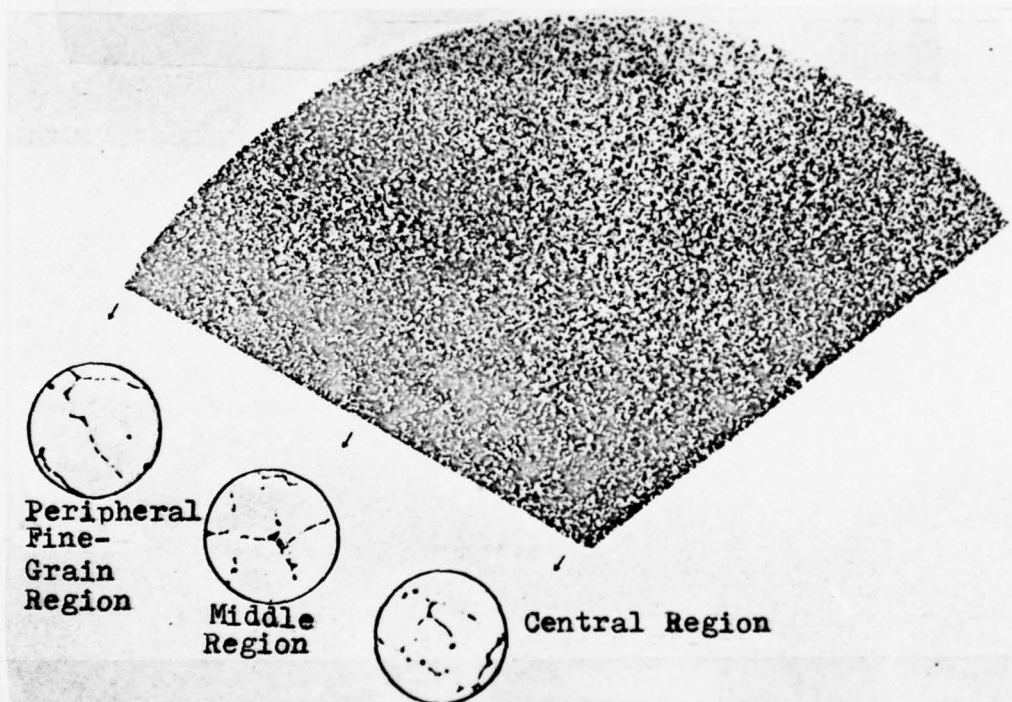


Figure 9 Structures of LD2 Alloy $\phi 272\text{mm}$ Round Ingot under Low Power and High Power Microscope

The rate of crystallization during casting directly influences the size of the cells in the dendritic network: the higher the rate of crystallization, the smaller the average size of the cells in the dendritic network. The properties of the ingot are heavily dependent on the size of the cells in the dendritic network. This effect is especially pronounced for alloys with high contents of alloy elements. The reason is that the sizes and distribution of interdendritic compounds (eutectic structures) are directly affected by it. When the cells in the dendritic network are small, which means that the compounds are small and evenly distributed, the structural quality of the ingot is good.

When improper chemical compositions and technical methods are used, accumulations of preferentially precipitated proeutectic compounds will also appear in the ingot. Their structural features are discussed in Chapter Seven on Al-Cu-Mg-Fe-Ni System Alloys.

During semi-continuous casting, subgrains can also be found within the dendritic network of the ingot (Figure 10). Their sizes are related to the rate of crystallization during casting: their sizes are large when crystallization is slow, and small when crystallization is fast. Besides, they grow in size with temperature during homogenization.

The size and distribution of crystal grains are dependent on alloy casting techniques. For industrial-pure Al that does not contain any modifier such as titanium, and for Al-Mg alloys with low content of magnesium, there are three grain regions, namely, the peripheral fine-grain region, the columnar grain region, and the central equiaxed region

(For details, see the macrographs of ingots in Chapter One on Industrial-Pure Aluminium and Chapter Two on Al-Mg Alloys). The structures of the above alloys will undergo marked changes when a modifier (titanium) has been added. The columnar grain region becomes poorly developed, while the size of the equiaxed grains diminishes (Figure 11a). When cast improperly, the ingots of industrial-pure aluminium LF5 and LC4 alloys can exhibit coarse equiaxed grains, coarse columnar grains, and lacy structures (Figures 11b and 11c). When cast properly, the ingots of multi-component alloys that contain high amounts of alloy elements (LY12, LD8, LC4) are basically composed of equiaxed fine grains, the columnar grains being poorly developed (Figure 11d).

2. Structures of Alloys under Various Working Conditions

(1) Structures of Alloys under Hot Rolling

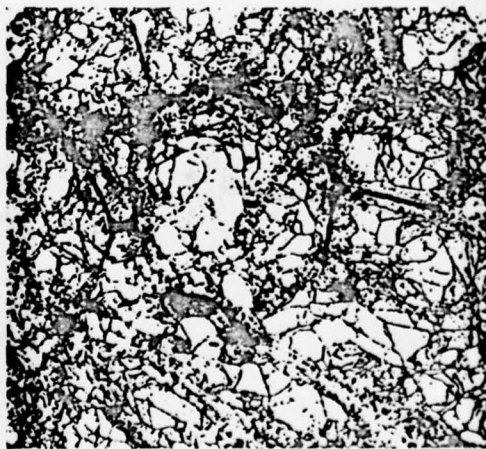


Figure 10 Subgrains in the Dendritic Network of Ingot Made by Semi-continuous Casting

After the ingot has been hot-rolled its sheet structure is dependent on the final temperature in hot rolling. In practical production, final temperatures in hot rolling for alloys vary widely. In most cases, the final temperatures in hot rolling for sheets are either below the recrystallization temperature or within the recrystallization temperature range. Therefore, the structures of hot-rolled sheets are often those of incomplete recrystallization. Some of them may not even have undergone recrystallization and still remain in the recovery condition (Figure 12).

During the hot rolling of an alloy, its cast grains and dendritic residues are being crushed. The grains will be stretched along the direction in which rolling is applied. The compounds are arranged into arrays, showing markedly directionality. At this time, if the alloy undergoes recrystallization, the grains will be refined and the structure will be changed.

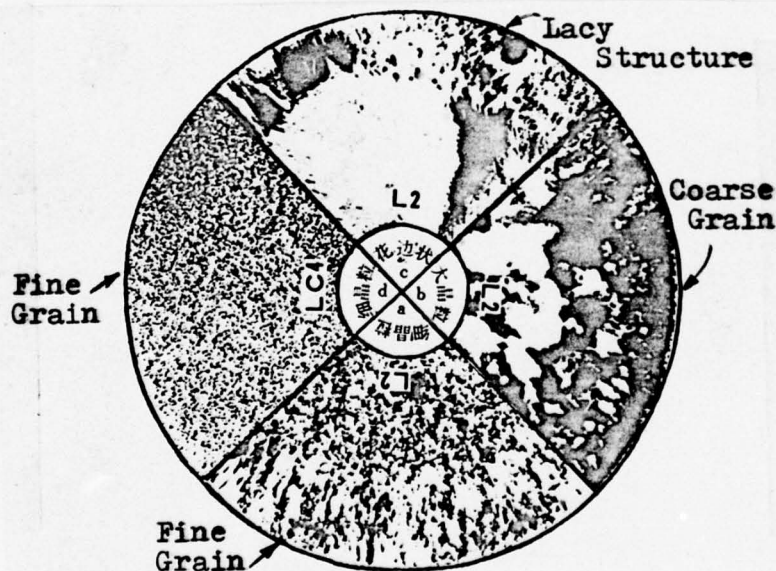


Figure 11 Comparison of Grain Sizes of Aluminium Alloy Ingots Made by Semi-continuous Casting

stallization, the shape of the grains will become flat. If there is no recrystallization, its structure will consist of fibres elongated along the principal deformation direction in which **rolling** is applied (Figure 8D). When recrystallization is not complete, the structure of the alloy is a combination of the above two structures.

Surprisingly, the extent of deformation due to stretching along the principal **rolling** direction at the surface area of the alloy in contact with the roller is less than that in the central region. When the industrial-pure Al alloy L2 has been hot-rolled at 520°C , the surface has **undergone** recrystallization and exhibits equiaxed grains, but there are some residual cast structures left; whereas in the central region of the sheet, the dendritic network has been completely destroyed (Figure 13).

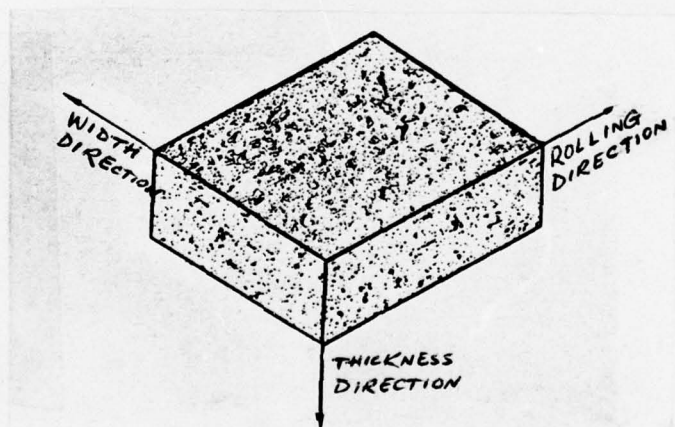


Figure 12 Three Dimensional Structure of a Hot-Rolled 8mm Thick LY12 Alloy Sheet

The structure of the hot-rolled sheet is not uniform throughout. In the inner layer right next to the surface of the sheet, the flow of metal is not in order. The characteristics of the distribution of this disordered layer are as shown in Figure 14 for two 6.0mm thick sheets, one of which is hot-rolled at 480°C, and the other at 490°C. The thickness of the disordered layer increases from the side to the center of the sheet gradually, and remains constant in the middle region.

(2) Structures of Alloys under Hot Extrusion

When the ingot is being worked on under forward extrusion in the absence of lubrication, the dendritic network is broken. In the process of extrusion, the flow of metal is in the form of layers, and exhibits strong directionality. The grains are elongated along the principal deformation direction in which extrusion is applied. The greater the degree of deformation, the more severe the elongation, and at the same time the greater the degree of compounds being

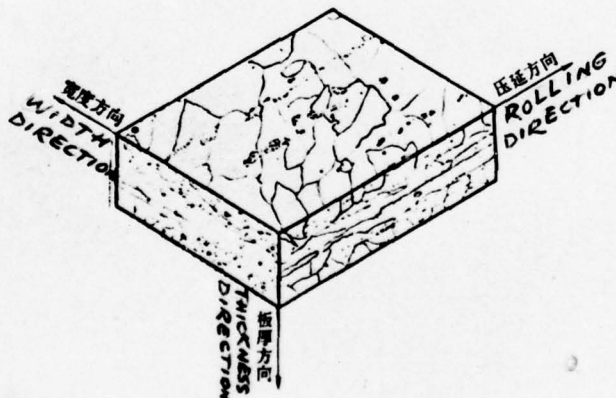


Figure 13 Three Dimensional Structure of a 10mm Thick Hot-Rolled L2 Industrial-Pure Al Sheet (Hot Rolling Temperature 520°C)

broken (Figure 8F).

Under hot extrusion most manganese-containing and chromium-containing alloys do not undergo recrystallization. There is a large amount of subgrains in the layered

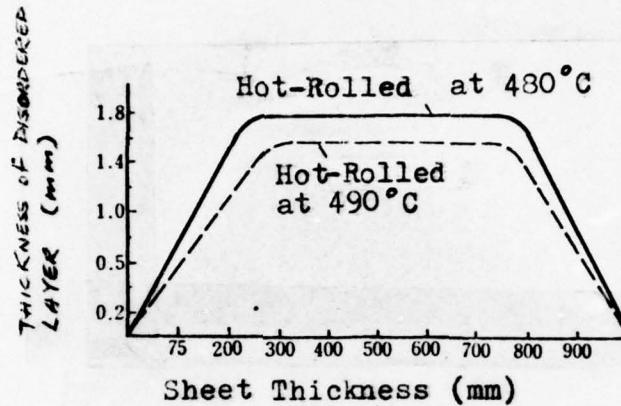


Figure 14 Distribution of Disordered Layer Thickness along the Width Direction in a 6.0mm Thick Hot-Rolled Sheet



Figure 15 Subgrains in the Structure of an LY12 Alloy under Hot Extrusion

structure (Figure 15). For those alloys which have low recrystallization temperatures (e.g. Industrial-Pure Al, LY16, and LD8), their structures are those of recrystallization when the hot extrusion final temperature is high enough. When the hot extrusion final temperature is low, recrystallization will not be complete, so that the structures formed are partially recrystallized and deformed fibre structures.

Most aluminium alloy products that have undergone hot extrusion and subsequent quenching and ageing have greater strength than other products that have undergone other methods of hot working (e.g. Rolling, Forging, and Die-Pressing) and cold working (Cold spinning and Cold drawing) with similar quenching and ageing conditions. The increase in strength is especially marked along the extrusion direction. This phenomenon is called the Extrusion Effect.

The structures of extruded products are dependent on the alloy compositions, shapes of orifices in the dies, extrusion temperatures, deformation rates, and numbers of extrusions applied. Under usual circumstances, alloy compositions, deformation rates, numbers of extrusions applied, and extrusion temperatures are the principal factors that influence the structures of the products. A second extrusion can reduce the variation in directionality in the first extrusion. This is because the second extrusion alters the fibre structures formed in the first extrusion,^(Figures 16 and 17) causing the compounds that are originally in arrays to intermingle with the broken pieces of the crystal grains. Moreover, the heating of additional numbers of times induces further decomposition of manganese in $\alpha(\text{Al})$, thereby lowering the recrystallization temperature of the alloy and diminishing or eliminating the Extrusion Effect (Figures 18 and 19). The effects of the above mention-

ed structural changes on the mechanical properties of extruded products are listed in Table 3 in the Appendixes.

During extrusion, the alloy is not uniformly deformed, so that the structure of the extruded product is not homogeneous. Figure 20 is a diagram of the structure of an LD2 alloy rod. The diagram shows a coarse grain region at the surface. The depth of the coarse grain region increases gradually from the non-coarse grain region at the front end of the rod (Figure 20a) to the coarse grain region at the rear end of the rod (Figure 20b). The shape of the coarse grain region distributed on the cross-section of the product is related to the shape of the orifice in the die and to the number of orifices present. For example, the coarse grain region of a rod is of annular form in the case of single orifice, and of crescent form in the case of more than one orifices. Also, the extent of physical deformation at the front end is less than that at the rear end. On the same cross-section, the extent of physical deformation at the edge portion is bigger than those at the middle and center portions, that of the center portion being the least; this kind of variation is most pronounced at the front end of the rod, and diminishes as the rear end is approached. Since the extent of deformation is small at the front end, residual cast structures can still be found. Consequently, the mechanical properties of the front end of the rod are not as good as those of the rear end of the rod. In particular, the elongation rate is lower than, and the properties are not as even as, those at the rear end of the rod.

(3) Structures of Alloys under Forging

The thickness of the flow-lines of forged products is

dependent on the structures of the materials to be forged and on the forging techniques. When a previously extruded billet is die-pressed, the metal flow along the outline of the die exhibits strong directionality. After quenching, fine flow lines are formed. When a previously cast material is die-pressed, or when a product has undergone different kinds and many times of forging, the directionality of the metal flow is rather weak. After quenching, thick flow lines are formed. The structures of forged materials are rather complicated, and are dependent on the sizes of the forged materials, the die-forging techniques used, and the shapes of the forged materials. The structures of the forged materials after quenching and artificial ageing are similar to those of extruded products, namely, they have either complete recrystallized structures or a combination of partially recrystallized and deformed fibre structures. The compounds are broken and rearranged in arrays along either the outlines of the dies or along the principal deformation direction during forging (Figure 21). (Details of the structural features of forged materials can be found in Chapter Five on Al-Mg-Si-Cu Alloys and Chapter Six on Al-Zn-Mg-Cu Alloys)

N.B. In most hot die-forged products recrystallized structures as well as regionally distributed subgrains can be found when under quenching and artificial ageing conditions. (see Chapter Five on Al-Mg-Si-Cu Alloys and Chapter Six on Al-Zn-Mg-Cu Alloys).

The inhomogeneity of the structure of a forged material appears mainly in the thick-walled portion, which, because of the small extent of deformation, contains residual cast structures. It is apparent from Figure 21 and the comparison of figures in Table 3 in the Appendixes that the smaller the deformation rate, the smaller the extent of the cast structure

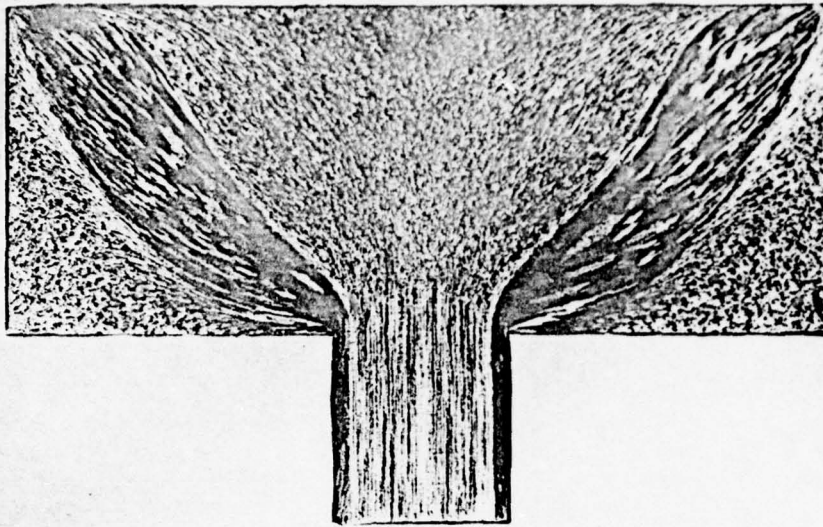


Figure 16 Metal Flow During First Extrusion

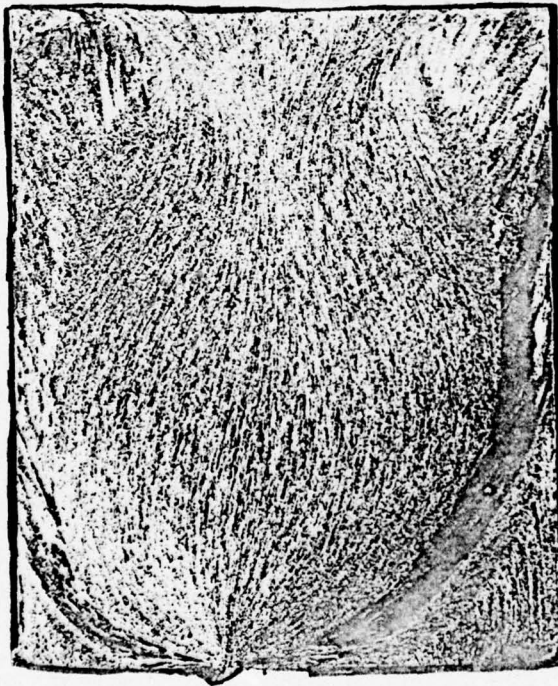


Figure 17 Metal Flow During Second Extrusion

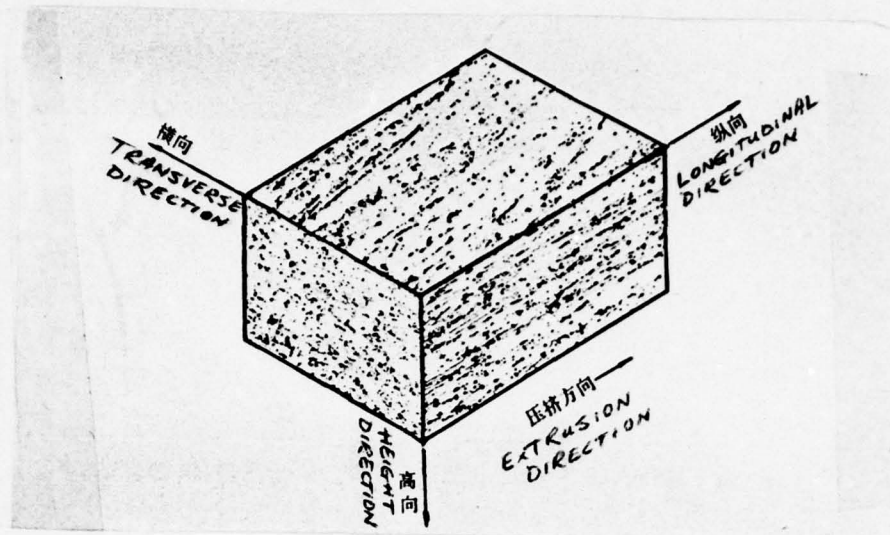


Figure 18 Three Dimensional Structure under Hot Extrusion Condition of a Once-Extruded LD2 Alloy Ribbon (Specification : 90 x 230 mm; Deformation : 87.6%)

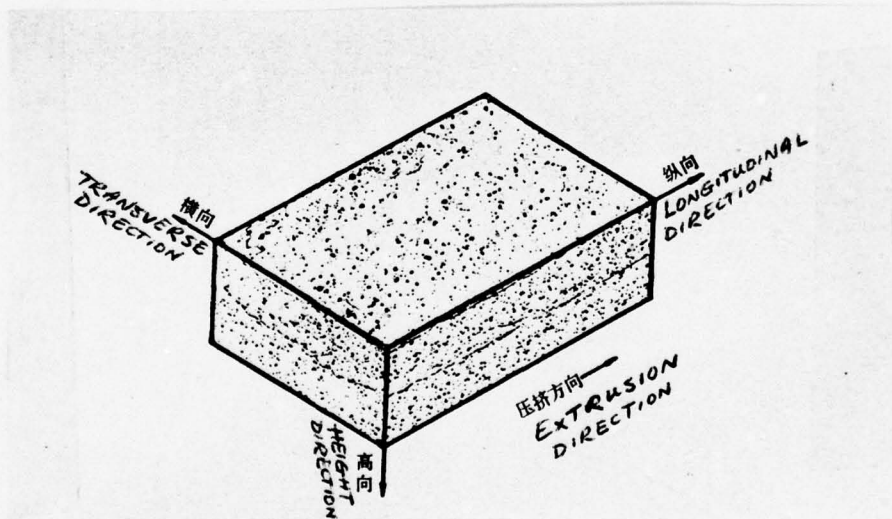
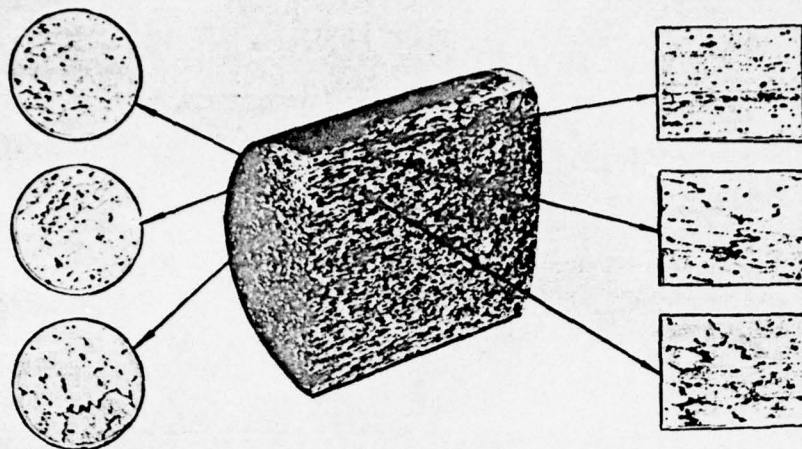
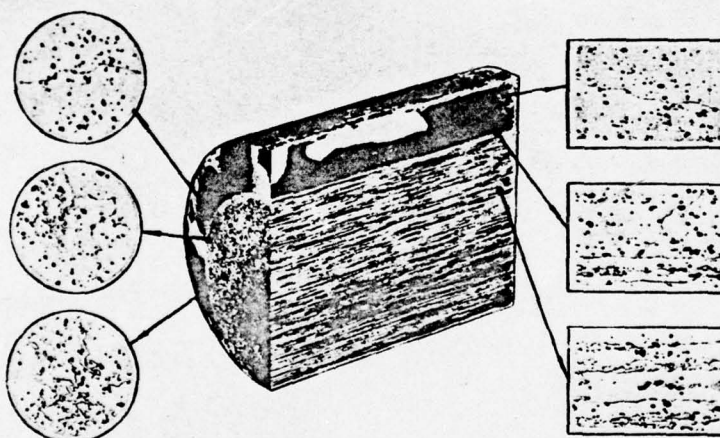


Figure 19 Three Dimensional Structure under Hot Extrusion Condition of a Twice-Extruded LD2 Alloy Structural-shape (Specification : AP-218; Deformation : 94.2%)



a



b

Figure 20

Diagram Showing the Structure of an LD2 Alloy Rod

a --- Front End; b --- Rear End

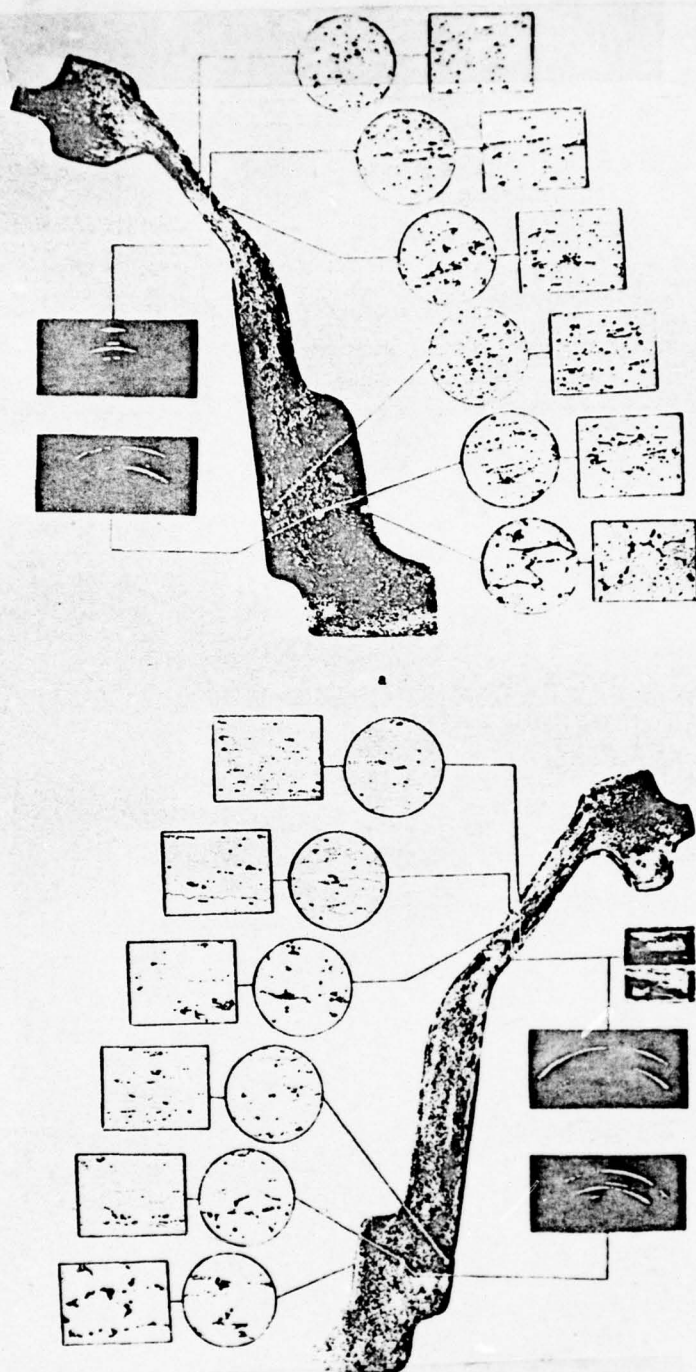


Figure 21

**Summary of the Structural Features of an
LD2 Die-Forged Material**

a --- Forged; b --- Quenched & Artificially
Aged

being broken, and that the clearer the outlines of the dendritic network, which means the more the residual cast structures, the lower the transverse elongation rate of the forged material. Figure 22 are macrographs of the structures of different portions of a forged LY11 alloy. In the portion where the deformation rate is large, the cast grains are clearly deformed, and the transverse elongation rate can reach as high as 20%. In the portion where the deformation rate is small, the outlines of the cast grains can still be discerned, and the elongation rate is only 2%.

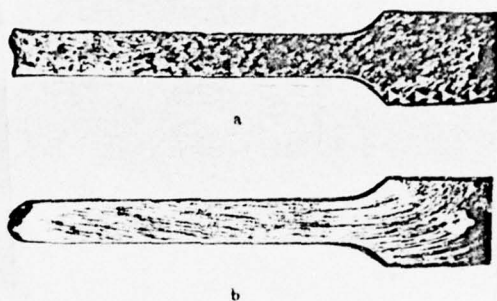


Figure 22 Macrostructures of Different Portions of an Forged LY11 Alloy

- a --- Elongation rate of small deformation rate portion is 2%
- b --- Elongation rate of large deformation rate portion is 20%

(4) Structures of Alloys under Cold-Rolling, Cold-Drawing, and Cold-Spinning

The structures of alloys under cold deformation processes are closely related to the amount of deformation. When

the cold deformation rate is small, the shapes of the original grains can still be recognized, but the grains are elongated somewhat along the deformation direction. As the deformation rate increases, the extent of grains being broken also increases, and the outlines of the original grains gradually disappear. Figure 23 shows the structural features of various kinds of cold-wrought products.

3. Structures of Cast and Wrought Products under Heat Treatments

(1) Structures of Ingots under Homogenization

The homogenization of an ingot consists of heating the metal close to the solidus line or close to the eutectic temperature, annealing it at the same temperature for a long period, and then slowly cooling it to room temperature. The purpose of homogenization is to eliminate or diminish the inhomogeneities in the structures and the chemical compositions within the grains, thereby improving the alloy texture, increasing the malleability of the alloy, and facilitating deformation during working. For most aluminium alloys with high strength and low malleability, homogenization can help eliminate or reduce the internal stresses caused by the rapid cooling of the metal during casting, so that the danger of rupture can be avoided when the ingot is being sawed or is subject to an impact.

When the ingot is heated in the process of homogenization, it undergoes two opposite stages of structural changes. In one stage, non-equilibrium eutectic mixtures (e.g. $\alpha(\text{Al}) + \text{CuAl}_2$, $\alpha(\text{Al}) + \text{MgSi}_2$, etc.) dissolve in $\alpha(\text{Al})$ to form solid solutions, so that the dendritic network structures disappear,

or only a small amount of residual dendritic network traces remains. In the other stage, compounds containing manganese, chromium, zirconium are precipitated from supersaturated solid solutions. During subsequent cooling, particles of soluble compounds (e.g. the CuAl_2 , $\text{S}(\text{CuMgAl}_2)$ phases, etc.) are also precipitated from the solid solutions (Figure 8C).

The tensile strength and yield strength of the ingot do not change appreciably after homogenization, but the elongation rate is immensely enhanced (confer Table 3 in the Appendixes).

In the process of homogenization, if the alloy is heated and subsequently cooled at a very slow rate, Widmanstätten structures will be formed (Figure 24), which means that needle-shaped compounds will be precipitated from $\alpha(\text{Al})$ along fixed crystalline planes, while maintaining fixed orientations with respect to one another. The higher the temperature during heating, and the slower the cooling rate, the thicker the precipitates.

(2) Structures of Products under Recovery and Recrystallization

When a wrought product has undergone the process of recovery, it can recover its physical and mechanical properties that it had before working, but its structure has not undergone significant changes. During the process of recovery of the metal, polygonization occurs as a result of climb of dislocations out of their slip planes, followed by their motion by slip into the lower energy arrays. The subgrains thus obtained are very small in size, unobservable under ordinary optical microscopes. They can be

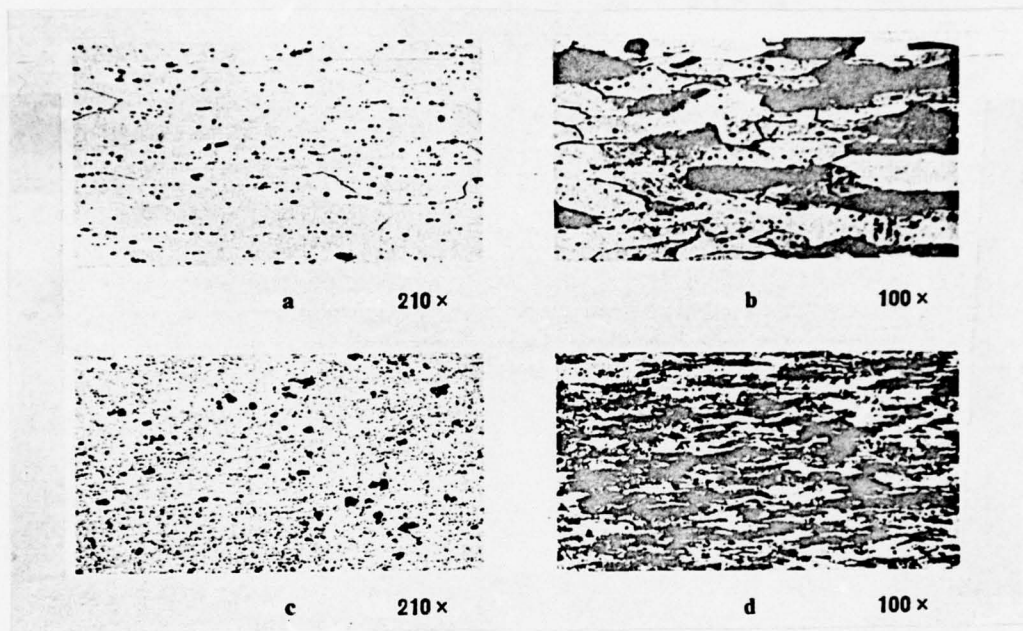
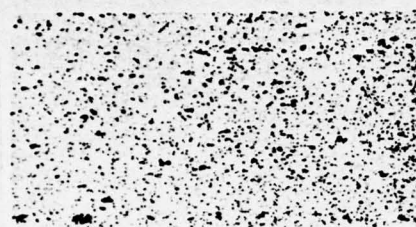


Figure 23 Structures of Alloys under Various Cold Working Conditions

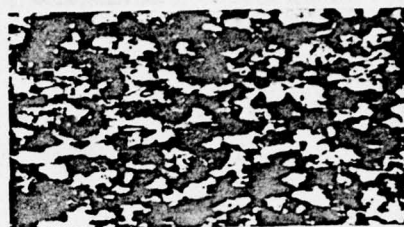
a & b --- Cold-Drawn Tube; Cold Deformation Rate 14%

c & d --- Cold-Rolled Sheet; Cold Deformation Rate 80%

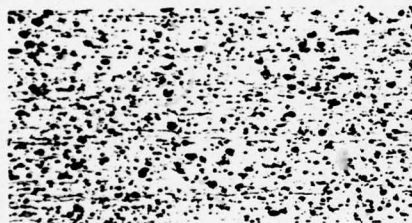
(to be continued on next page)



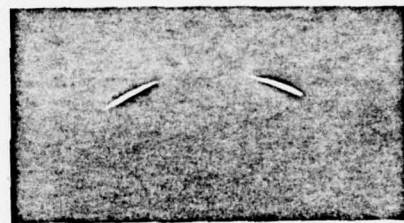
e 210x



f 100x



g 210x



h

Figure 23 Structures of Alloys under Various Cold
(con't) Working Conditions

e & f --- Cold-Drawn Wire; Cold Deformation Rate 45%

g & h --- Cold-Spun Tube; Cold Deformation Rate 35%

(continued from last page)



Figure 24 Widmanstatten Structure Obtained after
Homogenization of an LY12 Alloy Ingot
(600 x)

discerned only by means of x-ray diffractions or by means of electron microscopes.

The recrystallized structural features of deformed aluminium alloy products are closely related to the alloy compositions, working methods, and heat treatment techniques. Industrial pure aluminium and alloys that have low recrystallization temperatures, such as Al-Mg system alloys, have rather simple recrystallized structures. After complete recrystallization, the grains become equiaxed or closely equiaxed, and the grain boundaries are rather straight. If alloy elements (e.g. manganese, chromium, zirconium, etc.) which can raise the recrystallization temperature markedly are added to the alloys, the recrystallized structures will be pronouncedly different from those mentioned above. When such an alloy is heated to the temperature range bounded by the initial recrystallization temperature and the final recrystallization temperature, the recrystallized grains will appear to have incompletely closed or tooth-shaped grain

boundaries, and will appear elongated as fibres along the principal deformation direction. For some zirconium-added alloys, their grains retain their fibre shape after recrystallization even though the temperature during heating is higher than the recrystallization temperature (For details, see Al-Cu-Mg, and Al-Zn-Mg-Cu system alloys).

When the alloy is heated to the initial recrystallization temperature, the first new grain or a saw-tooth shaped local grain boundary appears. As the temperature continues to be raised, tooth-shaped or straighter grain boundaries of completely recrystallized structures will ultimately be formed. When observed under polarized light, there first appear in the deformed fibre structures of the matrix small spots or short and narrow bands that are uniformly colored and look brighter than the matrix. These regions grow in size and quantity with increasing temperature until the deformed fibre structures completely disappear. At this time, the alloy has undergone complete recrystallization (see the recrystallized structural features of Industrial-Pure Aluminium and Al-Mg system Alloys). We feel that the appearance of especially coarse and non-uniform recrystallized structures in alloy products are due to the occurrence of a second recrystallization.

The rate of heat application has a pronounced effect on the final granular sizes of deformed aluminium alloys. In particular, manganese-containing aluminium alloys are very sensitive in this respect. Rapid heating produces fine grains. This is because during rapid heating, the distorted grains do not have enough time to recover, and as the diffusion coefficient increases drastically with temperature, the number of recrystallization nuclei is greatly augmented, so that every

part of the alloy undergoes recrystallization at the same time. Slow application of heat produces coarse grains, because in this process, the deformed metal has already undergone partial recovery before the recrystallization temperature is reached, thereby reducing the number of recrystallization nuclei, so that the grains obtained after recrystallization are coarse.

Rolled sheets (especially cold-rolled sheets) have low recrystallization temperatures and narrow recrystallization temperature ranges. The grains after complete recrystallization are equiaxed grains, and the grain boundaries are not very curved.

The recrystallization temperatures of hot-extruded products, especially those that are extruded once and those that contain recrystallization temperature raising elements, are higher than those of rolled products, and the recrystallization temperature ranges of the former are wider than the latter. When manganese-containing alloys are heated in the recrystallization temperature range, incompletely closed recrystallized structures with curved grain boundaries are formed. Besides, equiaxed grains are hard to obtain even when the alloys are heated above the final recrystallization temperature.

(3) Structures of Alloys under Annealing

The annealing of deformed aluminium alloy products can be classified into two types, namely, low-temperature annealing and high-temperature annealing. Low-temperature annealing includes the recovery treatment that eliminates the internal stresses in cold-deformed products, the stabilizat-

ion treatment of high magnesium content alloys, and partial softening annealing for alloys of different hardness. The structural changes in recovery treatment has been discussed previously. In the process of stabilization, $\beta(\text{Mg}_2\text{Al}_3)$ are precipitated on the grain boundaries. The temperature of partial-softening annealing is between the initial recrystallization temperature and the final recrystallization temperature. Therefore, the structural features in partial-softening annealing are that on the fibre structures of the matrix, there appear recrystallized grains, which increases in number as the temperature rises (For details, see the structural diagrams in Figure I-5 of Chapter One on Industrial-Pure Aluminium).

In high-temperature annealing, alloy structures undergo marked changes. After high-temperature annealing, industrial-pure Al has gone through recrystallization only, but for other alloys, decomposition of the $\alpha(\text{Al})$ solid solution and accumulation of residual soluble compounds also occur in addition to recrystallization. Besides the compounds, decomposed products are also found densely distributed on the $\alpha(\text{Al})$ matrix. Since the recrystallization temperatures of extruded products are usually high, most of them do not have complete recrystallization during annealing. Recrystallized grains are hard to be distinguished one from another because of the densely distributed decomposed products (Figures 8I and 8J), and have to be discerned under polarized light.

Wrought products exhibit decrease in tensile strength and yield strength but increase in elongation rate. These changes in properties are more pronounced in cold-wrought products than in hot-wrought products (confer Table 3 in the

Appendixes).

(4) Structures of Alloys under Quenching and Ageing

The application of heat to semi-finished wrought aluminium alloy products before quenching can cause the soluble hardening phases (e.g. CuAl_2 , $\text{S}(\text{CuMgAl}_2)$, Mg_2Si , etc.) to dissolve maximally into $\alpha(\text{Al})$. Subsequent quenching will make the $\alpha(\text{Al})$ supersaturated with alloy elements that comprise the hardening phases. Accordingly, under the new quenching condition, the structures of the products will contain markedly fewer compounds than they had before heating, while the matrices have undergone recrystallization. If the alloys contain elements such as manganese, chromium, and zirconium, particles of compounds formed by these elements with aluminium are also found to be distributed over the $\alpha(\text{Al})$ matrices. For alloys containing copper or zinc, the spaces between the recrystallized grains exhibit different degrees of contrast in color. Bigger contrast will indicate that there are higher contents in the solid solutions of the alloys (Figures 8G, 8H, and 8K).

After quenching, the structural changes in the alloys caused by ageing can only be seen by means of an electron microscope. Recently, x-rays and electron microscopes are used in combination. Investigations of the structural changes in alloys under the ageing process reveal that the decomposition process of $\alpha(\text{Al})$ is rather complicated in low temperature ageing. Table 2 lists the decomposition gradations of supersaturated $\alpha(\text{Al})$ for several alloys during ageing (Shown in parentheses are alloy elements of the richly congregated solute atoms, or are precipitated phases formed in the process of ageing).

Of the ageing gradations of alloys mentioned above, the GP1 and GP2 stages have complete lattice coherency with the $\alpha(\text{Al})$ matrix, thus causing the alloy to harden. In particular, the GP2 stage has the greatest hardening effect. In the transitional phase stage, there is partial lattice coherency with the $\alpha(\text{Al})$ matrix, but the hardening effect is not as great as that of the GP2 stage. When the stable phase appears, there is total lattice incoherency with the $\alpha(\text{Al})$ matrix, causing the alloy to soften.

Investigations by means of the electron microscope verify that the shape of the GP region is determined by the differences in size between the solute atoms and the solvent atoms. For example, the difference in atomic radii between Al and Cu is rather large, and the GP region is platelike in shape, so as to provide a wider contact area with the matrix and to minimize distortion of the lattice. Table 3 shows the shapes of the GP regions for several principal alloys.

We carried out some studies by means of the electron microscope on the structures of a forged LD10 alloy material and an LY12 alloy foil during artificial ageing. We found that after the LD10 alloy had been annealed at 500°C for 60 minutes, subsequently quenched in water, and then aged at 185°C for 12 hours, its structure exhibited a large quantity of platelike and needlelike bodies under the electron microscope (Figure 25a). Analysis by means of electron scattering verified that these platelike and needlelike bodies were both of the $\theta'(\text{CuAl}_2)$ metastable phase, which had partial lattice coherency with the $\alpha(\text{Al})$ matrix. Therefore, the platelike bodies appeared semi-circular in form, and the adjacent needlelike bodies were actually the cross-sections of some platelike bodies in another direction. Figure 25b is an electron

scattering picture of the portion indicated by the head of the arrow in Figure 25a.

Figure 26 is the structure of the LY12 alloy foil under the electron microscope after it has been annealed at 500°C for 30 minutes, subsequently quenched in water, and then aged at 170°C for 12 hours. The striplike structure indicated by the head of the arrow 1 is a dispersed particle of a manganese-containing phase. One can also see the dislocation lines (Arrow 2). The fingerprint-like feature that appears on the grain boundary is the light interference pattern (Arrow 3).

The shapes of metastable phases of several principal alloys are shown in Table 4.

The structural features under the optical microscope of deformed aluminium alloys in the natural ageing condition are the same as those in the new quenching condition.

The structures under the optical microscope of artificially aged alloys are similar to those of naturally aged alloys in general. In artificial ageing, since the decomposition of the $\alpha(\text{Al})$ solid solution is accelerated by the high temperature, the decomposed products are precipitated more along the grain boundaries and the subgrain boundaries than inside the grains and the subgrains. Consequently, the grain boundaries and the subgrain boundaries in this case are more susceptible to corrosion than in the case of natural ageing. We can utilize this feature to study the distribution of subgrains in the alloys (For details, see the structural features of extruded products and die-forged materials under artificial ageing in Chapter Four on Al-Cu-Mg System Alloys, Chapter Five on Al-Mg-Si-Cu System Alloys, and

Table 2 Decomposition Gradations of Supersaturated Solid Solutions during Ageing for Several Principal Alloys

Alloy	Ageing Gradations
Al-4%Cu	SS \rightarrow GP(1)(Al,Cu) \rightarrow GP(2)(Cu) \rightarrow θ' \rightarrow θ (CuAl ₂)
LY12	SS \rightarrow GP(Al,Cu,Mg) \rightarrow ordered GP \rightarrow S' \rightarrow S(CuMgAl ₂)
LY11	SS \rightarrow GP(Al,Cu) \rightarrow θ' \rightarrow θ (CuAl ₂)
Al-Mg-Si	SS \rightarrow GP(Mg,Si) \rightarrow ordered GP region \rightarrow β' \rightarrow β (Mg ₂ Si)
Al-Zn-Mg	SS \rightarrow GP(Al,Mg,Zn) \rightarrow M' \rightarrow M(MgZn ₂) \rightarrow T' \rightarrow T(Mg ₃ Zn ₃ Al ₂)

Table 3 Shapes of GP Regions for Several Principal Alloys

Alloy System	Condition of the GP Region	
	Shape	Existence Situation
Al-Cu	Platelike	Lattice Coherency
Al-Mg-Si	Needlelike	Lattice Coherency
Al-Cu-Mg	Needlelike or Spherical	Lattice Coherency
Al-Zn-Mg	Spherical	Lattice Coherency

Table 4 Shapes of Metastable Phases for Several Principal Alloys

Alloy System	Condition of the Metastable Phase	
	Metastable Phase	Shape
Al-Cu	θ'	Platelike
Al-Cu-Mg	S'	Spherical
Al-Mg-Si	β'	Rodlike
Al-Zn-Mg	M'	Platelike

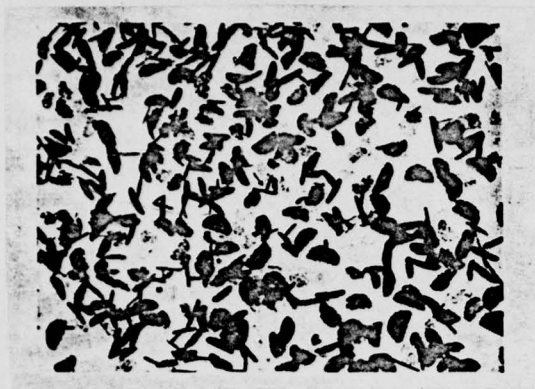


Figure 25a 12000 x
Electron Micrograph Taken by
Once-Collected Sprayed-Carbon
Duplication Method

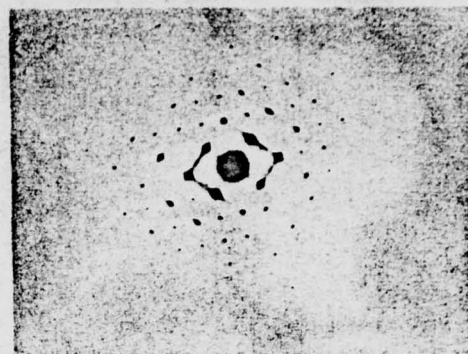


Figure 25b
Electron Scattering Picture
of the Portion Indicated by
the Arrow Head in Figure 25a



Figure 26 Electron Micrograph Taken by Means of
Metal Thin-Film Method
26000 x

Chapter Six on Al-Zn-Mg-Cu System Alloys).

Cold working of the alloys after quenching can facilitate the decomposition of α (Al) solid solutions and accelerate ageing. However, cold working following artificial ageing will not cause the above structural changes. The structures will only exhibit the broken features peculiar to cold working.

If the temperature is too high when heating the alloy before quenching, over-firing will result. At this time, the alloy structures will exhibit re-melted eutectoids that are spherical in shape, and the grain boundaries become coarsened. Moreover, some portions become shuttle-shaped, and the grain boundaries appear "frayed"; the junctions where three grains meet will take on triangular shapes. These are some of the over-fired structural features (Figure 27), which are the results of the re-melting of the eutectic structures when the temperature during heating exceeds the minimum eutectic temperature of the alloy. When an alloy product is over-fired, the above-mentioned over-fired structural features do not necessarily appear simultaneously. Any slight over-firing of the alloy will seriously diminish its ability against fatigue, even though its strength does not decrease, or may even increase. Therefore, over-fired products must be declared unusable. For coated aluminium sheets, prolonged annealing will cause the Cu atoms of the alloys in the matrices to diffuse into the coated aluminium layers. Moreover, since diffusion takes place more easily along the grain boundaries than inside the grains, a concentration gradient of Cu atoms are formed. Therefore, beardlike structures will appear in the coated Al layers at the end, which is an indication of the diffusion of Cu (Figure 28). As soon as the beardlike

structures penetrate the coated aluminium layers, the ability of the sheets against corrosion will be drastically reduced. Accordingly, the duration of annealing at constant temperature before quenching has to be properly adjusted. During quenching, if the temperature of the quenching medium is too high or if the product is exposed to air too long, decomposition of the $\alpha(\text{Al})$ solid solution will ensue. Precipitates will begin to emerge along the grain boundaries, causing the latter to become coarsened, which are often mistaken as due to over-firing. When the cooling rate is too slow, particles of precipitation will also be found inside the grains (Figure 29).

N.B. In the General Discussion and the following chapters in this book, we introduce summarily the structural features of deformed aluminium alloys under various working and heat treatment conditions. The appearance of these structures is restricted to cases under the usual existing technical conditions. In regard to the structural changes in some special working and heat treatment conditions, they can be treated as special topics of interest.

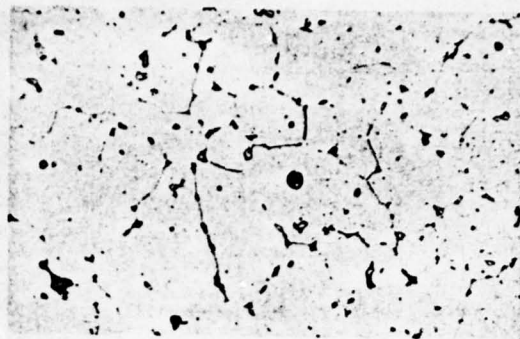


Figure 27 Over-Fired Structure of a Quenched LY12 Extruded Rod (Annealed at 515°C for One Hour, Quenched, and Etched in an Aqueous Solution of Mixed Acids; 210x)



Figure 28 Diffusion of copper into the coated Aluminium Layers of an LY12 CZ Sheet (Etched in an Aqueous Solution of Mixed Acids; 150x)



Figure 29 An LY12 Alloy Sheet Annealed at 500°C for 45 Minutes and Quenched in a Furnace at 150°C (Etched in an Aqueous Solution of Mixed Acids; 210x)

Pure aluminium has the following properties : low specific gravity, good electrical conductivity, high thermal conductivity, high latent heat of fusion , high optical reflectivity, small neutron absorption cross-section, and lustrous appearance. When it is exposed to air, a thick and firm film of oxide is formed on its surface which prevents further entrance of oxygen, thus rendering it corrosion resistant.

Section 1 Impurity Contents and Phases Formation

Labels and impurity limits of currently available pure aluminium are listed in Table I-1 :

Table I-1 Labels and Impurity Limits of Pure Aluminium

Label	Impurity Content, not greater than (%)								Al Content not more than (%)
	Cu	Mg	Mn	Fe	Si	Fe+Si	其它	总和	
L03	0.005			0.003	0.0025			0.01	99.99
L02	0.005			0.015	0.015			0.03	99.97
L01	0.01			0.04	0.04			0.07	99.93
L1	0.01			0.16	0.16	0.26		0.30	99.70
L2	0.01			0.25	0.20	0.36		0.40	99.60
L3	0.015			0.30	0.30	0.45		0.50	99.50
L4	0.05			0.30	0.35	0.60	0.10	0.70	99.30
L5	0.02			0.50	0.50	0.90		1.00	99.00
L6	0.10	0.10	0.10	0.50	0.55	1.00	0.10	1.20	98.80
L7	0.05			1.10	1.00	1.80		2.00	98.00

Iron and silicon are the chief impurities in industrial-pure aluminium. Other impurities include copper, zinc, mag-

Table I-2 Effects of Impurities on $\sigma_{0.2}$, σ_b , and δ of Pure Aluminium

IMPURITY CONTENT (%)	WORK - HARDENED			300°C ANNEALED			500°C ANNEALED		
	$\sigma_{0.2}$ (Kg/mm ²)	σ_b (Kg/mm ²)	δ (%)	$\sigma_{0.2}$ (Kg/mm ²)	σ_b (Kg/mm ²)	δ (%)	$\sigma_{0.2}$ (Kg/mm ²)	σ_b (Kg/mm ²)	δ (%)
ULTRA-PURE AL:	11.0	13.3	3.5	3.8	6.9	29	1.3	4.6	28
WITH Fe 0.014	11.1	13.6	3.2	7.6	9.2	19	1.4	5.0	34
0.10	12.2	14.5	3.5	9.5	10.4	15	2.1	6.4	34
0.31	13.6	15.8	3.5	10.6	11.8	12	2.5	7.2	36
0.66	15.0	17.5	4.6	11.5	12.7	10	3.2	8.5	40
WITH Si 0.051	12.0	14.2	3.1	3.1	7.3	33	1.7	5.2	25
0.11	12.6	14.4	3.4	3.0	6.4	32	1.8	5.4	20
0.19	13.3	15.1	4.1	3.1	7.7	37	1.9	6.0	18
0.50	14.8	17.0	4.5	3.3	8.1	37	2.0	7.3	20
0.89	16.2	19.0	4.6	3.5	8.7	34	3.2	9.7	28
WITH Cu 0.050	11.5	14.3	4.3	3.0	6.3	27	1.5	4.6	21
0.060	12.5	14.0	3.4	3.0	6.7	31	1.6	4.7	19
0.20	13.0	15.5	2.9	3.3	7.8	31	1.7	5.3	25
0.43	15.0	17.6	2.6	3.4	8.1	31	1.9	5.9	24
0.66	17.0	18.6	2.7	3.6	8.6	32	1.9	6.8	22
WITH Zn 0.053	11.5	13.6	4.6	2.5	6.4	32	1.4	4.3	27
0.10	11.7	13.6	2.9	2.4	6.1	33	1.4	4.4	31
0.20	11.1	13.0	3.4	2.5	6.2	37	1.3	4.4	30
0.47	11.6	13.7	2.6	2.5	6.0	35	1.4	4.3	24
0.69	11.4	13.3	2.9	2.6	6.3	34	1.4	4.5	24
WITH Mg 0.057	12.3	14.1	2.6	2.8	6.7	28	1.4	4.5	25
0.11	13.3	14.6	3.2	3.2	7.6	30	1.5	4.7	26
0.20	14.5	15.5	2.9	4.1	8.0	26	1.8	5.1	24
0.47	16.2	17.4	3.0	4.4	9.5	24	2.4	6.3	22
0.87	16.4	19.6	3.1	5.7	11.8	21	3.3	8.2	20
WITH Mn 0.047	12.1	14.0	4.2	5.9	8.4	18	1.5	4.4	27
0.10	12.8	14.0	3.8	7.8	9.8	14	1.6	4.9	28
0.20	13.0	14.3	3.2	10.4	10.9	9	1.9	5.9	29
0.465	13.0	15.8	4.5	12.9	14.1	7.3	2.8	7.0	26
0.75	14.5	16.8	3.5	13.7	15.4	6.3	3.5	8.0	25

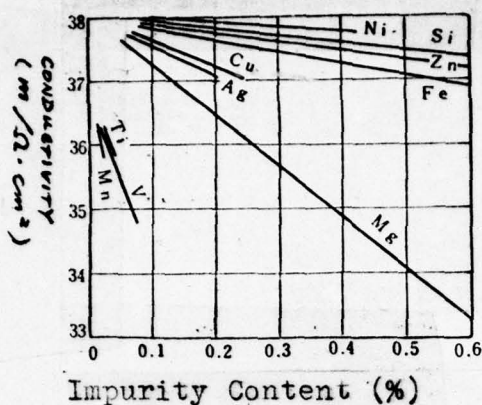


Figure I-1 Effects of Impurities on the Electrical Conductivity of Highly Pure Aluminium (320°C, 3 hr., Annealed)

Impurities have a definite effect on the electrical conductivity of pure Al. When the contents of impurities increase, its electrical conductivity decreases. From Figure I-1, it can be seen that manganese, titanium, and vanadium lower the electrical conductivity markedly, followed by silver and magnesium. Copper, silicon, nickel and iron have rather little influence.

The existence of impurities disrupts the continuity of the oxide film formed on the surface of aluminium, thereby decreasing its corrosion resistance. Accordingly, the higher the contents of impurities in Al, the lower its corrosion resistance. For example, copper and iron can decrease the corrosion resistance of aluminium markedly. However, when the ratio of impurities $\text{Fe/Si} \geq 2$, the ability of Al against corrosion in agitated media at high temperature can be improved. The solid solubility of Si in Al decreases with temperature, so the precipitation of Si from the $\alpha(\text{Al})$ solid solution at low temperature can accelerate the corrosion of Al.

Some figures of the physical and technical properties of pure aluminium are listed in Table I-3 :

Table I-3 Physical and Technical properties of Pure Al

Physical and Technical Properties	High-Purity Al (99.996% Al)	Industrial-Pure Al (99.0% Al)
Specific Gravity (20°C)	2.6989 gm/c.c.	2.71 gm/c.c.
Resistivity 20°C	2.6548 micro-ohm-cm	2.900 micro-ohm-cm
Young's Modulus	6999.2 kg/mm	7087.1 kg/mm
Neutron Absorption Cross-section	0.22 barns	
Melting Point	660.2°C	
Liquid Phase Point		657°C
Solid Phase Point		643°C
Crystalline Structure	Face Center Cubic $a = 4.0497 \text{ \AA}$	Face Center Cubic $a = 4.0400 \text{ \AA}$
Casting Temperature		675~730°C
Crystallization Contraction		6.6 %
Hot Deformation Temperature Range		210~520°C

From the Al-Fe equilibrium diagram (Figure I-2), it is apparent that at the eutectic temperature the maximum solubility of Fe in Al is 0.52%. When the Fe content exceeds 0.52%, the structures formed are proeutectic $\alpha(\text{Al})$ and the eutectic $\alpha(\text{Al}) + \text{FeAl}_3$ mixture. When the iron content exceeds 1.9% (as in Al-Fe intermediate alloy), the structures formed are proeutectic FeAl_3 and the eutectic $\alpha(\text{Al}) + \text{FeAl}_3$ (Figure I-6).

According to the Al-Si equilibrium diagram (Figure I-3), at the eutectic temperature, the maximum solubility of Si in

Al is 1.65%, but at room temperature, it drops below 0.05%. When the Si content exceeds 12.6% (as in Al-Si intermediate alloy), the structures formed are proeutectic Si and the eutectic $\alpha(\text{Al}) + \text{Si}$ mixture (Figure I-7).

It is apparent from Figure I-4 that in the liquid phase zone near the Al-rich portion of the Al-Fe-Si equilibrium diagram, there also exist, besides the Si and FeAl phases, the $\alpha(\text{Fe}_3\text{SiAl}_{12})$ and $\beta(\text{Fe}_2\text{Si}_2\text{Al}_9)$ phases. $\alpha(\text{Fe}_3\text{SiAl}_{12})$ can be found in an alloy containing 2.3% Si and 5.5% Fe. There is also some residual FeAl_3 surrounded by $\alpha(\text{Fe}_3\text{SiAl}_{12})$ due to incomplete peritectic reaction (Figure I-8). Proeutectic $\beta(\text{Fe}_2\text{Si}_2\text{Al}_9)$ and the eutectic $\alpha(\text{Al}) + \beta(\text{Fe}_2\text{Si}_2\text{Al}_9) + \text{Si}$ mixture can be found in an alloy containing 8.1% Si and 2.2% Fe (Figure I-9). For an alloy containing 0.26% Fe and 2.5% Si, the $\alpha(\text{Al})$, $\alpha(\text{Fe}_3\text{SiAl}_{12})$, $\beta(\text{Fe}_2\text{Si}_2\text{Al}_9)$ and Si phases exist simultaneously (Figures I-10 to I-13).

After the re-melting and subsequent slow-cooling of ingots of industrial-pure Al made by semi-continuous casting, the $\alpha(\text{Al})$, $\alpha(\text{Fe}_3\text{SiAl}_{12})$ and FeAl_3 phases can be found in the structures of the L6 and L4 alloys, while free Si and $\beta(\text{Fe}_2\text{Si}_2\text{Al}_9)$ phases can be found only in industrial Al with higher impurity contents. (Figures I-14 to I-17)

The features of the phases are described as follows :

FeAl_3 : Proeutectic FeAl_3 appear in the form of needles or slender strips. Before etching, they are greyish in color. ^(Figure I-6) After etching in a solution of 20 ml $\text{H}_2\text{SO}_4 + 80 \text{ ml } \text{H}_2\text{O}$ at 70°C for 5-10 seconds, some of the FeAl_3 dissolve into the solution, and the remaining FeAl_3 appear dark brown in color. When observed under polarized light, FeAl_3 shows

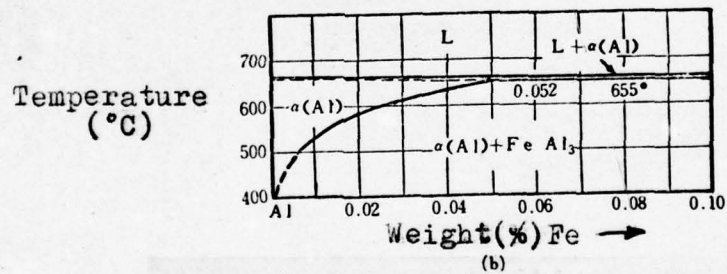
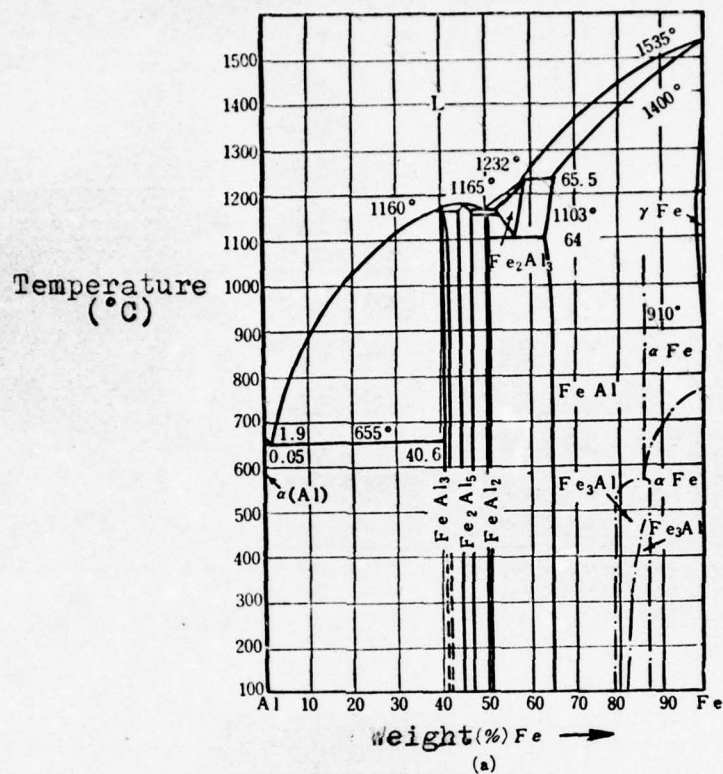


Figure I-2 Al-Fe Equilibrium Diagram

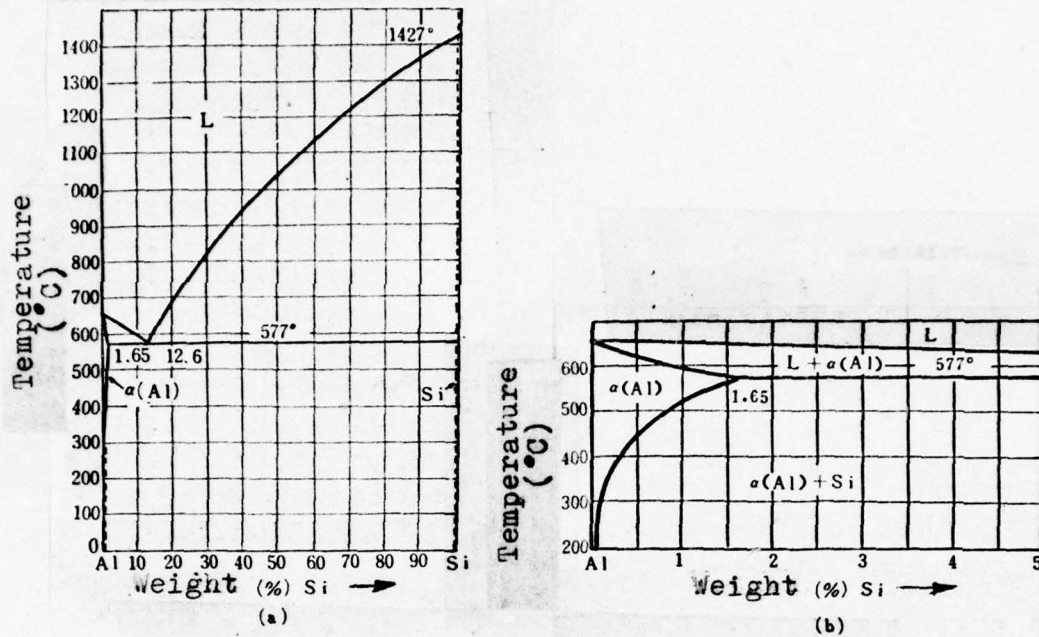


Figure I-3 Al-Si Equilibrium Diagram

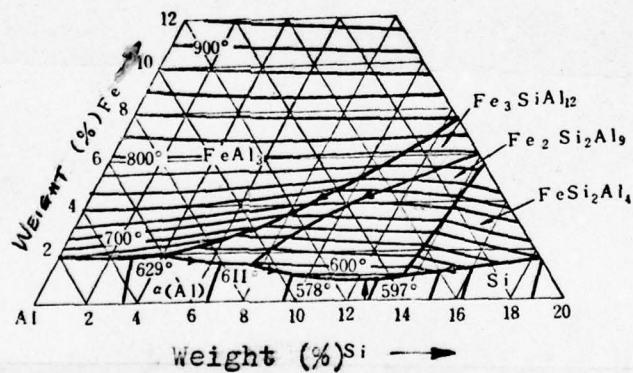


Figure I-4 Liquid Phase Section of Al-Fe-Si Equilibrium Diagram

a dark-colored rim. Its microhardness is 960 kg/mm².

$\alpha(\text{Fe}_3\text{SiAl}_{12})$: This phase contains 31.9% Fe and 5.6% Si. Proeutectic $\alpha(\text{Fe}_3\text{SiAl}_{12})$ has an irregular laminar shape, whereas $\alpha(\text{Fe}_3\text{SiAl}_{12})$ in the eutectic mixture is bone-shaped. Before etching, it is bright grey in color. After etching with a solution of 20 ml H_2SO_4 + 80 ml H_2O , the color turns dark. There are black rims at the junction where it meets with $\alpha(\text{Al})$ (Figure I-11). Its microhardness is 330 ~ 360 kg/mm².

$\beta(\text{Fe}_2\text{Si}_2\text{Al}_9)$: This phase contains 29.1% Fe and 14.6% Si, and has the shape of a pine-needle or a slender strip. (Figure I-7) Before etching, it is greyish in color. After etching with a solution of 0.5 ml HF + 99.5 ml H_2O , the color turns to dark brown. When observed under polarized light, it shows a bright-colored rim. Its microhardness is 578 kg/mm².

Si : Proeutectic Si appear to be polygons with smooth edges, whereas Si in the eutectic mixture assume the form of strips. (Figure I-7) Si is not easily etched. Before etching, it has a sparkling grey color. After etching, the sparkling is reduced. When observed under polarized light, it shows a pink reflection. Its microhardness is 1380 kg/mm².

Except for Si, the above phases can be made visible by various other etching reagents. See Table 4 in the Appendixes for details.

Section 2 Properties under Heat Treatments

Industrial-pure Al cannot be hardened by means of heat treatments. Its strength can only be improved by cold work-

ing methods. The structures and properties of pure Al sheets made by continuous casting and spinning and subsequent cold-hardening will exhibit changes during the heating cycle of the annealing process. From Figure I-5, it can be seen that the strength and elongation rate do not change appreciably when annealing is taken place below 200°C. The material still maintains its deformed fibre structure. At 200°C, the strength decreases markedly, while the elongation rate increases. There appear a small number of recrystallized grains in the deformed fibre structure, thus proving that recrystallization has already been taken place in the material. At 300°C, the strength and elongation rate exhibit drastic changes. A large number of recrystallized grains of various sizes appear in the deformed fibre structure of the material, although recrystallization is still not yet complete. At 400°C, the strength continues to decrease, while the elongation rate increases markedly. At this time recrystallization is complete. The deformed fibre structure has changed entirely into one that contains uniform crystal nuclei. When the annealing temperature reaches 550°C, the strength remains the same, whereas the elongation rate decreases. At this time, the crystal grains of the material become very coarse and non-uniform. During the annealing of pure Al, the change in strength occurs 100°C earlier than the change in elongation rate. This fact is worth noticing when choosing the annealing technique for half-hard temper products.

The structures and properties of industrial-pure Al are determined by the impurity contents, working methods, and annealing techniques. From the recrystallization temperature figures in table I-4, it is apparent that the recrystallization temperature increases with the impurity content. The impurities iron and silicon have a definite effect on the

crystal grain sizes. When the content of Fe is greater than that of Si, the grains obtained are smaller in size than those when the content of Si is greater than that of Fe. The higher the temperature used in hot rolling the smaller will the grain size be for the Al sheet after annealing.

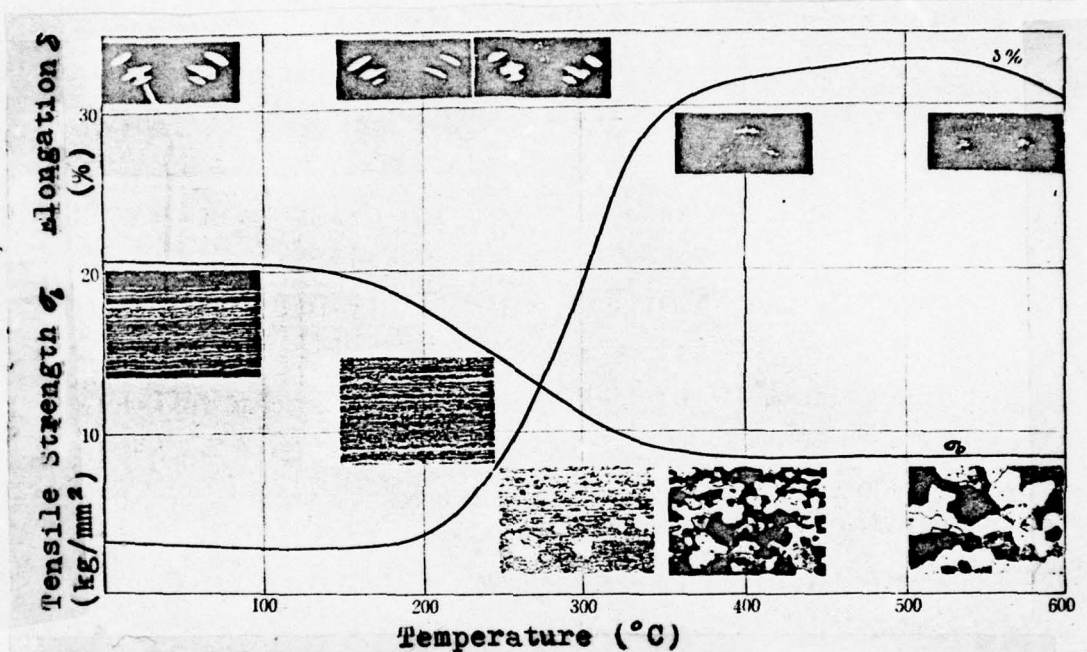


Figure 1-5 Effects of Annealing Temperature on the Structures and Properties of a 1.0 mm thick L2 Industrial-Pure Aluminium Sheet Made by Continuous Casting and Spinning and Subsequent Rolling

Table I-4 Recrystallization Parameters for Various Industrial-Pure Aluminium Products

Label	Product	Speci- ficate- ion (mm)	Technical Conditions						RECRYSTALLIZA- TION TEMPERATURES (°C)		Remarks
			Rolling		Extru- sion		Annealing Condition		ini- tial	final	
			TEMP. (°C)	DEFORM- ATION (%)	TEMP. (°C)	DEFORM- ATION (%)	SALT BATH OR AIR FURNACE	TIME (min.)			
L2	HOT- ROLLED SHEET	10.5	300~350	96			AIR FURNACE	120		400~405	HOT-ROLLED STRUCTURE HAS BEGUN RECRY- STALLIZATION, BUT INCOMPLETE
L4		8.0	300~350	97			SALT BATH	10		400~415	
L2	COLD- ROLLED SHEET	0.5	ROOM TEMP.	92			AIR FURNACE	480	190~200	260~270	
L4		1.0	ROOM TEMP.	87.5			SALT BATH FURNACE	10 20	230~235 200~205	305~310 285~290	
L2	Rod	φ 10.5			350	98					EXTRUDED STRUCTURE HAS UNDERGONE COMPLETE RECRYSTALLIZATION
L4	ROD	φ 10			350	92					
L4	THIN- EXTRUDED TUBE	50 × 41			350	96					
L4	RIBBON	60 × 6			350	96	SALT BATH	10		455~460	EXTRUDED STRUCTURE HAS BEGUN RECRYSTALLIZATION
L4	COLD- SPUN TUBE	18 × 16			ROOM TEMP. (COLD SPINNING)	59		10	280~285	355~360	

Section 3 Structures of Cast and Wrought Products

1. Formation of Phases

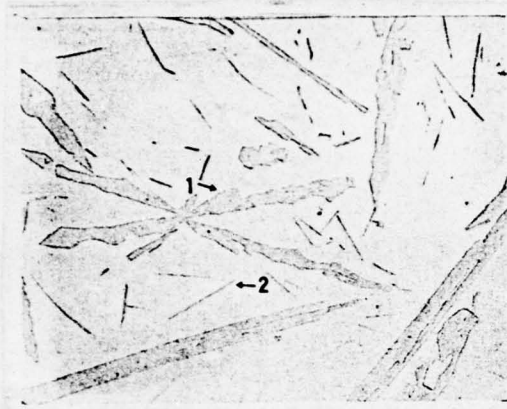


Figure I-6

210x

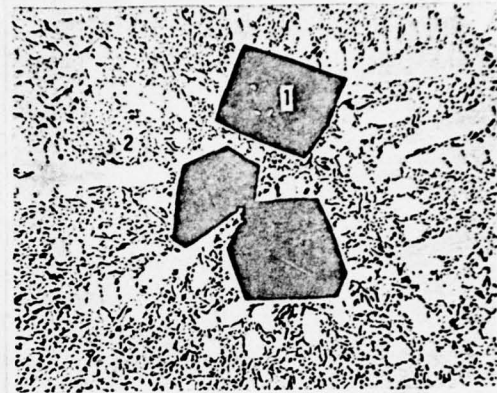


Figure I-7

210x

Alloy	Al-10.38%Fe
Condition	Remelted at 800°C, cooled slowly to 580°C, annealed for 3 hours, and quenched in water
Etching	Not etched
Structural features	1 -- Primary FeAl_3 2 -- FeAl_3 in the $\alpha(\text{Al}) + \text{FeAl}_3$ eutectic mixture.

Alloy	Al-17.25%Si
Condition	Remelted at 710°C, cooled rapidly to room temperature
Etching	Not etched
Structural features	1 -- Primary Si 2 -- $\alpha(\text{Al}) + \text{Si}$ eutectic mixture.

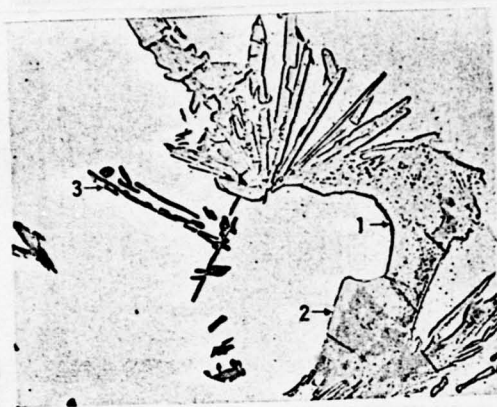


Figure I-8

210x



Figure I-9

210x

Alloy	Al-5.5%Fe-2.3%Si
Condition	As cast (Slow-cooled)
Etching	Not etched
Structural features	1 -- $\alpha(\text{Fe}_3\text{SiAl}_{12})$ 2 -- FeAl_3 3 -- Si in the $\alpha(\text{Al}) + \text{Si}$ eutectic mixture.

Alloy	Al-2.2%Fe-8.18%Si
Condition	As cast (Slow-cooled)
Etching	Not etched
Structural features	1 -- Proeutectic $\beta(\text{Fe}_2\text{Si}_2\text{Al}_9)$ grey strips 2 -- Si in the $\alpha(\text{Al}) + \text{Si}$ eutectic mixture.

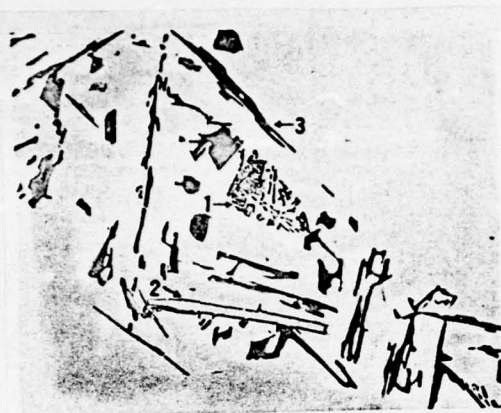


Figure I-10

210x

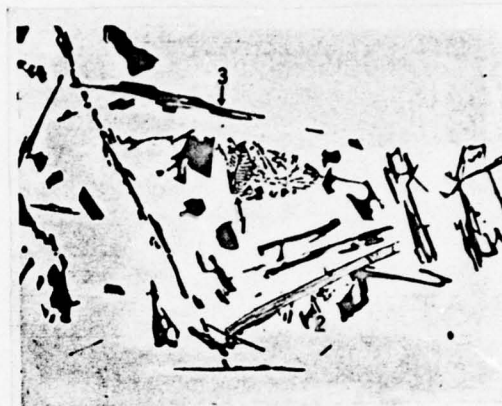


Figure I-11

210x

Alloy	Al-0.26%Fe-2.5%Si
Condition	As cast (Slow-cooled)
Etching	Not etched
Structural features	1 -- $\alpha(\text{Fe}_3\text{SiAl}_{12})$ bright grey, bone-shaped 2 -- $\beta(\text{Fe}_2\text{Si}_2\text{Al}_9)$ bright grey, needlelike or strip-shaped 3 -- Si, deep grey, strip-shaped.

Alloy	Same as Figure I-10
Condition	As cast (Slow-cooled)
Etching	20ml H_2SO_4 + 80ml H_2O
Structural features	1 -- $\alpha(\text{Fe}_3\text{SiAl}_{12})$ dark grey 2. -- $\beta(\text{Fe}_2\text{Si}_2\text{Al}_9)$ light grey 3 -- Si, not affected by etching, re- mains deep grey.

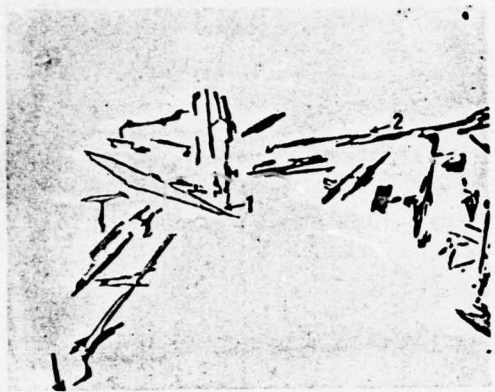


Figure I-12

210x



Figure I-13

210x

Alloy	Same as Figure I-10
Condition	As cast(Slow-cooled)
Etching	Not etched
Structural features	1 -- $\beta(\text{Fe}_2\text{Si}_2\text{Al}_9)$ bright grey, needlelike
	2 -- Si in the $\alpha(\text{Al}) + \text{Si}$ eutectic mixture.

Alloy	Same as Figure I-10
Condition	As cast(Slow-cooled)
Etching	0.5ml HF + 99.5ml H_2O
Structural features	1 -- $\beta(\text{Fe}_2\text{Si}_2\text{Al}_9)$ brown
	2 -- Si in the $\alpha(\text{Al}) + \text{Si}$ eutectic mixture is not affected by etching.

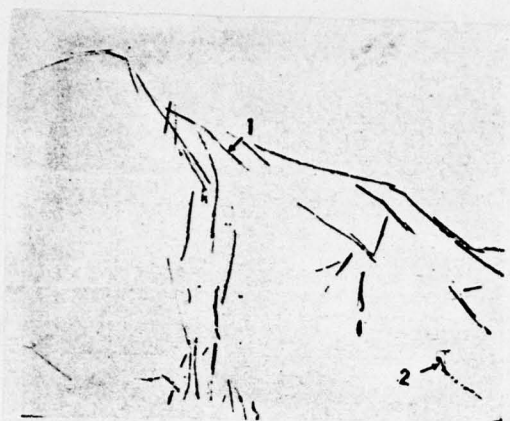


Figure I-14

210x

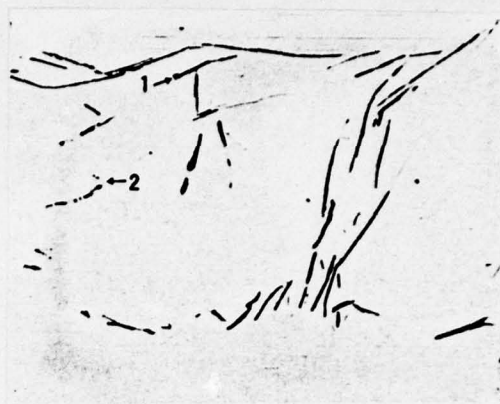


Figure I-15

210x

Alloy I4
Condition As cast (Ingot made by semi-continuous process was remelted at 750°C, slow-cooled to 600°C, annealed for 3 hours, cooled in furnace to 400°C, and quenched in water.)

Etching Not etched

Structural features 1 -- FeAl_3
light grey,
strip-shaped
2 -- $\alpha(\text{Fe}_3\text{SiAl}_{12})$
bright grey,
bone-shaped.

Alloy I4
Condition Same as Figure I-14
Etching 20ml H_2SO_4 +
80ml H_2O
Structural features 1 -- FeAl_3
black
2 -- $\alpha(\text{Fe}_3\text{SiAl}_{12})$
color
becomes
dull.



Figure I-16

210x

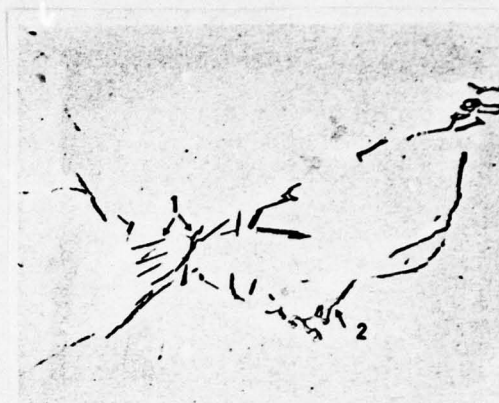


Figure I-17

210x

Alloy	L6
Condition	Semi-continuously cast
Etching	20ml H_2SO_4 + 80ml H_2O
Structural features	1 -- $\alpha(Fe_3SiAl_{12})$ color becomes dull
	2 -- $FeAl_3$ black.

Alloy	L6
Condition	As cast(Ingot made by semi-continuous process was remelted at $750^\circ C$, cooled in furnace to $400^\circ C$ and quenched in water.)
Etching	20ml H_2SO_4 + 80ml H_2O
Structural features	1 -- $FeAl_3$, black
	2 -- $\alpha(Fe_3SiAl_{12})$ color becomes dull.

2. Structures of Ingots

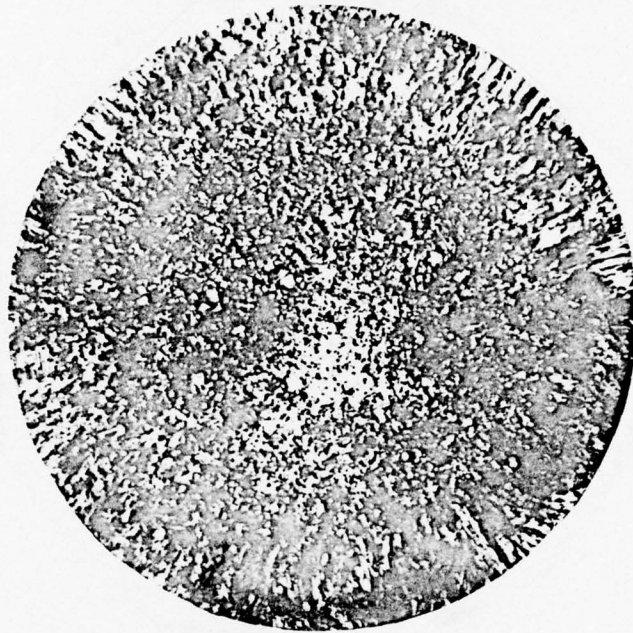


Figure I-18

Alloy and Condition	L2, made by semicontinuous casting
Specification	Ø192mm
Etching reagent	75ml HCl + 25ml HNO ₃ + 5ml HF
Structural features	Macrograph: the peripheral region, about 3mm thick, are composed of small equiaxed grains sprinkled with columnar grains; the next layer is the columnar grain region, about 20mm thick; the remaining portion is composed of relatively large equiaxed grains.

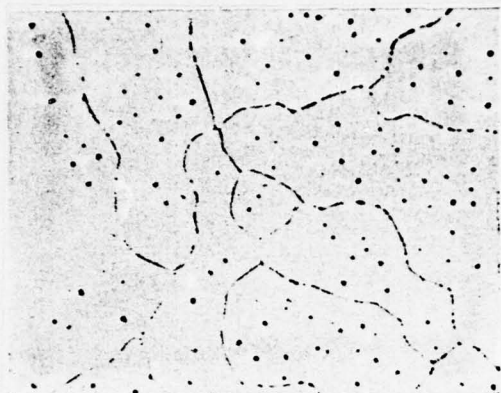


Figure I-19

210x

Alloy and condition	L2, made by semi-continuous casting
Specification	Ø192mm
Etching reagent	50% HF aqueous solution
Structural features	Structure in the transverse direction of the middle region at the base of the ingot, appears as a dendritic network; cells of the network are sparse and discontinuous.



Figure I-20

100x

Specimen has been electro-polished and Anodized

Alloy and Condition	Same as Figure I-19
Specification	Same as Figure I-19
Structural features	Structure of Figure I-19 under polarised light; size and shape of the grains are visible.

3. Structures of Sheets and Foils

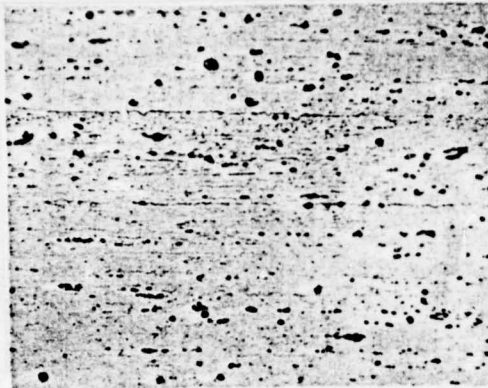


Figure I-21
Etched in 50% HF Aqueous
Solution

210x

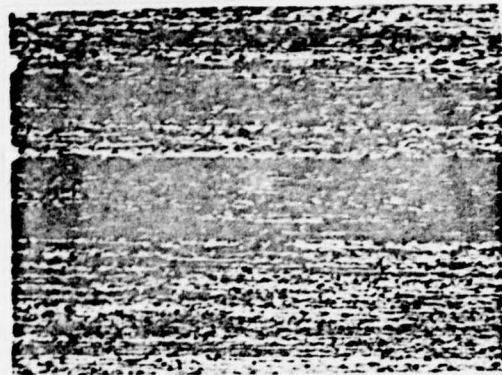


Figure I-22
Structures of an Electro-
polished and Anodized
Specimen under Polarized
Light (Color)

100x

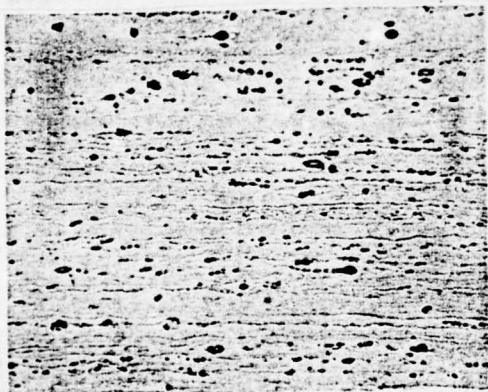


Figure I-23
Etched in 50% HF Aqueous
Solution

210x

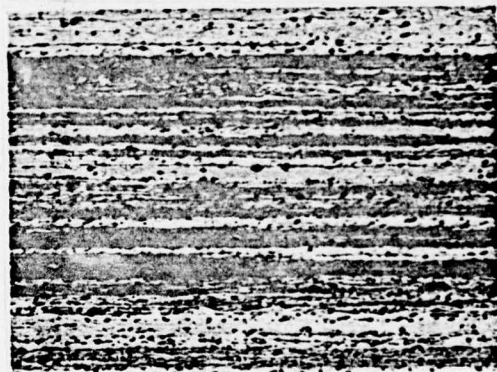


Figure I-24
Structures of an Electro-
polished and Anodized
Specimen under Polarized
Light (Color)

100x

Alloy and Condition	L2R (Hot-rolled at 360°C)
Specification	10mm thick
Structural features	<p>Figures I-21 and I-22 are the longitudinal structures of the portions close to the sheet surface. Figures I-23 and I-24 are the longitudinal structures of the central region of the sheet. Compounds have been broken and re-arranged in arrays along the principal deformation direction in which rolling is applied. The structures have not undergone recrystallization; they are of the deformed fibre structures.</p>



Figure I-25
Etched in 50% HF Aqueous
Solution

210x



Figure I-26
Structure of an Electro-
polished and Anodized Specimen
under Polarized Light (Color)

100x

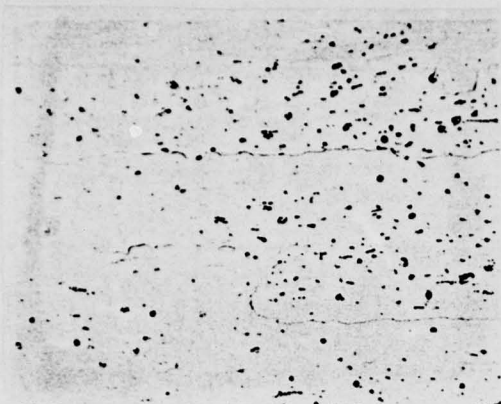
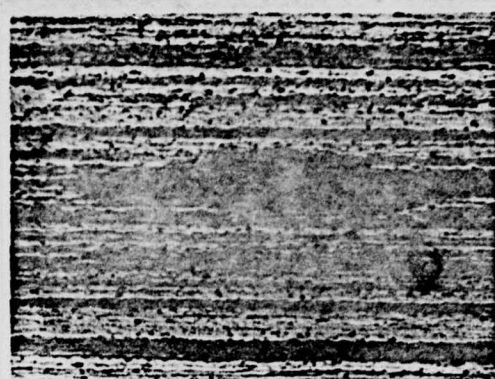


Figure I-27
Etched in 50% HF Aqueous
Solution



210x Figure I-28 100x
Structure of an Electro-
polished and Anodized Specimen
under Polarized Light (Color)

Alloy and Condition
Specification

L2R (Hot-rolled at 520°C)
10mm thick

Structural features

Figures I-25 and I-26 are longitudinal structures of portions close to the sheet surface. Figures I-27 and I-28 are longitudinal structures of the central region of the sheet. Compounds have been broken. When compared with Figures I-21 and I-24, the sheet is known to be undergone recrystallization after hot rolling at 520°C. The portion close to the surface has undergone complete recrystallization, and the grains approach equiaxed shapes. The central region has undergone lesser extent of recrystallization, and retains the deformed fibre structure.

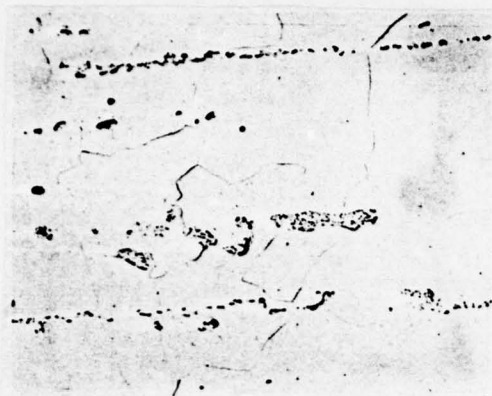


Figure I-29
Etched in 50% HF Aqueous
Solution

210x



Figure I-30
Structure of an Electro-
polished and Anodized Specimen
under Polarized Light (Color)

100x



Figure I-31
Etched in 50% HF Aqueous
Solution

210x

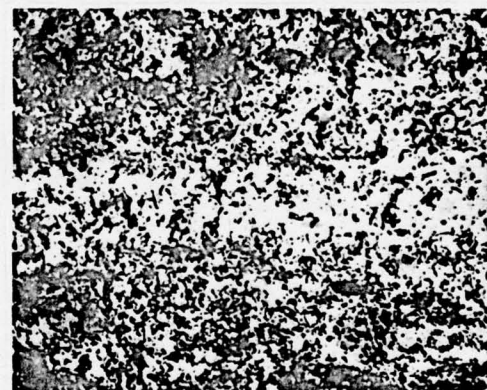


Figure I-32
Structure of an Electro-
polished and Anodized Specimen
under Polarized Light (Color)

100x

Alloy and Condition
Specification

L2R
10mm thick

Structural features

Figures I-29 and I-30 are the structures
of the outermost surface where the

the sheet comes into contact with the roller when the sheet is hot-rolled at 520°C. This area has undergone complete recrystallization. Since the central does not suffer much deformation due to elongation, the compounds are not uniformly distributed after they have been broken, and the residual cast structure is clearly visible.

Figures I-31 and I-32 are the structures of the outermost surface where the sheet comes into contact with the roller when the sheet is hot-rolled at 360°C. This area has not undergone complete recrystallization. There are only small traces of recrystallized grains in the deformed structure of the matrix. The compounds are not broken to as good an extent as in the case of 520°C hot rolling.



Figure I-33

210x



Figure I-34

100x

Specimen has been electro-polished and anodized

Alloy and
condition

L2Y

Specifi-
cation

0.8mm

Etching
reagent

50% HF aqueous
solution

Structural
features

Longitudinal
structure of the
sheet: the deformed
structure is finer
and denser than
that due to hot-
rolling deformation.
Compounds that have
been broken are
arranged along the
hot-rolling direction
in arrays.

Alloy and
condition

L2Y

Specifi-
cation

0.8mm

Etching
reagent

50% HF aqueous
solution

Structural
features

Structure of
Figure I-33 under
polarized light;
appears as deformed
fibre structure.

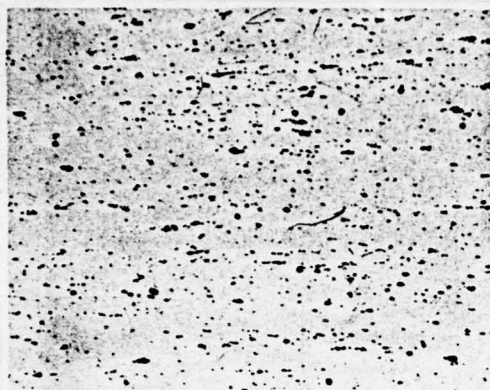


Figure I-35

210x

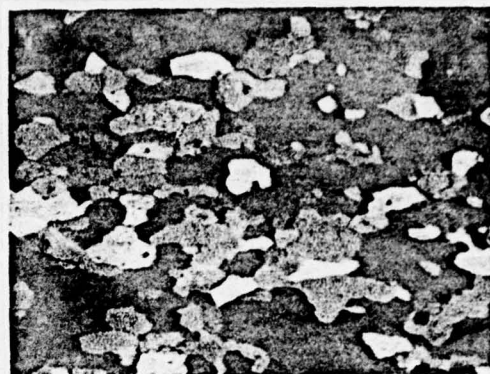


Figure I-36

100x

Specimen has been electro-polished and anodized

Alloy and condition	L2M
Specification	0.8mm
Etching reagent	50% HF aqueous solution
Structural features	Longitudinal structure of the sheet. Deformed fibre structure is no longer visible after annealing. Compounds are still arranged in arrays along the hot-rolling direction.

Alloy and condition	L2M
Specification	0.8mm
Etching reagent	50% HF aqueous solution
Structural features	Structure of Figure I-35 under polarized light. The material has undergone complete recrystallization. The grains are fine and uniform.

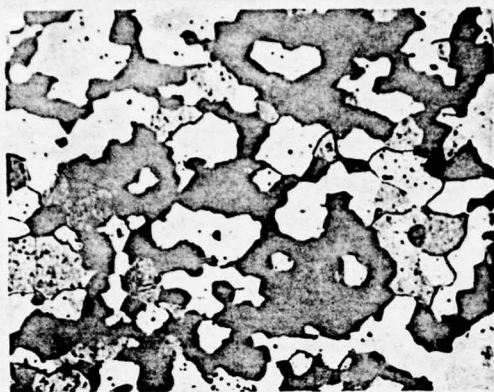


Figure I-37 100x
Specimen has been electro-
polished and anodized



Figure I-38 100x
Specimen has been electro-
polished and anodized (color)

Alloy and condition	L1M
Specifi- cation	0.12mm
Structural features	Completely recrystallized. Equiaxed grains.

Alloy and condition	L1M
Specifi- cation	0.05mm
Structural features	Completely recrystallized. Equiaxed grains.



Figure I-39

100x

Specimen has been electropolished and anodized

Alloy and condition	L1M
Specification	0.007 mm
Structural features	Completely recrystallized. Grain boundaries are smooth and straight. Grains are fine and uniform.

4. Structures of Extruded Products

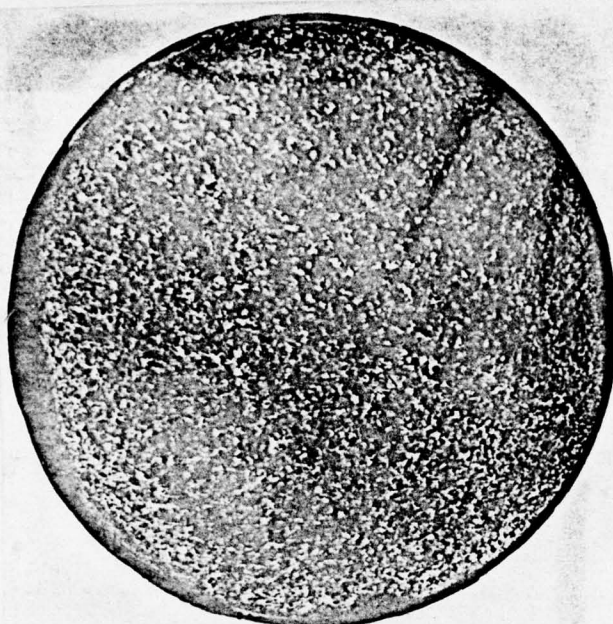


Figure I-40

0.8:1

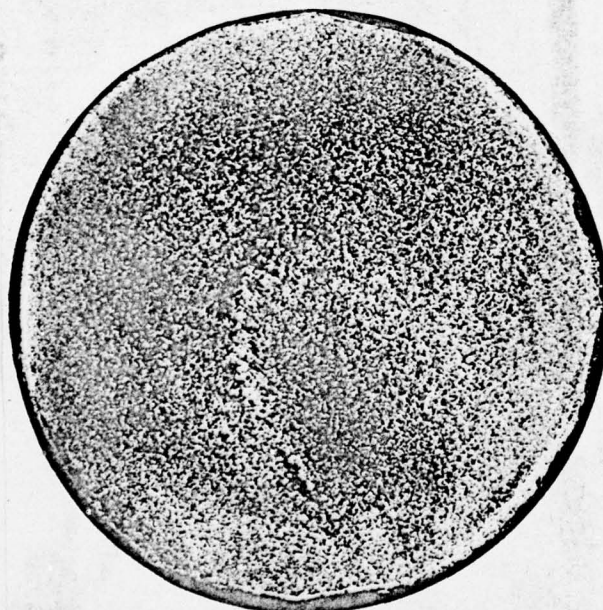


Figure I-41

0.8:1

Alloy L2R
and
condition
Specification - \varnothing 90 mm rod

Etching 75 ml HCl + 25 ml
HNO₃ + 5 ml HF

Structural Figures I-40 &
featu- I-41 are the
ures transverse macro-
structures of the
front and rear
ends respectively.
The peripheral re-
gion at the front
end is the fine-
grain region, about
10mm thick. The
middle and central
portions still re-
tain the cast grain
outlines. The rear
end has recrystal-
lized structure
with fine grains.
The half-moon shaped
crystallization zone
at the center is a
mark left by the
retraction of metal
flow at the end of
extrusion.

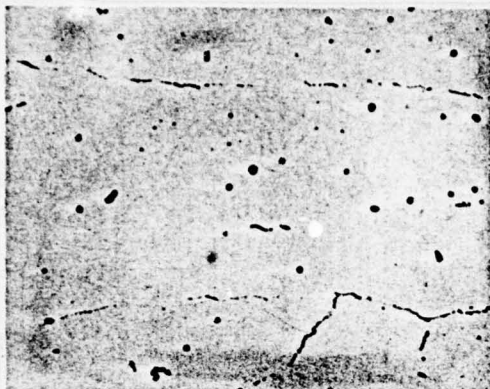


Figure I-42
Etched in 50% HF Aqueous
Solution

210x



Figure I-43
Structure of an Electro-
polished and Anodized Specimen
under Polarized Light

100x

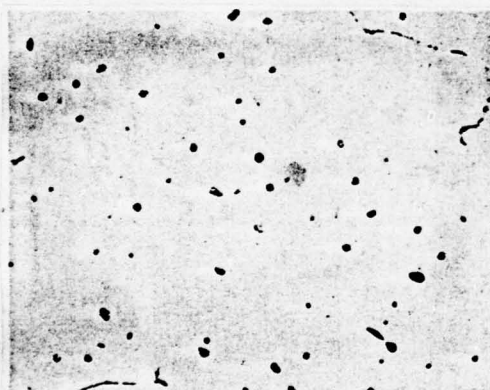


Figure I-44
Etched in 50% HF Aqueous
Solution

210x

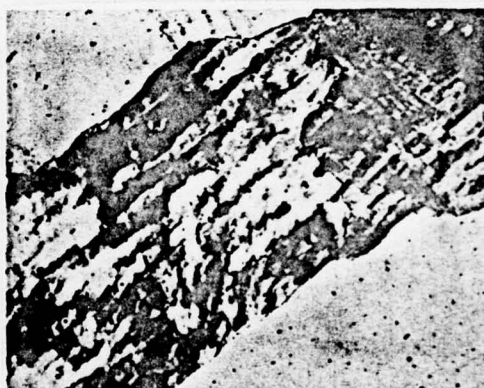


Figure I-45
Structure of an Electro-
polished and Anodized Specimen
under Polarized Light

100x

Alloy and condition

L2R

Specification

Ø90mm rod

Structural features

Figures I-42 and I-43 are the longitudinal

structures of the portion close to the surface at the front end of the rod. This portion has undergone complete recrystallization. The compounds have been broken, and are rearranged in arrays along the extrusion direction. Figures I-44 and I-45 are the longitudinal structures of the central portion at the front end of the rod. Since the extent of deformation is small, the compounds are broken to a lesser extent here than at the surface. The subgrains formed due to deformation (broken pieces of the grains) are clearly visible in the structure.

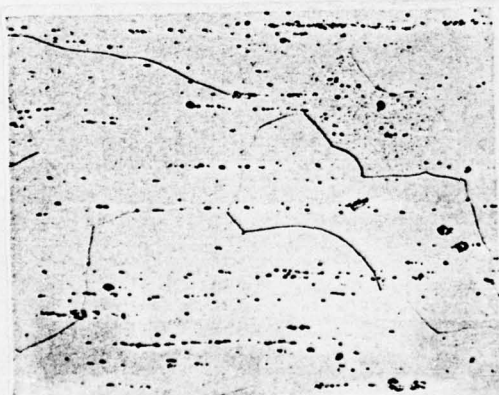


Figure I-46
Etched in 50% HF Aqueous
Solution

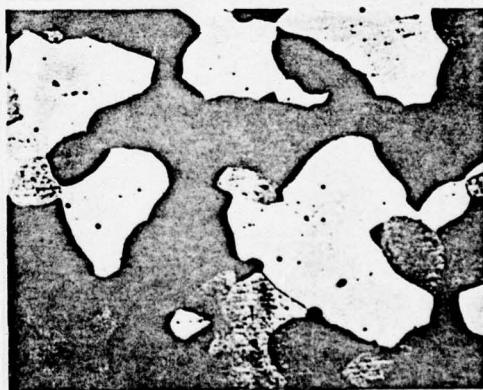


Figure I-47
Structure of an Electro-
polished and Anodized Specimen
under Polarized Light



Figure I-48
Etched in 50% HF Aqueous
Solution

210x

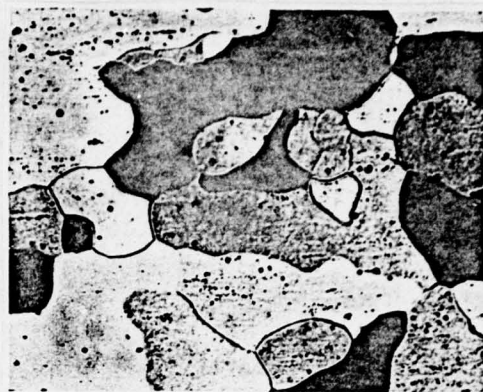


Figure I-49
Structure of an Electro-
polished and Anodized Specimen
under Polarized Light

100x

Alloy and condition
Specification
Structural features

L2R

Ø85mm rod

Figures I-46 and I-47 are the longitudinal structures of the portion close to the edge at the rear end of the rod. This portion has undergone complete recrystallization and exhibits equiaxed grains. The compounds have been broken and are rearranged in arrays along the extrusion direction.

Figures I-48 and I-49 are the longitudinal structures of the central portion at the rear end of the rod. This portion has undergone recrystallization, and exhibits equiaxed grains. The compounds have been broken and rearranged in arrays along the extrusion direction; the directionality here is weaker than at the edge portion.



Figure I-50
Etched in 50% HF Aqueous
Solution

210x



Figure I-51
Structure of an Electro-
polished and Anodized Specimen
under Polarized Light

100x

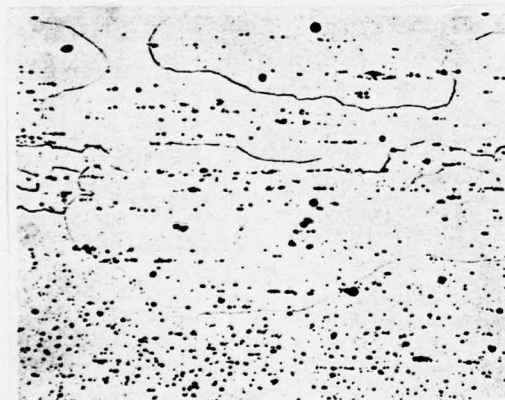


Figure I-52
Etched in 50% HF Aqueous
Solution

210x

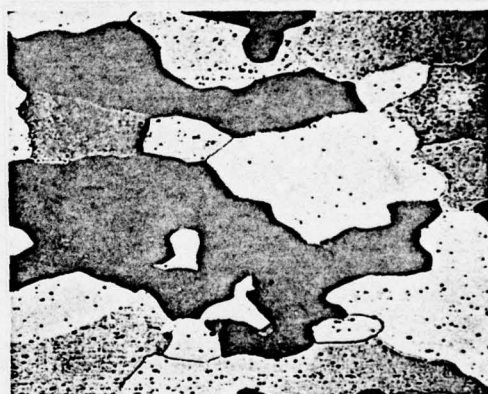


Figure I-53
Structure of an Electro-
polished and anodized Specimen
under Polarized Light

100x

Alloy and condition L2R

Specification Structural shape

Structural features Figures I-50 and I-51 are the longitudinal

structures of the thin-walled portion at the rear end of the structural shape. This portion has undergone complete recrystallization and exhibits equiaxed grains. The compounds have been broken and rearranged in arrays along the extrusion direction.

Figures I-52 and I-53 are the longitudinal structures of the thick-walled portion at the rear end of the structural shape. This portion has undergone complete recrystallization and exhibits grains somewhat coarser than those in the thin-walled portion. The compounds have been broken and rearranged along the the extrusion direction, which are more clearly visible than those in the thin-walled portion.

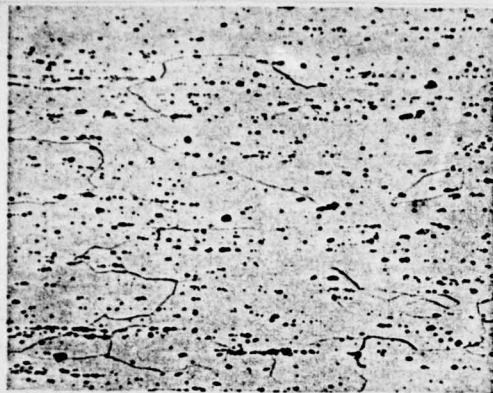


Figure I-54

210x



Figure I-55

100x

Structure of an Electro-polished and Anodized Specimen under Polarized Light

Alloy and condition	L4Y
Specification	φ80x77mm cold-drawn tube
Etching reagent	50% HF aqueous solution
Structural features	Longitudinal structure of the rear end of the tube. Grains are elongated along the drawing direction. Compounds are arranged in arrays.

Alloy and condition	L4Y
Specification	φ80x77mm cold-drawn tube
Structural features	Structure of Figure I-54 under polarized light. Grains are elongated along the drawing direction.

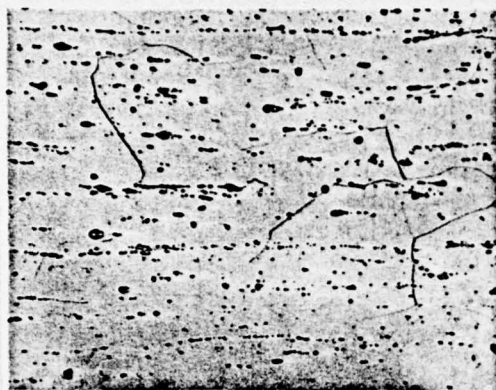


Figure I-56

210x

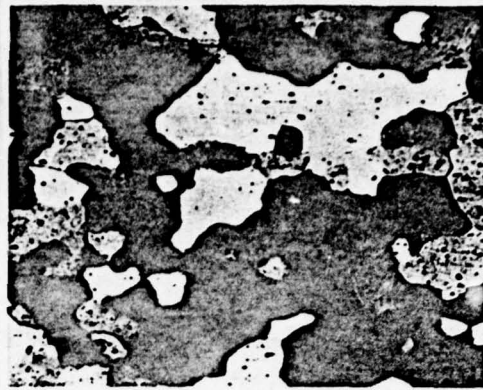


Figure I-57

100x

Structure of an Electro-polished and Anodized Specimen under Polarized Light

Alloy and condition	L4M
Specification	φ80x77mm cold-drawn tube
Etching reagent	50% HF aqueous solution
Structural features	Longitudinal structure of the rear end of the tube. After annealing, the compounds are still arranged in arrays along the drawing direction.

Alloy and condition	L4M
Specification	φ80x77mm cold-drawn tube
Structural features	Structure of Figure I-56 under polarized light. The tube has undergone complete recrystallization and exhibit equiaxed grains.

CHAPTER TWO

ALUMINIUM-MAGNESIUM ALLOYS

Aluminium-magnesium system alloys have high corrosion resistivity, good solderability, and good malleability. They can be wrought into semi-finished products such as sheets, rods, structural shapes, tubes, wires and forgings.

Section 1 Chemical Compositions and
Phase Formations

Chemical compositions of this class of alloys are listed in Table II-1. Magnesium is the principal constituent element of the alloys, in which lesser amounts of manganese, titanium, and other elements are also added. The impurities in the alloys are mainly iron, copper, and zinc.

Table II-1 Chemical Compositions of Aluminium-Magnesium System Alloys

Alloy Label	Principal Constituent(%)					Impurity, not more than (%)						
	Mg	Mn	Si	Cr	Ti	Fe	Si	Cu	Zn	Fe+Si	OTHERS	TOTAL
LF2	2.0~2.8	0.15~0.4 or Cr				0.4	0.4	0.1		0.6	0.1	0.8
LF3	3.2~3.8	0.3~0.6	0.5~0.8			0.5		0.05	0.2		0.1	0.85
LF5	4.0~5.5	0.3~0.6				0.5	0.5	0.05	0.2		0.1	
LF6	5.8~6.8	0.5~0.8		Be 0.0001~ 0.005	0.02~0.1	0.4	0.4	0.1	0.2		0.1	
LF7	6.0~7.5	0.3~0.6				0.5	0.5	0.05	0.2			
LF10	4.7~5.7	0.2~0.6				0.4	0.4	0.2		0.6	0.1	1.10
LF12	8.3~9.6	0.4~0.8	Sb ≥0.004		0.05~ 0.15	0.3	0.3	0.05	0.2			

As the content of magnesium is increased, the mechanical properties of the alloys are also correspondingly increased

(Table II-2). When the magnesium content exceeds 5%, the ability of the alloys against stress corrosion will deteriorate. When the magnesium content exceeds 7%, the malleability of the alloy will decrease, and the solderability will also deteriorate.

Table II-2 Effects of Magnesium Content on the Mechanical Properties of the Aluminium-Magnesium Alloys

Alloy Label	Condition	Sheet Thickness (mm)	Mechanical Properties		
			σ_b (kg/mm ²)	$\sigma_{0.2}$ (kg/mm ²)	δ (%)
LF2	Annealed	2.0	18.9		21.2
LF3	Annealed	2.0	22.5	12.0	21.5
LF5	Annealed	2.0	30.5	16.5	25.0
LF6	Annealed	2.0	33.5	17.0	23.0

The addition of manganese not only benefits the alloys in their corrosion resistivity, but also improve the strength of the alloys. The addition of small quantity of titanium and vanadium can help reduce the sizes of the grains. The purpose of the addition of a small amount of silicon to LF3 alloy is to improve the solderability of the alloy.

Impurities such as iron, copper, and zinc can cause the corrosion resistivity and technical properties of the alloys to deteriorate. Therefore, they should be strictly regulated.

Minute amount of sodium impurity can cause caustic brittleness to develop in alloys that contain more than 3%

of magnesium. Therefore, refining using sodium baths should be avoided whenever possible.

From the Al-Mg system alloy equilibrium diagram (Figure II-1) and the range of alloy compositions, and from the verifications through the use of metallographic analysis and electron microprobing^{quality} analysis, the following phases can be found when the alloys are subject to the slow-cooling condition during casting:

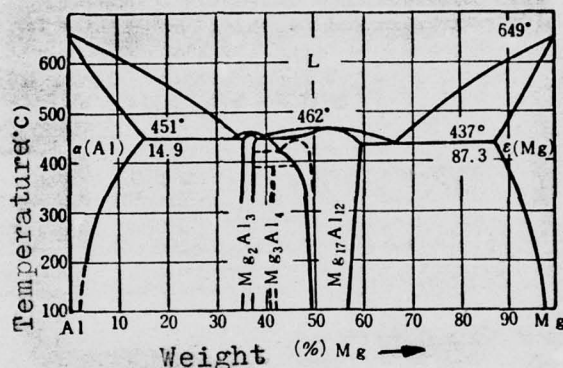


Figure II-1 Binary Al-Mg System Equilibrium Diagram

$\beta(\text{Mg}_2\text{Al}_3)$ phase : The $\beta(\text{Mg}_2\text{Al}_3)$ in the eutectic structure of $\alpha(\text{Al}) + \beta(\text{Mg}_2\text{Al}_3)$ is bone-shaped, which is light grey in color before etching. After etching in 10% H_3PO_4 aqueous solution, the boundaries are more clearly displayed, as shown in Figure II-6. The $\beta(\text{Mg}_2\text{Al}_3)$ phase has face-center cubic lattice. It is very brittle at room temperature, so the malleability of the alloy is decreased when the content of this phase in the alloy is increased.

$(\text{FeMn})\text{Al}_6$ phase : Appears as polygon pieces, as shown in

Figure II-7. Its structural features in details can be found in Chapter Three.

Mg_2Si phase : Since 0.5-0.8% Si is added to the alloy LF3, this very alloy is rich in the eutectic $\alpha(Al) + Mg_2Si$ mixture, as shown in Figure II-8. The structural features of this phase in details can be found in Chapter Five.

$FeAl_3$ phase : The iron impurity in the alloy can combine with aluminium to form the compound $FeAl_3$, which appears in the form of eutectic $\alpha(Al) + FeAl_3$ mixture, as shown in Figure II-9. Its detailed structural features can be found in Chapter One.

In the structure of a semi-continuously cast ingot, it can be seen that these phases are the principal components of the dendritic network veins, as shown in Figures II-10 through II-14.

Under the semi-continuous casting condition, the appearance of the non-equilibrium eutectic $\alpha(Al) + \beta(Mg_2Al_3)$ mixture is closely related to the magnesium content. For example, the result obtained through the analysis of phases for a round $\phi 192mm$ ingot is as follows: the $\beta(Mg_2Al_3)$ phase is not found in the LF2 and LF3 alloys; in the LF5 alloy, small amount of $\beta(Mg_2Al_3)$ phase can be found; and in the LF6 and LF12 alloys, the amount of $\beta(Mg_2Al_3)$ phase increases with the magnesium content (as shown in Figure II-2).

Section 2 Properties of Alloys under Heat Treatment

Under different temperatures, although the variation of

the solid solubility of magnesium is large, it does not produce pronounced age-hardening effect on the alloys in reality. This is because there is no lattice coherency between the new phase β' that is formed after quenching and aging and the matrix, so that hardening due to lattice coherency is not obtained in this case. Accordingly, the strength of this class of alloys is not improved by means of quenching and aging. The semi-finished products of this class of alloys are usually in the annealed condition or in the cold-working hardened condition.

During annealing, the aluminium-magnesium alloys undergo changes in structures and properties. These changes are more pronounced as the temperature rises gradually. After the temperature has reached a certain value, the structures and properties of the alloys will remain stable even though the annealing temperature continues to increase. For example, as is shown in Figure II-3, when the cold-^{rolled} LF6 alloy sheet is annealed at 240°C (fired at constant temperature for 1 hour, and air-cooled), the sheet begins to recrystallize. At this time, small amount of recrystallized grains appear in the deformed fibre structure, and clear spots due to scattering also begin to show in its corresponding x-ray picture. The strength of the alloy begins to decrease, while the elongation rate increases. When the annealing temperature reaches 280°C, its microstructure has changed from the deformed fibre structure completely into one that contain^{equiaxial} recrystallized grains. Clear spots due to scattering completely appear on the x-ray picture. When the temperature reaches 320°C, there are no significant changes in structures and properties.

It is seen from our studies that the recrystallization temperature of the alloy is closely related to the magnesium

AD-A049 264

FOREIGN TECHNOLOGY DIV WRIGHT-PATTERSON AFB OHIO
DEFORMED ALUMINUM ALLOY METALLOGRAPHY. (U)
AUG 77

F/G 11/6

UNCLASSIFIED

FTD-ID(RS)T-0577-77

NL

4 OF 5
AD
A049 264





Figure VI-38

210x

Corroded in Mixed Acid
Liquid Solution

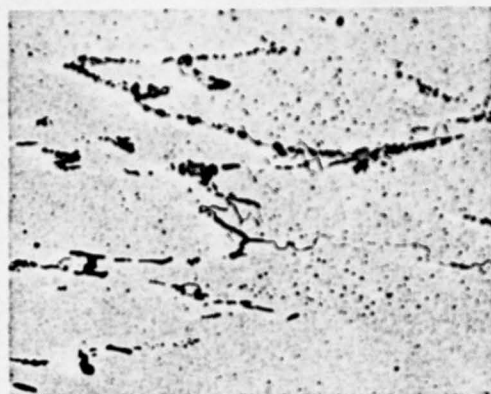


Figure VI-39

210x

Corroded in Mixed Acid
Liquid Solution

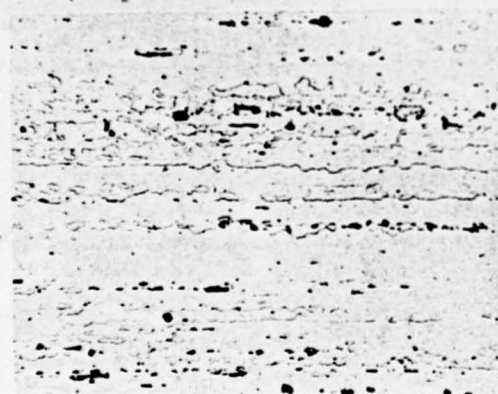


Figure VI-40

210x

Corroded in Mixed Acid
Liquid Solution

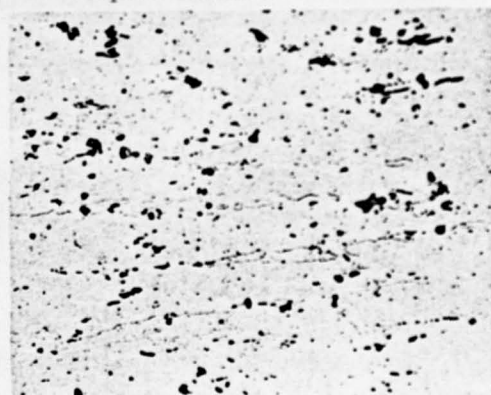


Figure VI-41

210x

Corroded in Mixed Acid
Liquid Solution

Alloy and Condition LC4CS

Specification ϕ 60 mm. multiple-holed extruded bar

Features of Structure Figure VI-38 and Figure VI-39 respectively show the longitudinal structure of the central part and the edge part at the (continued)

front end of the bar. Recrystallization is not complete, and the grains stretch along the direction of extrusion. There are remanant phases $S(CuMgAl_2)$ and $T(AlZnMgCu)$, which are not in solid solution, and phase $AlMnFeSi$, which is hard to dissolve.

Figure VI-40 and Figure VI-41 respectively show the longitudinal structure of the central part and the edge part at the rear end of the bar. The crystal grains at the edge part are small and the degree of recrystallization at the central part is low.

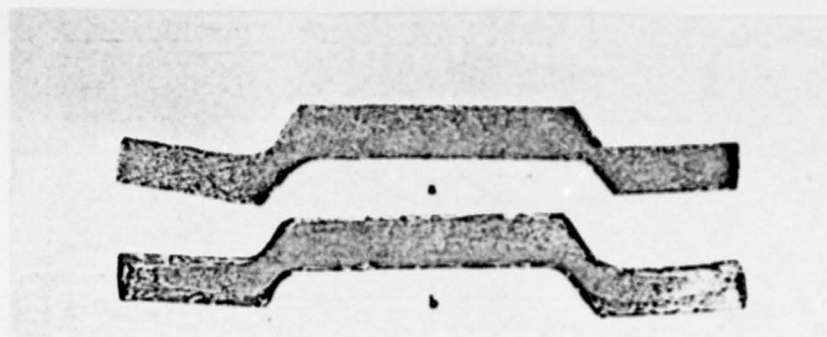


Figure VI-42

Alloy and Condition	LC4CS
Specification	XC3124 mold
Corrosion	25%NaOH liquid solution
Features of Structure	<p>In this Figure, a shows the transverse macroscopical structure at the front end. The size of the crystal grains are homogeneous.</p> <p>b shows the transverse macroscopical structure at the rear end. At the edge, there are coarse crystal links and the grains at the central part are small and fine.</p>

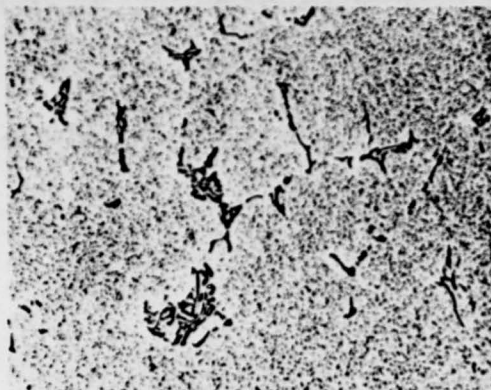


Figure VI-43 210x

Corroded in Mixed Acid
Liquid Solution

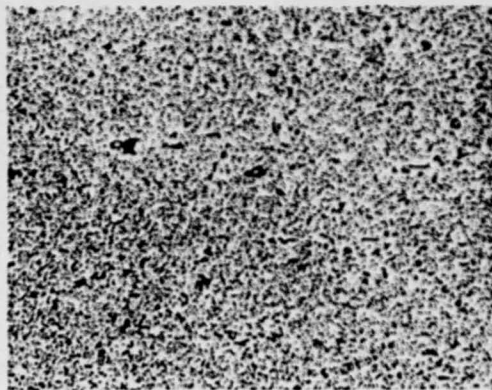


Figure VI-44 210x

Corroded in Mixed Acid
Liquid Solution

Alloy and Condition LC4R

Specification XC3L24 mold

Features of
Structure

Figure VI-43 shows the transverse structure of the central part at the front end. Because the degree of deformation is low, there are remnant casting structures. On the matrices of $\alpha(Al)$, there are many particles separated from the soluble phases.

Figure VI-44 shows the transverse structure of the central part at the rear end. Because the deformation is complete, chemical compounds are noticeably all broken.

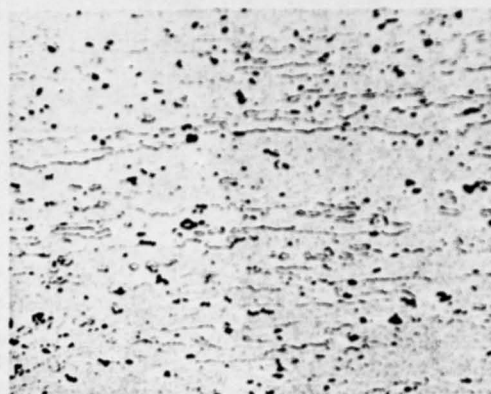
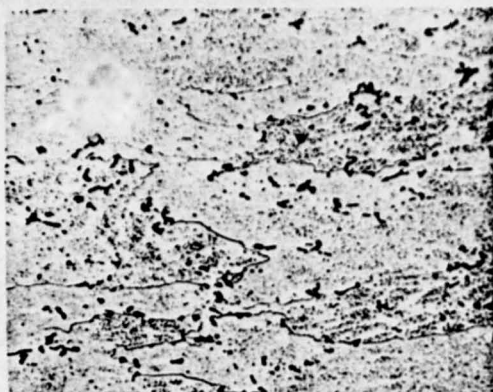


Figure VI-45 210x
Corroded in Mixed Acid
Liquid Solution

Figure VI-46 210x
Corroded in Mixed Acid
Liquid Solution

Alloy and Condition LC4CS

Specification XC3124 mold

Features of
Structure

Figure VI-45 shows the transverse structure of the central part at the front end. The alloy has recrystallized and the grains are coarse. On the matrices of $\alpha(Al)$, scatter the remnants of the soluble phase $S(CuMgAl_2)$ and $T(AlZnMgCu)$ and $AlMnFeSi$, which is hard to dissolve.

Figure VI-46 shows the transverse structure of the central part at the rear end. The alloy has recrystallized and the grains are smaller than those at the front end.

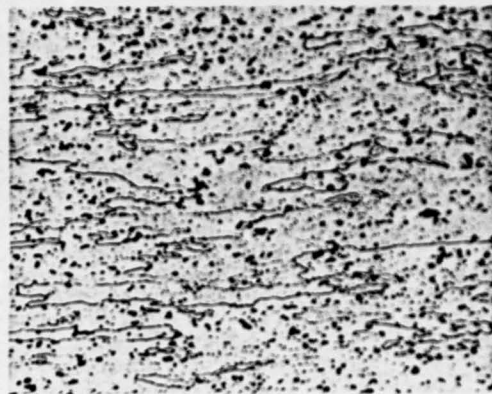


Figure VI-47 210x
Corroded in Mixed Acid
Liquid Solution

Figure VI-48 210x
Corroded in Mixed Acid
Liquid Solution

Alloy and Condition LC4CS

Specification ϕ 76 x 64 mm. tube

Features of Structure Figure VI-47 shows the longitudinal structure of the central part. The alloy has recrystallized and the grains still stretch along the direction of extrusion.

Figure VI-48 shows the transverse structure of the central part.

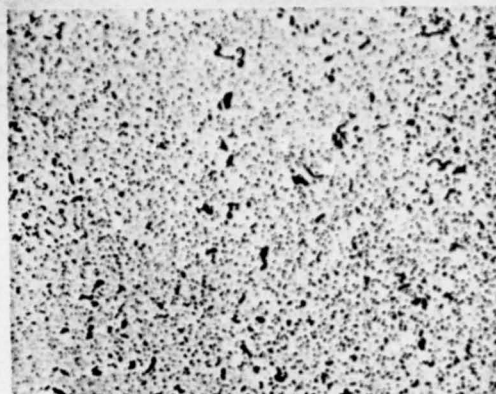


Figure VI-49 210x
Corroded in Mixed Acid
Liquid Solution

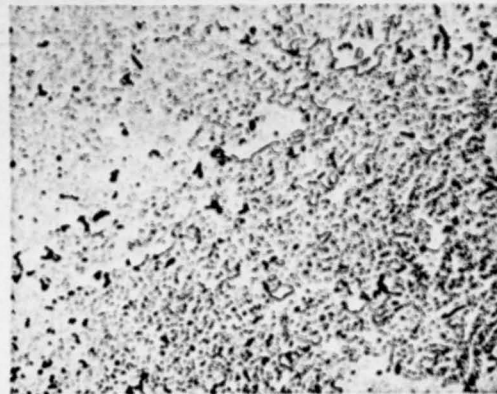


Figure VI-50 210x
Corroded in Mixed Acid
Liquid Solution

Alloy and LC4Y
Condition

Specification ϕ 6 mm. cold draw
wire

Features of The Figure shows
Structure the transverse
 structure of the
 central part. The
 chemical compounds
 are further broken
 and become finer.
 On the matrices of
 α (Al) spread par-
 ticles separated
 from soluble phases
 and phases which
 contain Mn and Cr.

Alloy and LC4CS
Condition

Specification ϕ 6 mm. cold draw
wire

Features of The Figure shows the
Structure **transverse structure**
 of quenched central
 part. The alloy has
 recrystallized. On the
 matrices of α (Al),
 spread particles se-
 parated from phase
 Mn and Cr and the
 remnant soluble phase and
 impurity phase.

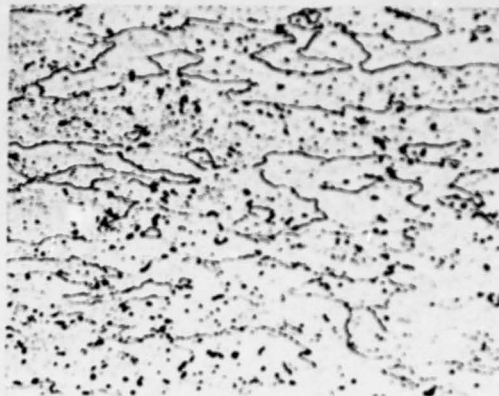
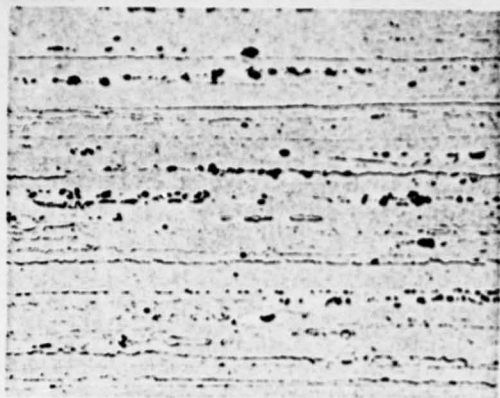


Figure VI-51 210x
Corroded in Mixed Acid
Liquid Solution

Figure VI-52 210x
Corroded in Mixed Acid
Liquid Solution

Alloy and Condition LC6CS

Specification ϕ 35 x 19 mm. tube

Features of Structure Figure VI-51 shows the longitudinal structure of the central part. The alloy has recrystallized and the grains stretch along the direction of extrusion.

Figure VI-52 shows the transverse structure of the central part.

5. The Structure of Die-forged Articles

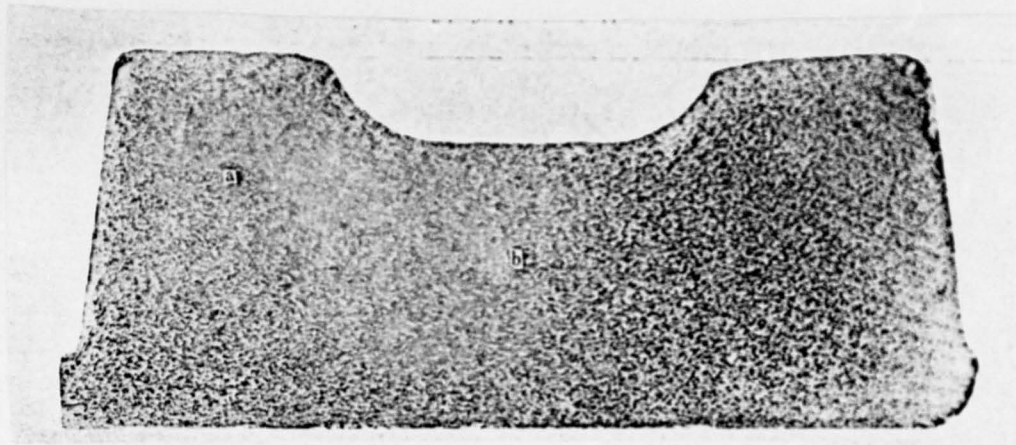


Figure VI-53

Alloy and Condition	LC4CS
Specification	A 5 die-forged article
Corrosion	25%NaOH liquid solution

Features of
Structure

In the Figure, a is the sinew part and b is the thick-board part. The ~~stream~~-lines of the alloy run along the outline of the die-forged piece and they run homogeneously. The degree of deformation in the edge region is great and the structure is much finer.

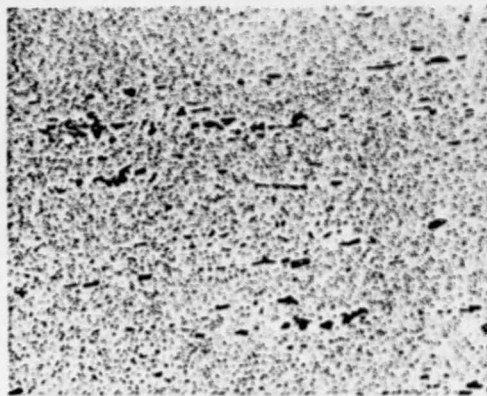
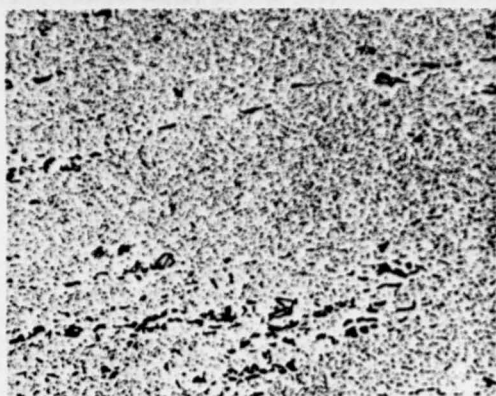


Figure VI-54 210x

Corroded in Mixed Acid
Liquid Solution

Figure VI-55 210x

Corroded in Mixed Acid
Liquid Solution

Alloy and Condition LC4R

Specification A 5 die-forged article

Features of
Structure

Figure VI-54 and Figure VI-55 respectively show the longitudinal structure of the central region of the sinew part and the thick-board part. The broken chemical compounds caused by die pressing arrange themselves along the direction of deformation. From the matrices of $\alpha(\text{Al})$ separate a great many particles of soluble phase $\text{S}(\text{CuMgAl}_2)$ and $\text{T}(\text{AlCuMgZn})$, and phases which contain Mn and Cr.

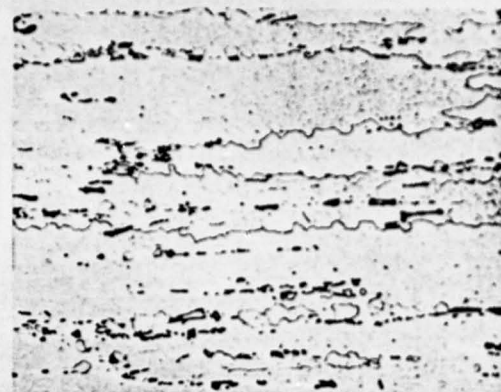


Figure VI-56 210x
Corroded in Mixed Acid
Liquid Solution



Figure VI-57 210x
Corroded in Mixed Acid
Liquid Solution

Alloy and Condition LC4CS

Specification A 5 die-forged article

Features of Structure Figure VI-56 and Figure VI-57 respectively show the longitudinal structure of the central region of the sinew part and the thick-board part. The recrystallization of the alloy is not complete and the grains arrange themselves along the direction of deformation. In Figure VI-57, some hypo-crystallites can be seen.

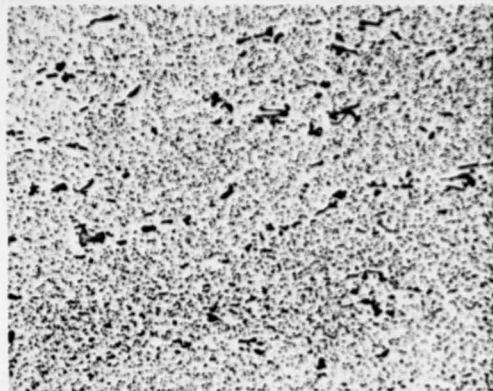


Figure VI-58 210x

Alloy and Condition LC4R

Specification A 5 die-forged article

Corrosion Mixed acid liquid solution

Features of Structure This Figure shows the transverse structure of the central region of the thick-board part. The broken chemical compounds scatter on the matrices of $\alpha(\text{Al})$ and show no clear directionality. The segregated phase particles also scatter on the matrices of $\alpha(\text{Al})$.

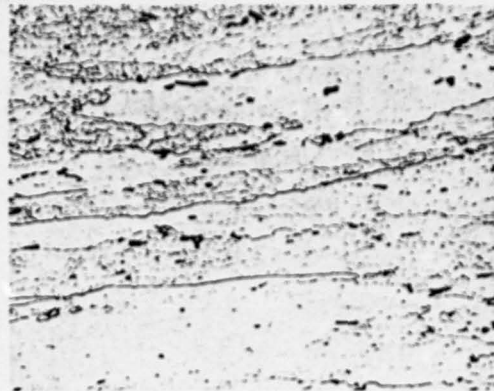


Figure VI-59 210x

Alloy and Condition LC4CS

Specification A 5 die-forged article

Corrosion Mixed acid liquid solution

Features of Structure This Figure shows the transverse structure of the central region of the thick-board part. The recrystallization is not complete, and some hypo-crystallites grains can be seen.

6. The Structure of Welded Articles

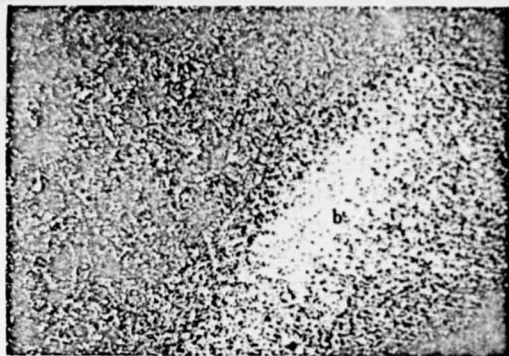


Figure VI-60

12x

Alloy and Condition	LC6+0.12%Zr (Mg2.9%, Zn 8.1%, Cu 2.5%, Mn 0.35%, Cr0.17%, Zr0.12%, Fe<0.5%, Si<0.3%) welding.
Specification	Plate of thickness 3.0 mm. Argon arc-welded article
Corrosion	Mixed acid liquid solution
Features of Structure	a - welded region b - heat affected region

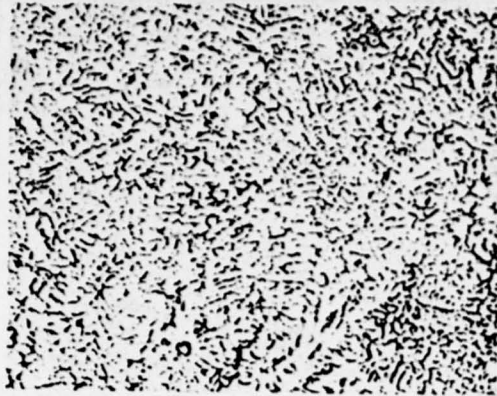


Figure VI-61 100x

Corroded in Mixed Acid
Liquid Solution

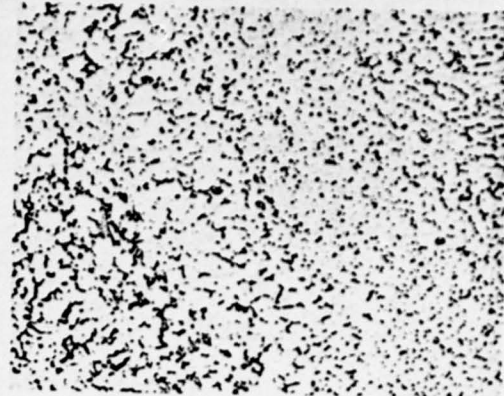


Figure VI-62 100x

Corroded in Mixed Acid
Liquid Solution

Alloy and Condition Same as Figure VI-60

Specification Same as Figure VI-60

Features of Structure Figure VI-61 shows the structure of welded region. It is of some characteristics of casting structure, and it looks like dendritic crystals.

Figure VI-62 shows the structure of the heat affected region. The closer it is to the seaming region, the larger the crystal boundaries are. The chemical compounds are more aggregated.

Chapter 7

Alloy of Aluminum-Copper-Magnesium-Iron-Nickel Group

For the heat-resisting aluminum alloy of aluminum-copper-magnesium-iron-nickel group, there are three brand marks, LD7, LD8 and LD9, which are used often. Among them, alloy LD7 has the best quality of heat-resisting, and LD8 and LD9 follow in order. In industrial production, alloy LD7 is therefore used widely. Alloy LD9, however, because it has such characteristics as small thermal coefficient of expansion and good heat conductivity, still holds definite useful value.

This kind of alloy has good manufacturing property and can be processed into various kinds of bars, forged items and component parts good to be used when the temperature is at 150-225°C. Under certain conditions, it can also be used to make plates.

Section I

Chemical Composition and Phase Formation

The chemical composition of alloy LD7, LD8 and LD9 can be found in Table VII-1:

Table VII-1 Chemical Composition of Alloy LD7, LD8 and LD9

Brand Mark	Principal Constituents (%)							Impurity no more than (%)				
	Cu	Mg	Ni	Fe	Si	Ti	Al	Mn	Si	Zn	other	total
LD7	1.9~ 2.5	1.4~ 1.8	1.0~ 1.5	1.0~ 1.5	—	0.02~ 0.1	sur- plus	0.2	0.35	0.3	0.1	0.95
LD8	1.9~ 2.5	1.4~ 1.8	1.0~ 1.5	1.1~ 1.6	0.5~ 1.2	—	sur- plus	0.2	—	0.3	0.1	0.6
LD9	3.5~ 4.5	0.4~ 0.8	1.8~ 2.3	0.5~ 1.0	0.5~ 1.0	—	sur- plus	0.2	—	0.3	0.1	0.6

From the above table it can be seen that the chemical composition of these alloys is relatively complex. In addition to copper and magnesium, there is a considerable amount of iron and nickel. And there is also silicon in alloy LD8 and LD9, and titanium in LD7.

The principal heat-resisting phase of this kind of alloy is $S(CuMgAl_2)$ phase. Therefore, the quantity of $S(CuMgAl_2)$ phase in this alloy must be made to reach its utmost. A $FeNiAl_9$ phase is another principal phase which also has important effect on its quality of heat-resistance.

Compared with hard aluminum, the ratio between copper and magnesium contained in this kind of alloy is low. Under the condition of low rate of copper, the amount of magnesium is proportionally increased. Then the composition of the alloy falls into two phase zones of $\alpha(Al) + S(CuMgAl_2)$ as indicated in the Al-Cu-Mg three-element equilibrium diagram (see Figure VII-1). This insures that the alloy has the largest quantity of $S(CuMgAl_2)$ phase, and

thereby it can have a good quality of heat-resistance. At the same time, because of the low rate of copper, the concentration of copper in the solid solution $\alpha(\text{Al})$ becomes low accordingly. The solid solution $\alpha(\text{Al})$ of low ^{concentration} has small decomposing tendency and high heat stability; it is therefore good for the quality of heat-resistance of the alloy.

Iron and nickel have good effects upon the heat-resisting capability of the alloy. Nevertheless, if iron or nickel is added alone, the heat-resisting capability will become low. From the Al-Cu-Fe and Al-Cu-Ni three-element equilibrium diagrams (see Figures VII-2 and VII-3) it can be seen that when iron is added alone, following the increase of the amount of iron, it forms a Cu_2FeAl_7 phase (when iron is low), which is difficult to dissolve, and a CuFeAl_3 phase (when iron is high). When only nickel is added, following the increase of the amount of nickel, it forms a AlCuNi phase (when nickel is low), which is difficult to dissolve, and a $(\text{CuNi})_2\text{Al}_3$ phase (when nickel is high). Copper is contained in all these four phases. The formation of any of these phases reduces the quantity of the principal heat-resisting phase $\text{S}(\text{CuMgAl}_2)$ in the alloy and lowers its heat-resisting capability.

From the cross-section of the Al-Cu-Fe-Ni four-element equilibrium diagram with Cu at 2.2% (Figure VII-4), it can be seen

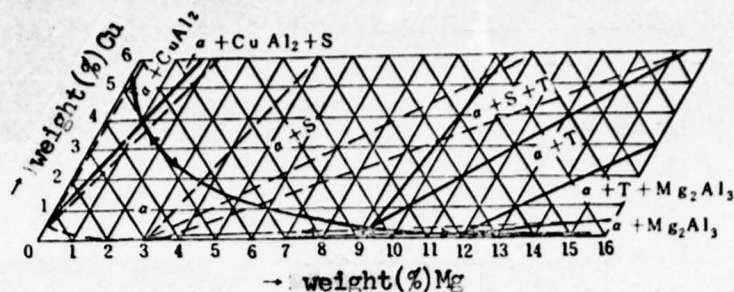


Figure VII-1 Distribution of phase zones of Al-Cu-Mg three elements after solidification.

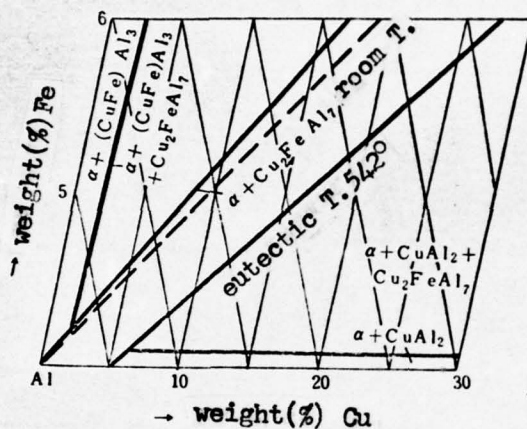


Figure VII-2 Distribution of aluminum phase angle zones of Al-Cu-Mg three elements in solidity.

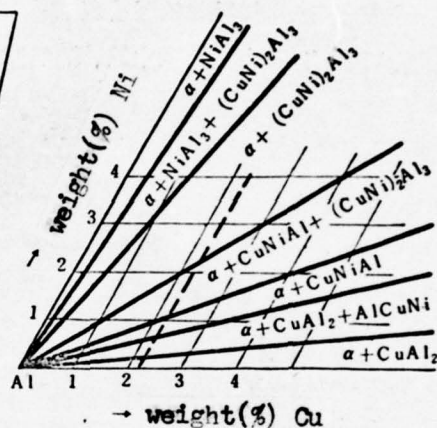


Figure VII-3 Distribution of aluminum phase angle zones of Al-Cu-Ni three elements in solidity.

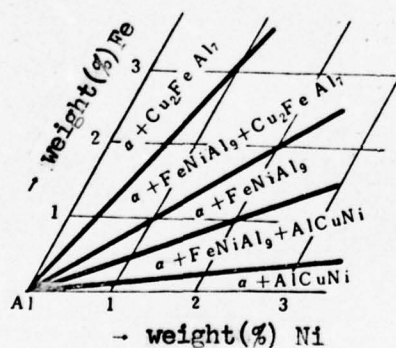


Figure VII-4 Distribution of aluminum phase angle zones on the cross-section of Al-Cu-Fe-Ni four elements containing 2.2% Cu.

when 1.0 - 1.5% of iron and nickel, by a ratio of 1:1, are added to the alloy, it will basically not affect the quantity of $S(CuMgAl_2)$ phase and the alloy is mainly within two phase zones of $\alpha(Al) + FeNiAl_9$. Under such condition, iron and nickel will no longer combine with copper to form $(Cu_2FeAl_7, CuFeAl_3, AlCuNi, (CuNi)_2Al_3)$ phase which contains copper and is hard to dissolve, but iron and nickel together form a hard-to-dissolve $FeNiAl_9$ phase. Thus it enables copper in the alloy to form a great quantity of $S(CuMgAl_2)$ phase and insures the heat-resisting capability of the alloy.

After the formation of $FeNiAl_9$ phase, if iron remains surplus, it will form a Cu_2FeAl_7 phase; if nickel is surplus, it will form a $AlCuNi$ phase. Because of the varying amount of iron and nickel in the alloy, it is therefore possible that Cu_2FeAl_7 phase or $AlCuNi$ phase appears.

Due to the formation of the hard-to-dissolve $FeNiAl_9$ phase, the structure of the alloy becomes more complex and its heat-resisting capability is further promoted. $FeNiAl_9$ phase, following the rise of temperature, becomes very difficult to dissolve in the solid solution $\alpha(Al)$. In casting, it is of the shape of long narrow piece and scatters on the matrices of solid solution $\alpha(Al)$. After deformation, the fragments scatter inside or on the edges of the crystal grains. And they will obstruct the alloy deformation under high temperature. This has good effect on the heat-resisting capability of the alloy (see Figure VII-56 and VII-57).

When silicon is added to the alloy, it forms Mg_2Si phase and reduces the quantity of $S(CuMgAl_2)$ phase which is the principal heat-strengthening phase. After artificial aging, Mg_2Si will help to increase the toughness of the alloy, and under high temperature, ^{over-}because of its great aging sensitivity, it acts to reduce the high temperature instantaneous strength and durability of the alloy. In alloy LD7, Si is regarded as impurity and controlled at the level below 0.35%, so only a small quantity of Mg_2Si phase can be found in the alloy. But Si can lower the thermal coefficient of expansion of the alloy and increase the degree of room temperature. Silicon is therefore an important constituent of alloy LD7 and LD8 and it may reach as high as 1.0-1.2%. It is evident that the quantity of Mg_2Si contained in these two alloys is larger than that in LD9.

Titanium is the important modifying agent to fine the structure of alloy and has good effect on its manufacturing property and the transverse-directional property of its products.

Based on the analyses in the equilibrium diagrams and the proofs made by metallographic microprobe minute examination, alloy LD7 under the condition of gradual cooling contains $\alpha(Al)$, $S(CuMgAl_2)$, $FeNiAl_9$, $AlCuNi$, and Mg_2Si phases. The formation of these phases in alloy LD8 is similar to that in LD7 except that the quantity of Mg_2Si phase is larger. And these various phases also exist in alloy LD9.

Under the condition of semicontinuous casting, the phase formation

in the cast ingot is generally similar to that under the condition of gradual cooling. But each phase is smaller and separate.

The phases mentioned above, according to their forms and different reaction to corroding agent, can be easily differentiated. (see Figure VII-7 through VII-18).

$S(CuMgAl_2)$ phase: For details of its characteristics, see Chapter 4, Alloy of Al-Cu-Mg Group.

$FeNiAl_9$ phase: Its primary crystallization is of the shape of long narrow pieces or schists with bright white color; while the eutecticum is a cluster of fine long narrow pieces. After being corroded in the mixed liquid acid solution or liquid solution with 0.5% hydrofluoric acid, its color becomes brown. But it will not be corroded in nitric acid.

$AlCuNi$ phase: It has a skeleton-shaped appearance with bright grey color, but it is darker than $FeNiAl_9$ phase before corroding. Because of its high degree of hardness ($H_v = 1000 \text{ kg./mm}^2$), after being polished, it is more noticeable than other phases on the surface of the test piece. And it can be easily corroded in the liquid solution which contains 25% of nitric acid.

Mg_2Si phase and $W(Cu_4Mg_5Si_4Al_x)$ phase: For their special features, see Chapter 5, Alloy of Al-Mg-Si-Cu Group.

Section 2

Characteristics of Heat Treatment

To this kind of alloy, the heat treatment is applied under the condition of quenching and artificial aging. The important strengthening phase of this alloy is $S(CuMgAl_2)$ phase, and, in addition, there is Mg_2Si phase in alloy LD8 and LD9. Therefore, they have high sensitivity to the strengthening work in heat treatment. In the process of solid solution heat treatment, $S(CuMgAl_2)$ has important strengthening effect when it is dissolved in solid solution. Only a part of Mg_2Si phase can be dissolved in solid solution, so its strengthening effect is relatively small. $FeNiAl_9$ phase and $AlCuNi$ phase (or Cu_2FeAl_7 phase) perform no strengthening function in heat treatment.

The system of heat treatment of this kind of alloy will be indicated in Table VII-2:

Table VII-2 System of Heat Treatment of Alloy LD7, LD8 and LD9

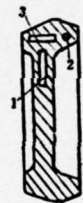
Brand Mark	Quench Heating T. (°C)	System of Artificial Aging	
		Heating T. (°C)	Heat Retaining (hrs.)
LD7	525~540	165~180	10~16
LD8	525~540	185~195	8~12
LD9	510~520	150~180	6~16

In order to reduce the internal stress caused during quenching and to avoid the occurrence of cracking and curling up, it is better to adopt stage quenching method for articles of large size made of this alloy.

Because of its limited content of manganese, this alloy has greater tendency of recrystallization. It is, therefore, easy to have a

complete recrystallization after hot processing (hot pressing or die forging). For instance, except for its far front end where the deformation is less and the recrystallization is incomplete, the other parts of a hot-pressed stick-shaped piece of alloy LD7 (the press temperature is 370-450°C) all have complete recrystallization. For the same reason, after hot-die-forging, the alloy will also have a complete recrystallization. If it undergoes another quenching heat treatment, it will be fully recrystallized and the crystal grains are large.

Table VII-3 Three Directional Mechanical Properties of Alloy LD7 K9 Forged Articles

Testing Piece No.	Mechanical Properties		Die-forging Position
	σ_b (kg./mm ²)	δ (%)	
1	40.4~41.4	18.4~20.8	
2	40.2~41.7	16.0~20.0	
3	40.6~42.6	14.4~18.8	

The stick-shaped articles and forged pieces, after quenching, exhibit large and approximate isometric recrystallized grains on their cross-sections, and this causes the mechanical properties of this alloy product to have no noticeable anisotropy. And because the crystal grains are large, it is helpful to the heat-resisting capability of the alloy.

The three directional mechanical properties of alloy LD7 K9 forged articles after quenching and artificial aging can be seen in Table VII-3.

Section 3

Structure of Cast Ingot and Processed Articles

The general rules of affecting the structure and quality of products of this kind of alloy by the type of processing have been discussed in detail in the Introduction as well as in the related diagrams and figures in this chapter. But the structure and the quality of the alloy itself have their own characteristics, and the major ones are as follows:

I. The segregation of FeNiAl_9 primary crystallization. This kind of alloy contains high quantity of iron and nickel, when its constituents and the casting techniques are not correct, it will possibly result in rough segregation of FeNiAl_9 primary crystallization. The cluster of shining acicular primary crystals of FeNiAl_9 (for its characteristics, see Figure VII-18), is very hard to break when it is under hot processing. Because of its existence, the manufacturing and mechanical property of the alloy are reduced. In casting, therefore, it should be avoided.

2. Special features of the structure of fractures. When the fractures on the forged articles of this kind of alloy are examined, it is often found that there are lamellar cracks on the fracture (Figure VII-5). The alloys of this kind all contain great amount of chemical compounds -- FeNiAl_9 phase and AlCuNi phase (or Cu_2FeAl_7 phase), which are hard to dissolve in solid solution $\alpha(\text{Al})$. Heat treatment cannot change the conditions and distributions of these phases, and deformation

can make them broken and dissociated. But in the location where those chemical compounds are in cluster, it is possible that they form lamellae there. The lamellar cracks on the fractures of forged articles of alloy LD7 and LD8 are indications that the lamellae of those chemical compounds exist there. Through microstructural observation, it can be seen that the lamellar cracks are developed out of the chemical compounds which are arranged in a shape of string (Figure VII-6). There is an essential difference between this kind of lamellar structure and the schistose structure of α in alloy LD2. In production, this structure is usually treated as a normal phenomenon.



Figure VII-5 Structure of fractures on the projecting spots of forged article of alloy LD7 S6 type. There are lamellar cracks on the fracture. The arrow pointed spots are cracks.

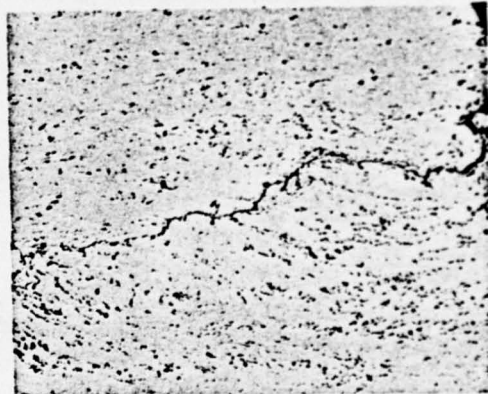


Figure VII-6 Microstructure of cracks in Figure VII-5.

I. Phase Formation

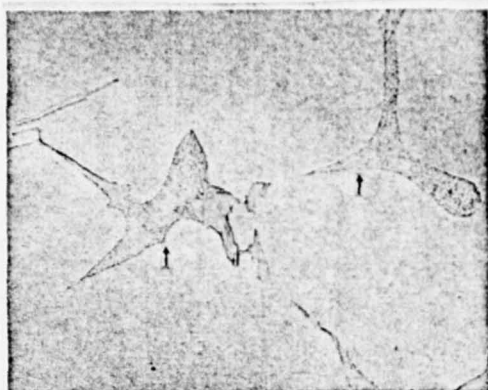


Figure VII-7

210x

Alloy LD7
 Condition After fusing at 750°C, the cast ingot gradually cooled to 500°C in furnace, then water cooling.
 Corrosion Not corroded.
 Features of Structure The arrow pointed honeycomb structure is a(Al)+S(CuMgAl₂) eutecticum.

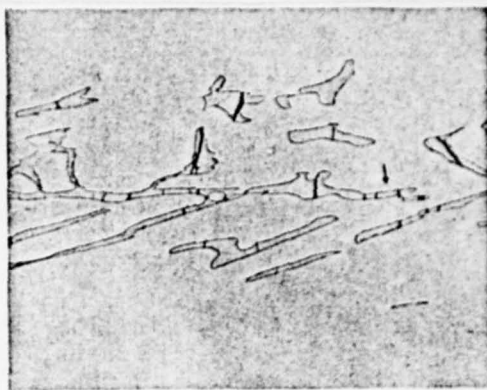


Figure VII-8

210x

Alloy LD7
 Condition Same as in Figure VII-7.
 Corrosion Not corroded.
 Features of Structure The arrow pointed spot is FeNiAl₉ phase of grey color in the shape of long narrow pieces and schists. Because the speed of cooling is slow, they appear bulky.



Figure VII-9

210x

Alloy LD7
 Condition Same as in Figure VII-7.
 Corrosion Not corroded.
 Features of Structure The arrow pointed AlCuNi phase is of grey color in the shape of a skeleton. Because of its degree of hardness, after polishing, it becomes more noticeable than others on the foundation.



Figure VII-10

210x

Alloy LD7
 Condition Same as in Figure VII-7.
 Corrosion Not corroded.
 Features of Structure 1 - $\alpha(\text{Al}) + \text{S}(\text{CuMgAl}_2)$ eutecticum;
 2 - FeNiAl_9 phase;
 3 - AlCuNi phase;
 4 - Mg_2Si phase.



Figure VII-11

210x

Alloy	LD7
Condition	Same as in Figure VII-7.
Corrosion	25% nitric acid liquid solution, 70°C, 30 seconds.
Features of Structure	<p>1 - $S(CuMgAl_2)$ phase is of black color;</p> <p>2 - $FeNiAl_9$ phase, cannot be corroded;</p> <p>3 - $AlCuNi$ phase, can be corroded severely, and has a rough surface;</p> <p>4 - Mg_2Si phase is dissolved, and its color becomes black.</p>

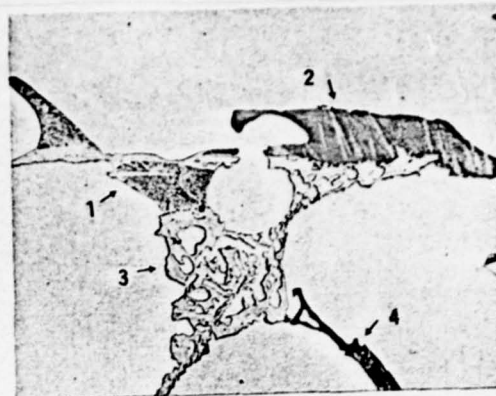


Figure VII-12

210x

Alloy	LD7
Condition	Same as in Figure VII-7.
Corrosion	Mixed acid liquid solution, 5 seconds.
Features of Structure	<p>1 - $S(CuMgAl_2)$ cannot be corroded;</p> <p>2 - $FeNiAl_9$ can be corroded, brown color;</p> <p>3 - $AlCuNi$ phase cannot be corroded;</p> <p>4 - Mg_2Si phase is dissolved, and its color becomes black.</p>

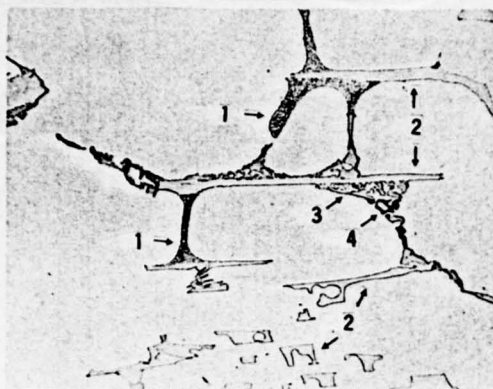


Figure VII-13

210x

Alloy	LD7
Condition	Same as in Figure VII-7.
Corrosion	10g. NaOH + 100ml. liquid solution, 50°C, 15 seconds.
Features of Structure	<p>1 - $S(CuMgAl_2)$ can be corroded, its color becomes dark;</p> <p>2 - $FeNiAl_9$ phase can be corroded, its color becomes dark;</p> <p>3 - $AlCuNi$ phase cannot be corroded;</p> <p>4 - Mg_2Si phase cannot be corroded.</p>

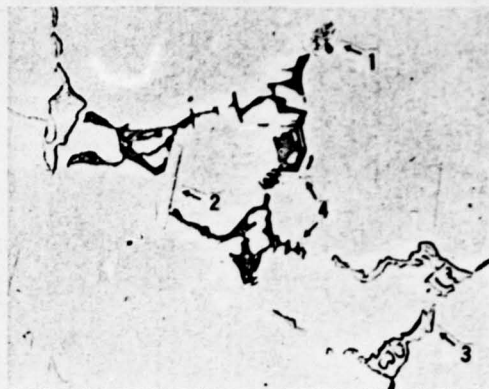


Figure VII-14

210x

Alloy	LD8
Condition	Cast ingot after fusing at 750°C, gradually cooled to 500°C in furnace, then water cooling.
Corrosion	Not corroded.
Features of Structure	<p>1 - $S(CuMgAl_2)$ phase;</p> <p>2 - $FeNiAl_9$ phase;</p> <p>3 - $AlCuNi$ phase;</p> <p>4 - Mg_2Si phase.</p>



Figure VII-15

210x

Alloy	LD9
Condition	Cast ingot after fusing at 750°C, gradually cooled to 500°C in furnace, then water cooling.
Corrosion	25% nitric acid liquid solution, 70°C, 15 seconds.
Features of Structure	1 - S(CuMgAl ₂) phase; 2 - FeNiAl ₉ phase; 3 - AlCuNi phase; 4 - Mg ₂ Si phase.

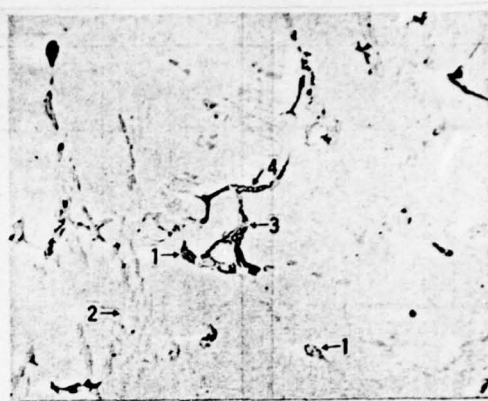


Figure VII-16

320x

Alloy	LD7
Condition	Semicontinuous ingot casting.
Corrosion	Not corroded.
Features of Structure	1 - α (Al) + S(CuMgAl ₂) eutecticum; 2 - FeNiAl ₉ phase in the shape of clustered fine long narrow pieces; 3 - AlCuNi phase; 4 - Mg ₂ Si phase.

Compared with testing piece which is cooled gradually, the phases in semicontinuous ingot casting are all finer.

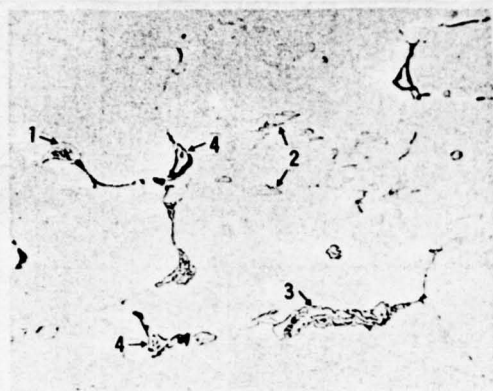


Figure VII-17

320x

Alloy	LD8
Condition	Semicontinuous ingot casting.
Corrosion	Not corroded.
Features of Structure	1 - $\alpha(\text{Al}) + \text{S}(\text{CuMgAl}_2)$ eutecticum; 2 - FeNiAl_9 phase; 3 - AlCuNi phase; 4 - Mg_2Si phase.



Figure VII-18

210x

Alloy	LD7
Condition	Semicontinuous ingot casting.
Corroding Agent	Mixed acid liquid solution.
Features of Structure	Structure of segregation of primary crystallization of cast ingot of FeNiAl_9 ; 1 - FeNiAl_9 primary crystallization; 2 - $\alpha(\text{Al}) + \text{FeNiAl}_9$ eutecticum.

2. Structure of Cast Ingot

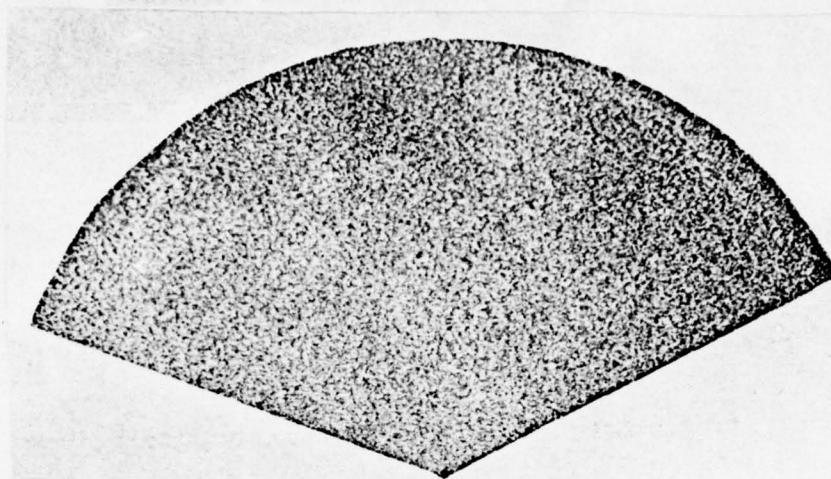


Figure VII-19 Corrosion of 15% NaOH Liquid Solution

Alloy and Condition	Semicontinuous ingot casting of alloy LD7.
Specification	Ø 192 mm.
Features of Structure	Structure of the macroscopic of the transverse section of a cast ingot. The lines of crystal boundary are not clear, this is because that the alloy contains numerous chemical compounds.

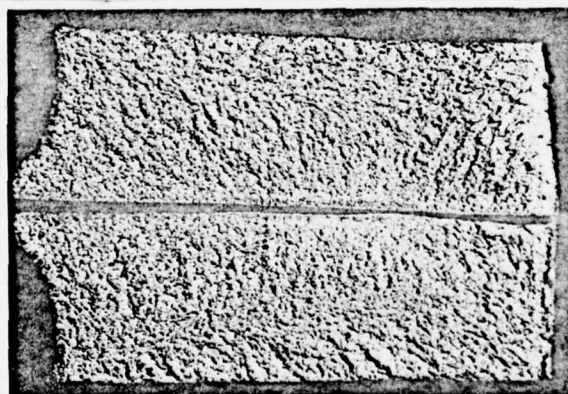


Figure VII-20

Alloy and Condition	Same as in Figure VII-19
Specification	Same as in Figure VII-19
Features of Structure	Structure of fracture of semi-continuous ingot casting of alloy LD7.

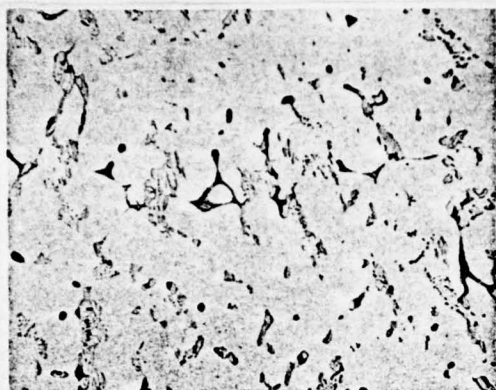


Figure VII-21

210x

Corrosion of Mixed Acid
Liquid Solution



Figure VII-22

210x

Corrosion of Mixed Acid
Liquid Solution

Alloy and Condition

Specification
Features of
Structure

Semicontinuous ingot casting of alloy
LD7.

φ 192 mm.

Both figures show the net-structure of
dendritic crystal.

Figure VII-22 is the transverse structure
of the edge of ingot. The meshes among
the dendritic crystals are large and the
network is not all connected.

Figure VII-23 is the transverse structure
of the center of ingot. The meshes
among the dendritic crystals are smaller.
A great quantity of FeNiAl₉ and AlCuNi
phase pile up and scatter on the network
of dendritic crystal, and the network is
connected.

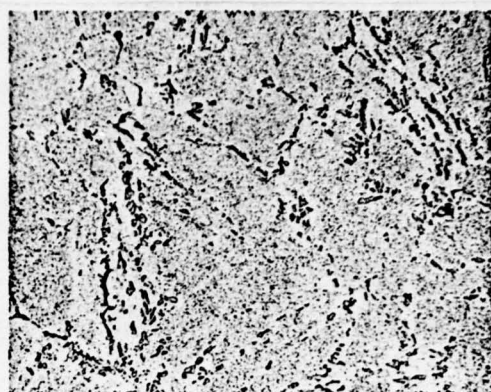
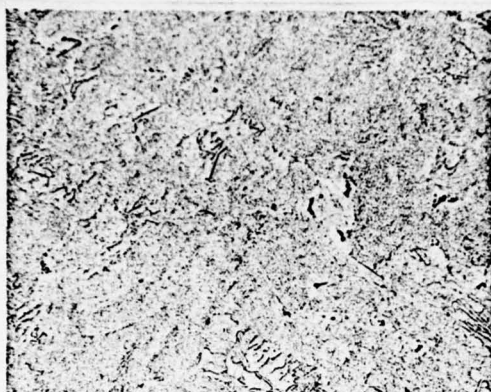


Figure VII-23

210x

Corrosion of Mixed Acid
Liquid Solution

Figure VII-24

210x

Corrosion of Mixed Acid
Liquid Solution

Alloy and Condition

Semicontinuous ingot casting of alloy LD7, and in homogenizing (500°C, 12 hours, cooled in furnace).

Specification

ø 192 mm.

Features of
Structure

Figure VII-23 and VII-24 respectively show the transverse structure of the edge and the center of an ingot; After the homogenizing of the ingot and the soluble excess of $S(CuMgAl_2)$ and Mg_2Si are dissolved in solid solution $\alpha(Al)$, there still some net-structure of dendritic crystal remains, and $FeNiAl_9$ phase and $AlCuNi$ phase, which are difficult to dissolve, remain unchanged. And from the matrices of $\alpha(Al)$, a great amount of particles of $S(CuMgAl_2)$ and Mg_2Si comes out.

3 Structure of Pressure Castings

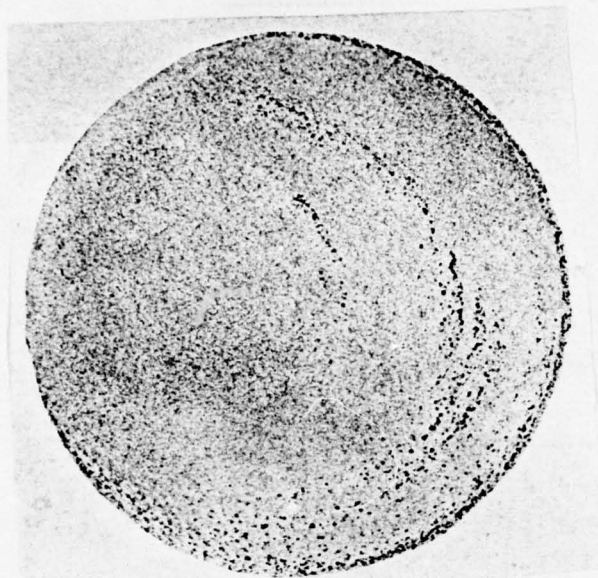


Figure VII-25

1:1

Corrosion of Mixed Acid
Liquid Solution

Alloy and Condition LD7
Specification ϕ 80 mm.
Features of Structure Macroscopical
structure of the transverse
section of a
rod shaped piece. After pressing,
it recrystallized. In the areas
around its edge, many recrystallized
grains which have become large,
can be seen.

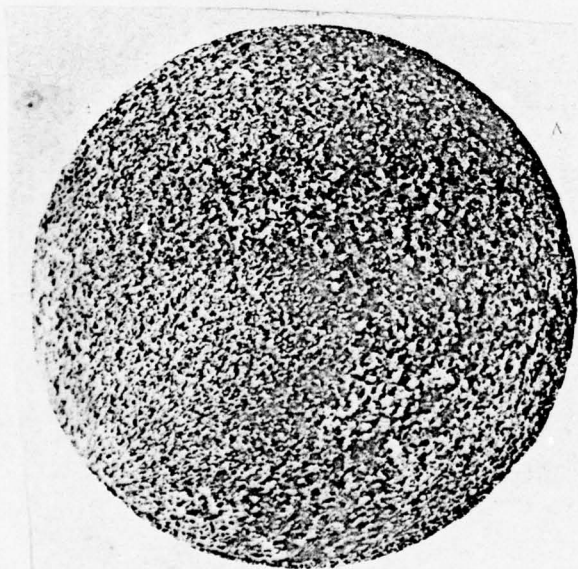


Figure VII-26

1:1

Corrosion of Mixed Acid
Liquid Solution

Alloy and Condition LD7CS
Specification ϕ 80 mm.
Features of Structure Macroscopical
structure of the transverse
section of a
rod shaped piece. After aging,
it recrystallized and the grains
all become large. On the surface
of the whole cross-section all
the crystal grains are large,
especially in the areas where
the deformation is larger, the
grains are even larger.

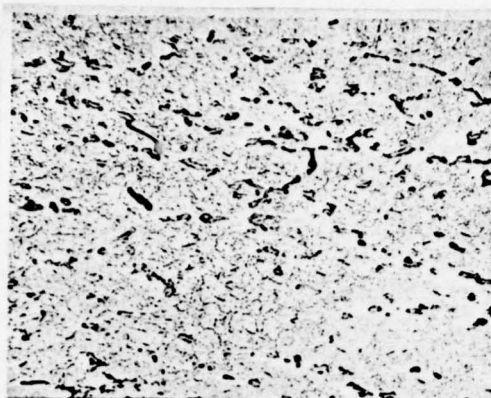


Figure VII-27 210x
Corrosion of Mixed Acid
Liquid Solution

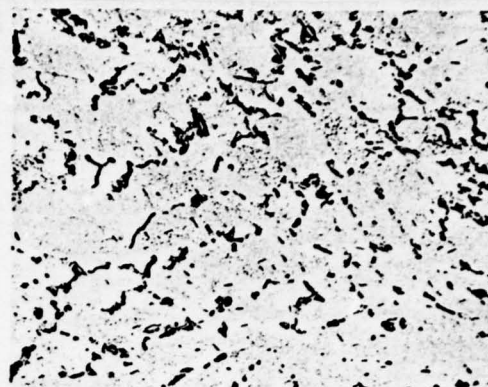


Figure VII-28 210x
Corrosion of Mixed Acid
Liquid Solution

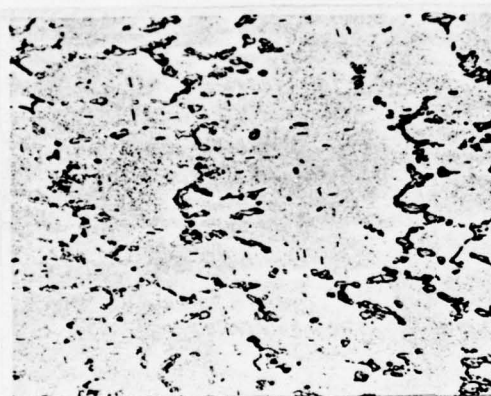


Figure VII-29 210x
Corrosion of Mixed Acid
Liquid Solution

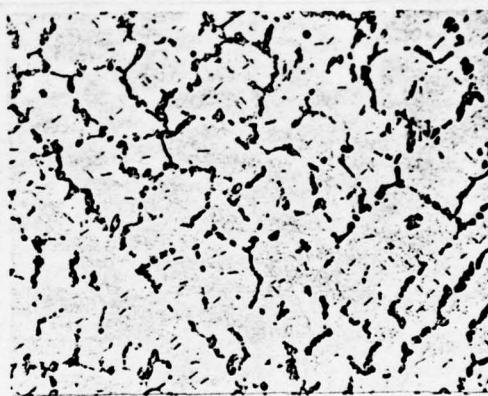


Figure VII-30 120x
Corrosion of Mixed Acid
Liquid Solution

Alloy and Condition
Specification
Features of Structure

LD7R
ø 80 mm.
Figure VII-27 and VII-29 respectively
show the longitudinal microstructure
of the edge and the center of the (contd.)

far front end of a pressure cast piece. After deformation, the cast crystal grains break into fragments, and the broken chemical compounds are arranged along the direction of deformation of the pressure cast article. Because the deformation at the far front end, especially the central part of the rod-type article is small, some cast remnants remain there. Solid solution (Al) is fully decomposed, so from its matrices, great many particles of $S(CuMgAl_2)$ and Mg_2Si come out.

Figure VII-28 and VII-30 respectively show the transverse structure at the edge and the central part of the far front end of the rod-type article.

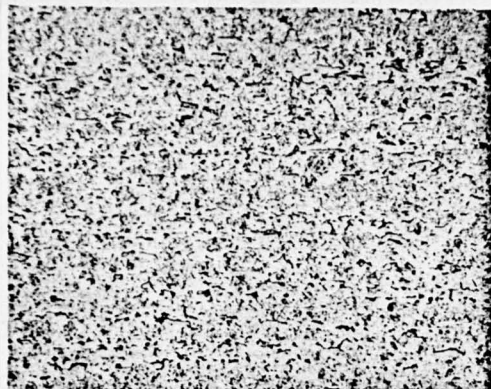


Figure VII-31 210x
Corrosion of Mixed Acid
Liquid Solution

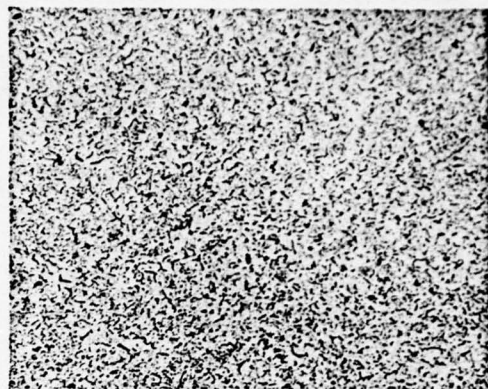


Figure VII-32 210x
Corrosion of Mixed Acid
Liquid Solution

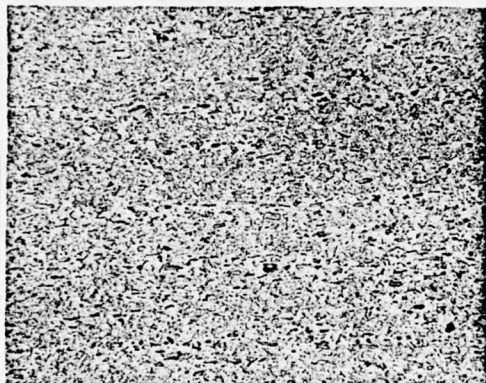


Figure VII-33 210x
Corrosion of Mixed Acid
Liquid Solution

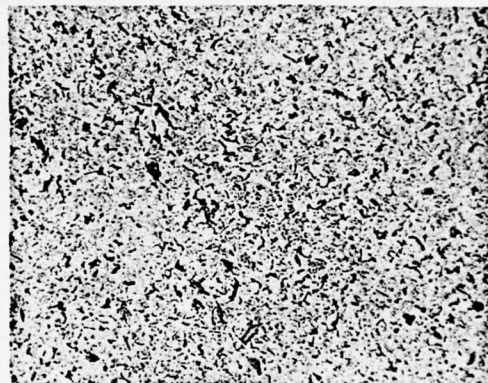


Figure VII-34 210x
Corrosion of Mixed Acid
Liquid Solution

Alloy and Condition
Specification
Features of Structure

LD7R
ø 80 mm.
Figure VII-31 and VII-33 show the
longitudinal microstructure of the
edge and the center of the (contd.)

rear end of a pressure cast piece. Compared with the structure of its far front end, the deformation of the rear end is greater. The cast structure broke completely, and the remnant chemical compounds give a clear directionality to arrange them along the direction of the main deformation. Solid solution $\alpha(\text{Al})$ decomposes more fully and the segregated particles are in clusters and coarse in appearance.

Figure VII-32 and VII-34 respectively show the transverse structure of the edge and the central part of the rear end of the pressure cast rod-type article.

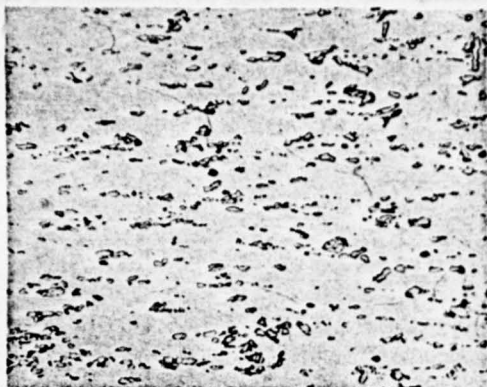


Figure VII-35 210x

Corrosion of Mixed Acid
Liquid Solution

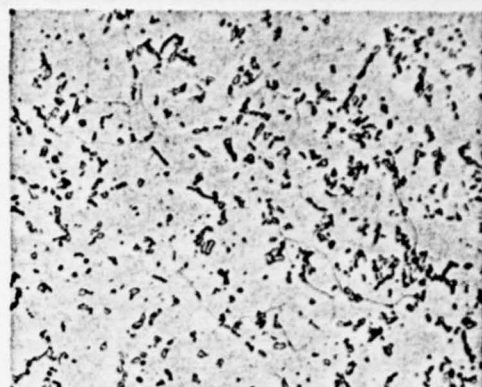


Figure VII-36 210x

Corrosion of Mixed Acid
Liquid Solution

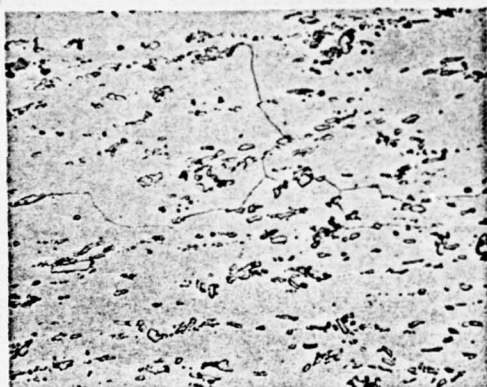


Figure VII-37 210x

Corrosion of Mixed Acid
Liquid Solution

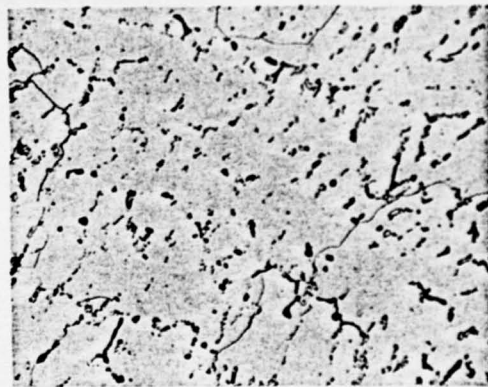


Figure VII-38 210x

Corrosion of Mixed Acid
Liquid Solution

Alloy and Condition

Specification

Features of Structure

LD7CS (530°C, 40 minutes, water
cooling, 185°C, 8 hours)
ø 80 mm.

Figure VII-35 and VII-37 show the
longitudinal microstructure (contd.)

of the edge and the center of the far front end of a pressure cast rod-type piece. After quenching, alloy has completely crystalized, and the grain is a large **isometric crystal**. The soluble chemical compounds of $S(CuMgAl_2)$ are dissolved in solid solution $\alpha(Al)$, and $FeNiAl_9$ phase, $AlCuNi$ phase and the fractional remnant of Mg_2Si remains on the matrices of $\alpha(Al)$.

Figure VII-36 and VII-38 respectively show the transverse microstructure of the edge and the central part of the far front end of a rod-type article.

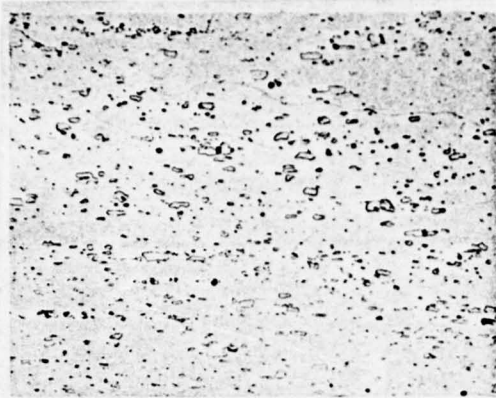


Figure VII-39 210x

Corrosion of Mixed Acid
Liquid Solution

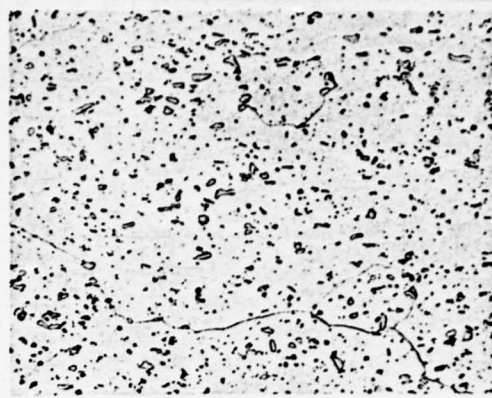


Figure VII-40 120x

Corrosion of Mixed Acid
Liquid Solution

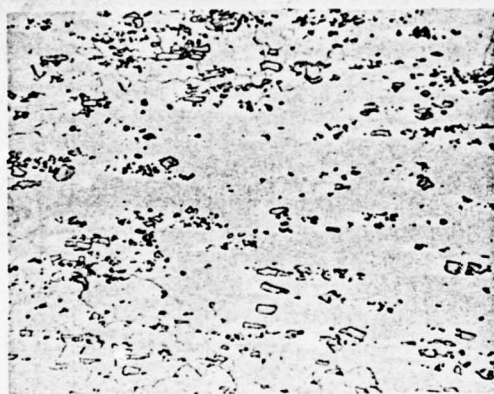


Figure VII-41 210x

Corrosion of Mixed Acid
Liquid Solution

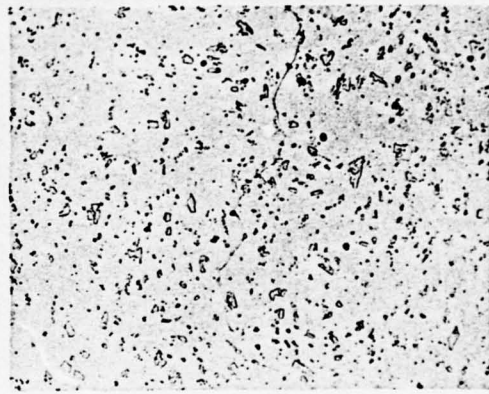


Figure VII-42 120x

Corrosion of Mixed Acid
Liquid Solution

Alloy and Condition

LD7CS (530°C, 40 minutes, water cooling,
185°C, 8 hours)

Specification

Ø 80 mm.

Features of Structure

Figure VII-39 and VII-41 show the
longitudinal microstructure (contd.)

of the edge and the central part of the rear end of a pressure cast rod-type piece. It is similar to the structure of the far front end (Figure VII-35 through VII-38), but because the degree of deformation of the rear end is greater, the recrystallized grains are more coarse. The cast structure broke completely, and the directionality of arrangement of the chemical compounds becomes very clear.

Figure VII-40 and VII-42 respectively show the transverse microstructure of the edge and the central part of the rear end of the rod-type article.

4. The Structure of Die-forged Articles

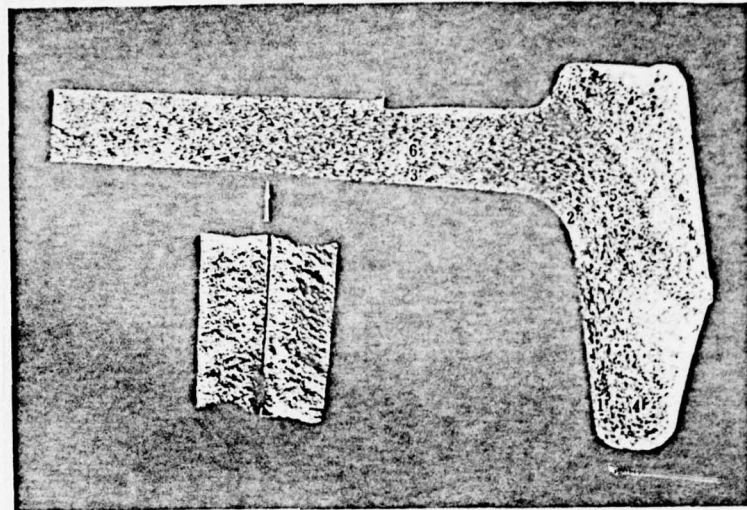


Figure VII-43

Corrosion of Mixed Acid
Liquid Solution

Alloy and Condition

LD7 CS (530°C, 90 minutes, water
cooling, 185°C, 8 hours)

Specification

K9 die-forged piece

Feature of Structure

The Figure illustrates the radial
macroscopical structure of a die-
forged article. The alloy has com-
pletely recrystallized and the grains
are relatively large. The fracture
testing piece is taken from the broad-
plate part of the article and its
structure is fine and homogeneous.

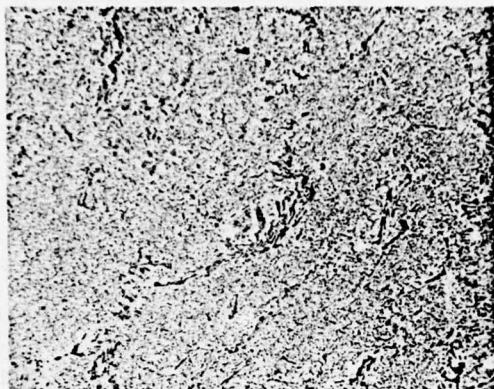


Figure VII-44 210x
Corrosion of Mixed Acid
Liquid Solution

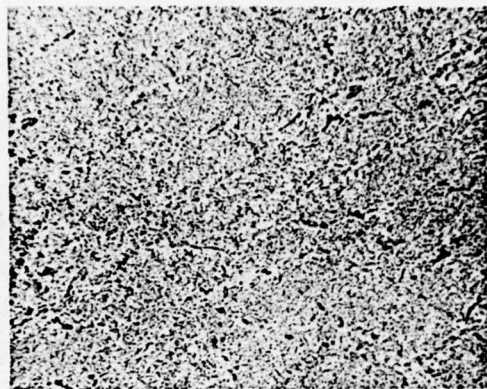


Figure VII-45 210x
Corrosion of Mixed Acid
Liquid Solution

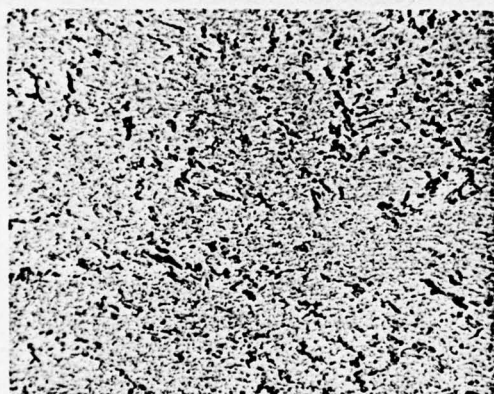


Figure VII-46 210x
Corrosion of Mixed Acid
Liquid Solution

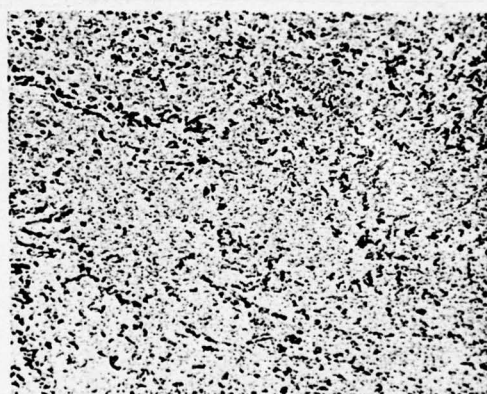


Figure VII-47 210x
Corrosion of Mixed Acid
Liquid Solution

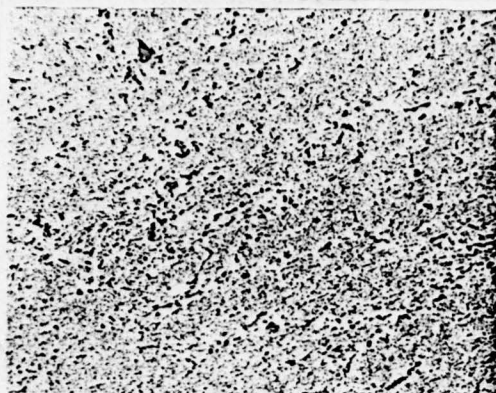


Figure VII-48 210x
Corrosion of Mixed Acid
Liquid Solution

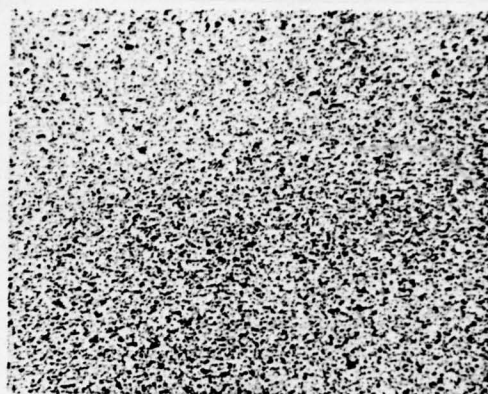


Figure VII-49 210x
Corrosion of Mixed Acid
Liquid Solution

Alloy and Condition
Specification
Features of Structure

LD7R
K9 die-forged piece
Figure VII-44, VII-46 and VII-48 illustrate the microstructure of various locations on the surface of a die-forged article (corresponding to the locations 1, 2, and 3 in Figure VII-43). The deformation in these locations is small, and many remnant cast structures can be seen.

Figure VII-45 and VII-47 illustrate the microstructure of the centers of the thick parts of the die-forged article (corresponding to the locations 4 and 5 in Figure VII-43). The deformation in those two locations is small, and the remnant cast structure can still be seen.

Figure VII-49 (corresponding to location 6 in Figure VII-43) shows the structure at the center of the thick part of the die-forged article. The deformation is full and the cast structure broke completely. There is a strong directionality of arranging the chemical compounds along the direction of deformation. After hot-forging, solid solution α (Al) decomposed fully and on its matrices there are great many segregated particles.

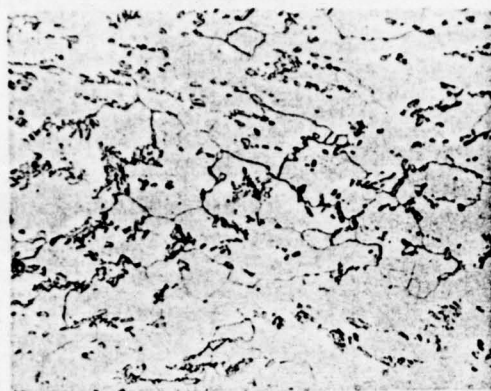


Figure VII-50 210x

Corrosion of Mixed Acid
Liquid Solution

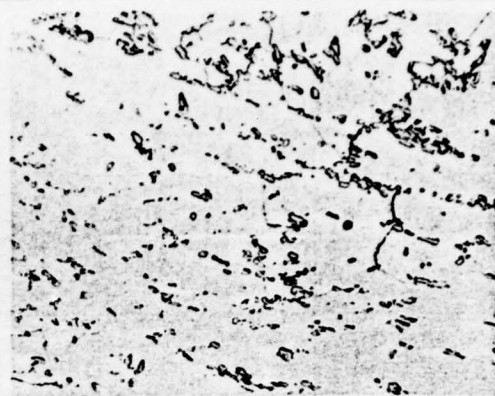


Figure VII-51 210x

Corrosion of Mixed Acid
Liquid Solution

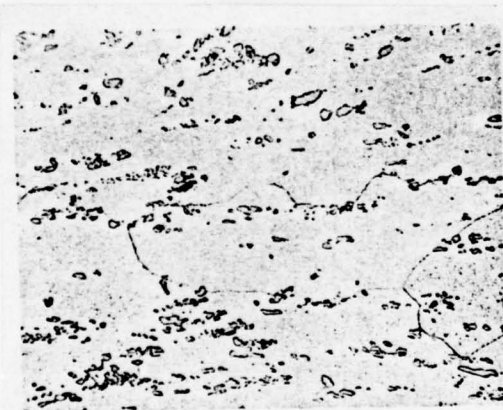


Figure VII-52 210x

Corrosion of Mixed Acid
Liquid Solution

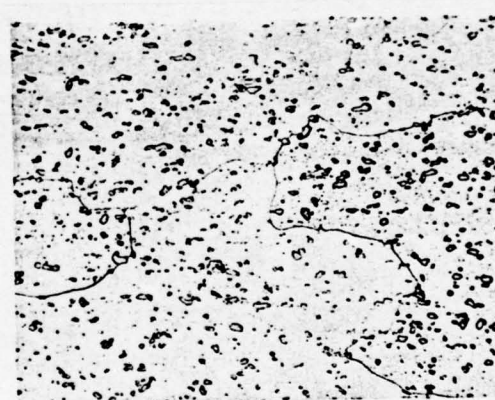


Figure VII-53 210x

Corrosion of Mixed Acid
Liquid Solution

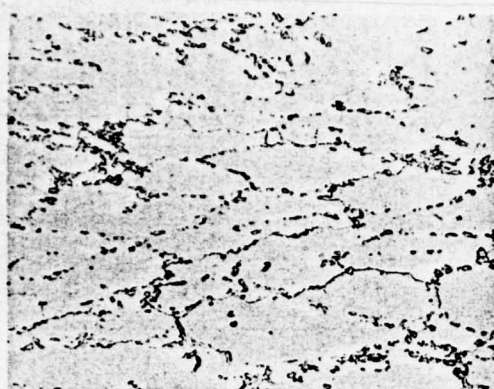


Figure VII-54 210x

Corrosion of Mixed Acid
Liquid Solution

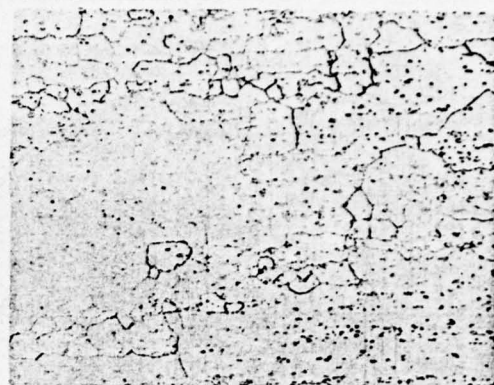


Figure VII-55 210x

Corrosion of Mixed Acid
Liquid Solution

Alloy and Condition

Specification

Features of Structure

LD7CS (530°C, 90 minutes, water cooling
185°C, 8 hours)

K9 die-forged piece

Figure VII-50, VII-52 and VII-54
respectively illustrate the micro-
structure of the various locations on
the surface of the die-forged article
(see location 1, 2, and 3 in Figure VII-43).

Figure VII-51, VII-53 and VII-55 respec-
tively illustrate the microstructure of
the thick and the broad-plate parts of the
die-forged article (see location 4, 5, and
6 in Figure VII-43).

The forged article after quenching has
completely recrystallized and the grains
are in the isometric shape. The soluble
phase is dissolved in solid solution α (Al),
and only FeNiAl_9 phase, AlCuNi phase and a
part of Mg_2Si phase, which are insoluble,
remain. In locations where the deformation
is small (see Figure VII-50, 51, 52 and 54),
the outline of the structure of the dendritic
crystal can be seen from the manner of
distribution of the insoluble phases. In
location where deformation is great (see
Figure VII-55), the directionality of
arranging the remnant phases along the
direction of deformation is strong.

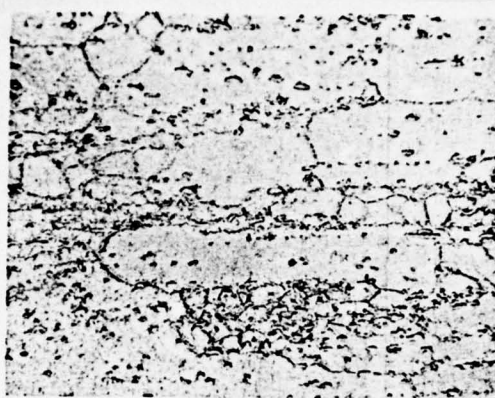


Figure VII-56 210x

Corrosion of Mixed Acid
Liquid Solution

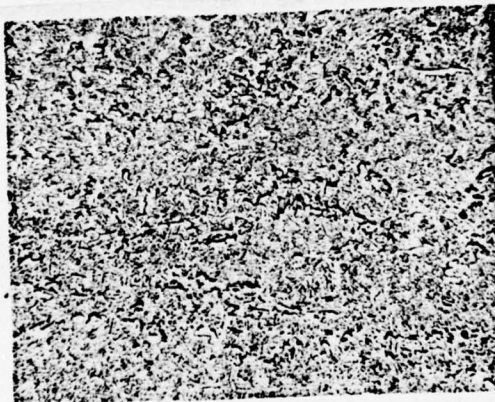


Figure VII-57 210x

Corrosion of Mixed Acid
Liquid Solution

Alloy and Condition

LD7CS, testing of strength of high
temperature retention which is processing
under 250°C, then 300°C for a period of
100 hours.

Specification

K9 die-forged piece (contd.)

Features of Structure

Figure VII-56 illustrates the structure under the condition of downward stretching for 100 hours at 250°C (loading 7 kg./mm²).

Figure VII-57 illustrates the structure under the condition of downward stretching for 100 hours at 300°C (loading 5 kg./mm²).

From the Figures it can be seen that after the testing of strength of high temperature retention at 250°C, the solid solution $\alpha(\text{Al})$ in the alloy has begun to decompose, and the particles of $\text{S}(\text{CuMgAl}_2)$ phase first come out along the crystal boundaries. The form of FeNiAl_9 phase and AlCuNi phase remains unchanged.

After the testing at 300°C, great quantity of $\text{S}(\text{CuMgAl}_2)$ comes out and grows and collects into a cluster. FeNiAl_9 phase and AlCuNi phase remain unchanged.

This test illustrates that when temperature reaches above 250°C, $\text{S}(\text{CuMgAl}_2)$ phase, which has decomposed, begins to come out and tries to assemble in a cluster, so its hot-strengthening capability has greatly weakened. FeNiAl_9 phase and AlCuNi phase, which scatter on the matrices and the crystal boundaries, remain unchanged when temperature rises. So they have good effect on the heat-resisting capability of the alloy.

Chapter 8

Alloy of Aluminum-Copper-Manganese Group

Alloy of aluminum-copper-manganese group is a kind of heat-resisting and deformable aluminum alloy, which began to develop in the early 1950's. For alloys of this group, two brand marks, which are used often, are LY16 and LY17. The alloys can be processed into semi-finished items, such as plates materials, stick-shaped pieces, moulds and forged-pieces. The pressure cast and die-forged semi-finished items made of this alloy can be used to make component parts, which can work at 200-300°C, and the plate materials can be processed into welded articles, which can be used to work under constant heat or high temperature.

Section I

Chemical Composition and Phase Formation

The chemical composition of alloy LY16 and LY17 can be found in Table VIII-I:

Table VIII-I Chemical Composition of Aluminum-Copper-Manganese Group Alloy

Brand Mark	Principal Constituents (%)				Impurity no more than (%)					
	Cu	Mn	Mg	Ti	Fe	Si	Mg	Zn	others	total
LY16	6.0~7.0	0.4~0.8	—	0.1~0.2	0.3	0.3	0.05	0.1	0.1	1.05
LY17	6.0~7.0	0.4~0.8	0.25~0.45	0.1~0.2	0.3	0.3	—	0.1	0.1	—

Copper and manganese are the principal constituents of Al-Cu-Mn group alloy. According to what the findings of researches indicate, when ^{its} copper content is 6.0-6.5% this alloy has high recrystallization temperature, and this is good to its heat-resisting capability. The presence of copper helps the alloy to produce a strengthening phase CuAl_2 , which, after quenching and artificial aging, increases the strength of the alloy.

Manganese in the alloy is the important element that insures the heat-resisting capability of the alloy. Manganese in aluminum has small coefficient of diffusion and it can also lower the coefficient of diffusion of copper in aluminum. As a result, not only is the decomposition tendency of $\alpha(\text{Al})$ diminished, and the congregation tendency of CuAl_2 under high temperature is also reduced. When manganese content is .4-0.5%, there will be a $\text{T}(\text{CuMn}_2\text{Al}_{12})$ phase formed in the alloy. The dispersed and fine $\text{T}(\text{CuMn}_2\text{Al}_{12})$ phase has good effect to the heat-resisting capability of the alloy. Following the increase of manganese content, not only is the quantity of $\text{T}(\text{CuMn}_2\text{Al}_{12})$ increased and it also becomes bulky in size. When manganese content reaches 1.2%, because the quantity of $\text{T}(\text{CuMn}_2\text{Al}_{12})$ phase is increased, the phase area will, as a result, be expanded. Then its diffusibility is speeded up, and the heat-resisting capability of the alloy is reduced. The manganese content in the alloy is therefore regulated to be 0.4-0.8%. Besides, the addition of manganese lowers the cracking tendency when the alloy is used in welding.

When titanium is added, not only it helps to make the crystal grain finer during casting, and it can also raise the recrystallization

temperature of the alloy. Besides, it can help to reduce the decomposition tendency of the supersaturated solid solution whether there is stress or not, and make the structure of the alloy stable under high temperature. When titanium content is 0.2%, a chemical compound $TiAl_3$ of high fusing point is formed. When the content increases to 0.3%, $TiAl_3$ will show a coarse acicular shape. At this point, the heat-resisting capability of the alloy becomes low. Therefore, titanium content in this alloy is decided to be 0.1-0.2%.

Because magnesium can act to lower the weldability of alloy LY16, its content must be controlled at the level below 0.05%. If 0.25-0.45% of magnesium is added, the strength of alloy LY17 under room temperature will be promoted. This is good in improving the heat-resisting capability of the alloy at 150-250°C, but it is not good to the weldability of the alloy.

The impurity zinc can accelerate the speed of diffusion of copper in aluminum, so it is not good to the alloy. Iron can, together with copper contained in the alloy, form Cu_2FeAl_7 , and lower copper concentration in $\alpha(Al)$. Thus, the quality of the alloy under room temperature and high temperature is lowered, so its content should be controlled at the level below 0.3%. Silicon can lower the high temperature durability of the alloy at 300°C. So zinc, iron and silicon should all be regarded as impurities and put under control.

Based on the Equilibrium Diagram of Al-Cu-Mn group alloy (Figure VIII-1) and the chemical composition of the alloy, alloy LY16 lies in

$\alpha(\text{Al}) + \text{CuAl}_2 + \text{CuMn}_2\text{Al}_{12}$, three phase zones. $\text{CuMn}_2\text{Al}_{12}$ is the solid solution of copper in MnAl_4 , and its structural formula has recently been made as $\text{CuMn}_2\text{Al}_{12}$. After, the alloy fused at 750°C and gradually cooled down to 400°C , then quenched in water. At this time, phases $\alpha(\text{Al})$, $\text{T}(\text{CuMn}_2\text{Al}_{12})$, CuAl_2 , CuFeAl_7 and $(\text{FeMn})\text{Al}_6$ are formed.

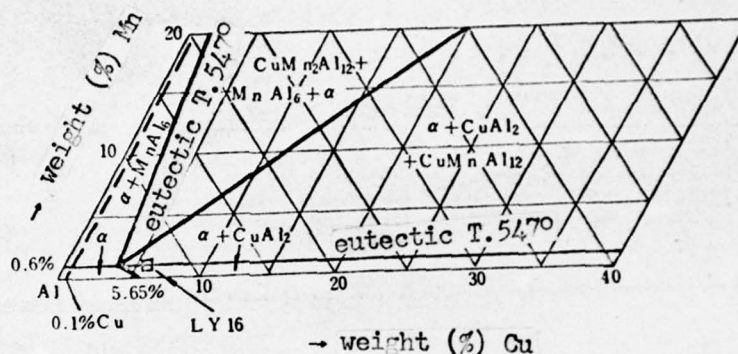


Figure VIII-I Distribution of dependent aluminum angle solid phase zone of Al-Cu-Mn group alloy.

Through metallographic and microprobe examination, it was pointed out that the phases mentioned above also exist in semicontinuous cast ingot. But most of them are $\alpha(\text{Al}) + \text{CuAl}_2$ binary eutecticum, next are $\alpha(\text{Al}) + \text{CuAl}_2 + \text{T}(\text{CuMn}_2\text{Al}_{12})$ ternary eutecticum, a few $(\text{FeMn})\text{Al}_6$ and Cu_2FeAl_7 can be seen only on the deviated swellings of cast ingot. Because titanium content in this alloy is relatively small, TiAl_3 is so tiny that it is hard to be recognized.

CuAl₂ phase: When it is in the process of gradual crystallization, $\alpha(\text{Al}) + \text{CuAl}_2$ eutecticum appears in a shape of honeycomb (see Figure

VIII-5 through VIII-11). Under semicontinuous casting, $\alpha(\text{Al}) + \text{CuAl}_2$ eutecticum maintains in the shape of bar and honeycomb, and also some in the shape of sphere or bar (see Figure VIII-12 through VIII-15). For their characteristics, see Chapter 4, Alloy of Al-Cu-Mg-Mn Group.

T($\text{CuMn}_2\text{Al}_{12}$) phase: Under condition of gradual cooling, it appears in the shape of bar and irregular cakes. Before corroding, its color is grey, and after corroding in 0.5% HF liquid solution at room temperature for 5 seconds, it becomes brown. If it is corroded in liquid solution of 20ml HCl + 20ml HNO_3 + 5ml HF + 55ml H_2O at room temperature for 1-2 seconds, it becomes blue. This color response of T phase is the unique feature of the deformable aluminum alloy.

(FeMn) Al_6 phase: For detail, see Chapter 3, Alloy of Al-Mn Group.

Cu_2FeAl_7 phase: Before corroding, it is of a light grey color and an acicular shape. It is insensitive to various corroding agents.

The phase formation of alloy LY17 is similar to that of alloy LY16.

Section 2

Characteristics of Heat Treatment

The characteristics of this kind of alloy after heat treatment are twofold: 1. It has high hot strengthening property, and 2. Its pressure castings show no pressed effect.

1. Hot Strengthening Property of the Alloy

The effect of natural aging to this kind of alloy is much less noticeable than that of artificial aging. Under conditions of artificial aging, the alloy has relatively high strength and high heat-resisting capability. The quenching temperature of alloy LY16 is 535°C, at 160-170°C and retaining the temperature for 10-16 hours, artificial aging can take place. The quenching temperature of alloy LY17 is 520°C, and its procedures of artificial aging are similar to that of LY16.

At the same time, this alloy can have two opposite processes when quench heating takes place. One is that the eutectic structure of $\alpha(\text{Al}) + \text{CuAl}_2$ and $\alpha(\text{Al}) + \text{CuAl}_2 + \text{T}(\text{CuMn}_2\text{Al}_{12})$ is dissolved in $\alpha(\text{Al})$, and after quenching, there comes super-saturated solid solution $\alpha(\text{Al})$. During artificial aging, the alloy is strengthened. The other is that from solid solution $\alpha(\text{Al})$ separates $\text{T}(\text{CuMn}_2\text{Al}_{12})$ phase, which contains manganese, and it disperses on the matrices of $\alpha(\text{Al})$ like a number of small dots.

From the data in Table VIII-2, it can be seen that the microhardness of $\text{T}(\text{CuMn}_2\text{Al}_{12})$ phase under high temperature is higher than that of CuAl_2 , but the percentage of softening under high temperature and long-period of loading is smaller than that of CuAl_2 . Following the increase of phase content, T phase can promote the durable hardness of the alloy under high temperature more noticeably than CuAl_2 can (see Figure VIII-2 and Figure VIII-3).

Table VIII-2 Microhardness of $T(\text{CuMn}_2\text{Al}_{12})$ and CuAl_2 at 20°C . and 300°C .

chemical compound	microhardness H_v (kg./mm ²)							
	at 20°C load -ing (30sec)	300°C						
		load -ing (30sec)	load -ing (30min)	load -ing (60min)	difference of hardness when loading for 30sec. and 30min.			
					difference (%)		difference (%)	
CuAl_2	531	481	266	201	215	44.4	280	58.2
$T(\text{CuMn}_2\text{Al}_{12})$	628	628	534	452	94	15	176	28.02

It must be pointed out that alloy LYL6 at 525°C and after having retained that temperature for 24 hours, CuAl_2 in the eutectic remnants has apparently gathered together, but there is no obvious change in the form of $T(\text{CuMn}_2\text{Al}_{12})$ (see Figure VIII-21). It is therefore evident that $T(\text{CuMn}_2\text{Al}_{12})$ phase has higher stability than CuAl_2 phase and it is not easy to congregate under high temperature.

To sum up what has been mentioned above, after quench artificial aging, the alloy, on the one hand, due to the strengthening of solid solution of CuAl_2 , begins to have relatively high degree of strength under room temperature; and, on the other hand, due to the strengthening of diffusibility of $T(\text{CuMn}_2\text{Al}_{12})$, it begins to have high heat-resisting capability. So, although the strength of this alloy under room temperature is smaller than that of alloy LYL2, LYL4, and LD10, its hot strengthening ability is much higher than that of hard aluminum-type alloy at high temperature of $225-250^\circ\text{C}$.

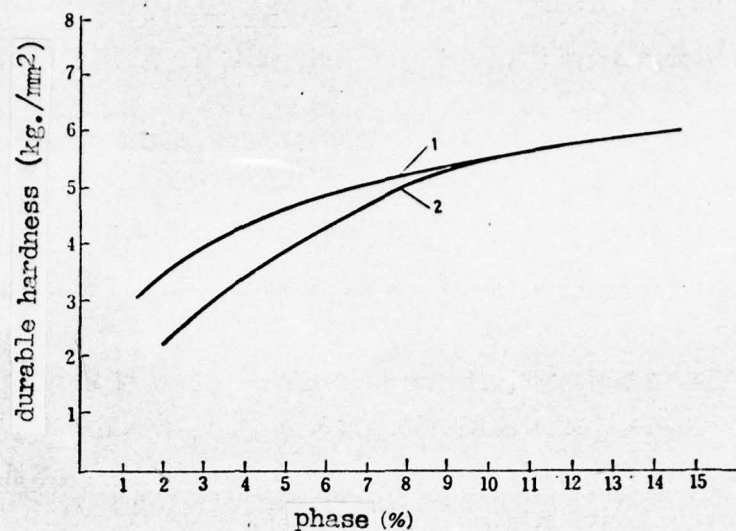


Figure VIII-2 The relationship between durable hardness of the alloy at 300°C and phase content after quenching and stabilizing.
1 - $T(\text{CuMn}_2\text{Al}_{12})$ phase; 2 - CuAl_2 phase

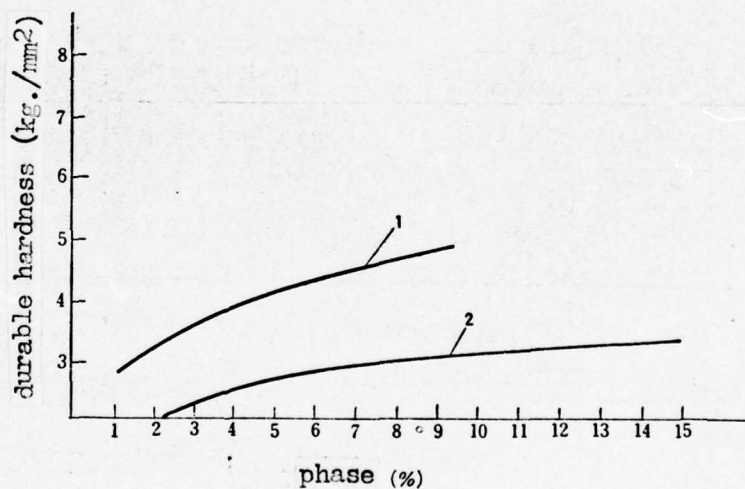


Figure VIII-3 The relationship between durable hardness of the alloy at 350°C and phase content after quenching and stabilizing.
1 - $T(\text{CuMn}_2\text{Al}_{12})$ phase; 2 - CuAl_2 phase

2. No Pressed Effect on Pressure Castings

Although manganese content in alloy LY16 is similar to that in LY12, in production, however, no pressed effect can be found on the quench-finished articles. When 25 x 16 mm. pressed cast belt items (press temperature is 320-450°C) and 3.0 mm. cold reduced plates are respectively given heat treatment according to the following procedures:- belt items at 535°C and retaining the temperature for one hour, take quenching in water, and at 165°C take artificial aging for 16 hours; the plates at 535°C and retaining the temperature for 20 minutes, take quenching in water, and at 165°C take artificial aging for 14 hours. The results of testing the mechanical property of these two items can be found in Table VIII-3 and VIII-4.

Table VIII-3 The Longitudinal Mechanical Property of
25 x 16 mm. Pressure Cast Belt Item of Alloy
LY16 After Quenching and Artificial Aging.

testing specimen position	testing specimen No.	$\sigma_{0.2}$ (kg./mm ²)	σ_b (kg./mm ²)	δ (%)
belt head	1	33.5	43.2	22.7
	2	32.4	43.4	20.5
	3	30.6	43.4	20.0
belt tail	4	31.3	44.4	20.0
	5	30.3	43.5	20.5
	6	31.4	43.6	20.5

Table VIII-4 The Longitudinal Mechanical Property of
3.0 mm. Cold Reduced Plate of Alloy LY16
After Quenching and Artificial Aging.

testing speci- men No.	$\sigma_{0.2}$ (kg./mm ²)	σ_b (kg./mm ²)	δ (%)
1	32.6	45.9	14.8
2	33.5	45.6	14.0
3	32.6	45.5	16.3
4	32.6	45.5	16.3
5	31.5	45.2	16.5
6	33.7	45.2	16.3
平均	32.6	45.5	15.7

From the above Tables it can be known that the longitudinal strength of the pressure cast belt items is almost the same as that of the plates, and the extensibility of the belt item is higher than that of the plate. The result of X-ray analysis has pointed out that the belt item when it is under pressing, it has begun to recrystallize (see Figure VIII-4a). After quenching and artificial aging, it has completely recrystallized and the crystal grains are coarse and large (see Figure VIII-4b). The plate when it is under pressing does not recrystallize (see Figure VIII-4c), but after quenching and artificial aging, it will have completely recrystallized (see Figure VIII-4d), but the crystal grains are fine and small.

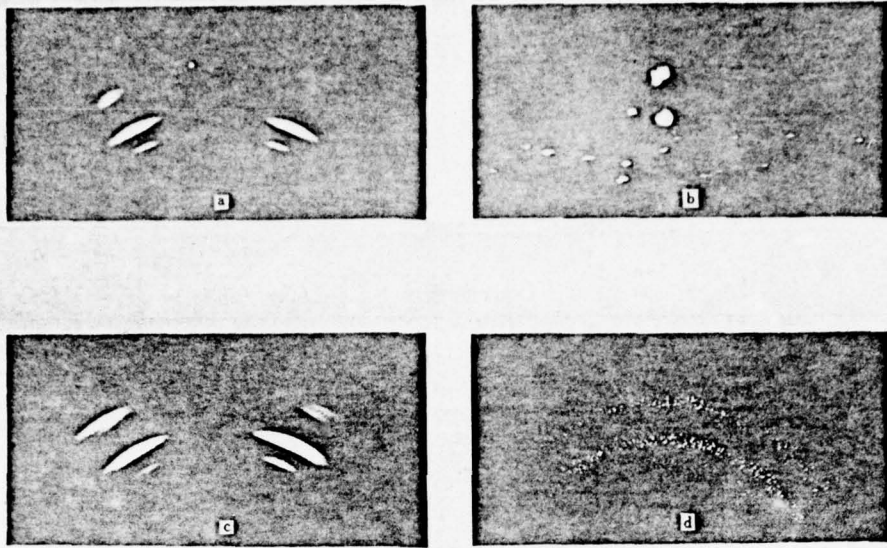


Figure VIII-4 X-ray Photograph of Recrystallization of Alloy LY16 Pressure Cast Belt Item and Cold Reduced Plate.

- a - 25 x 6 mm. pressure cast belt item under pressing has begun to recrystallize;
- b - 25 x 6 mm. pressure cast belt item under the condition of quenching and artificial aging has completely recrystallized, and the grains are coarse and large;
- c - 3.0 mm. cold reduced plate under cold pressing recrystallization does not take place;
- d - 3.0 mm. cold pressure plate under the condition of quenching and artificial aging has completely recrystallized, and the grains are fine and small.

Section 3

The Structure of Cast Ingots and Processed Articles

1. Phase Formation

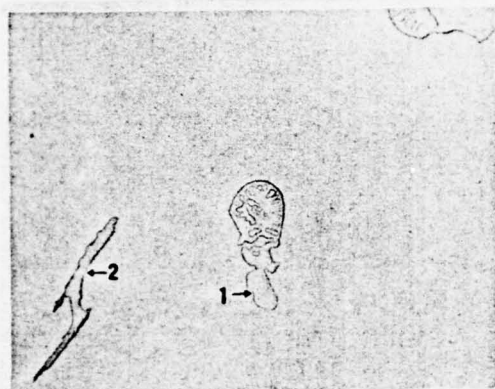


Figure VIII-5

210x

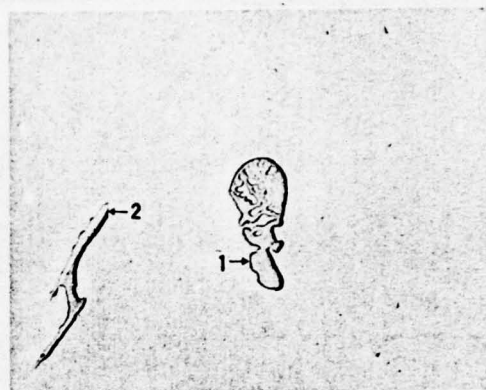


Figure VIII-6

210x

Alloy	LY16
Condition	Cast ingot after fusing at 750°C, gradually cooled to 650°C, then in furnace cooled to 400°C and quenching in water.
Corrosion	Not corroded.
Features of Structure	1 - CuAl ₂ in eutecticum displays weak pink color; 2 - Cu ₂ FeAl ₇ displays bright grey color.

Alloy	LY16
Condition	Same as in Figure VIII-5
Corroding Agent	25% HNO ₃ liquid solution.
Features of Structure	1 - CuAl ₂ displays copper-red color; 2 - Cu ₂ FeAl ₇ can not be corroded.

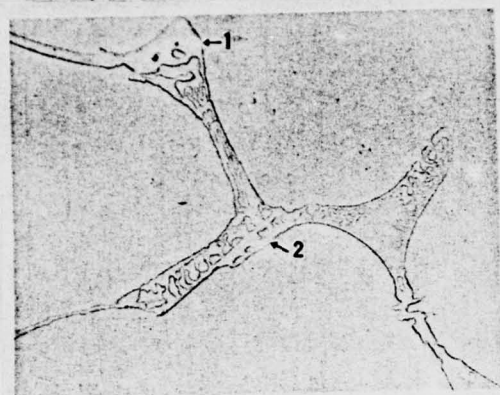


Figure VIII-7 210x

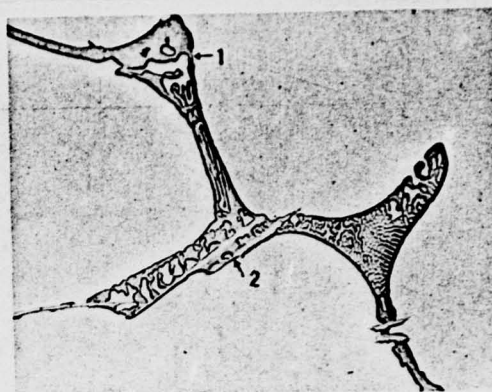


Figure VIII-8 210x

Alloy	LY16
Condition	Same as in Figure VIII-5
Corrosion	Not corroded
Features of Structure	1 - CuAl ₂ displays weak pink color; 2 - Cu ₂ FeAl ₇ displays bright grey color.

Alloy	LY16
Condition	Same as in Figure VIII-5
Corroding Agent	25% HNO ₃ liquid solution
Features of Structure	1 - CuAl ₂ displays copper-red color; 2 - Cu ₂ FeAl ₇ displays bright grey color.

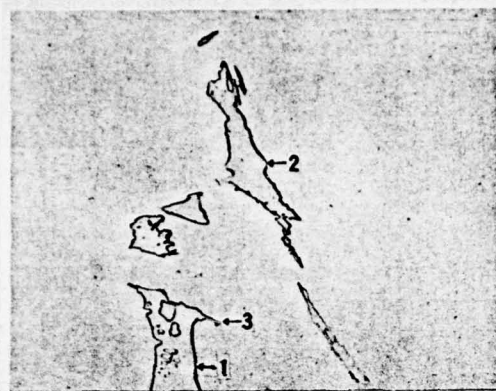


Figure VIII-9

210x

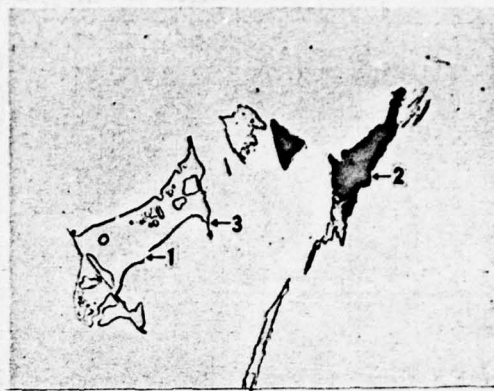


Figure VIII-10

210x

Alloy	LY16
Condition	Same as in Figure VIII-5
Corrosion	Not corroded
Features of Structure	<p>1 - CuAl_2 displays weak pink color;</p> <p>2 - $\text{T}(\text{CuMn}_2\text{Al}_{12})$ displays grey color;</p> <p>3 - Cu_2FeAl_7 displays bright grey color.</p>

Alloy	LY16
Condition	Same as in Figure VIII-5
Corroding Agent	20 ml. HCl + 20 ml. HNO_3 + 5ml. HF + 55ml. H_2O
Features of Structure	<p>1 - CuAl_2 can not be corroded;</p> <p>2 - $\text{T}(\text{CuMn}_2\text{Al}_{12})$ phase displays blue color;</p> <p>3 - Cu_2FeAl_7 can not be corroded.</p>

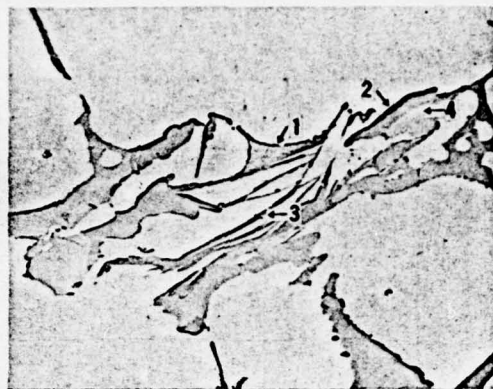


Figure VIII-11

210x

Alloy	LY16
Condition	Same as in Figure VIII-5
Corrosion	Not corroded
Features of Structure	<p>1 - $\alpha(\text{Al}) + \text{CuAl}_2$ binary eutecticum;</p> <p>2 - $\text{T}(\text{CuMn}_2\text{Al}_{12})$ displays grey color;</p> <p>3 - Cu_2FeAl_7 of acicular shape and bright grey color;</p> <p>4 - $(\text{FeMn})\text{Al}_6$ displays bright grey color.</p>

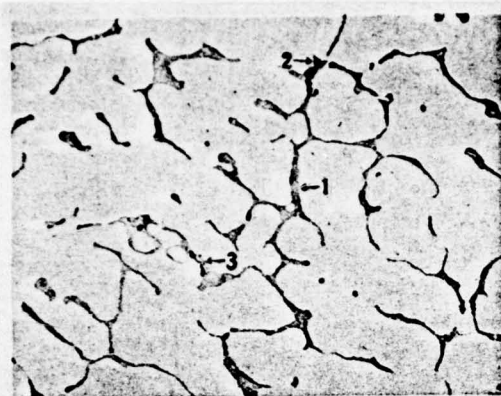


Figure VIII-12

210x

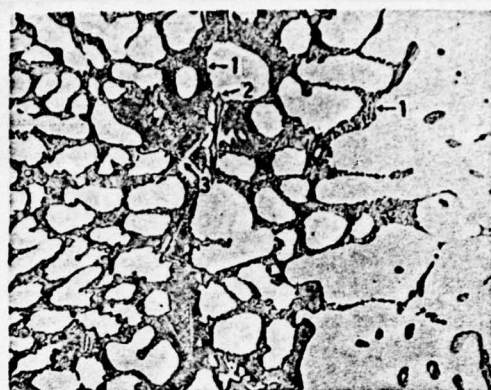


Figure VIII-13

210x

Alloy	LY16
Condition	Semicontinuous casting
Corroding Agent	Mixed acid liquid solution
Features of Structure	<p>1 - $\alpha(\text{Al}) + \text{CuAl}_2$ binary eutecticum of honeycomb shape;</p> <p>2 - $\text{T}(\text{CuMn}_2\text{Al}_{12})$ displays dark brown color;</p> <p>3 - $(\text{FeMn})\text{Al}_6$ displays bright grey color.</p>

Alloy	LY16
Condition	Same as in Figure VIII-12
Corroding Agent	25% HNO_3 liquid solution
Features of Structure	<p>Microstructure of the segregated swellings on the surface of the cast ingot</p> <p>1 - $\alpha(\text{Al}) + \text{CuAl}_2$ binary eutecticum of honeycomb shape;</p> <p>2 - $(\text{FeMn})\text{Al}_6$ displays grey color;</p> <p>3 - Cu_2FeAl_7 of acicular shape and grey color.</p>

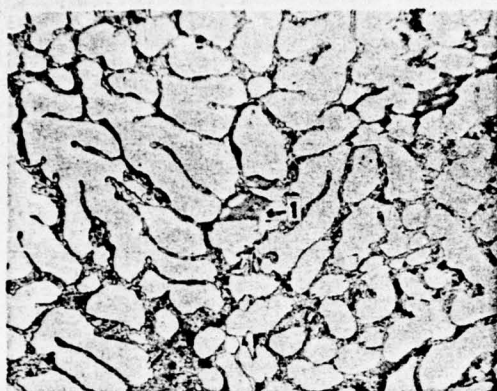


Figure VIII-14

210x

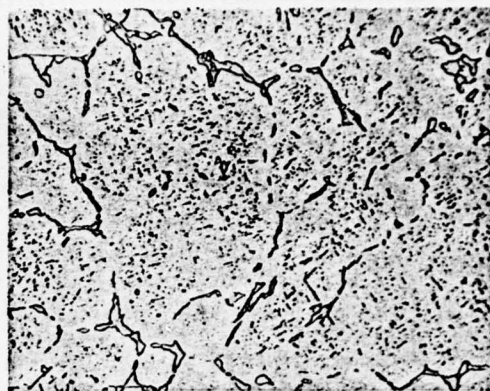


Figure VIII-15

210x

Alloy	LY16
Condition	Same as in Figure VIII-12
Corroding Agent	10g. NaOH + 100ml. H ₂ O solution (20°C)
Features of Structure	1 - (FeMn)Al ₆ displays grey cake-shapes.

Alloy	LY16
Condition	Under condition of homogenizing (525°C soaking for 24 hours, then cooling in furnace)
Corroding Agent	Mixed acid liquid solution
Features of Structure	Besides eutectic structure of $\alpha(\text{Al}) + \text{CuAl}_2$ remaining in the alloy, the acicular shaped fragments of decomposed CuAl_2 and dispersed particles from $\text{T}(\text{CuMn}_2\text{Al}_{12})$ closely spread on the matrices of $\alpha(\text{Al})$.

2. The Structure of Cast Ingots

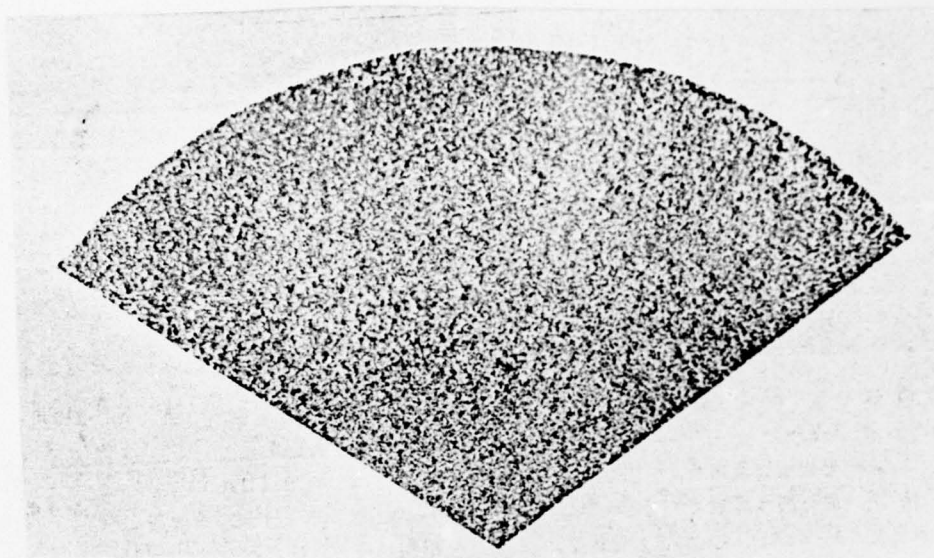


Figure VIII-16

Alloy and Condition
Specification
Corroding Agent
Features of Structure

LY16 semicontinuous casting
ø 172 mm. round ingot
15% NaOH liquid solution
The transverse macroscopical structure
of a cast ingot. There are fine isometric
crystals from the edge to the center.

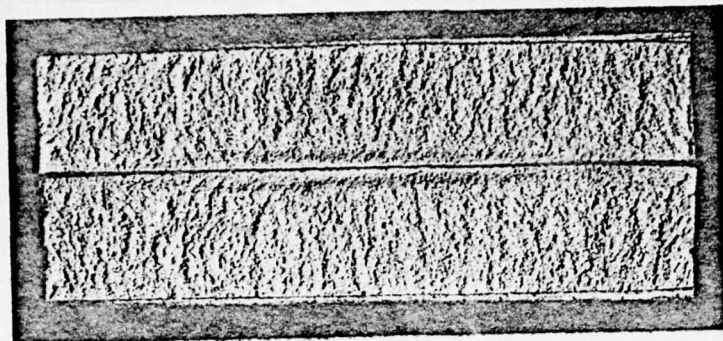


Figure VIII-17

1
— x
2

Alloy and Condition
Specification
Features of Structure

LY16 semicontinuous casting
ø 172mm. round cast ingot
The structure of fractures of
a cast ingot, and the structure
is homogeneous and fine.

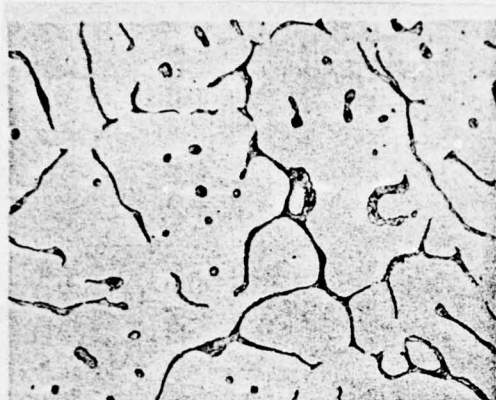


Figure VIII-18

210x

Corrosion of Mixed Acid
Liquid Solution



Figure VIII-19

210x

Corrosion of Mixed Acid
Liquid Solution

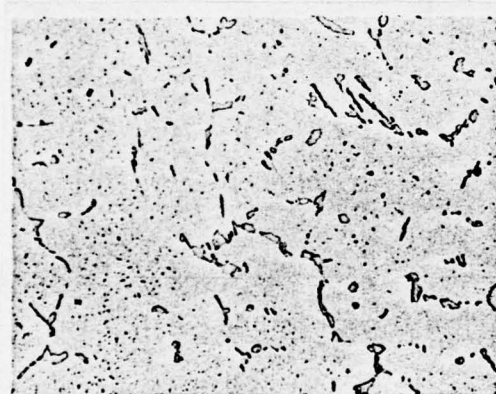


Figure VIII-20

210x

Alloy and Condition

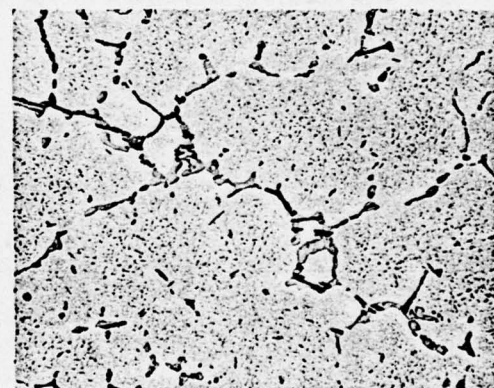


Figure VIII-21

210x

Specification

LY16. Figure VIII-18 and VIII-19 show the condition of semicontinuous casting; Figure VIII-20 and VIII-21 show the condition of homogenizing (525°C, 24 hours, cooled in furnace).
 ϕ 172mm. round cast ingot
 (contd.)

Features of Structure

Figure VIII-18 illustrates the transverse structure of the edge of a cast ingot. The meshes of the dendritic crystal are big and the network is thin;

Figure VIII-19 illustrates the transverse structure of the central part of a cast ingot. The meshes of the dendritic crystal are very small and the network is relatively thick.

Figure VIII-20 and VIII-21 show the condition of homogenizing and the eutectic structure remains. There are acicular shaped and dot-shaped phases of CuAl_2 and $\text{T}(\text{CuMn}_2\text{Al}_{12})$ segregated from the matrices of $\alpha(\text{Al})$. Of the remnants on the network of dendritic crystal, CuAl_2 from honeycomb shape, in casting assembles into cake shape, and $\text{T}(\text{CuMn}_2\text{Al}_{12})$ phase shows no obvious change.

3. The Structure of Plates

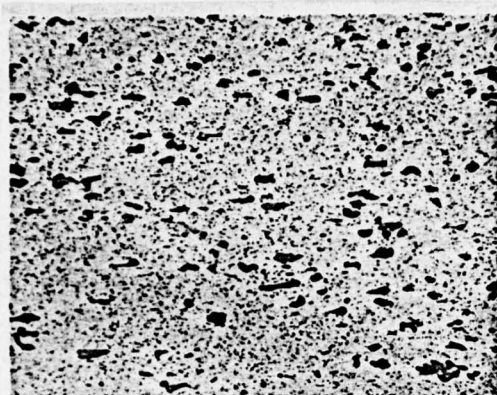


Figure VIII-22

210x

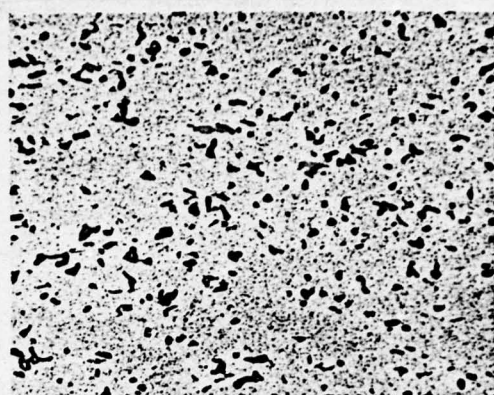


Figure VIII-23

210x

Corrosion of Mixed Acid
Liquid Solution

Corrosion of Mixed Acid
Liquid Solution

Alloy and Condition
Specification
Features of Structure

LY16R

8.0 mm. thick

Figure VIII-22 illustrates the longitudinal structure of the central part of a plate. When the chemical compounds are broken they arrange themselves in row along the direction of pressure extension. Among them the black ones are $T(CuMn_2Al_{12})$ phase and the grey ones are $CuAl_2$. On the matrices of $\alpha(Al)$, there are segregated particles of $CuAl_2$ and $T(CuMn_2Al_{12})$.

Figure VIII-23 illustrates the transverse structure of the central part of a plate.

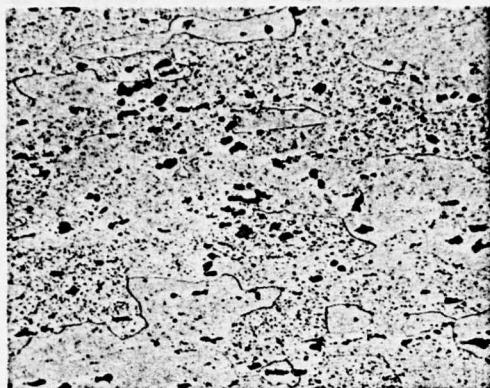


Figure VIII-24 210x

Corrosion of Mixed Acid
Liquid Solution

Alloy and Condition
Specification
Features of Structure

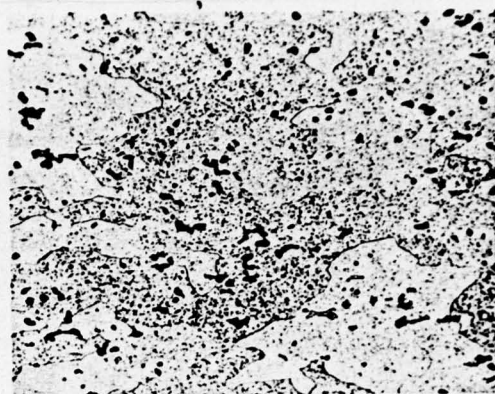


Figure VIII-25 210x

Corrosion of Mixed Acid
Liquid Solution

LY16CS
8.0 mm. thick
Figure VIII-24 illustrates the longitudinal structure of the central part of a plate. The alloy has completely recrystallized and the soluble chemical compounds have partially been in solid solution but the remnants arrange themselves in row along the direction of pressure extension. On the matrices of $\alpha(\text{Al})$, there are segregated particles of T(CuMn₂Al₁₂) phase.

Figure VIII-25 illustrates the transverse structure.

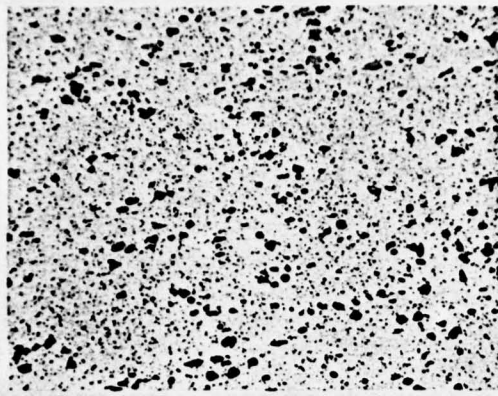


Figure VIII-26

210x

Corrosion of Mixed Acid
Liquid Solution

Alloy and Condition
Specification
Features of Structure

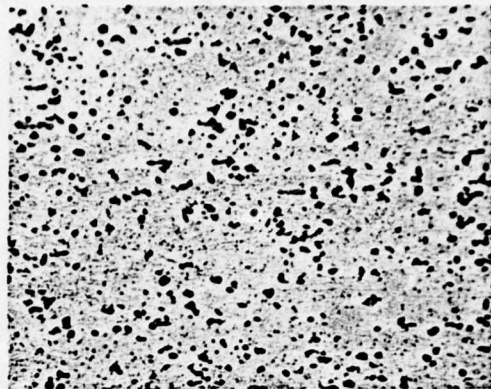


Figure VIII-27

210x

Corrosion of Mixed Acid
Liquid Solution

LY16Y
3.0 mm. thick
Figure VIII-26 illustrates the longitudinal structure of the central part of a plate. The chemical compounds are obviously broken into fragments and the fragments arrange themselves along the direction of pressure extension. On the matrices of $\alpha(\text{Al})$, there are great many segregated particles of CuAl_2 .

Figure VIII-27 illustrates the transverse structure.

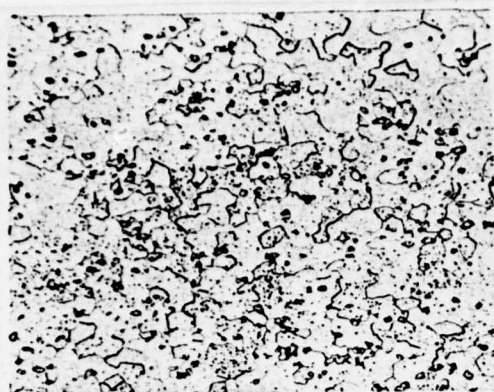


Figure VIII-28

210x

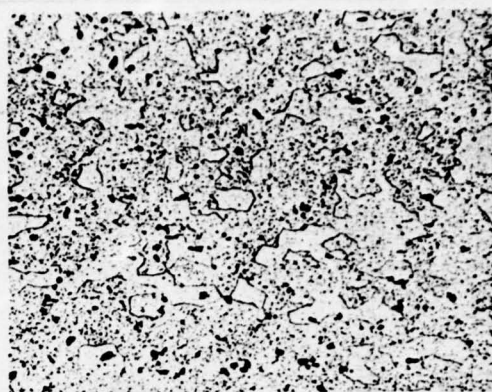


Figure VIII-29

210x

Corrosion of Mixed Acid
Liquid Solution

Corrosion of Mixed Acid
Liquid Solution

Alloy and Condition
Specification
Features of Structure

LY16CS
3.0 mm. thick
Figure VIII-28 illustrates the longitudinal structure of the central part of a plate. The alloy has completely recrystallized and a great amount of phase particles segregated from the chemical compound are in solid solution. The remaining soluble phase becomes remarkably few. On the matrices of α (Al), there are more segregated particles of $T(CuMn_2Al_{12})$.

Figure VIII-29 illustrates the transverse structure.

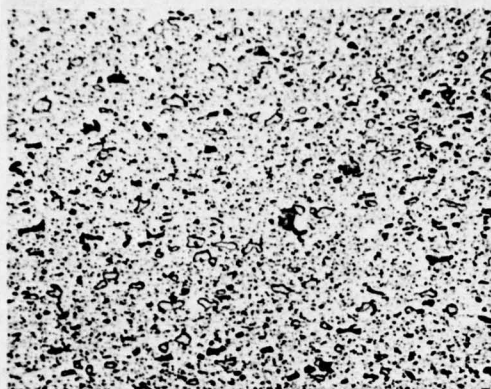


Figure VIII-30

210x

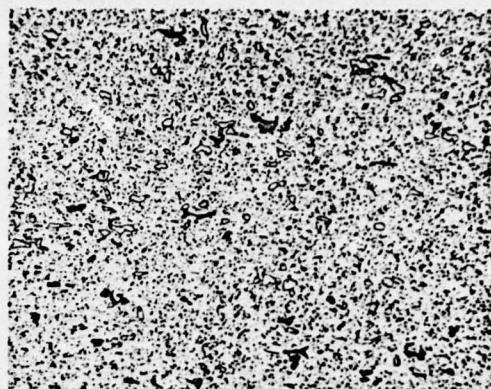


Figure VIII-31

210x

Corrosion of Mixed Acid
Liquid Solution

Corrosion of Mixed Acid
Liquid Solution

Alloy and Condition
Specification
Features of Structure

LY17R

5.0 mm. thick

Figure VIII-30 illustrates the longitudinal structure of a plate. The chemical compounds have been broken into pieces and the pieces arrange themselves along the direction of pressure extension. The dark ones are $T(CuMn_2Al_{12})$ phase and the bright ones are $CuAl_2$ phase. On the matrices of $\alpha(Al)$, there are particles segregated from $CuAl_2$ and T phase.

Figure VIII-31 illustrates the transverse structure.

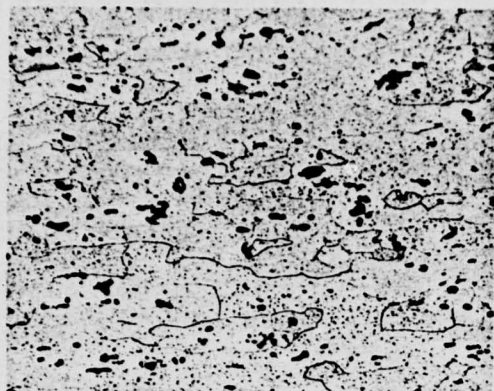


Figure VIII-32 210x

Corrosion of Mixed Acid
Liquid Solution

Alloy and Condition
Specification
Features of Structure

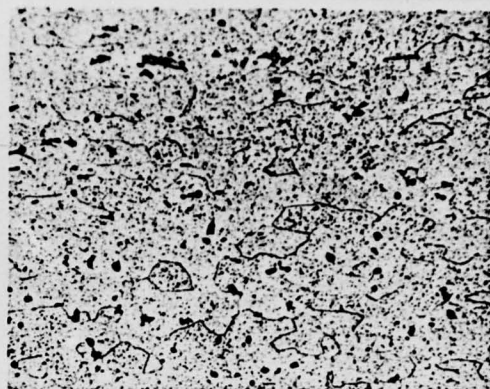


Figure VIII-33 210x

Corrosion of Mixed Acid
Liquid Solution

LYL7CS
5.0 mm. thick
Figure VIII-32 illustrates the longitudinal structure of a plate. The alloy has completely recrystallized, and the remnant soluble phases arrange themselves along the direction of pressure extension. On the matrices of $\alpha(\text{Al})$, there are more particles segregated from $\text{T}(\text{CuMn}_2\text{Al}_{12})$ phase.

Figure VIII-33 illustrates the transverse structure.

4. The Structure of Pressure Castings

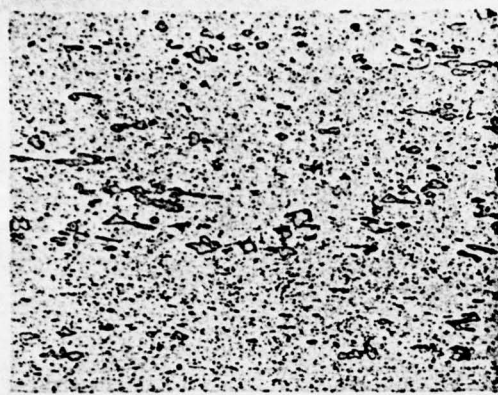


Figure VIII-34

210x

Corrosion of Mixed Acid
Liquid Solution

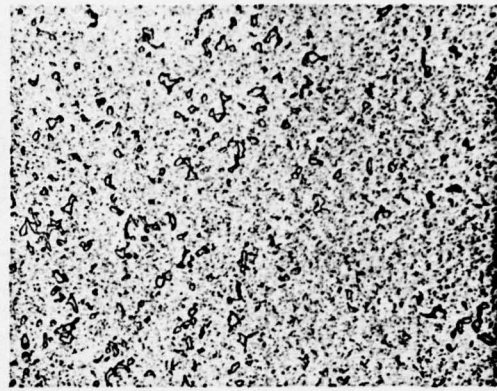


Figure VIII-35

210x

Corrosion of Mixed Acid
Liquid Solution

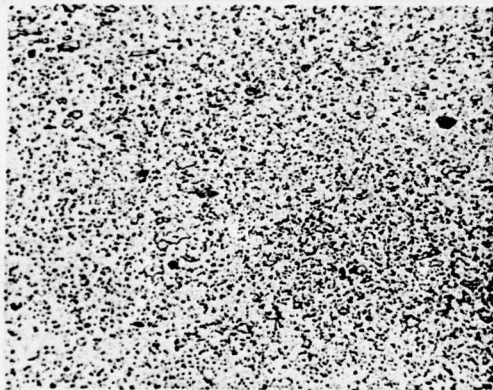


Figure VIII-36

210x

Corrosion of Mixed Acid
Liquid Solution

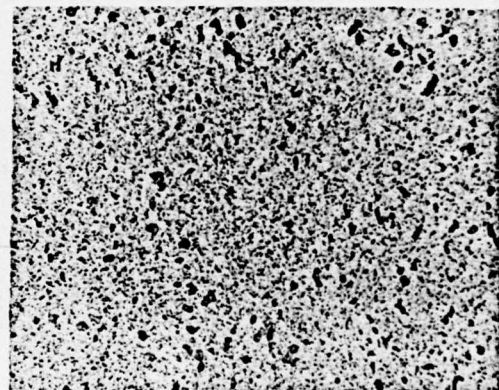


Figure VIII-37

210x

Corrosion of Mixed Acid
Liquid Solution

Alloy and Condition
Specification

LY16R
25 x 16 mm. belt item

(contd.)

Features of Structure

Figure VIII-34 illustrates the longitudinal structure of the central part of the far front end of a belt item. The chemical compounds are broken into pieces, and the pieces arrange themselves along the direction of pressure extension. The black ones are $T(CuMn_2Al_{12})$ phase and the white and bright ones are $CuAl_2$. From the matrices of $\alpha(Al)$ separate great many dispersing particles of $T(CuMn_2Al_{12})$ and $CuAl_2$.

Figure VIII-35 illustrates its transverse structure.

Figure VIII-36 illustrates the structure of the central part of the rear end of the belt item. The degree of decomposition of the chemical compounds is greater than that of the far front end, but the directionality of arranging the fragments along the direction of pressure extension is weaker.

Figure VIII-37 illustrates its transverse structure.

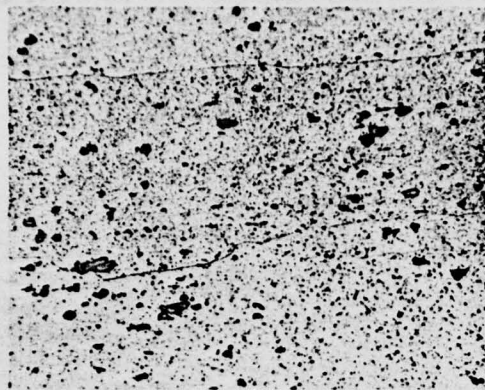


Figure VIII-38

210x

Corrosion of Mixed Acid
Liquid Solution

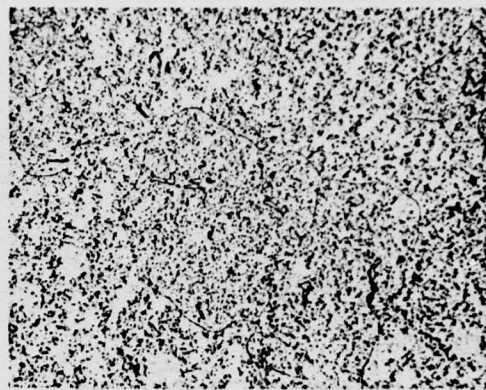


Figure VIII-39

210x

Corrosion of Mixed Acid
Liquid Solution

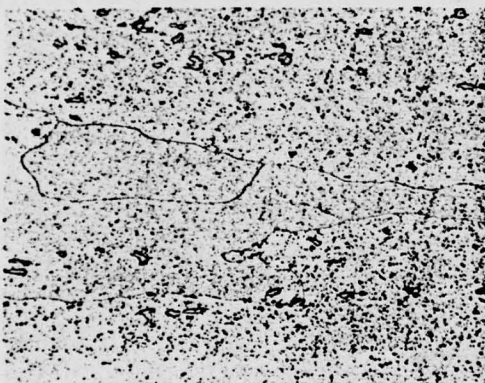


Figure VIII-40

210x

Corrosion of Mixed Acid
Liquid Solution

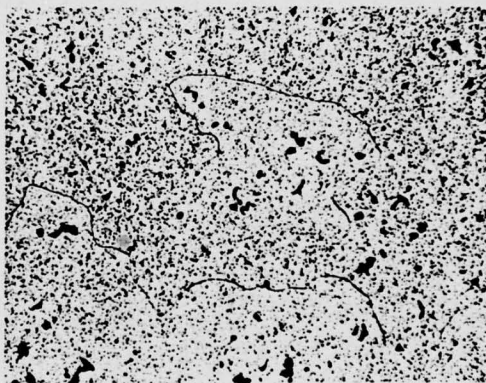


Figure VIII-41

210x

Corrosion of Mixed Acid
Liquid Solution

Alloy and Condition
Specification
Features of Structure

LY16CS
25 x 16 mm. belt item
Figure VIII-38 illustrates the longitudinal
structure of the central part (contd.)

of the far front end of a belt item. The alloy has completely recrystallized, and the grains are coarse and large and they grow along the direction of pressure. The soluble phases are already in solid solution and the remnant chemical compounds arrange themselves along the direction of pressure extension. Among them, CuAl_2 phase is white and bright and $\text{T}(\text{CuMn}_2\text{Al}_{12})$ phase is dark brown.

Figure VIII-39 illustrates its transverse structure.

Figure VIII-40 illustrates the longitudinal structure of the central part of the rear end of the belt item. Its recrystallized grains are finer and smaller than those of the far front end and grow along the direction of pressure. The remnant and soluble chemical compounds are smaller than at the front end.

Figure VIII-41 illustrates its transverse structure.

APPENDICES

Appendix 1. Chemical Composition of Deformable Aluminum Alloy

Number of Order	Alloy Group	Kind of Heat Treatment	Brand of Alloy	Symbol
1	pure aluminum	heat treatment of non-strengthening alloy	No.1 industrial highly pure Al	L 0
2	pure aluminum	heat treatment of non-strengthening alloy	No.2 industrial highly pure Al	L 00
3	pure aluminum	heat treatment of non-strengthening alloy	No.1 industrial pure aluminum	L 1
4	pure aluminum	heat treatment of non-strengthening alloy	No.2 industrial pure aluminum	L 2
5	pure aluminum	heat treatment of non-strengthening alloy	No.3 industrial pure aluminum	L 3
6	pure aluminum	heat treatment of non-strengthening alloy	No.4 industrial pure aluminum	L 4
7	pure aluminum	heat treatment of non-strengthening alloy	No.5 industrial pure aluminum	L 5
8	pure aluminum	heat treatment of non-strengthening alloy	No.6 industrial pure aluminum	L 6
9	pure aluminum	heat treatment of non-strengthening alloy	No.7 industrial pure aluminum	L 7
10	Al-Mg	heat treatment of non-strengthening alloy	No.1 rust-proof aluminum	LF1
11	Al-Mg	heat treatment of non-strengthening alloy	No.2 rust-proof aluminum	LF2
12	Al-Mg	heat treatment of non-strengthening alloy	No.3 rust-proof aluminum	LF3
13	Al-Mg	heat treatment of non-strengthening alloy	No.5 rust-proof aluminum	LF5
14	Al-Mg	heat treatment of non-strengthening alloy	No.6 rust-proof aluminum	LF6
15	Al-Mg	heat treatment of non-strengthening alloy	No.7 rust-proof aluminum	LF7
16	Al-Mg	heat treatment of non-strengthening alloy	No.10 rust-proof aluminum	LF10
17	Al-Mg	heat treatment of non-strengthening alloy	No.11 rust-proof aluminum	LF11
18	Al-Mg	heat treatment of non-strengthening alloy	No.21 rust-proof aluminum	LF21
19	Al-Cu-Mg	heat treatment of strengthening alloy	No.1 hard aluminum	LY1
20	Al-Cu-Mg	heat treatment of strengthening alloy	No.2 hard aluminum	LY2
21	Al-Cu-Mg	heat treatment of strengthening alloy	No.6 hard aluminum	LY6

Appendix 1. (continued)

(a)

Chemical Composition (%)								
Principal Constituents								
copper	magnesium	manganese	zinc	iron	nickel	silicon	chromium	titanium
-	-	-	-	-	-	-	-	-
-	-	-	-	-	-	-	-	-
-	-	-	-	-	-	-	-	-
-	-	-	-	-	-	-	-	-
-	-	-	-	-	-	-	-	-
-	-	-	-	-	-	-	-	-
-	-	-	-	-	-	-	-	-
-	-	-	-	-	-	-	-	-
-	-	-	-	-	-	-	-	-
-	-	-	-	-	-	-	-	-
-	-	-	-	-	-	-	-	-
-	0.8-1.3	0.9-1.4	-	-	-	-	-	-
-	2.0-2.8	or or 0.15-0.4	-	-	-	-	-	-
-	3.2-3.8	0.3-0.6	-	-	-	0.5-0.8	-	-
-	4.0-5.5	0.3-0.6	-	-	-	-	-	-
-	5.8-6.8	0.5-0.8	-	-	-	-	Be 0.0001- 0.005	0.02-0.1
-	6.0-7.5	0.3-0.6	-	-	-	-	-	-
-	4.7-5.7	0.2-0.6	-	-	-	-	-	-
-	4.8-5.5	0.3-0.6	-	-	-	-	-	0.02-0.1 0.02-0.2
-	-	1.0-1.6	-	-	-	-	-	-
2.2- 3.0	0.2-0.5	-	-	-	-	-	-	-
2.6- 3.2	2.0-2.4	0.45-0.7	-	-	-	-	-	-
3.8- 4.5	1.7-2.3	0.5-1.0	-	-	-	Be 0.001- 0.005	-	0.03- 0.15

Appendix 1. (continued)

(b)

aluminum	Impurity no more than								total
	iron	silicon	copper	zinc	manganese	Fe + Ni	Fe + Si	other	
99.90	0.06	0.06	0.005	-	-	-	0.095	-	0.10
99.85	0.1	0.08	0.008	-	-	-	0.142	-	0.15
99.7	0.16	0.16	0.01	-	-	-	0.26	-	0.30
99.6	0.25	0.20	0.01	-	-	-	0.36	-	0.40
99.5	0.30	0.30	0.015	-	-	-	0.45	-	0.50
99.3	0.30	0.35	0.05	-	-	-	0.60	0.1	0.7
99.0	0.50	0.50	0.02	-	-	-	0.90	-	1.0
98.8	0.50	0.55	0.1	0.1	0.1	Mg 0.1	1.0	0.1	1.2
98.0	1.1	1.0	0.05	-	-	-	1.8	-	2.0
sur- plus	0.7	0.7	0.1	-	-	-	-	0.1	1.6
sur- plus	0.4	0.4	0.1	-	-	-	0.6	0.1	0.8
sur- plus	0.5	-	0.05	0.2	-	-	-	0.1	0.85
sur- plus	0.5	0.5	0.05	0.2	-	-	-	0.1	-
sur- plus	0.4	0.4	0.1	0.2	-	-	-	0.1	1.2
sur- plus	0.5	0.5	0.05	0.2	-	-	-	-	-
sur- plus	0.4	0.4	0.2	-	-	-	0.6	0.1	1.1
sur- plus	0.5	0.5	0.05	0.2	-	-	-	0.1	1.35
sur- plus	0.7	0.6	0.2	0.1	-	-	Mg 0.05	0.1	1.75
sur- plus	0.5	0.5	-	0.1	0.2	-	-	0.1	1.4
sur- plus	0.3	0.3	-	0.1	-	-	-	0.1	0.8
sur- plus	0.5	0.5	-	0.1	-	-	-	0.1	1.2

Appendix 1. (continued)

(c)

Number of Order	Alloy Group	Kind of Heat Treatment	Brand of Alloy	Symbol
22	Al-Cu-Mg	heat treatment of strengthening alloy	No.9 hard aluminum	LY9
23	Al-Cu-Mg	heat treatment of strengthening alloy	No.10 hard aluminum	LY10
24	Al-Cu-Mg	heat treatment of strengthening alloy	No.11 hard aluminum	LY11
25	Al-Cu-Mg	heat treatment of strengthening alloy	No. 12 hard aluminum	LY12
26	Al-Cu-Mg	heat treatment of strengthening alloy	No.16 hard aluminum	LY16
27	Al-Cu-Mg	heat treatment of strengthening alloy	No.17 hard aluminum	LY17
28	Al-Cu-Mg-Si-Mn	heat treatment of strengthening alloy	No.2 forged aluminum	LD2
29	Al-Cu-Mg-Si-Mn	heat treatment of strengthening alloy	No.5 forged aluminum	LD5
30	Al-Cu-Mg-Si-Mn	heat treatment of strengthening alloy	No.6 forged aluminum	LD6
31	Al-Cu-Mg-Si-Mn	heat treatment of strengthening alloy	No.10 forged aluminum	LD10
32	Al-Cu-Mg-Fe-Ni	heat treatment of strengthening alloy	No.7 forged aluminum	LD7
33	Al-Cu-Mg-Fe-Ni	heat treatment of strengthening alloy	No.8 forged aluminum	LD8
34	Al-Cu-Mg-Fe-Ni	heat treatment of strengthening alloy	No.9 forged aluminum	LD9
35	Al-Zn-Mg-Cu	heat treatment of strengthening alloy	No.3 superhard aluminum	LC3
36	Al-Zn-Mg-Cu	heat treatment of strengthening alloy	No.4 superhard aluminum	LC4
37	Al-Zn-Mg-Cu	heat treatment of strengthening alloy	No.5 superhard aluminum	LC5
38	Al-Zn-Mg-Cu	heat treatment of strengthening alloy	No.6 superhard aluminum	LC6

Appendix 1. (continued)

(d)

Chemical Composition (%)								
Principal Constituents								
copper	magnesium	manganese	zinc	iron	nickel	silicon	chromium	titanium
3.8-4.5	1.2-1.6	0.3-0.7	-	-	-	-	-	-
3.9-4.5	0.15-0.3	0.3-0.5	-	-	-	-	-	-
3.8-4.8	0.4-0.8	0.4-0.8	-	-	-	-	-	-
3.8-4.9	1.2-1.8	0.3-0.9	-	-	-	-	-	-
6.0-7.0	-	0.4-0.8	-	-	-	-	-	0.1-0.2
6.0-7.0	0.25-0.45	0.4-0.8	-	-	-	-	-	0.1-0.2
0.2-0.6	0.45-0.9	0.15-0.35	-	-	-	0.5-1.2	-	-
1.8-2.6	0.4-0.8	0.4-0.8	-	-	-	0.7-1.2	-	-
1.8-2.6	0.4-0.8	0.4-0.8	-	-	-	0.7-1.2	0.01-0.2	0.02-0.1
3.9-4.8	0.4-0.8	0.4-1.0	-	-	-	0.6-1.2	-	-
1.9-2.5	1.4-1.8	-	-	1.0-1.5	1.0-1.5	-	-	0.02-0.1
1.9-2.5	1.4-1.8	-	-	1.1-1.6	1.0-1.5	0.5-1.2	-	-
3.5-4.5	0.4-0.8	-	-	0.5-1.0	1.8-2.3	0.5-1.0	-	-
1.8-2.4	1.2-1.6	-	6.0-6.7	-	-	-	-	0.02-0.08
1.4-2.0	1.8-2.8	0.2-0.6	5.0-7.0	-	-	-	0.1-0.25	-
0.3-1.0	1.2-2.0	0.3-0.8	7.0-8.0	-	-	-	-	-
2.2-2.9	2.5-3.2	0.2-0.5	7.6-8.6	-	-	-	0.1-0.25	-

Appendix 1. (continued)

(e)

aluminum	Impurity no more than								
	iron	silicon	copper	zinc	manganese	Fe + Ni	Fe + Si	other	total
sur-plus	0.5	0.5	-	0.1	-	-	-	0.1	1.2
sur-plus	0.2	0.25	-	0.1	-	-	-	0.1	0.65
sur-plus	0.7	0.7	-	0.3	Ni 0.1	0.7	-	0.1	1.8
sur-plus	0.5	0.5	-	0.3	Ni 0.1	0.5	-	0.1	1.5
sur-plus	0.3	0.3	-	0.1	Mg 0.05 Zr 0.2	-	-	0.1	1.05
sur-plus	0.3	0.3	-	0.1	-	-	-	0.1	-
sur-plus	0.5	-	-	0.2	-	-	-	0.1	0.8
sur-plus	0.7	-	Ni 0.1	0.3	-	0.7	-	0.1	1.1
sur-plus	0.7	-	Ni 0.1	0.3	-	0.7	-	0.1	1.1
sur-plus	0.7	-	Ni 0.1	0.3	-	-	-	0.1	1.2
sur-plus	-	0.35	-	0.3	0.2	-	-	0.1	0.95
sur-plus	-	-	-	0.3	0.2	-	-	0.1	0.6
sur-plus	-	-	-	0.3	0.2	-	-	0.1	0.6
sur-plus	0.2	0.2	-	Cr 0.05	0.1	-	-	0.1	0.65
sur-plus	0.5	0.5	-	-	-	-	-	0.1	1.1
sur-plus	0.6	0.4	-	-	-	-	-	0.3	-
sur-plus	0.5	0.3	-	-	-	-	-	0.1	0.9

Appendix 2 The Crystal Structure of Main

Phase	Crystal Structure	Lattice Constant (Å)			Number of Atoms in Each Cell
		a	b	c	
S CuMgAl ₂ or Cu ₂ Mg ₂ Al ₅ or Cu ₇ Mg ₈ Al ₁₃	face-centered oblique lattice	4.01	9.25	7.15	16
Mg ₂ Si	face-centered cubic lattice	6.351			12
CuAl ₂	body-centered square lattice	6.066		4.874	12
MgZn ₂	hexagonal lattice	5.18		8.517	12
W Cu ₄ Mg ₅ Si ₄ Al _x	body-centered cubic lattice	12.63			
T Mg ₃ Zn ₃ Al ₂	body-centered cubic lattice	14.19			162
T CuMn ₂ Al ₁₂ or Cu ₂ Mn ₃ Al ₁₃	oblique lattice	24.11	12.51	7.77	150
FeNiAl ₉ or FeNi ₂ Al ₁₂ or FeNi ₂ Al ₁₃	single oblique lattice				
TiAl ₃	body-centered square lattice	3.848		8.596	8

Appendix 2 (continued)

Phase of Deformable Aluminum Alloy and The Characteristics Before

Color and Form of Phase Before Corroding	2ccHF + 3ccHCl + 5ccHNO ₃ + 250ccH ₂ O *	0.5ccHF + 99.5ccH ₂ O	1g NaOH + 100ccH ₂ O	10g NaOH + 100ccH ₂ O	20cc H ₂ SO ₄ + 80ccH ₂ O
congregated crystals of yellowish grey and honey-comb shape	dark brown (strong)	slightly corroded color becomes brown	no	color becomes dark	dark brown
sea blue color, usually of fish-bone shape, primary crystal of rhombic cake shape	black (strong)	black	no	blue color becomes deeper.	black
light rose color, primary crystal congregated, secondary crystals dispersed inside a(Al) + CuAl ₂ , the elliptical eutecticum	no	no	color becomes dark	copper-red color	no
light grey color, schistose crystal	black (strong)	brown	no	no	slightly corroded color becomes black
light grey, skeleton shaped, sometimes congregated crystal of cake shape	slightly corroded	dark brown (sensitive)	no	no	slightly corroded
light grey, darker than MgZn ₂ , honey-comb shaped	brown	no	no	no	severely corroded
grey, schistose or congregated crystal	black	light brown and brown	slightly corroded	dark brown	slightly corroded
bright grey, coarse schistose crystal brighter than AlCuNi	brown to dark brown	brown	color becomes dark	brown	no
bright grey, schistose crystal	slightly corroded	very slightly corroded	no	light brown	no

* Mixed liquid acid solution adopted here.

and After Corroding

Appendix 2 (continued)

25cc HNO ₃ + 75ccH ₂ O	0.5ccHF + 1.5ccHCl + 2.5cc HNO ₃ + 99.5ccH ₂ O	20ccHCl + 20cc HNO ₃ + 5ccHF + 55ccH ₂ O	10cc H ₃ PO ₄ + 90ccH ₂ O	10g Fe(NO ₃) ₃ + 75ccH ₂ O	micro- hard- ness H ₅ V	fusing point °C
black brown	dark brown	dark brown	becomes brown after corroding	becomes dark brown after cor- roding	449	550
black (strong)	black (strong)	black	becomes dark af- ter cor- roding	becomes dark af- ter cor- roding	450	1102
copper- red (strong)	no	no	no	copper- red and brown (strong)	560	591
black	black	black	becomes dark af- ter cor- roding	becomes dark af- ter cor- roding		590
dark brown	slightly corroded	black	no	no	495	
black brown	brown	brown			427	530
no	black	blue	no	no	702	
no	brown and black brown	brown and black brown	no	no	700	810
no	slightly corroded	slightly corroded	no	no		1340

Appendix 2 (continued)

(a)

Phase	Crystal Structure	Lattice Constant (\AA)			Number of Atoms in Each Cell
		a	b	c	
FeAl_3	single oblique lattice	15.520	8.099	12.501	100
NiAl_3	oblique lattice	6.611	7.366	4.812	16
MnAl_3	oblique lattice	6.498	7.552	8.870	28
MnAl_4	hexagonal lattice	28.41		12.38	
Si					
Mg_2Al_3 or Mg_3Al_4	face-centered cubic lattice	28.16			1166
$(\text{FeMn})\text{Al}_6$ solid solution					
$\alpha (\text{Fe}_3\text{SiAl}_{12})$		12.548			
$\beta (\text{Fe}_2\text{Si}_2\text{Al}_4)$		6.12	6.12	41.48	

Appendix 2 (continued)

(b)

Color and Form of Phase Before Corroding	2ccHF + 3ccHCl + 5ccHNO ₃ + 250ccH ₂ O *	0.5ccHF + 99.5ccH ₂ O	1g NaOH + 100ccH ₂ O	10g NaOH + 100ccH ₂ O	20cc H ₂ SO ₄ + 80ccH ₂ O
grey, schistose crystal	slightly corroded	no	color becomes dark	color becomes dark	brown corroded
grey, schistose crystal	black brown (strong)	deep grey or deep brown	color becomes dark	dark light brown sometimes deep blue	light dark
bright grey, rhombic crystal with holes on it	no	slightly corroded	brown then blue as position changes	blue changes into black (strong)	no
bright grey, darker than MnAl ₆	no	no	becomes brown (strong)	strong not even, corroded becomes dark	no
grey, light red under light, schistose crystal	very slightly corroded	no	no	no	no
light grey, primary crystal (skeleton shaped) looser than CuAl ₃	slightly corroded	very slightly corroded	no	no	dissolved
bright grey, same as MnAl ₆ , brighter than FeAl ₃	slightly corroded, color no change	no	becomes coarse	color becomes dark	no
bright grey, brighter than FeAl ₃ , FeSiAl ₃ , fish-bone shaped	no	no	no	no	slightly corroded
bright grey, darker than FeAl ₃ , coarse acicular crystal	easy to become light brown	corroded, brown color	no	corroded color changed	severely corroded

* Mixed liquid acid solution adopted here.

Appendix 2 (continued)

(c)

25cc HNO ₃ + 75ccH ₂ O	0.5ccHF + 1.5ccHCl + 2.5cc HNO ₃ + 99.5ccH ₂ O	20ccHCl + 20cc HNO ₃ + 5ccHF + 55ccH ₂ O	10cc H ₃ PO ₄ + 90ccH ₂ O	10g Fe(NO ₃) ₃ + 75ccH ₂ O	micro- hard- ness H ₅ p	fusing point °C
no	slightly corroded	dark color becomes brown	no	color becomes dark	960	1160
no	slightly corroded	slightly corroded	dark color	dark color	770	854
no	no	no	no	no	540	710
no	no	no			749	822
no	very slightly corroded	slightly corroded light blue	no	no	1320	
dissol- ved	slightly corroded	slightly corroded	no	no	340	452
no	slightly cor roded color no change	slightly corroded co- lor no change	no	no	704	
slightly corroded color no change	no change	no	no	no		860
slightly corroded color no change	light brown change	no	no	no	578	700

Appendix 2 (continued)

(d)

Phase	Crystal Structure	Lattice Constant (Å)			Number of Atoms in Each Cell
δ (FeSi ₂ Al ₄)	square lattice	6.16		9.49	
CrAl ₇	oblique lattice	24.8	24.7	30.2	1160
(FeMnSi) Al ₆					
^N Cu ₂ FeAl ₆ or Cu ₂ FeAl ₇	square lattice	6.336		14.870	40
Mn ₂ SiAl ₁₀	Cubic lattice	12.625			
^{Tni} Cu ₃ NiAl ₆ (AlCuNi)	body-centered cubic lattice	14.6			
^{Sni} (CuNi) ₂ Al ₃					

Appendix 2 (continued)

(e)

Color and Form of Phase Before Corroding	2ccHF + 3ccHCl + 5ccHNO ₃ + 250ccH ₂ O*	0.5ccHF + 99.5ccH ₂ O	1g NaOH + 100ccH ₂ O	10g NaOH + 100ccH ₂ O	20cc H ₂ SO ₄ + 80ccH ₂ O
light grey, usually schistose crystal	slightly corroded color become dark	slightly corroded	dark color	dark color	dark color
bright grey, schistose crystal	no	no	slightly corroded color becomes dark	light brown	no
light grey, branch shaped and cake shaped coarse crystal	very slightly corroded	yellowish brown to blue	slightly corroded	corroded mixed colors	black
bright grey, acicular crystal conglomerate with other phase crystal	corroded color becomes brown	slightly corroded light grey to dark grey	dark color	color changes as position changes	dark becomes black
bright grey, darker than MnAl ₆ , brighter than Si	no	no	no	no	no
grey, scattered branch-shaped crystal	no	no	no	no	no
dark grey, scattered branch-shaped crystal	slightly corroded	corroded light brown	slightly corroded	corroded light brown	slightly corroded

* Mixed liquid acid solution adopted here.

AD-A049 264

FOREIGN TECHNOLOGY DIV WRIGHT-PATTERSON AFB OHIO
DEFORMED ALUMINUM ALLOY METALLOGRAPHY. (U)
AUG 77

F/G 11/6

UNCLASSIFIED

FTD-ID(RS)T-0577-77

NL

2 OF 5
AD
A049 264



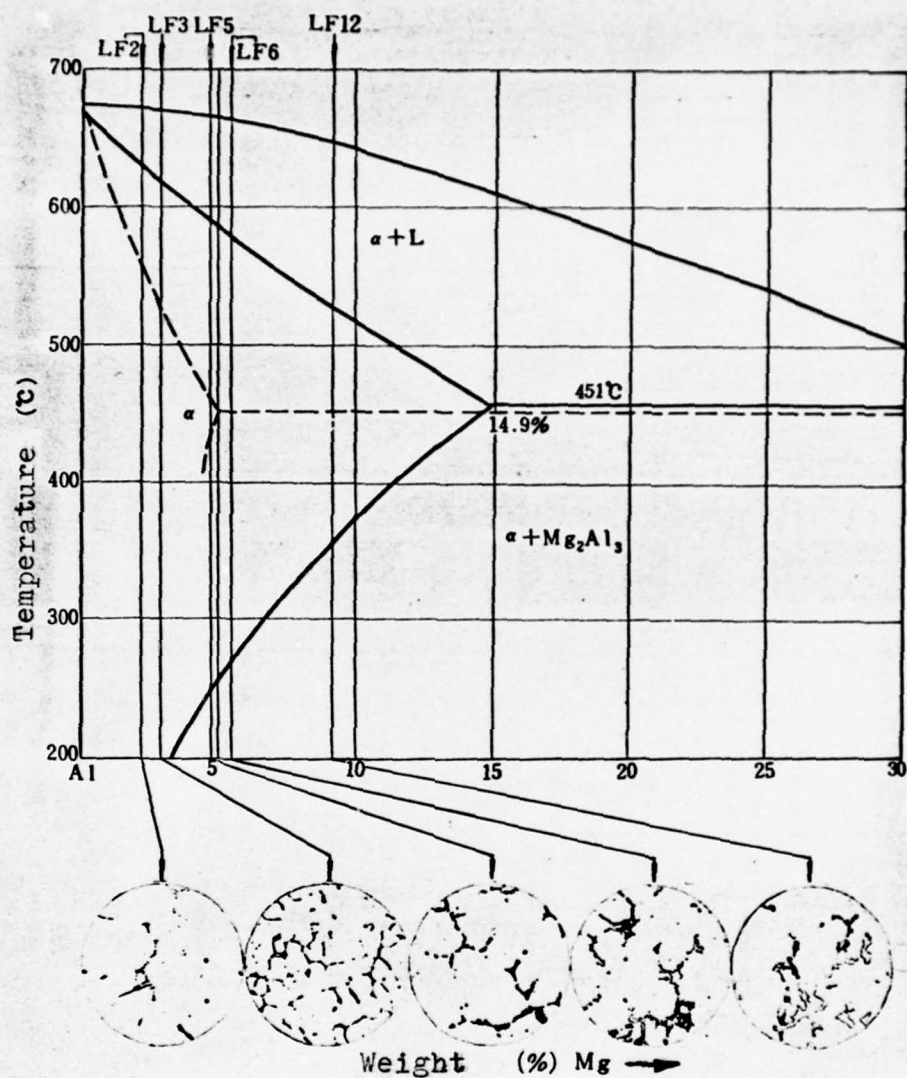


Figure II-2

Relation between Magnesium Contents and the Appearance of the $\beta(\text{Mg}_2\text{Al}_3)$ Phase in a Semi-Continuously Cast Aluminium-Magnesium Alloy

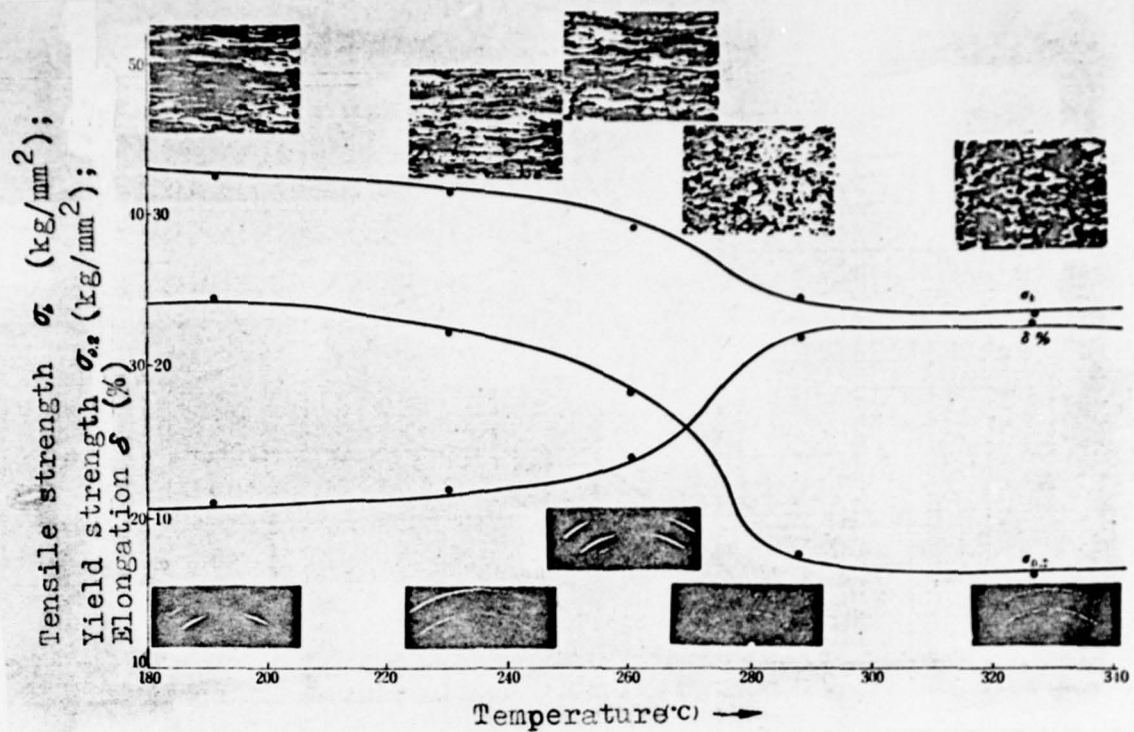


Figure II-3 Effects of Annealing Temperatures on the Mechanical Structures and Properties of a Cold-rolled LF6 Alloy Sheet (Cold Deformation Is 60%)

contents, as shown in Figure II-4. As the magnesium content is increased from 2% to 5%, the recrystallization temperature decreases correspondingly. As the magnesium content is increased from 5% to 9%, the recrystallization temperature increases with it. Moreover, when the magnesium content is about 5%, the solid-state solubility curve meets with the recrystallization temperature curves.

In addition to what is mentioned above, the recrystallization temperatures of alloys are also dependent on the process-

ing methods and the extents of cold-deformation before annealing. Recrystallization temperatures of some products of the industrial aluminium-magnesium system alloys are shown in Table II-3:

Table II-3 Recrystallization Temperatures of Partial Industrial Products of Aluminium-Magnesium System Alloys

Alloy Label	Variety	Specification (mm)	Technical Conditions						RECRYSTALLIZATION TEMPERATURE (°C)	
			Rolling		Extrusion		ANNEALING CONDITIONS		INITIAL	final
			TEMPERATURE (°C)	DEFORMATION (%)	TEMPERATURE (°C)	DEFORMATION (%)	SALT BATH OR FURNACE (min)	Time		
LF2	cold-rolled	2.0	room temperature	80%			air furnace	60	245~250	300~305
LF3	rolled	1.0							230~235	260~265
LF5	sheet	2.0							225~230	250~255
LF6	sheet	2.0							235~240	270~275

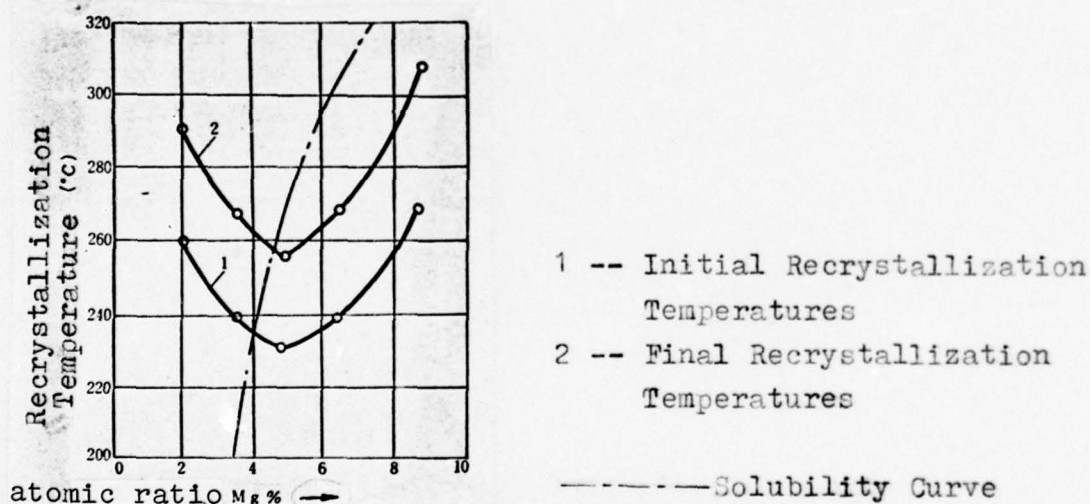


Figure II-4 Relationship of Recrystallization Temperature with Magnesium Content in Al-Mg System Alloys

The mechanical properties of a cold-^{rolled} alloy sheet of high magnesium content will undergo changes when the sheet is stored at room temperature for a long time. Figure II-5 is a curve showing the change in properties of a cold-rolled Al-Mg alloy sheet having 6% magnesium content when it is stored at room temperature for long periods of time. As the storage time increases, the strength of the sheet decreases. In particular, the yield strength decreases markedly, and the elongation rate increases markedly. This kind of softening phenomenon is even more pronounced when the extent of deformation and the magnesium content are increased. Under the microscope, the structure does not exhibit any changes.

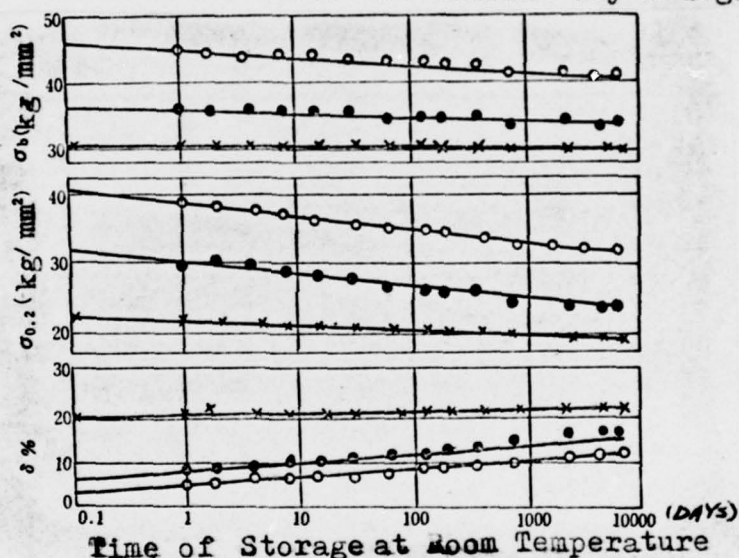


Figure II-5

Dependence of the Tensile Strength, the Yield Strength, and the Elongation Rate on the Storage Time of an Al-6%Mg Alloy Cold-rolled Sheet

Deformation ○—○ 60%
 ●—● 20%
 ×—× 5%

In order to avoid the softening phenomenon produced by the prolonged storage of an alloy after cold-working, the product must undergo low-temperature annealing treatment (150°C for 3 hours) subsequent to cold-deformation processes. In this way, the mechanical properties can **tend to stabilize** when stored at room temperature. This method is called Stabilization.

Section 3 Structures of Cast and Wrought Products

1. Phase Formations

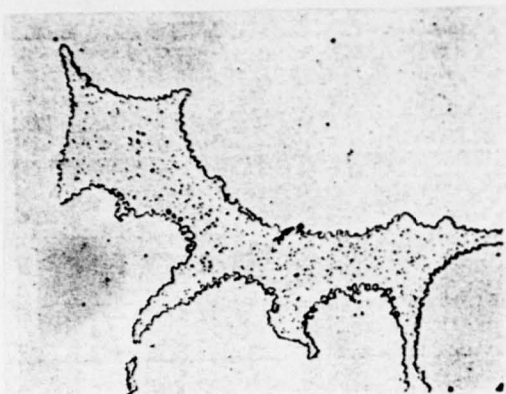


Figure II-6

210x



Figure II-7

210x

Alloy	LF12
Condition	Semi-continuous-ly cast ingot is remelted at 750°C, cooled slowly to 430°C, and quenched in water.
Etchant	10% H_3PO_4 aqueous solution
Structural features	Eutectic $\alpha(Al)$ + $\beta(Mg_2Al_3)$. $\beta(Mg_2Al_3)$ are bone-shaped.

Alloy	LF6
Condition	Same as Figure II-6
Etchant	20% H_2SO_4 aqueous solution
Structural features	$(FeMn)Al_6$ appear as polygons.



Figure II-8

210x



Figure II-9

210x

Alloy	LF3
Condition	Same as Figure II-6
Etchant	Not etched
Structural features	Eutectic $\alpha(\text{Al}) + \text{Mg}_2\text{Si}$. Mg_2Si are bone-shaped.

Alloy	LF3
Condition	Same as Figure II-6
Etchant	Mixed-acids aqueous solution
Structural features	1 -- FeAl_3 needle-like 2 -- Mg_2Si



Figure II-10

400x

Alloy	LF2
Condition	Semi-continuously cast
Etchant	Mixed-acids aqueous solution

Structural features	The veins of the dendritic network are composed of
---------------------	--

- 1 -- FeAl_3
- 2 -- Mg_2Si

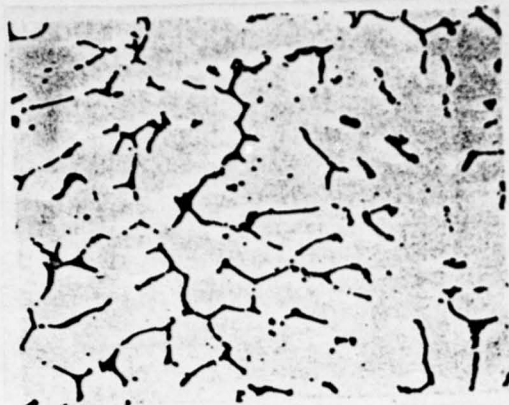


Figure II-11

400x

Alloy	LF3
Condition	Semi-continuously cast
Etchant	Mixed-acids aqueous solution
Structural features	The veins of the dendritic network are composed of $\alpha(\text{Al}) + \text{Mg}_2\text{Si}$

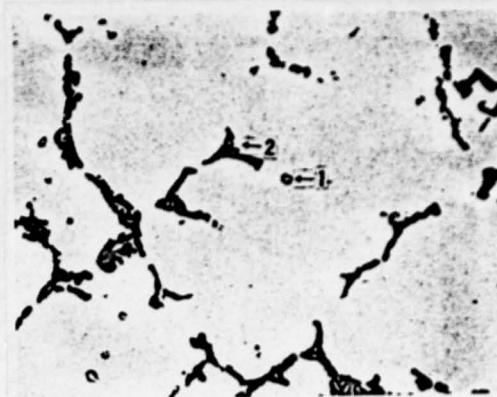


Figure II-12

400x

Alloy	LF5
Condition	Semi-continuously cast
Etchant	Mixed-acids aqueous solution
Structural features	1 -- $\beta(\text{Mg}_2\text{Al}_3)$ 2 -- Mg_2Si_2

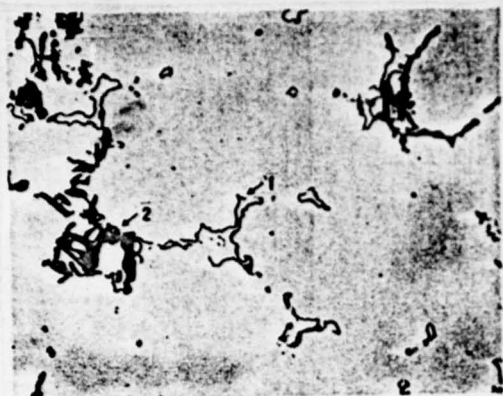


Figure II-13 400x

Alloy	LF6
Condition	Semi-continuous-ly cast
Etchant	Mixed-acids aqueous solution
Structural features	1 -- $\beta(\text{Mg}_2\text{Al}_3)$ 2 -- Mg_2Si

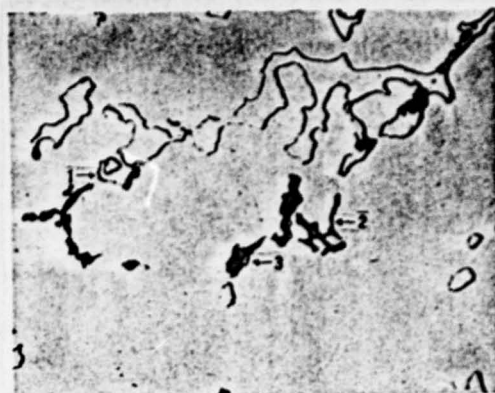


Figure II-14 400x

Alloy	LF12
Condition	Semi-continuously cast
Etchant	Mixed-acids aqueous solution
Structural features	1 -- $\beta(\text{Mg}_2\text{Al}_3)$ 2 -- Mg_2Si 3 -- $(\text{FeMn})\text{Al}_6$

2. Structures of Ingots

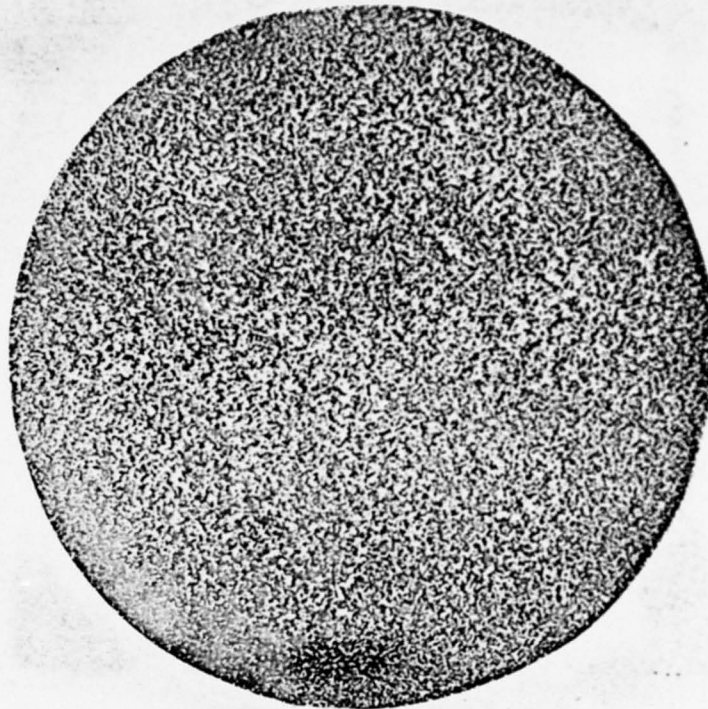


Figure II-15

Alloy and Condition	LF6 semi-continuously cast
Specification	Ø192mm
Etchant	15% NaOH aqueous solution
Structural features	Macrostructure. The grains are finer at the edge portion than at the middle and central portions.



Figure II-16 210x
Etched in Mixed-Acids Aqueous
Solution

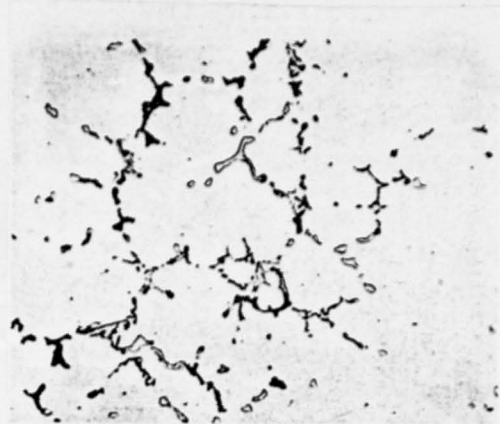


Figure II-17 210x
Etched in Mixed-Acids Aqueous
Solution

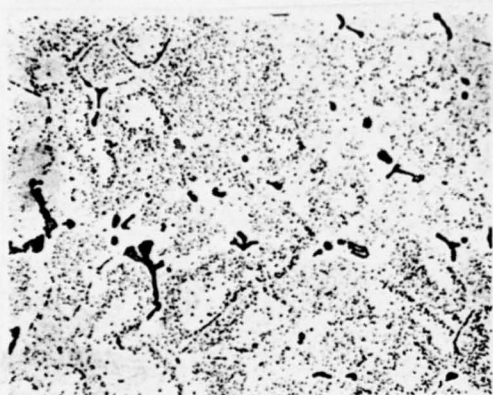


Figure II-18 210x
Etched in Mixed-Acids Aqueous
Solution

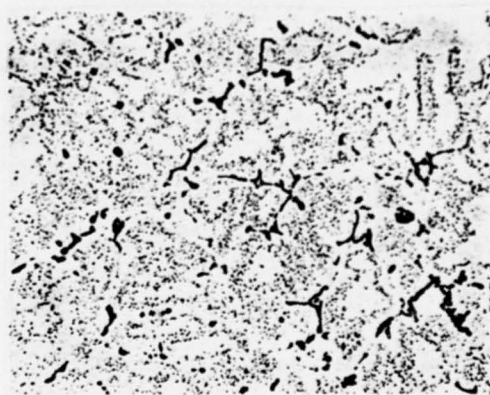


Figure II-19 210x
Etched in Mixed-Acids Aqueous
Solution

Alloy and Condition

Figure II-16 & Figure II-17: a semi-continuously cast alloy ingot. Figure II-18 & Figure II-19: the same ingot after homogenization (475°C, 24 hours, air-cooled)

Specification

Structural features

φ192mm

Figure II-16 is the structure of the edge portion of the transverse cross-section of the ingot. The dendritic network is discontinuous.

Figure II-17 is the structure of the middle portion of the transverse cross-section of the ingot. The dendritic network shows more continuity than that at the edge portion.

Figure II-18 and Figure II-19 are the structures of the edge portion and the middle portion of the homogenized ingot respectively. The dendritic network constituents have partially dissolved into the solid solution. Large quantity of dispersed particles of phases such as $\beta(\text{Mg}_2\text{Al}_3)$ are precipitated from the $\alpha(\text{Al})$ matrix.

3. Structures of Sheets

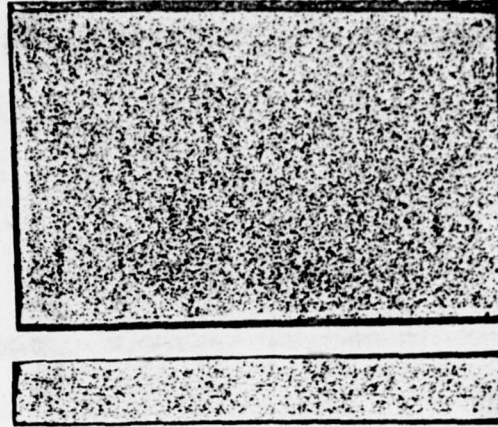


Figure II-20

1:1

Alloy and Condition	LF6R
Specification	6.0mm thick
Etchant	15% NaOH aqueous solution
Structural features	<p>The upper portion of the figure is the macrostructure of the sheet surface, which exhibits equiaxed fine grain structure.</p> <p>The lower portion of the figure is the macrostructure of the longitudinal cross-section of the sheet. The grains are fine at the edge. The grains at the center are elongated along the rolling direction.</p>

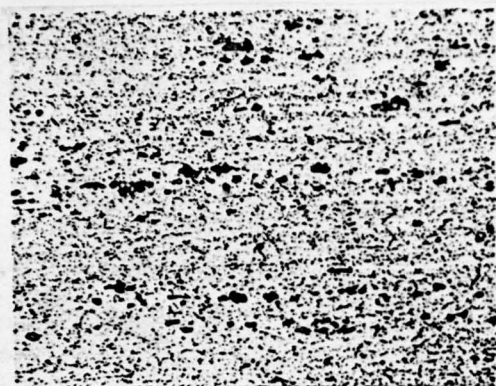


Figure II-21 210x
Etched in Mixed-Acids Aqueous
Solution



Figure II-22 210x
Etched in Mixed-Acids Aqueous
Solution



Figure II-23 100x
Structure of Electropolished
and Anodized Specimen under
Polarized Light



Figure II-24 100x
Structure of Electropolished
and Anodized Specimen under
Polarized Light

Alloy and Condition LF6R
Specification 6.0mm thick

Structural features Figure II-21 and Figure II-23 are the
structures of the middle portion of
the longitudinal cross-section of the

sheet. After the sheet has been hot-deformed, the compounds are arranged in arrays along the rolling direction. Large quantity of particles of phases such as $\beta(\text{Mg}_2\text{Al}_3)$ are precipitated from the $\alpha(\text{Al})$ matrix. The sheet has undergone recrystallization. The grains are elongated along the rolling direction. Figure II-22 and Figure II-24 are the structures of the middle portion of the transverse cross-section of the sheet.

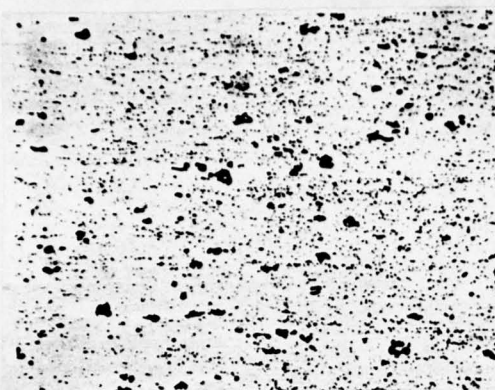


Figure II-25 210x
Etched in Mixed-Acids Aqueous
Solution



Figure II-26 100x
Structure of Electropolished
and Anodized Specimen under
Polarized Light

Alloy and Condition	LF6Y
Specification	1.0mm thick
Structural features	<p>Figure II-25 is the structure of the middle portion of the longitudinal cross-section of the sheet. After it has been cold-deformed, the compounds are broken and are arranged in arrays along the rolling direction. Large quantity of particles of phases such as $\beta(\text{Mg}_3\text{Al}_2)$ are still distributed on the $\alpha(\text{Al})$ matrix.</p> <p>Figure II-26 is Figure II-25 under polarized light.</p>



Figure II-27 100x
Structure of Electropolished
and Anodized Specimen under
Polarized Light



Figure II-28 100x
Structure of Electropolished
and Anodized Specimen under
Polarized Light

Alloy and Condition

LF6M

Specification

3.6mm thick

Structural features

Figure II-27 is the structure of the sheet after 240°C annealing. Recrystallized grains appear in the fibre structure.

Figure II-28 is the structure of the sheet after 280°C annealing. Recrystallization is complete. The fibre structure is completely replaced by recrystallized grains.

4. Structures of Extruded Products

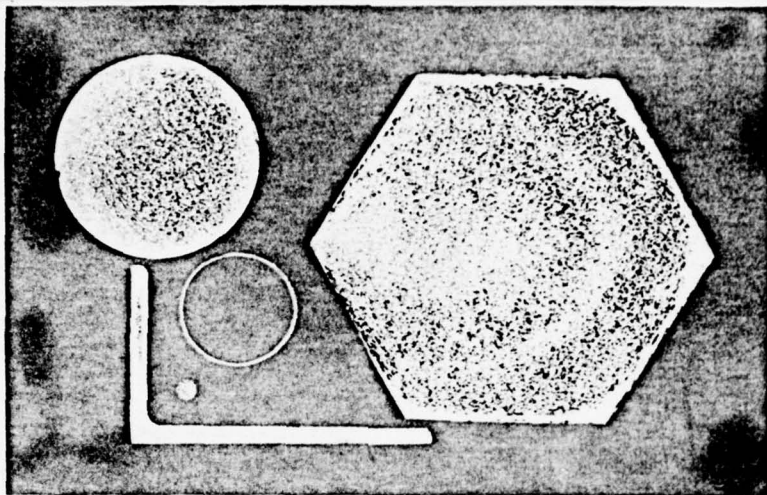


Figure II-29

Alloy and Condition	LF6R
Specification	$\phi 30$ mm rod XC113-55 structural-shape 20x18mm tube $\phi 4$ mm wire
Etchant	15% NaOH aqueous solution
Structural features	Shown in the figure are the macrostructures of the transverse cross-sections of the rear ends of the extruded products. Except for the surface layers where rings of coarse grains are found, the grains are finer in the edge portions than in central portions.

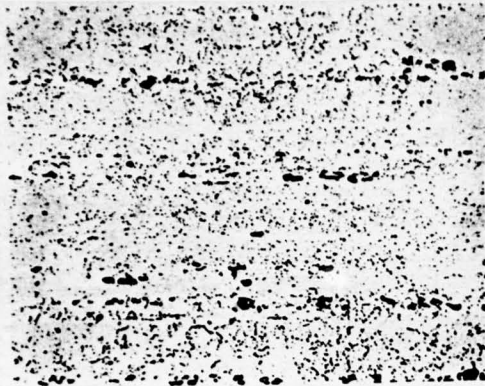


Figure II-30 210x
Etched in Mixed-Acids Aqueous
Solution

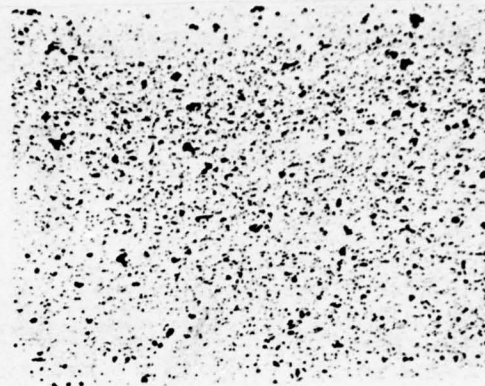


Figure II-31 210x
Etched in Mixed-Acids Aqueous
Solution



Figure II-32 100x
Structure of Electropolished
and Anodized Specimen under
Polarized Light



Figure II-33 100x
Structure of Electropolished
and Anodized Specimen under
Polarized Light

Alloy and Condition LF6R

Specification $\phi 35$ mm rod

Structural features Figure II-30 and Figure II-32 are the structures of the middle portion of the rear end of the rod. After it has been hot-deformed, the compounds are

broken and are arranged in arrays along the extrusion direction. Large quantity of particles of phases such as $\beta(\text{Mg}_2\text{Al}_3)$ are precipitated from the $\alpha(\text{Al})$ matrix. The sheet has undergone recrystallization. The grains are elongated along the extrusion direction. Small quantity of deformed structures still remain.

Figure II-31 and Figure II-33 are the structures of the middle portion of the transverse cross-section of the rear end of the rod. Grain sizes are not uniform.



Figure II-34 100x
Structure of Electropolished
and Anodized Specimen under
Polarized Light

Alloy and LF6R
condition

Specifi- XC113-55 struc-
cation tural-shape
Structural Structure, under
features polarized light,
of the middle
portion of the
longitudinal cross-
section of the
structural-shape.
The material has
undergone recrystal-
lization, but still
retains the deformed
structure.



Figure II-35 100x
Structure of Electropolished
and Anodized Specimen under
Polarized Light

Alloy and LF6M (fired iso-
condition thermally at 390°C
for 1 hour, and
cooled in air)

Specifi- XC113-55 struc-
cation tural-shape.
Structural Structure, under
features polarized light,
of the middle
portion of the
longitudinal cross-
section of the
structural-shape.
The material has
completely recrystallized. Grains are
elongated along the
extrusion direction.

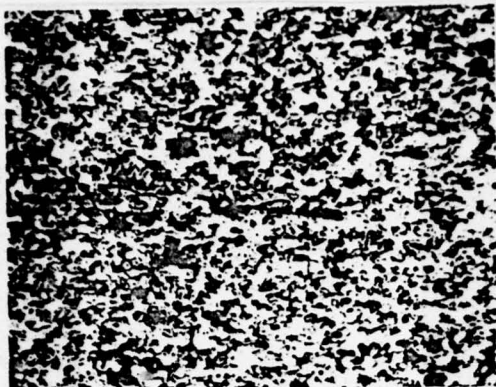


Figure II-36 100x

Structure of Electropolished and Anodized Specimen under Polarized Light

Alloy and condition LF6M (fired isothermally at 390°C, and air-cooled for one hour)

Specification 20x18mm tube

Structural features Structure, under polarized light, of the rear end of the tube in the longitudinal direction. It has undergone complete recrystallization, and exhibits fine equiaxed grains.

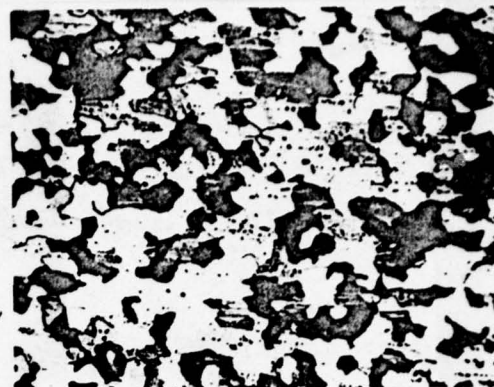


Figure II-37 100x

Structure of Electropolished and Anodized Specimen under Polarized Light

Alloy and condition LF6M (fired isothermally at 390°C, and air-cooled for one hour)

Specification \varnothing 4mm cold-drawn wire

Structural features Structure, under polarized light, of the rear end of the tube in the transverse direction. It has undergone complete recrystallization, and exhibits equiaxed grains.

5. Structures of Die-Forging



Figure II-38

Alloy and Condition	LF6R
Form number	A-4 Die-forging
Etchant	15% NaOH aqueous solution
Structural features	Structure of the radial cross-section of the forging under low power microscope. Flow lines travel uniformly along the outline of the die.



Figure II-39 210x
Etched in Mixed-Acids Aqueous Solution

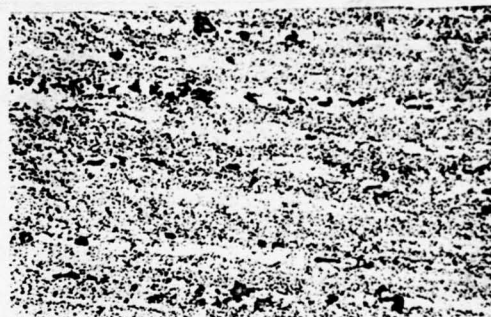


Figure II-40 210x
Etched in Mixed-Acids Aqueous Solution



Figure II 41 100x
Structure of Electropolished
and Anodized Specimen under
Polarized Light



Figure II-42 100x
Structure of Electropolished
and Anodized Specimen under
Polarized Light

Alloy and Condition

LF6R

Form number

A-4 Die-Forging

Structural features

Figure II-39 and Figure II-41 are the structures of the central portion of the elevated edge part of the forging. The compounds are distributed along the metal flow direction after they have been broken. Particles of phases such as $\beta(\text{Mg}_2\text{Al}_3)$ are precipitated profusely from the $\alpha(\text{Al})$ matrix. The material has undergone recrystallization, and still retains the deformed structure. Figure II-40 and Figure II-42 are the structures of the central portion of the body plate of the forging. Since its deformation rate is large, the directionality of the compound distribution is more pronounced here than in Figure II-39. The material has undergone recrystallization, but still retains the deformed structure.

Among the aluminium-manganese system alloys, the one that is most often produced is the LF21 labelled alloy. It has high malleability, good corrosion resistivity and solderability. It can be worked into semi-products such as sheets, rods and tubes.

Section 1 Chemical Composition and Phase Formations

The chemical compositions of the LF21 alloy can be found in Table III-1. Manganese is the principal constituent of this alloy system. As the content of manganese is increased, the strength of the alloy also increases correspondingly. When the manganese content is within the range of 1.0~1.6%, the alloy not only has high strength, but also good malleability and machinability. If the manganese content continues to be increased, the strength of the alloy will also increase, but because of the formation of a large quantity of the brittle compound $MnAl_6$, the alloy will fracture easily during deformation. Therefore, alloy that contains more than 1.6% of manganese is seldom use in practice.

Table III-1 Chemical Compositions of the
LF21 Alloy

Mn (%)	Impurity, not more than (%)						
	Fe	Si	Cu	Zn	Mg	others	total
1.0~1.6	0.7	0.6	0.2	0.1	0.05	0.1	0.75

The addition of manganese into aluminium can also improve the corrosion resistivity of the latter.

Iron impurity can lower the solid solubility of manganese in aluminium. For example, the addition of 0.03% Fe can reduce the solubility of manganese at 500°C from 0.35% to 0.15%. Iron dissolve into MnAl_6 to form $(\text{FeMn})\text{Al}_6$, which is a phase that is difficult to dissolve, hard and brittle, and whose microhardness is 704 kg/mm².

In practice, it is verified that the addition of a definite amount of iron into the alloy can help to reduce the grain sizes of the sheet. Therefore, in production, the content of iron is usually controlled within the range 0.4%-0.7%. However, the sum of the iron and manganese contents must not exceed 1.85%, for otherwise accumulations of large quantities of coarse and flake-shaped $(\text{FeMn})\text{Al}_6$ precipitates will be formed, which will markedly reduce the mechanical and technical properties of the alloy.

Silicon impurity can increase the tendency of the alloy to crack under thermal stress, and also reduce its castability. Therefore, the content of silicon should be strictly controlled.

According to the equilibrium diagram of the Al-Mg system alloys (Figure III-1), the following features can be found:

1. The slope of the liquidus line is very small, and the range of isothermal crystallization is very narrow.
2. The vertical ranges of crystallization along the liquidus and solidus lines are small, only 0.5-1.0°C.
3. At the eutectic temperature, the difference between

maximum solubility of manganese in aluminium and the content of manganese at the eutectic point is very small, only 0.1~0.13% Mn.

4. The solubility of manganese in aluminium varies widely, decreasing drastically with temperature.

Due to the aforementioned characteristics of the aluminium-manganese system alloys, together with the small diffusion constant of manganese in aluminium, serious preferential precipitation inside the grains occurs during the process of semi-continuous casting of the alloys, appearing as non-uniformity of distribution of manganese content within each grain and dendrite. The concentration of manganese decreases as one goes from the grain boundary or the edge of the dendrite towards the center, showing up as wave-shaped structures under the microscope (Figure III-2a). The LF21 alloy cannot obtain equilibrium structures even if it is cooled slowly during casting. Neither can precipitated particles of MnAl_6 be found on the $\alpha(\text{Al})$ matrix. When the alloy has been remelted at 760°C , cooled slowly to room temperature, and analyzed by means of metallography and electron microprobing, it has the following features:

$\alpha(\text{Al})$ phase: $\alpha(\text{Al})$ is in supersaturation and shows no signs of decomposition.

$\text{Mn}_3\text{SiAl}_{12}$ phase: $\text{Mn}_3\text{SiAl}_{12}$ appears in the form of eutectic structures, which turns from bright grey to yellowish brown in color after etching in 0.5% HF aqueous solution, and turns blue upon further etching. If 10% NaOH aqueous solution is used, it will appear dull grey, and its outline becomes more conspicuous (Figure III-8 and Figure III-9).

$(\text{FeMn})\text{Al}_6$ phase: It appears in the form of large bright

grey plates. Upon etching with 10% NaOH aqueous solution, the surfaces become rough, and the color changes slightly (Figure III-8).

Under the semi-continuous casting process of the alloys, MnAl_4 , $\text{Mn}_3\text{SiAl}_{12}$, and eutectic $\alpha(\text{Al}) + \text{MnAl}_4$ exist. The MnAl_4 in the eutectic mixture appears as bright grey rods, which turns to dark grey upon etching with 10% NaOH aqueous solution (Figure III-10).

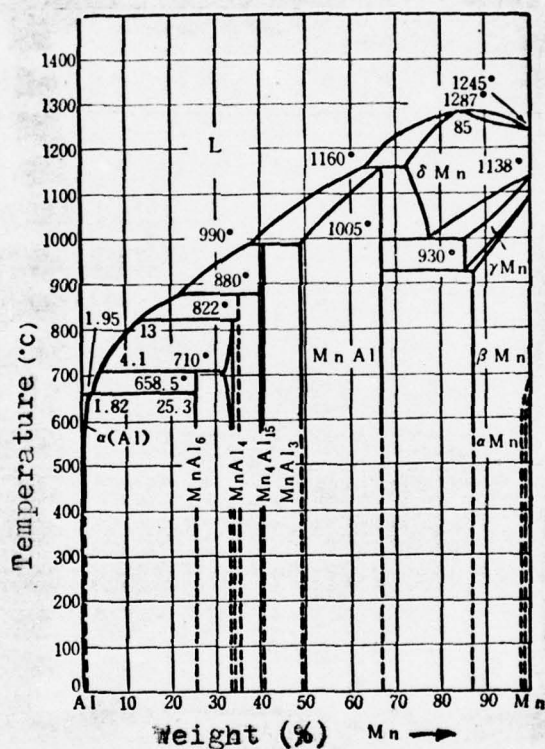


Figure III-1 Equilibrium Diagram of the Al-Mn System Alloys

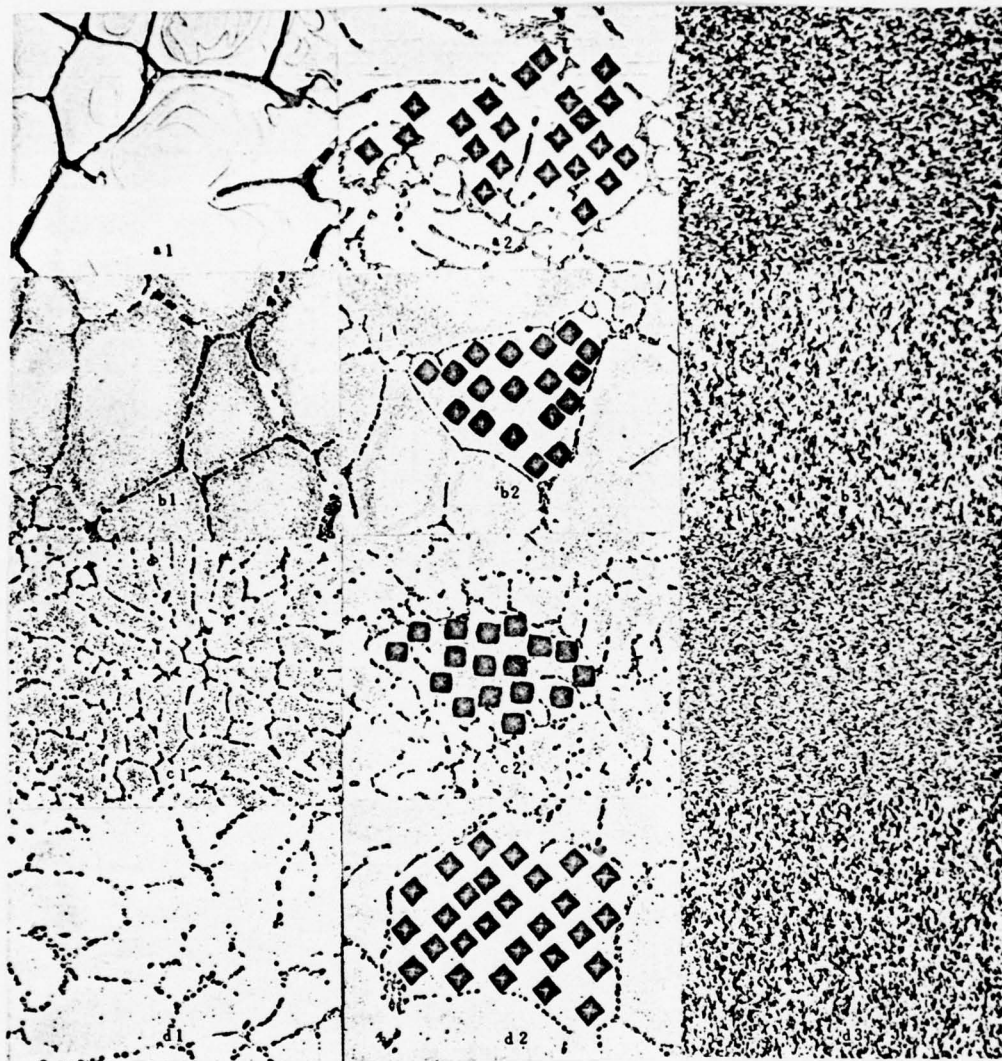


Figure III-2 Effects of Ingot Homogenization Procedures on the Preferential Precipitations within the Grains, on the Microhardnesses, and on the Grain Sizes of Sheets after Annealing

a --- The ingot is not homogenized. Wave-shaped preferentially precipitated matters inside the grains are clearly

visible. Microhardnesses are not even. The grains are coarse after it has been spun into a sheet with subsequent annealing.

- b --- The ingot has undergone homogenization at 500°C for 4 hours. Fine particles of compounds such as MnAl_6 and $(\text{FeMn})\text{Al}_6$ are precipitated along the boundaries of the dendritic network. Microhardnesses are still not even. The grains are still coarse after it has been spun into a sheet with subsequent annealing.
- c --- The ingot has undergone homogenization at 610-620°C for 4 hours. Particles of compounds such as MnAl_6 are precipitated within the entire dendrite and are evenly distributed. Microhardnesses are uniform throughout. The grains are fine after it has been spun into a sheet with subsequent annealing.
- d --- The ingot has undergone homogenization at 600°C for 4 hours. Since the precipitated particles re-dissolve into the solid solution, the microhardnesses are not uniform again. The grains are coarse after it has been spun into a sheet with subsequent annealing.

Section 2 Properties of Alloys under Heat Treatments

During the annealing of LF21 alloy products, coarse grains are produced extremely easily so that the surfaces become coarsened or cracks appear when the alloy semi-products are flushed or bent.

Testings verify the following: The appearance of coarse grains in the alloy is due mainly to the existence of serious preferential precipitation of manganese within the grains and dendrites of the semi-continuously cast ingots. Since manganese can raise the recrystallization temperature of the alloy considerably, the preferential precipitation of manganese inside the grains can cause the recrystallization range to widen, so that coarse grains are easily produced during the annealing of the alloy. In order to ensure the formation of fine grains in LF21 alloy sheets, the following measures should be adopted:

1. Homogenization of ingots. When an ingot is homogenized below 500°C, the effects of homogenization is difficult to obtain, no matter how long the firing at constant temperature is carried out. From the microstructure of the ingot, one can see that particles of compounds such as MnAl_6 , $(\text{FeMn})\text{Al}_6$, and $\text{Mn}_3\text{SiAl}_{12}$ are precipitated initially from the dendritic boundaries and the grains boundaries of $\alpha(\text{Al})$. This is a phenomenon known as congregated precipitation caused by the preferential precipitation within the grains (Figure III-2b). The grains of sheets made from this ingot remain coarse after annealing. As the homogenization temperature is increased, congregated precipitation will gradually be reduced. After homogenization at 600~620°C, distribution of precipitates such as MnAl_6 is even,

microhardnesses are the same from the dendritic boundaries to the centers (Figure III-3), and the sheets made from the ingot thus homogenized have fine and even grains. If the homogenization temperature is raised to 640°C close to the solidus line, preferential precipitation inside the grains will re-appear, due to the re-melting of compounds such as MnAl_6 that was precipitated from $\alpha(\text{Al})$. Distribution of microhardnesses is then uneven, and the corresponding sheets will develop coarse grains. Effects of ingot homogenization procedures on the preferential precipitation inside the grains, on the microhardnesses, and on the grain sizes of the sheets after annealing, are shown in Figure III-2.

2. High-temperature Rolling. Raising the ingot homogenization temperature from 390~440°C to 480~520°C can cause the sheets to obtain fine grains after annealing (Figure III-4). This is because high-temperature rolling can accelerate

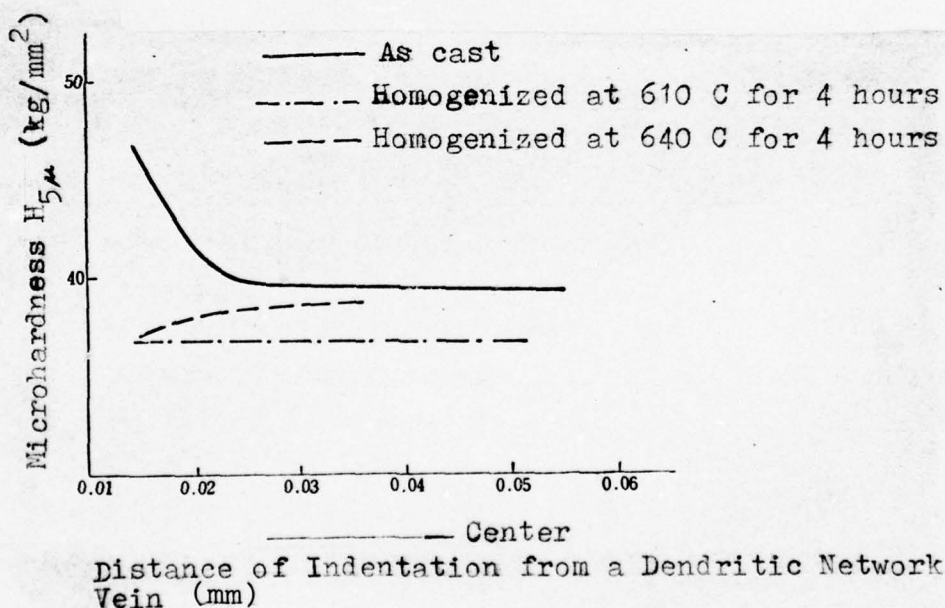


Figure III-3 Effects of Homogenization Temperature on the Microhardnesses and on the Preferential Precipitation within the Grains

the decomposition of the supersaturated solid solution.

3. Proper Control of Iron Content. In the situation where small amount of titanium is added into the alloy, the addition of iron of 4% or more can reduce the sizes of the grains markedly (Figure III-5).

4. Rapid Application of Heat. LF21 alloy is very sensitive to the rate of heat application in annealing. Rapid application of heat produces fine grains. This is because the rapid application of heat can cause the recrystallization range to narrow; the manganese-rich and manganese-poor portions nucleate at the same time, so that fine grains are produced. For example, annealing in salt baths can lead to fine grain structures. Figure III-6 shows the different grainularities obtained under different rates of heat application. Grains are finest when heated rapidly at high temperature, as shown in 8 of Figure III-6. It is apparent from Figure III-7 that grains are finer when annealed in salt baths than in box furnaces.

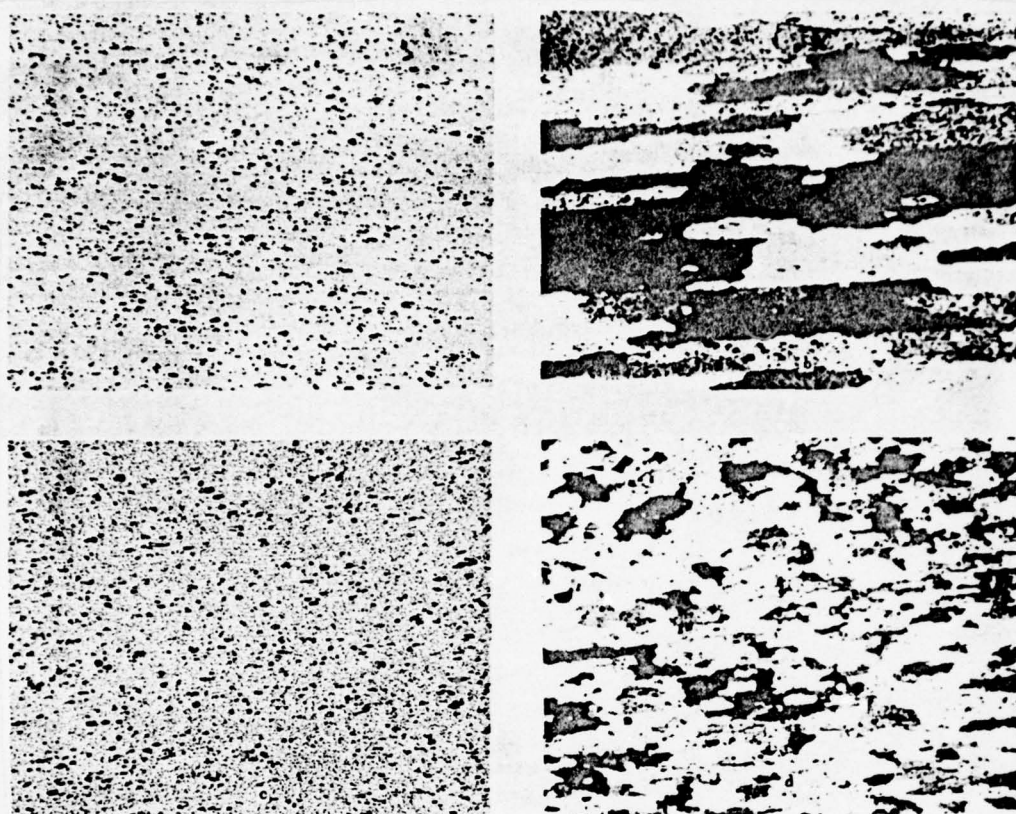


Figure III-4 Effects of Hot Spinning Temperature on the Granularity of an LF21 Alloy Sheet

- a -- A 6.0mm thick hot-spun sheet. Hot spinning temperature is 390°C. Precipitated Mn particles are few.
- b -- Structure, under polarized light, of a 2.0mm thick cold spun sheet (hot spinning temperature is 390°C) after annealing. Grains are coarse.
- c -- A 6.0mm thick hot-spun sheet. Hot spinning temperature is 520°C. Large quantity of fine and even Mn particles are precipitated.
- d -- Structure, under polarized light of a 2.0mm thick cold-spun sheet (hot spinning temperature is 520°C) after annealing. Grains are fine and even.

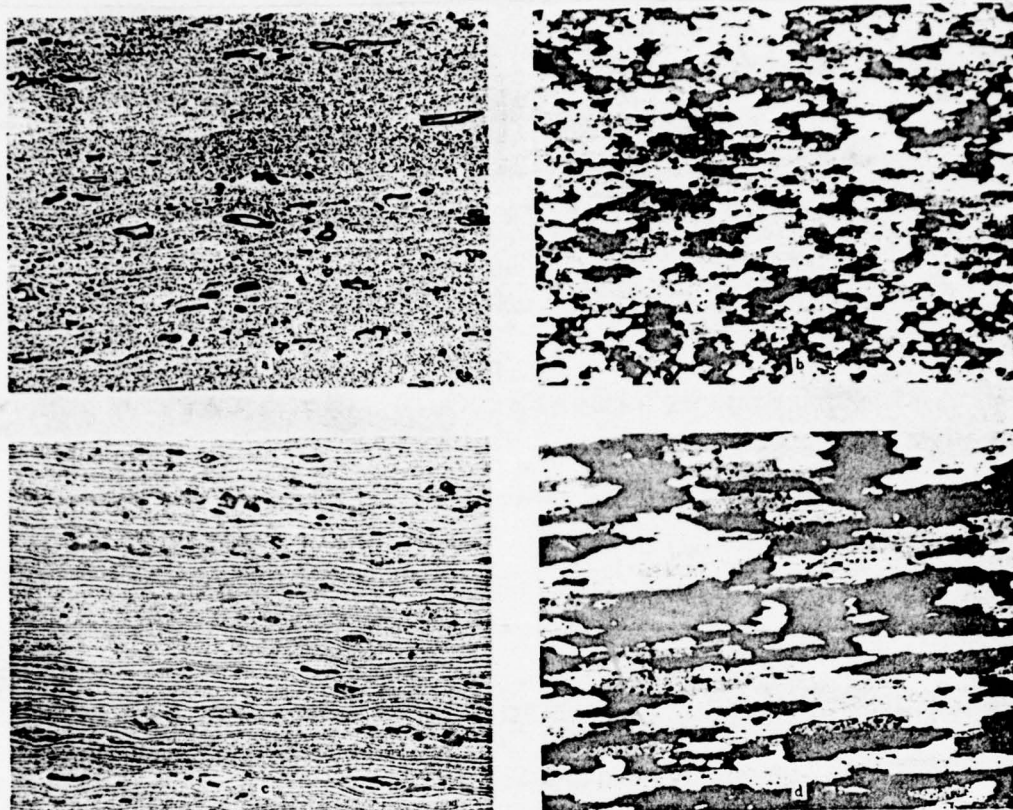


Figure III-5 Effects of Iron Contents on the Granularity of an LF21 Alloy Sheet

- a -- Hot-spun sheet with 0.47% iron. The large strips of compounds are the proeutectic $(\text{FeMn})\text{Al}_6$.
- b -- Structure of 0.47%-iron hot-spun sheet under polarized light after cold-spinning and annealing. Grains are fine and even.
- c -- 0.31%-iron hot-spun sheet. Primary $(\text{FeMn})\text{Al}_6$ are few and fine.
- d -- Structure of 0.31% iron hot-spun sheet under polarized light after cold spinning and annealing. Grains that contain higher content of iron are coarser than those that contain lower content of iron.

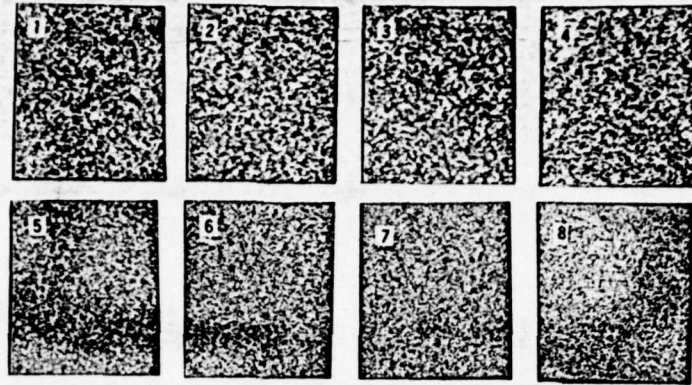


Figure III-6 Effect of the Rate of Heat Application on the Grain Sizes of an 1.5mm Thick LF21 Alloy Sheet

- 1,2,3,4 -- Macrostructures of the sheet after annealing in air furnace (heat is added slowly), and firing at constant temperatures 350°C, 400°C, 450°C, and 500°C, for 4 hours respectively.
- 5,6,7,8 -- Macrostructures of the sheet after annealing in salt bath (Heat is added rapidly), and firing at constant temperatures 350°C, 400°C, 450°C, and 500°C, for 20 minutes respectively.

Comparison between 1 and 5 reveals that the alloy is not very sensitive to the rate of heat application during low-temperature annealing, but comparison between 3,7,4, and 8 shows that the higher the temperature, the greater the effect of the rate of heat application on the grain sizes.

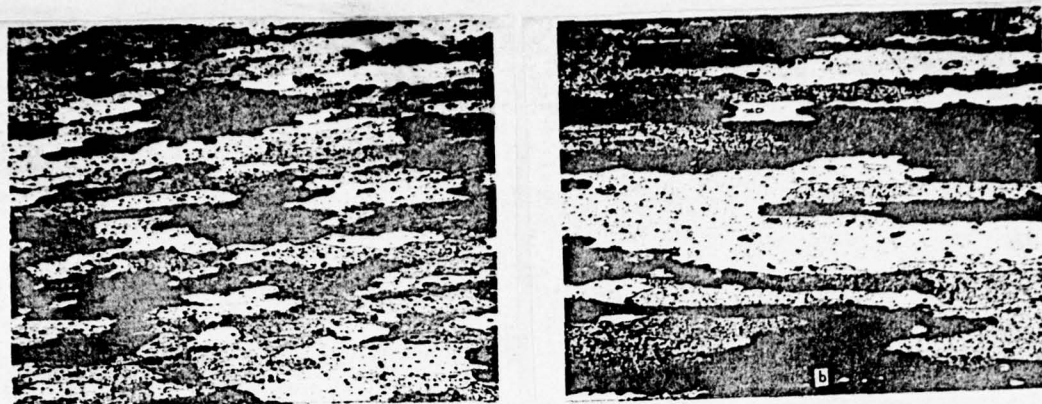


Figure III-7 Effects of Salt Bath Annealing and Box Furnace Annealing on the Granularity of an LF21 Alloy Sheet

a -- Salt bath annealing : firing at 500°C constant temperature for 20 minutes. Grains are fine.

b -- Box furnace annealing : firing at 500°C constant temperature for 4 hours. Grains are coarse.

Recrystallization parameters of LF21 wrought alloy products are listed in Table III-2:

Table III-2 Recrystallization parameters of LF21 Wrought Alloy Products

Variety	Speci- fication (mm)	Technical Conditions						Recrystallization Temperature (°C)	
		Rolling		Extrusion		Annealing Condition		initial	final
		TEMPER- ATURE (°C)	DEFORM- ATION (%)	TEMPER- ATURE (°C)	DEFORM- ATION (%)	SALT-BATH OR AIR FURNACE	TIME (min)		
Sheet	1.25	ROOM TEMPER- ATURE	84.4			AIR FURNACE	30	320~325	515~520
Sheet	1.25	ROOM TEMPER- ATURE	84.4			SALT-BATH	10	320~330	530~535
Rod	φ 110			380	90	AIR FURNACE	60	520~525	555~560 INCOMPLETE
"	"			380	90	SALT-BATH	60	520~525	555~560 COMPLETE
Tube	37 × 35			ROOM TEMPER- ATURE	85	SALT-BATH	10	330~335	525~530

Section 3. The Structures of Ingots and Processed products

1. The Phase Constitution

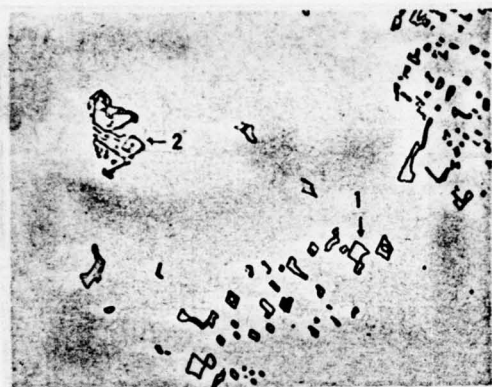


Figure III-8

210x

Alloy	LF21
Condition	Semi-continuously cast, remelted at 760°C for 4 hours, and cooled in furnace
Etchant	10% NaOH aqueous solution
Structural features	1 -- $(\text{FeMn})\text{Al}_6$ 2 -- $\text{Mn}_3\text{SiAl}_{12}$



Figure III-9

210x

Alloy	LF21
Condition	Same as Figure III-8
Etchant	10% NaOH aqueous solution
Structural features	Eutectic $\alpha(\text{Al}) + \text{Mn}_3\text{SiAl}_{12}$

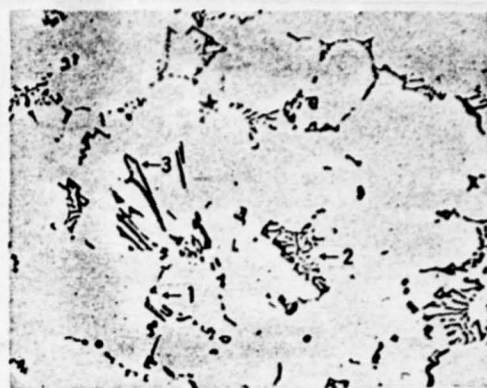


Figure II -10

210x

Alloy	LF21
Condition	Semi-continuously cast
Etchant	10% NaOH aqueous solution
Structural features	1 -- MnAl_4 2 -- $\alpha(\text{Al}) + \text{Mn}_3\text{SiAl}_{12}$ eutectic mixture 3 -- $(\text{FeMn})\text{Al}_6$

2. Structures of Ingots

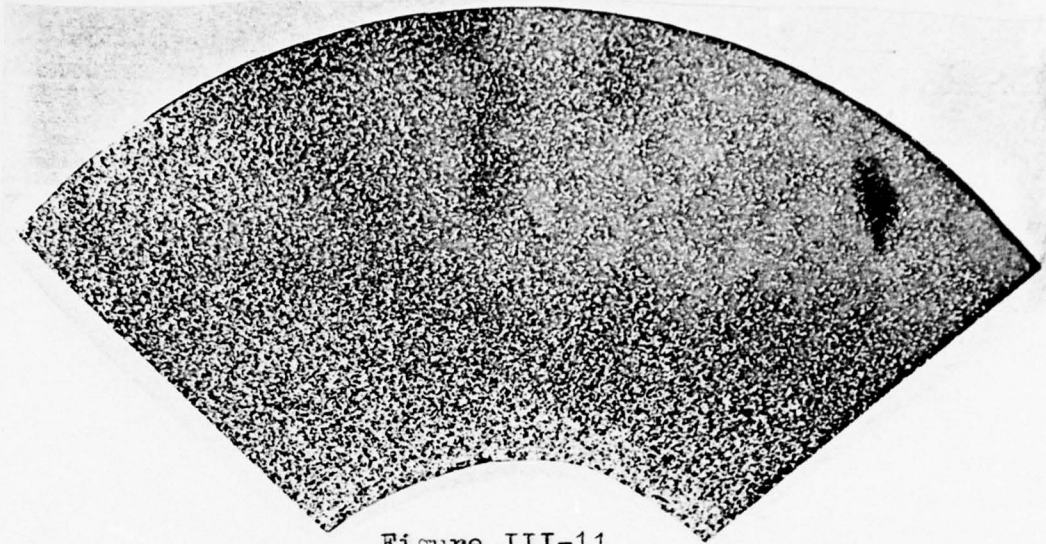


Figure III-11

Alloy and Condition	LF21 semi-continuously cast
Specification	φ270x130mm hollow ingot
Etchant	75ml HCl + 25ml HNO ₃ + 5ml HF
Structural features	Macrostructure of ingot. Grains are fine and uniform. Those at the edge of the inner wall are slightly coarser than the rest.

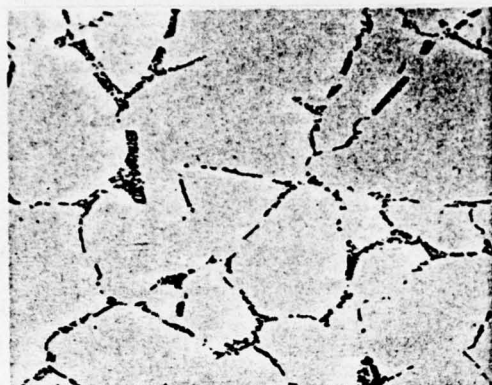


Figure III-12 210x



Figure III-13 100x
Structure of Electropolished
and Anodized Specimen under
Polarized Light

Alloy and condition	LF21 semi-continuously cast	Alloy and condition	Same as Figure III-12
Specification	φ270x130mm hollow ingot	Specification	φ270x130mm hollow ingot
Etchant	10% NaOH aqueous solution	Structural features	It is Figure III-12 under polarized light. Forms and sizes of grains are visible.
Structural features	Transverse structure of middle portion of ingot. The veins of the dendritic network are made of $\alpha(\text{Al}) + \text{MnAl}_4$ and $\alpha(\text{Al}) + \text{Mn}_3\text{SiAl}_{12}$ eutectic mixtures.		



Figure III-14 210x
Etched in 10% NaOH Aqueous
Solution

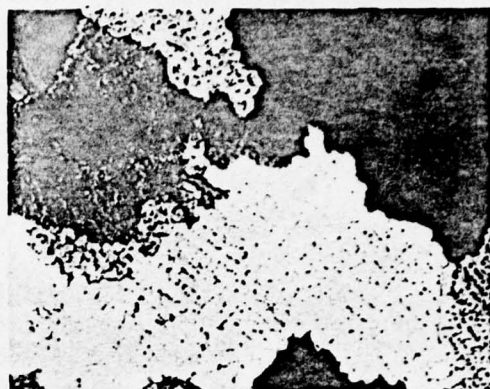


Figure III-15 100x
Structure of Electropolished
and Anodized Specimen under
Polarized Light

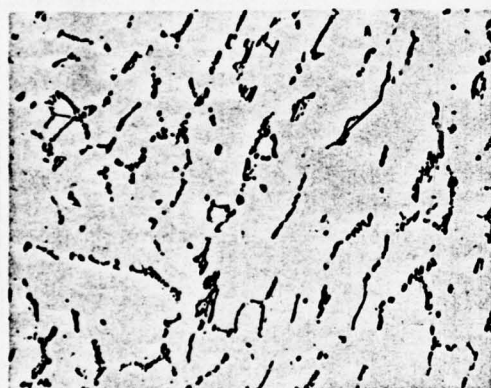


Figure III-16 210x
Etched in 10% NaOH Aqueous
Solution



Figure III-17 100x
Structure of Electropolished
and Anodized Specimen under
Polarized Light

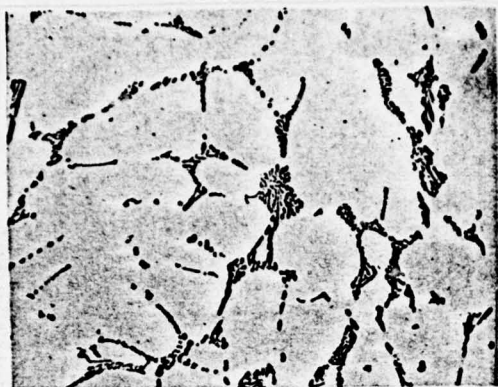


Figure III-18 210x
Etched in 10% NaOH Aqueous
Solution

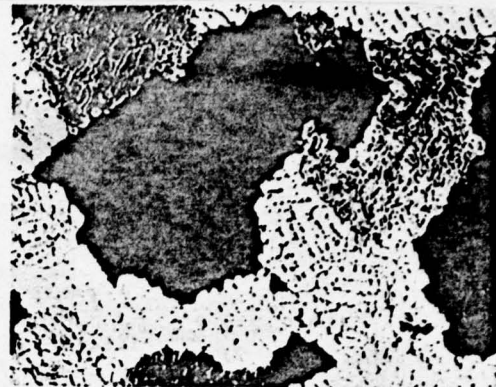


Figure III-19 100x
Structure of Electropolished
and Anodized Specimen under
Polarized Light

Alloy and condition
Specification
Structural features

LF21 semi-continuously cast
1500x200mm square ingot

Figure III-14 is the transverse structure of the edge portion of the ingot. The veins of the dendritic network are coarse and not continuous.

Figure III-15 is Figure III-14 under polarized light. The grains are coarse.

Figure III-16 is the transverse structure of the middle portion of the ingot. The veins of the dendritic network are thinner than those in the edge portion.

Figure III-17 is Figure III-16 under polarized light. The grains are fine.

Figure III-18 is the transverse structure of the central portion of the ingot. The veins of the dendritic network are thick.

Figure III-19 is Figure III-18 under

polarized light. The grains here are coarser than those in the middle portion.



Figure III-20

210x



Figure III-21

210x

Alloy and condition LF21 semi-continuously cast ingot, homogenized 610°C for 4 hours

Specification $\phi 270 \times 130$ mm hollow ingot

Etchant 10% NaOH aqueous solution

Structural features The dendritic network has partially dissolved into the solid solution. Particles of compounds such as MnAl_6 are precipitated from the $\alpha(\text{Al})$ matrix.

Alloy and condition Same as Figure III-20

Specification $\phi 192$ mm round ingot

Etchant 10% NaOH aqueous solution

Structural features The dendritic network has partially dissolved into the solid solution. Particles of compounds such as MnAl_6 are precipitated from the $\alpha(\text{Al})$ matrix.

3. Structures of Sheets

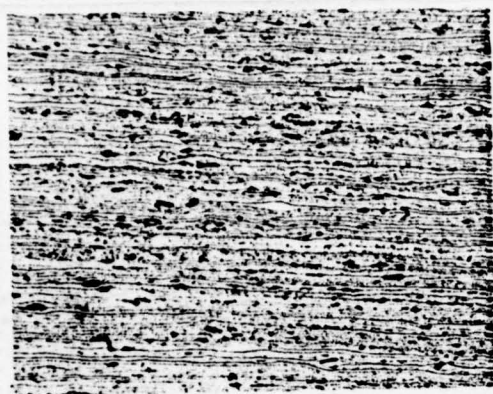


Figure III-22 210x
Etched in 10% NaOH Aqueous
Solution

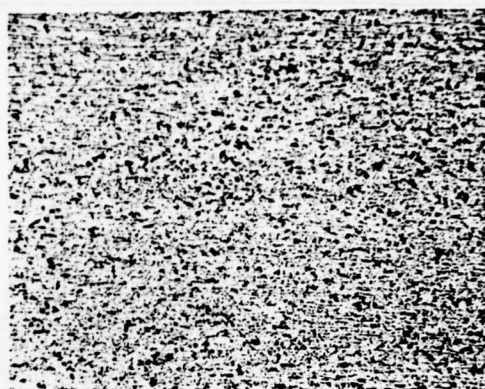


Figure III-23 210x
Etched in 10% NaOH Aqueous
Solution

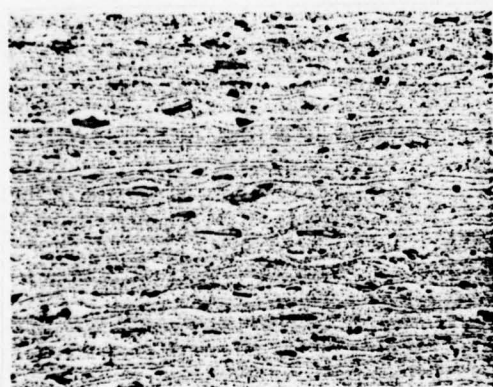


Figure III-24 210x
Etched in 10% NaOH Aqueous
Solution

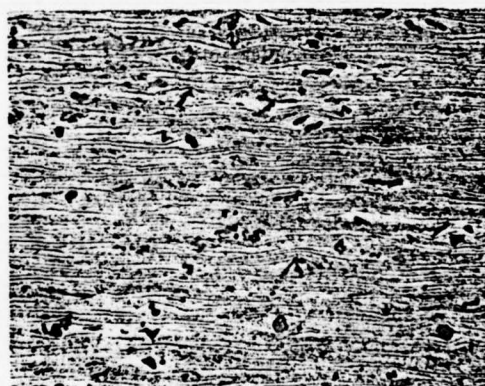


Figure III-25 210x
Etched in 10% NaOH Aqueous
Solution

Alloy and Condition	LF21R
Specification	6.0mm thick
Structural features	Figure III-22 and Figure III-24 are the

longitudinal structures of the edge portion and the central portion respectively. The compounds are arranged in arrays along the rolling direction after they have been broken. Particles of compounds such as MnAl_6 are precipitated from the $\alpha(\text{Al})$ matrix.

Figure III-23 and Figure III-25 are the transverse structures of the edge portion and the central portion of the sheet respectively. Compared with the central portion, the edge portion suffers greater deformation, and its layer structure, though irregular, is denser and finer than that of the central portion.

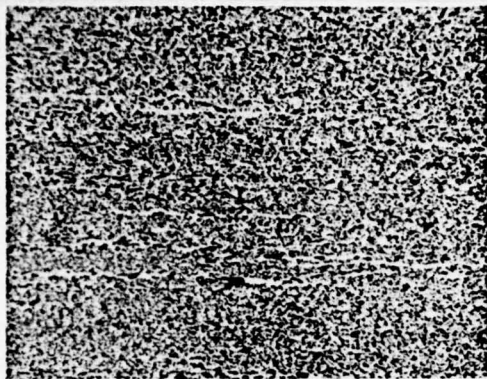


Figure III-26
Etched in 10% NaOH Aqueous
Solution 210x

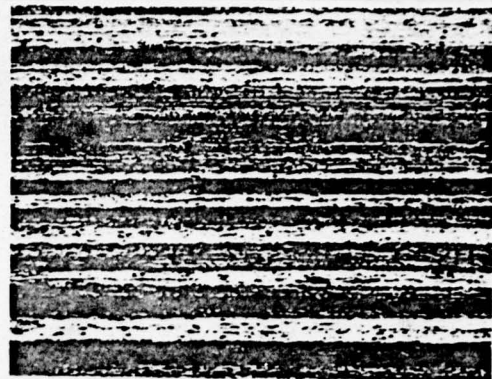


Figure III-27 100x
Structure of Electropolished
and Anodized Specimen under
Polarized Light

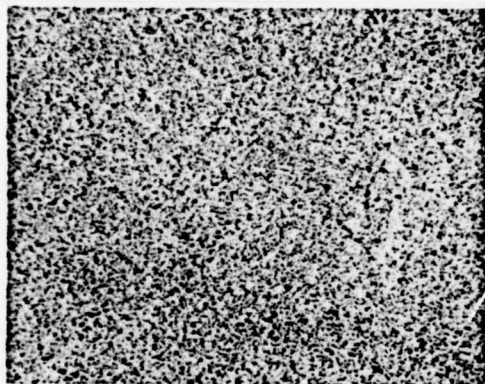


Figure III-28 210x
Etched in 10% NaOH Aqueous
Solution



Figure III-29 100x
Structure of Electropolished
and Anodized Specimen under
Polarized Light

Alloy and Condition	LF21Y (Deformation rate is 95%)
Specification	2.0mm thick
Structural features	Figure III-26 and Figure III-27 are the

longitudinal structures of the central portion of the sheet. The compounds are arranged in arrays along the rolling direction after they have been broken. The deformed fibre structure is clearly visible.

Figure III-28 and Figure III-29 are the transverse structures of the central portion of the sheet. The directionality of compounds being arranged in arrays is not as good.

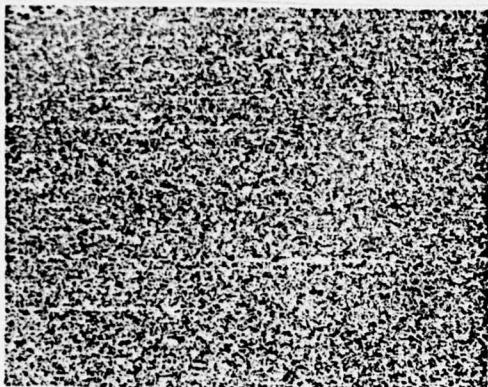


Figure III-30 210x
Etched in 10% NaOH Aqueous
Solution

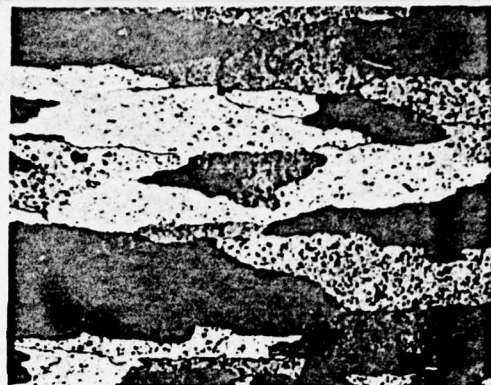


Figure III-31 100x
Structure of Electropolished
and Anodized Specimen under
Polarized Light

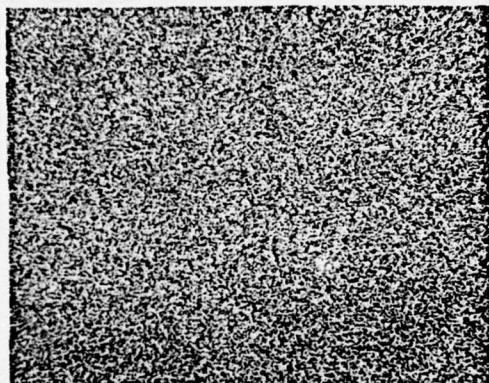


Figure III-32 210x
Etched in 10% Aqueous
Solution

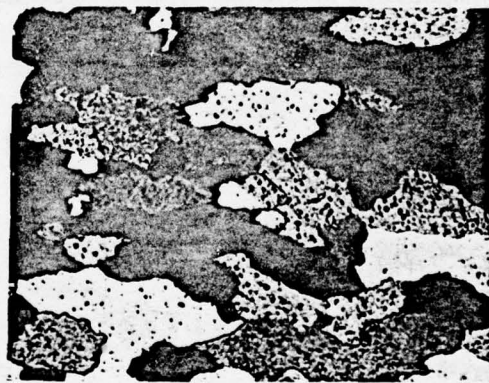


Figure III-33 100x
Structure of Electropolished
and Anodized Specimen under
Polarized Light

Alloy and Condition
Specification
Structural features

LF21M
1.0mm thick
Figure III-30 and Figure III-31 are the
longitudinal structures of the sheet.
Precipitated particles are uniformly

distributed. The sheet has undergone recrystallization. The grains are elongated along the rolling direction. Figure III-32 and Figure III-33 are the transverse structures of the sheet.

4. Structures of Extruded Products

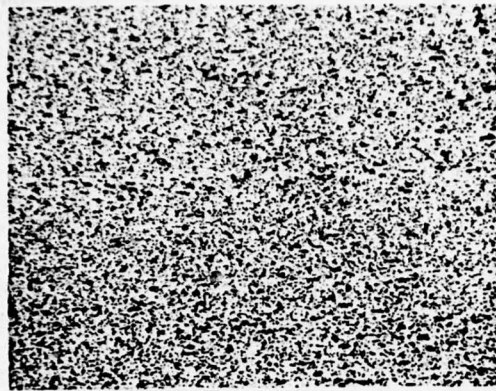


Figure III-34 210x
Etched in 10% NaOH Aqueous
Solution

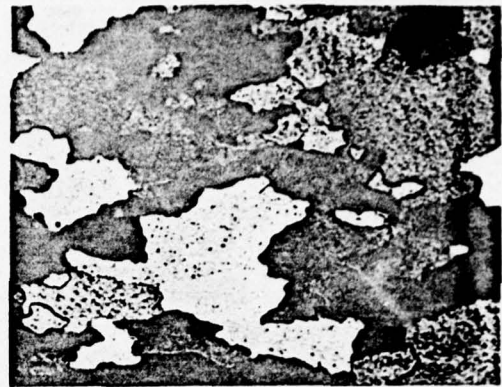


Figure III-35 100x
Structure of Electropolished
and Anodized Specimen under
Polarized Light

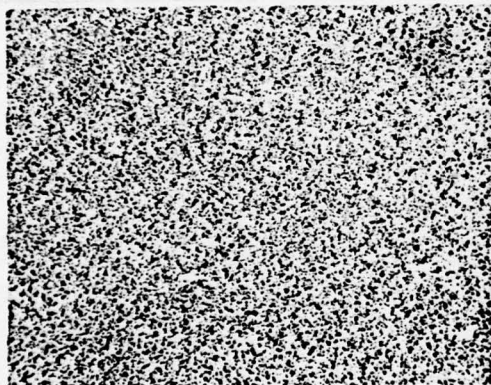


Figure III-36 210x
Etched in 10% NaOH Aqueous
Solution

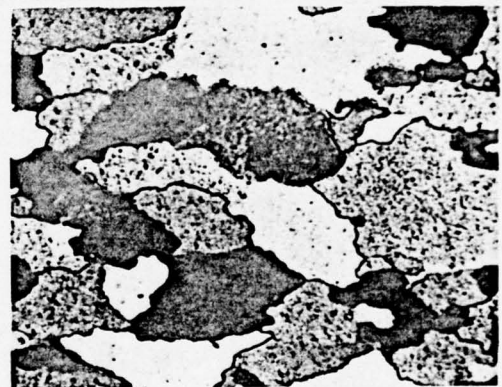


Figure III-37 100x
Structure of Electropolished
and Anodized Specimen under
Polarized Light

Alloy and Condition LF21M

Specification 27x25mm cold-spun tube

Structural features Figure III-34 and Figure III-35 are the

longitudinal structures of the tube. Precipitated particles are uniformly **distributed**. Compounds are arranged in arrays along the spinning direction. The tube has undergone complete recrystallization.

Figure III-36 and Figure III-37 are the transverse structures of the tube.

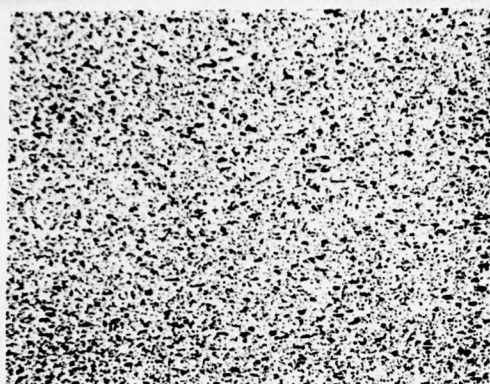


Figure III-38 210x
Etched in 10% NaOH Aqueous
Solution



Figure III-39 100x
Structure of Electropolished
and Anodized Specimen under
Polarized Light

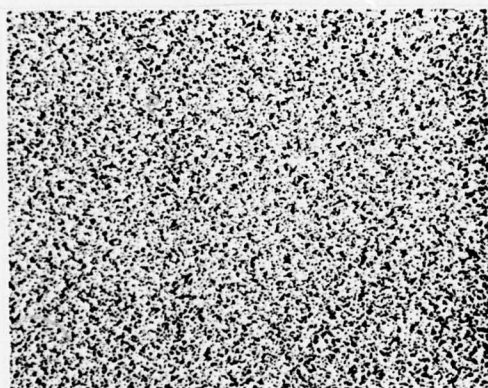


Figure III-40 210x
Etched in 10% NaOH Aqueous
Solution

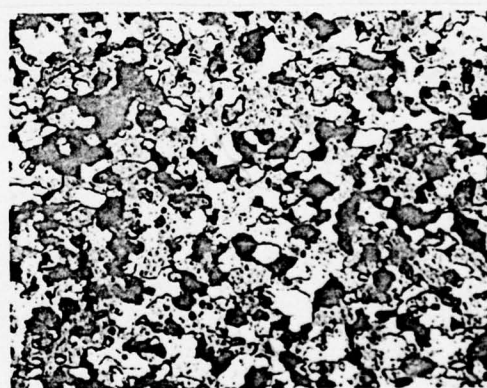


Figure III-41 100x
Structure of Electropolished
and Anodized Specimen under
Polarized Light

Alloy and Condition	LF21M
Specification	φ36x34mm cold-drawn tube
Structural features	Figure III-38 and Figure III-39 are the

longitudinal structures of the tube. The compounds are arranged in arrays along the drawing deformation direction. Precipitated particles are uniformly distributed. The tube has undergone recrystallization. The grains are elongated along the drawing direction, with directionality more marked than those of the cold-spun tube.

Figure III-40 and Figure III-41 are the transverse structures of the tube.

Aluminium-copper-magnesium system alloys are hard aluminium alloys that are used rather early and that find applications in many areas. They have good mechanical properties and working properties, and can be worked into semi-products such as sheets, rods, tubes, structural shapes and forgings. They are extensively used in the constructions of national economy and defense.

Under usual circumstances, the alloys of this system can be classified according to their strength and heat durability into the following four classes:

1. Low-strength hard aluminium such as LY1 and LY10;
2. Medium-strength hard aluminium such as LY11;
3. High-strength hard aluminium such as LY12;
4. Refractory hard aluminium such as LY2.

In order to improve the corrosion resistivity, the surfaces of hard aluminium sheets are coated with a layer of industrial-pure aluminium.

Section 1 Chemical Compositions and Phase Formations

The chemical compositions of alloys of this system are shown in Table IV-1. From the table, it is seen that the principal alloy elements are copper, magnesium, manganese, etc., and the impurities are iron, silicon, nickel and zinc. It can be seen from the analysis of the ratios between copper

and magnesium in the alloys that these ratios have a great effects on the properties of the alloys.

Table IV-1 Chemical Compositions of Al-Cu-Mg System Alloys

Alloy Label	Principal Constituents(%)					Impurity, not more than (%)							
	Cu	Mg	Mn	Cr	Ti	Fe	Si	Mn	Zn	Ni	Fe+Ni	Other	TOTAL
LY1	2.2~3.0	0.2~0.5	—	—	—	0.5	0.5	0.2	0.1	—	—	0.1	1.40
LY2	2.6~3.2	2.0~2.4	0.45~0.7	—	—	0.3	0.3	—	0.1	—	—	0.1	0.80
LY4	3.2~3.7	2.1~2.6	0.5~0.8	Be 0.001-0.01	0.05~0.4	0.3	0.3	—	0.1	—	—	0.1	0.80
LY6	3.8~4.3	1.7~2.3	0.5~1.0	Be 0.001-0.005	0.03~0.15	0.5	0.5	—	0.1	—	—	0.1	1.20
LY8	3.8~4.5	0.4~0.8	0.4~0.8	—	—	0.5	0.5	—	0.1	—	—	0.1	1.20
LY9	3.8~4.5	1.2~1.6	0.3~0.7	—	—	0.5	0.5	—	0.1	—	—	0.1	1.20
LY10	3.9~4.5	0.15~0.3	0.3~0.5	—	—	0.2	0.25	—	0.1	—	—	0.1	0.65
LY11	3.8~4.8	0.4~0.8	0.4~0.8	—	—	0.7	0.7	—	0.3	0.1	0.7	0.1	1.80
LY12	3.8~4.9	1.2~1.8	0.3~0.9	—	—	0.5	0.5	—	0.3	0.1	0.5	0.1	1.50

When the magnesium content in the alloy is low, copper will combine with aluminium to form CuAl_2 , which is the principal phase in both the low-strength and medium-strength hard aluminium alloys.

When the magnesium content is increased, especially in high-strength hard aluminium, magnesium, copper and aluminium will combine with one another to form $\text{S}(\text{CuMgAl}_2)$, which has better hardening effect than does CuAl_2 .

The addition of 0.3~1.0% of Mn into the alloys can reduce the detrimental effects caused by iron, and improve the corrosion resistivity of the alloys. Manganese can also reduce the grains sizes of the alloys, accelerate ageing effects, and

delay the recrystallization processes during extrusion and solid-solution treatments, thereby improving the mechanical properties of the products. When the manganese content exceeds 1%, accumulations of coarse $(FeMn)Al_6$, a brittle compound, appear, causing the technical properties of the alloys to deteriorate.

In the LY12 alloy, the elements copper, magnesium and manganese have the following effects on the stability of the solid solution:

1. As the total content of copper and magnesium is increased, the stability of the solid solution will decrease.
2. In copper-rich LY12 alloy, increasing the manganese content from 0.5% to 0.8% will increase the stability of the solid solution.
3. In copper-poor alloy, the increase in manganese content will cause the stability of the solid solution to decrease. If the magnesium content is increased, the stability of the solid solution will not be affected.
4. The minimum stability temperature of the solid solution is 350~375°C. If the manganese content in the alloy is increased, the stability of the solid solution at this temperature will further be reduced, causing the solid solution to decompose earlier than usual. However, at 450°C and even at 400°C, the time at which the solid solution begins to decompose will unusually be lengthened markedly.

The addition of titanium into the alloy can reduce the grain sizes, and lower the tendency of the alloy to develop

thermal cracks. In manufacturing alloys for soldering strips and fillings, small amount of titanium should be added.

Iron and silicon are the impurities elements in the alloys. Iron and copper can combine to form Cu_2FeAl_7 , an insoluble compound, thus causing the hardening phases CuAl_2 and $\text{S}(\text{CuMgAl}_2)$ to decrease in quantity in the alloys, so that the age-hardening effects of the alloys are reduced. Iron can also combine with silicon and manganese to form coarse $(\text{FeMnSi})\text{Al}_6$ and $(\text{FeMn})\text{Al}_6$, which are brittle compounds, causing the technical properties to deteriorate. Therefore, in the LY12 alloy, the iron content should be controlled below 0.5%.

In high-strength hard aluminium alloys, silicon can lower the hardening effects of the alloys. After the alloys have been naturally aged, the strength will decrease as the silicon content is increased. Therefore, its content should be controlled below 0.5%.

Production practices verify that the iron content should be larger than the silicon content, in order to lower the thermal brittleness of the alloys. However, in the LY11 alloy, the silicon content should be larger than the iron content, in order to improve the castability of the alloy.

Nickel is also a harmful impurity in hard aluminium alloys. Nickel in the alloys can combine with copper to form the insoluble compound AlCuNi , so that the hardening phases CuAl_2 and $\text{S}(\text{CuMgAl}_2)$ are reduced in quantity, causing the mechanical properties to decrease. Therefore, the nickel content in the alloys should be controlled.

Although zinc impurity does not have any effect on the

room temperature properties of the alloys, it can reduce the thermal strength of the alloys immensely. At the same time, zinc can increase the tendency of the alloys to develop cracks during casting and soldering, so it should be strictly controlled.

It is apparent from the Al-Cu-Mg system ternary equilibrium diagram^(Fig. IV-1) that the low-strength hard aluminium alloy LY10 is situated in the $\alpha(\text{Al}) + \text{CuAl}_2$ phase zone. Its principal hardening phase is CuAl_2 . The alloy LY1 is situated in the $\alpha(\text{Al}) + \text{CuAl}_2 + \text{S}(\text{CuMgAl}_2)$ phase zone boundary, and its principal hardening phase is also CuAl_2 . The medium-strength hard aluminium alloy LY11 is situated at the left side of the $\alpha(\text{Al}) + \text{CuAl}_2 + \text{S}$ phase zone. Its principal hardening phase is CuAl_2 , as well as a small amount of $\text{S}(\text{CuMgAl}_2)$ phase (when the silicon content in the alloy is low). The high-strength hard aluminium alloy LY12, owing to its higher content of magnesium, is situated at the right side of the $\alpha(\text{Al}) + \text{CuAl}_2 + \text{S}$ phase zone. Its principal hardening phase is $\text{S}(\text{CuMgAl}_2)$, followed by CuAl_2 . The refractory alloy LY2 is situated in the $\alpha(\text{Al}) + \text{S}$ phase zone. Its principal hardening phase is $\text{S}(\text{CuMgAl}_2)$. Because of the fluctuation of compositions, small amount of CuAl_2 can also appear.

The appearance of the principal hardening phases in the alloys should be determined by the following ratios. When Cu:Mg is equal to or less than 2.6, the $\text{S}(\text{CuMgAl}_2)$ phase is formed; when Cu:Mg exceeds 2.6, either the S and CuAl_2 phases or the CuAl_2 phase is formed.

Iron, silicon, manganese, and copper in the alloys react with one another to form FeAl_3 , $(\text{FeMn})\text{Al}_6$, Cu_2FeAl_7 , and $(\text{FeMnSi})\text{Al}_6$, which are brittle impurity phases. During heat

treatment processes, these impurity phases do not dissolve into the matrices easily. Silicon can also combine with magnesium to form Mg_2Si , which exists as a hardening phase in the LY11 alloy.

Through the analyses of metallography and electron microprobing, the hardening phases and some of the impurity phases of typical hard aluminium alloys under the semi-continuous casting condition are listed as follows: CuAl_2 in the LY10 alloy (Figure IV-4); CuAl_2 , Mg_2Si , and Cu_2FeAl_7 in the LY11 alloy (Figure IV-5 and Figure IV-11); CuAl_2 , $\text{S}(\text{CuMgAl}_2)$, and $(\text{FeMnSi})\text{Al}_6$ in the LY12 alloy (Figure IV-6, Figure IV-8, Figure IV-9, and Figure IV-10); and $\text{S}(\text{CuMgAl}_2)$ and CuAl_2 in the LY2 alloy (Figure IV-7).

CuAl_2 phase: Under the semi-continuous casting condition, it exists either in the binary eutectic $\alpha(\text{Al}) + \text{CuAl}_2$ mixture, or in the ternary eutectic $\alpha(\text{Al}) + \text{CuAl}_2 + \text{S}(\text{CuMgAl}_2)$ mixture.

Before etching, CuAl_2 has a very faint pink color. When etched in 25% HNO_3 aqueous solution (room temperature) followed by 10gm $\text{NaOH} + 100\text{ml H}_2\text{O}$ (70°C) for 3-5 min. each turn, CuAl_2 changes its color to copper-red. If CuAl_2 is etched by mixed-acids aqueous solution, and then rubbed with 25% HNO_3 aqueous solution to remove the black films, sometimes it can appear copper-red. This is due to the etching of 25% HNO_3 aqueous solution, and should not be mistaken as the etching effect caused by the mixed-acids aqueous solution.

$\text{S}(\text{CuMgAl}_2)$ phase: The eutectic structure formed by $\text{S}(\text{CuMgAl}_2)$ and $\alpha(\text{Al})$ appears greyish-yellow and honeycomb-like before etching, and turns blackish-brown after etching in 25% HNO_3 aqueous solution, and brown to dark brown after etch-

ing in mixed-acids aqueous solution.

Mg_2Si phase: See Chapter Five on Al-Mg-Si-Cu system alloys.

$(FeMnSi)Al_6$ phase: See Chapter Eight on Al-Cu-Mn system alloys.

Cu_2FeAl_7 : It appears needle-like, bright grey in color before etching, and brown in color after etching in mixed-acids aqueous solution.

Section 2 Properties of Alloys under Heat Treatments

The alloy composition of LY12 is situated in the shaded area in Figure IV-2. It is found from metallographical

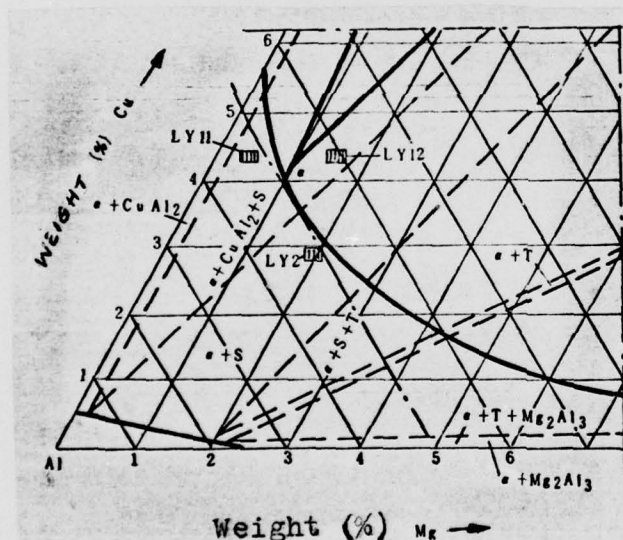


Figure IV-1 Distribution of Aluminium-Rich Solid-State Phase Zones of the Al-Cu-Mg System Alloys

analysis that when the LY12 alloy is quenched below $480^{\circ}C$, $CuAl_2$ in the binary eutectic mixture changes little, whereas the S and $CuAl_2$ phases in the ternary eutectic mixture dissolve markedly into the solid solution. If quenching is carried out at $490^{\circ}C$, $CuAl_2$ in the binary eutectic mixture will begin to dissolve, as well as the $CuAl_2$ and S phases in the ternary eutectic mixture. When the alloy is quenched at $502^{\circ}C$,

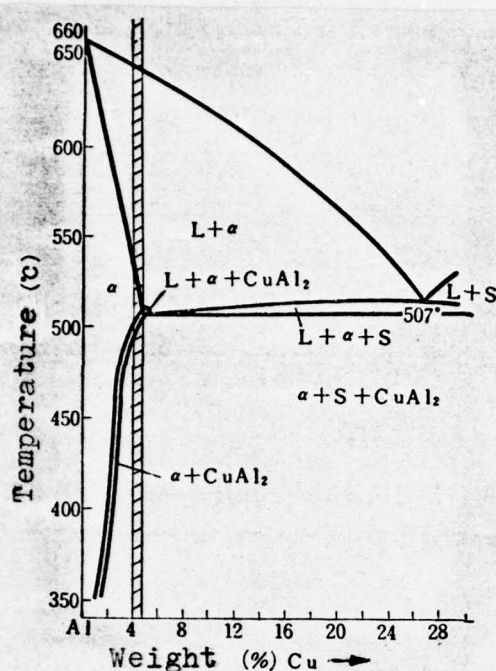


Figure IV-2 Vertical Cross-Section of Al-X in Figure 1 of the General Discussion

CuAl_2 in the binary eutectic mixture shows marked dissolution into the solid solution. The feature is that the content of the phase formed is less than that at low temperature, and the boundaries of the residual phase become smooth. When the alloy is quenched at 505°C , the dissolution of the phases proceeds more fully, and the principal hardening phases decrease in quantity markedly, but spherical alloy eutectic structures and local re-melting at the grain

boundaries (the alloy has been over-fired) appear. As the temperature is raised, the re-melting of the eutectic mixtures is more pronounced. Since the separation between the $\alpha(\text{Al}) + \text{S} + \text{CuAl}_2$ ternary eutectic temperature and the temperature at which the soluble phases in the LY12 alloy can dissolve into the solid solutions fully is very narrow, this alloy is extremely sensitive to over-firing. Under the production conditions, the quenching temperature of $495\text{--}500^\circ\text{C}$ can be used for the LY12 alloy.

When alloys of this system that are quenched and artificially aged are compared to those that are quenched and naturally aged, the former are more susceptible to intergranular

corrosion than the latter, so this type of treatment should only be used in making high-temperature structures. For ordinary structures, quenching and natural ageing is used. It can be seen from Figure IV-3 that the tensile strength and yield strength do not increase markedly until 1 hour after the alloy has been quenched. They then begin to rise rapidly. 12 hours after quenching, the rates of increase slow down. 48 hours after quenching, the tensile strength and yield strength remain basically constant, reaching their maximum values.

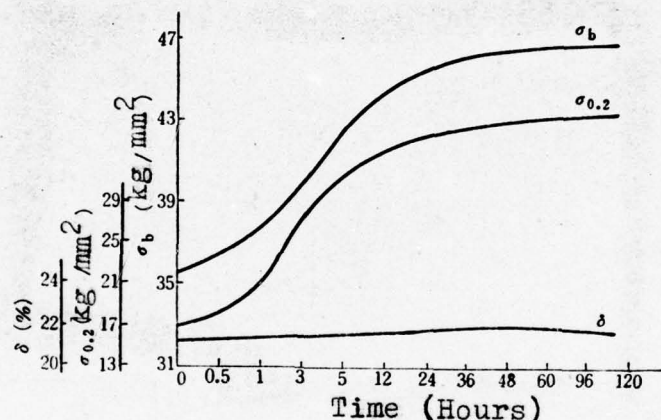


Figure IV-3 Dependence of the Mechanical Properties of the LY12 Alloy on the Natural Ageing Time After Quenching

The rate of quenching has a very strong effect on the corrosion resistivity of the alloys. Corrosion testings on LY11 and LY12 alloys show that their loss in strengths is related to the rate of quenching: the higher the rate of quenching, the smaller the loss in strengths, and the better

the corrosion resistivity. If the rate of quenching is lowered, compounds (such as CuAl_2) will precipitate profusely from the supersaturated solid solution along the grain boundaries, thereby lowering the corrosion resistivity of the alloy. For the LY11 and LY12 alloys, the quenching rates for the lowest corrosion resistivity are $20^\circ\text{C}/\text{sec}$ and $14^\circ\text{C}/\text{sec}$ respectively. However, slower rates than the above will increase the corrosion resistivity slightly. This could be due to the fact that under very slow quenching rate, very widespread decomposition and precipitation occurs.

Quenching for more than one times has definite effects on the properties of the alloys. For example, the yield strength of an LY12 alloy thick-walled structural-shape material generally decreases after quenching for more than one times. A thin-walled structural-shape material, when the extrusion effect exists, has its yield strength lowered by about $4\text{kg}/\text{mm}^2$ after multiple quenching.

The recrystallization features of the LY11 and LY12 alloys are as follows:

1. For the same type of alloy, working methods have very pronounced influence on the recrystallization of the alloy. The recrystallization temperatures of extruded products are generally higher than those of rolled products. The recrystallization temperature ranges of the former are also wider than those of the latter. In particular, for once-extruded products, the final recrystallization temperatures are usually above the over-firing temperatures.

2. The recrystallization temperatures of hot-rolled are higher than those of the cold-rolled products.

3. For hot-rolled sheets with low deformation rates

and rods of large specifications, they exhibit elongated recrystallized grains. For cold-drawn tubes, cold-spun tubes, and cold-rolled sheets that have large deformation rates, they exhibit equiaxed recrystallized grains during recrystallization.

The recrystallization temperatures of the LY11 and LY12 products are determined through testings and are listed in Table IV-2.

Table IV-2 Recrystallization Parameters of the LY11 and LY12 Alloys

Alloy	Variety	SPECIFICATION (mm)	Technical Conditions						RECRYSTALLIZATION TEMPERATURE (°C)	
			Rolling		Extrusion		Annealing Method		initial	final
			TEMP- ERATURE (°C)	DEFORM- ATION (%)	TEMP- ERATURE (°C)	DEFORM- ATION (%)	SALT BATH OR AIR FURNACE	* (min)		
LY11	Sheet	6.0	420	96			Furnace	20	310~315	355~360
		1.0	ROOM TEMPER- ATURE	84				20	250~255	275~280
	Rod	φ 10			370~420	97		20	360~365	535~540
LY12	Tube	18 × 15			ROOM TEMPER- ATURE	98	Furnace	20	270~275	315~320
	Sheet	6.0	420	96				20	350~355	495~500
		1.0	ROOM TEMPER- ATURE	83				20	270~275	305~310
	Rod	φ 90			370	94		20	380~385	530~535
	Tube	83 × 27			370~420	89		20	380~385	535~540

* Firing time at constant temperature

Section 3 Structures of Ingot and Processed Products

1. Phase Formations

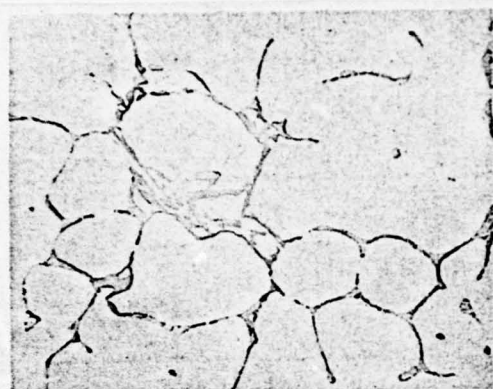


Figure IV-4 320x

Alloy	LY10
Condition	Semi-continuously cast
Etchant	Not etched
Structural features	Eutectic $\alpha(\text{Al}) + \text{CuAl}_2$, resembles veins of a net. CuAl_2 appears copper-red.

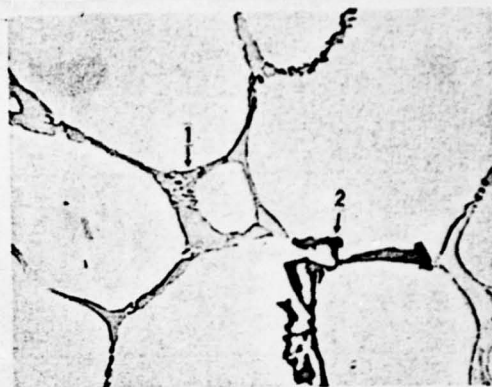


Figure IV-5 320x

Alloy	LY11
Condition	Semi-continuously cast
Etchant	25% HNO_3 aqueous solution
Structural features	<p>1 -- Eutectic $\alpha(\text{Al}) + \text{CuAl}_2$, resembles veins of a net. CuAl_2 appears copper-red.</p> <p>2 -- Eutectic $\alpha(\text{Al}) + \text{Mg}_2\text{Si}$. Mg_2Si is black and bone-shaped.</p>

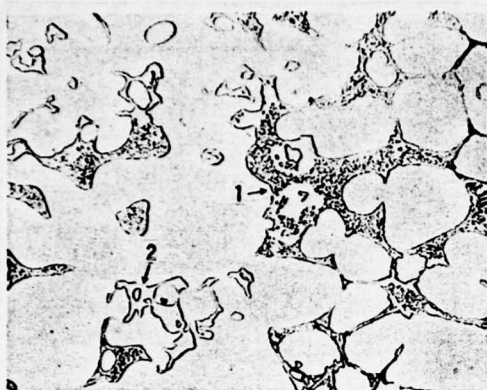


Figure IV-6

320x

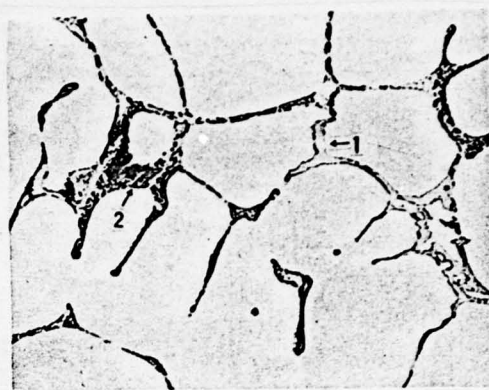


Figure IV-7

320x

Alloy	LY12
Condition	Semi-continuously cast
Etchant	25% HNO_3 aqueous solution
Structural features	<p>1 -- Eutectic $\alpha(\text{Al}) + \text{CuAl}_2$ + $\text{S}(\text{CuMgAl}_2)$, honeycomb-like. S-phase appears brown.</p> <p>2 -- Eutectic $\alpha(\text{Al}) + \text{CuAl}_2$. CuAl_2 appears copper-red.</p>

Alloy	LY12
Condition	Sem-continuously cast
Etchant	25% HNO_3 aqueous solution
Structural features	<p>1 -- Eutectic $\alpha(\text{Al}) + \text{CuAl}_2$. CuAl_2 appears copper-red.</p> <p>2 -- Eutectic $\alpha(\text{Al}) + \text{CuAl}_2$ + $\text{S}(\text{CuMgAl}_2)$. S-phase is brown and honeycomb-like.</p>

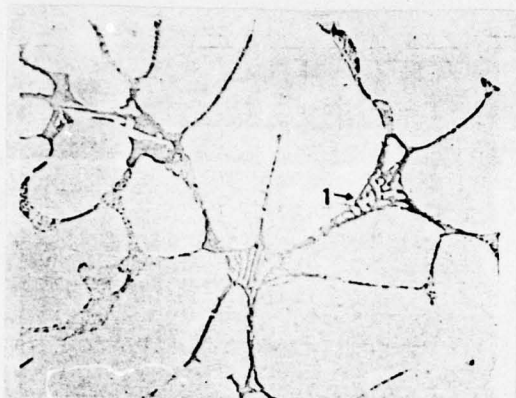


Figure IV-8

320x



Figure IV-9

320x

Alloy	LY12
Condition	Semi-continuously cast
Etchant	Not etched
Structural features	Structure of the elevated area where preferential precipitation takes place in the ingot 1 -- $(\text{FeMnSi})\text{Al}_6$, light grey in color, branch-shaped.

Alloy	LY12
Condition	Semi-continuously cast
Etchant	20% H_2SO_4 aqueous solution
Structural features	Structure of the elevated area where preferential precipitation takes place in the ingot 1 -- $(\text{FeMnSi})\text{Al}_6$, branch-shaped; becomes blackish brown in color after etching.



Figure IV-10 320x
 Alloy LY12
 Condition Semi-continuously cast
 Etchant Not etched
 Structural features Structure of the elevated area where preferential precipitation takes place in the ingot surface.
 1 -- Primary Mg_2Si , turquoise polygon.
 2 -- $\alpha(Al) + Mg_2Si$ eutectic. Mg_2Si is turquoise and bone-shaped.



Figure IV-11 320x
 Alloy LY11
 Condition Semi-continuously cast
 Etchant 20% H_2SO_4 aqueous solution
 Structural features Structure of the elevated area where preferential precipitation takes place in the ingot surface.
 1 -- Primary Mg_2Si , black polygon.
 2 -- $\alpha(Al) + Mg_2Si$ eutectic. Mg_2Si is black and bone-shaped.
 3 -- Cu_2FeAl_7 , deep grey and needle-like.

2. Structures of Ingots

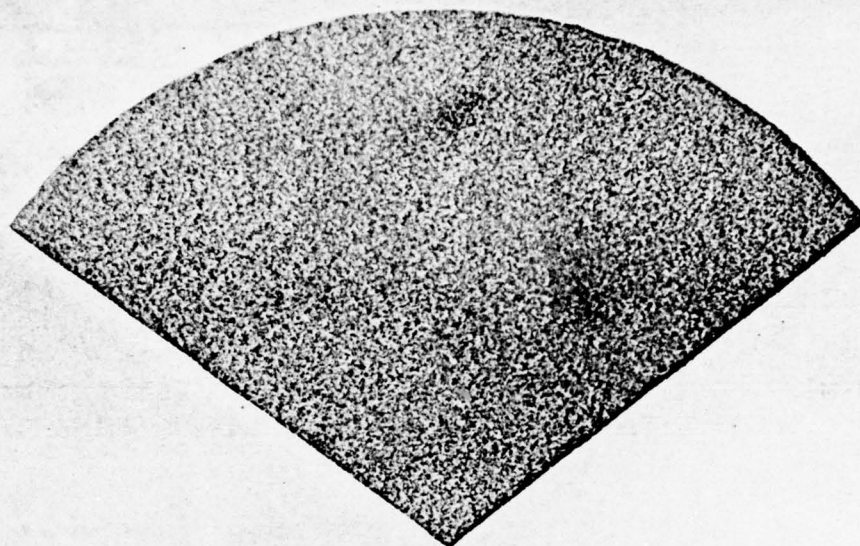


Figure IV-12 Etched in 12% NaOH Aqueous Solution

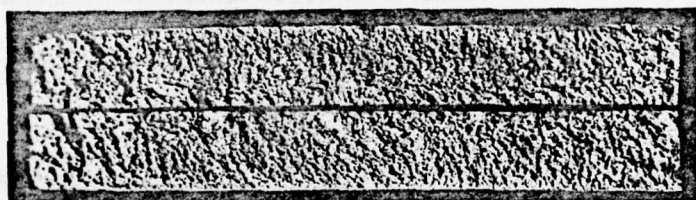


Figure IV-13

Alloy and Condition	LY12 semi-continuously cast
Specification	Ø192mm round ingot
Structural features	<p>Figure IV-12 is the transverse macro-structure of the head of the ingot. The grains are fine and uniform. Those in the 6~7 mm thick zone near the surface are finer than the rest.</p> <p>Figure IV-13 is the structure of the portion where the ingot cleaves. Grains are fine and even.</p>

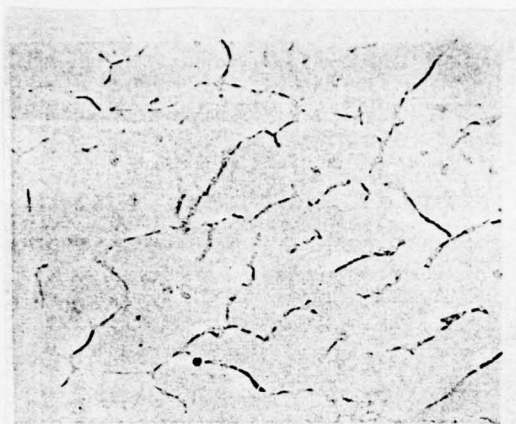


Figure IV-14 210x
Etched in Mixed-Acids Aqueous
Solution



Figure IV-15 100x
Structure of Electropolished
and Anodized Specimen under
Polarized Light

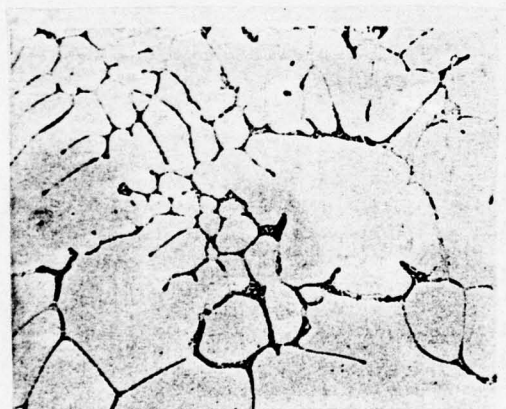


Figure IV-16 210x
Etched in Mixed-Acids Aqueous
Solution



Figure IV-17 100x
Structure of Electropolished
and Anodized Specimen under
Polarized Light

Alloy and Condition	LY12 semi-continuously cast
Specification	φ192mm round ingot
Structural features	Figure IV-14 is the transverse structure

of the edge portion of the ingot. The cells of the dendritic network are coarse and are evenly distributed.

Figure IV-15 is the same structure as Figure IV-14 under polarized light. The grains are fine and uniform. Preferential precipitation takes place inside the grains.

Figure IV-16 is the transverse structure of the central portion of the ingot. The cells of the dendritic network here is smaller than those in the edge portion, but they are not uniform.

Figure IV-17 is the same structure as Figure IV-16 under polarized light. The grains here are coarser than those in the edge portion. Preferential precipitation takes place inside the grains.

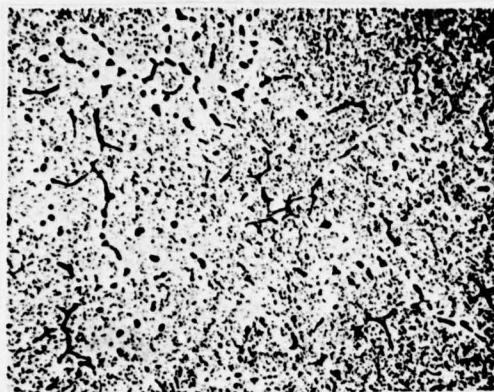


Figure IV-18
Etched in Mixed-Acids Aqueous
Solution

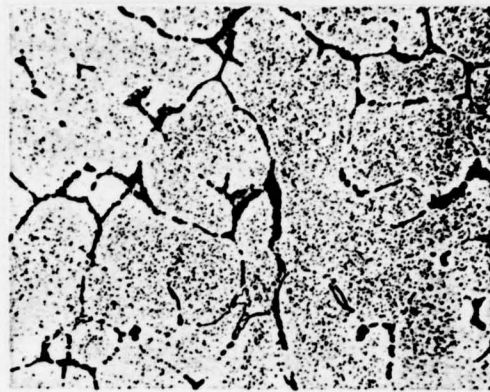


Figure IV-19
Etched in Mixed-Acids Aqueous
Solution

Alloy and Condition	LY12 semi-continuously cast, and homogenized at 485°C for 12 hours
Specification	φ192mm round ingot
Structural features	Figure IV-18 and Figure IV-19 are the transverse structure of the edge portion and of the central portion respectively. After homogenization, the dendritic network has partially dissolved into the solid solution, while a large amount of manganese-bearing compound particles are precipitated from the $\alpha(\text{Al})$ matrix.

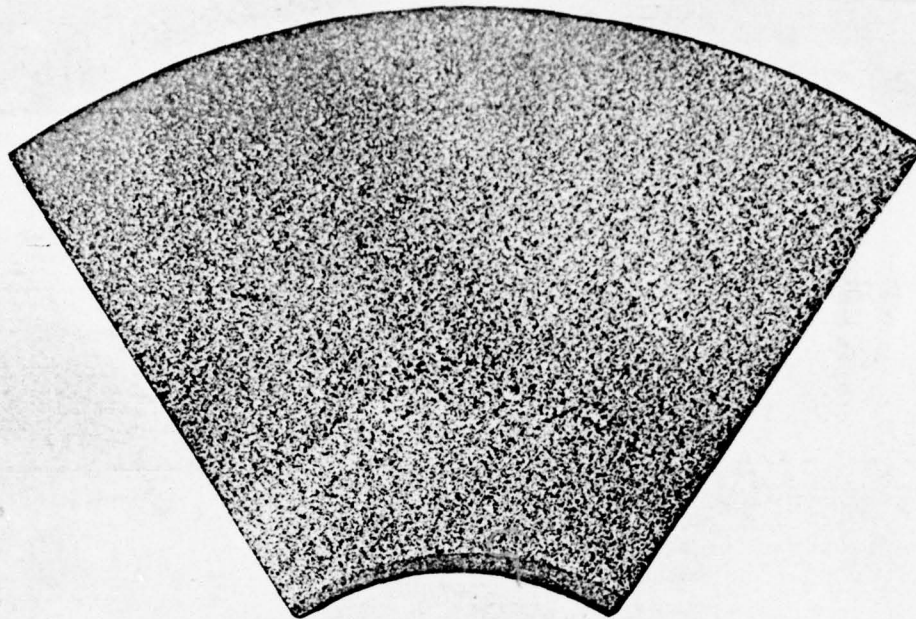


Figure IV-20 2:1
Etched in 18% NaOH Aqueous Solution

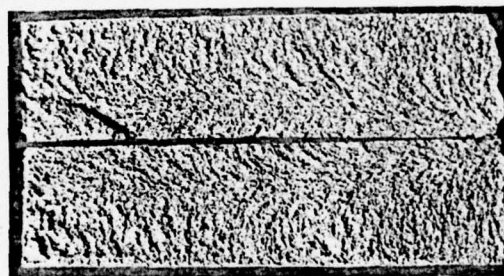


Figure IV-21 2:1

Alloy and Condition	LY12 semi-continuously cast
Specification	Ø270x106mm round hollow ingot
Structural features	Figure IV-20 is the macrostructure of the ingot. The grains are fine and uniform. Figure IV-21 is the structure of the portion where the ingot cleaves, which is fine and dense. The cleavage is smooth.

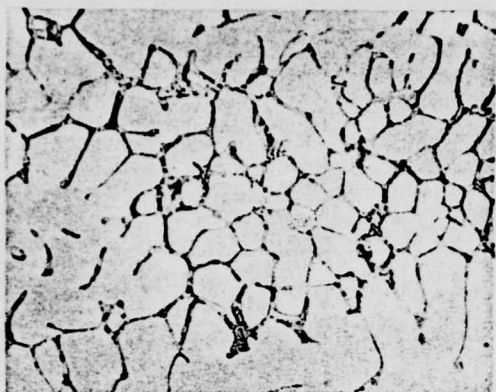


Figure IV-22 210x
Etched in Mixed-Acids Aqueous
Solution

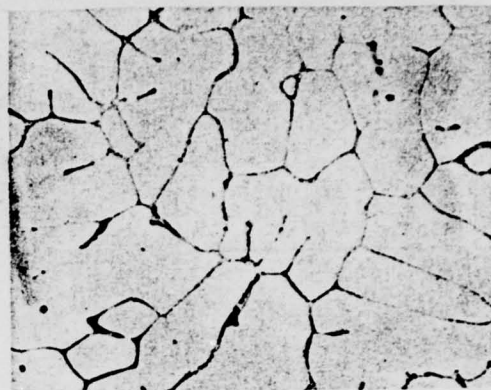


Figure IV-23 210x
Etched in Mixed-Acids Aqueous
Solution

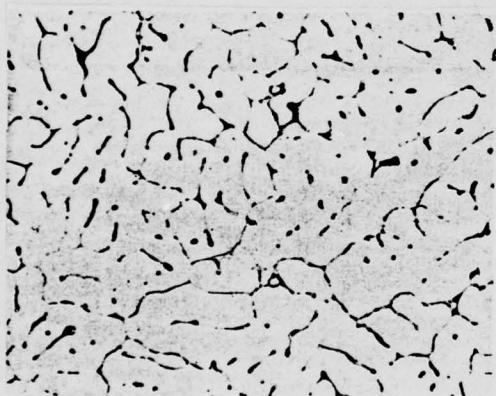


Figure IV-24 210x
Etched in Mixed-Acids Aqueous
Solution

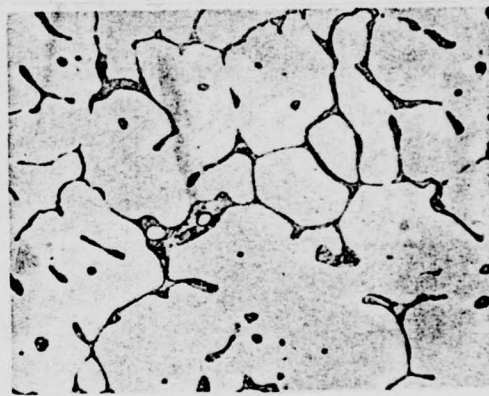


Figure IV-25 210x
Etched in Mixed-Acids Aqueous
Solution

Alloy and Condition	LY12 Semi-continuously cast
Specification	Ø270x106mm round hollow ingot
Structural features	Figure IV-22 is the structure of a hunch area in the inner surface where preferential precipiatation takes place.

The cells of the dendritic network are small in size and the separations between adjacent cells are thick. A large amount of impurity phases are visible.

Figure IV-23 is the structure of an area 15mm deep from the inner surface. The cells of the dendritic network are coarse and the separations between adjacent cells are thin.

Figure IV-24 is the structure of the middle portion of the ingot. The cells of the dendritic network are fine and uniform, but not entirely continuous. The separations between cells are thin compared with the preferentially precipitated hunch area.

Figure IV-25 is the structure of an area 20mm deep from the inner surface. The cells of the dendritic network is coarse, and the separations between adjacent cells are thick.

3. Structures of Sheets

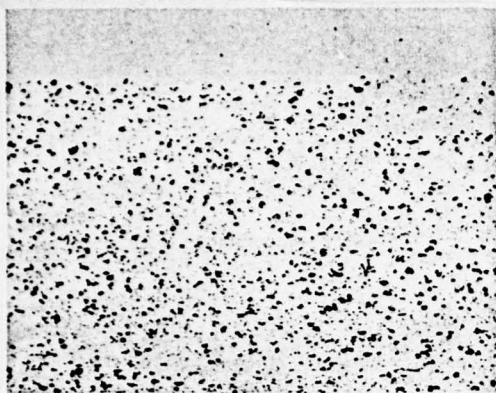


Figure IV-26 210x
Etched in Mixed-Acids Aqueous
Solution

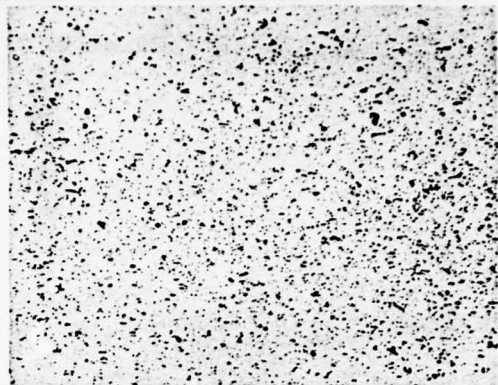


Figure IV-27 210x
Etched in Mixed-Acids Aqueous
Solution

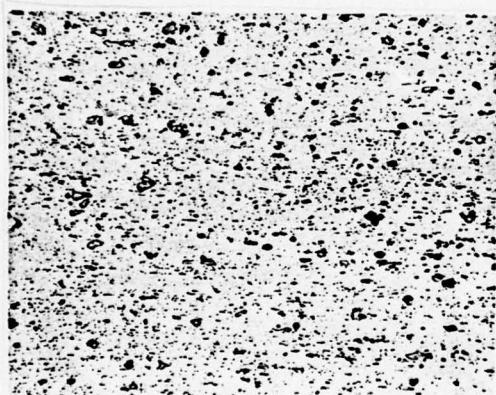


Figure IV-28 210x
Etched in Mixed-Acids Aqueous
Solution

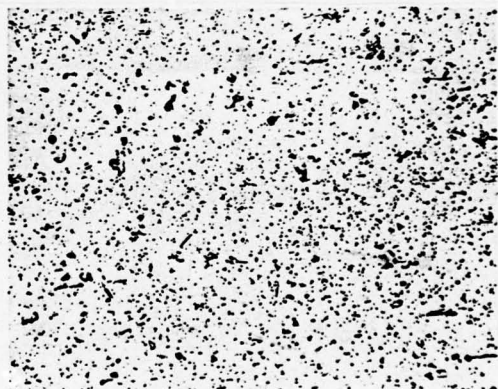


Figure IV-29 210x
Etched in Mixed-Acids Aqueous
Solution

Alloy and Condition	LY12R
Specification	10mm hot-rolled sheet
Structural features	Figure IV-26 and Figure IV-28 are the longitudinal structures of the portion close to the surface and of the central

portion respectively. Compounds are arranged in arrays along the rolling direction. They are finer and more evenly distributed in the portion close to the surface than in the central portion.

The bright white place in Figure IV-26 is the coated Al layer.

Figure IV-27 and Figure IV-29 are the transverse structures of the portion close to the surface and of the central portion respectively.

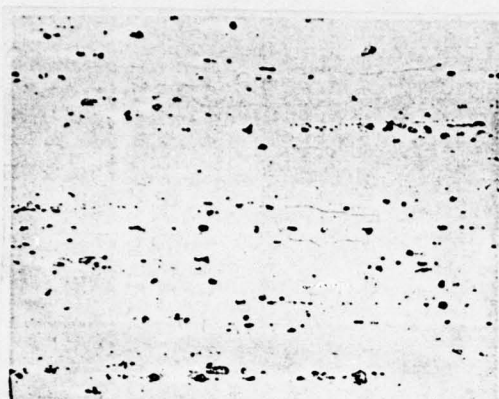


Figure IV-30
Etched in Mixed-Acids Aqueous
Solution

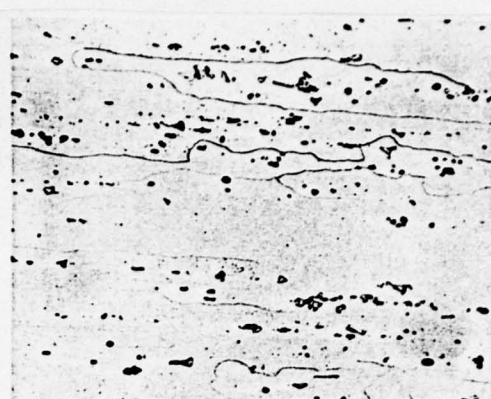


Figure IV-31
Etched in Mixed-Acids Aqueous
Solution

Alloy and Condition
Specification
Structural features

LY12CZ (500°C, 30 min., water-cooled)
10mm hot-rolled sheet
Figure IV-30 and Figure IV-31 are the longitudinal structures of the portion close to the surface and of the central portion respectively. After heating in the quenching process, the alloy has undergone complete recrystallization. The grains are elongated along the rolling direction. Hardening phases such as $S(CuMgAl_2)$ and $CuAl_2$ have already dissolved into the solid solution.



Figure IV-32
Etched in Mixed-Acids Aqueous
Solution

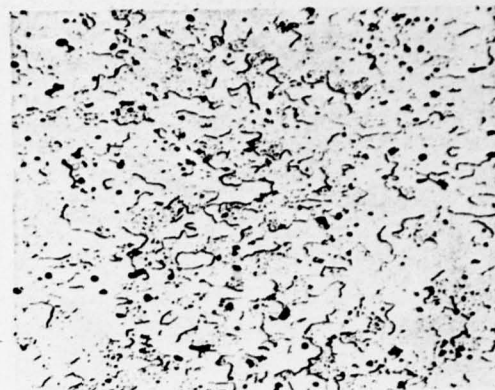


Figure IV-33
Etched in Mixed-Acids Aqueous
Solution

Alloy and Condition
Specification

LY12CZ (500°C, 20 min., water-cooled)
1.0mm cold-spun sheet

Structural features

Figure IV-32 and Figure IV-33 are the longitudinal structures of the portion close to the surface and of the central portion respectively. After heating in the quenching process, the alloy has undergone complete recrystallization, and exhibits equiaxed grains. Broken compounds are distributed rather evenly, but do not possess clear directionality. The hardening phases such as $S(CuMgAl_2)$ and $CuAl_2$ are more fully dissolved. The bright white zone in Figure IV-32 is the coated Al layer.

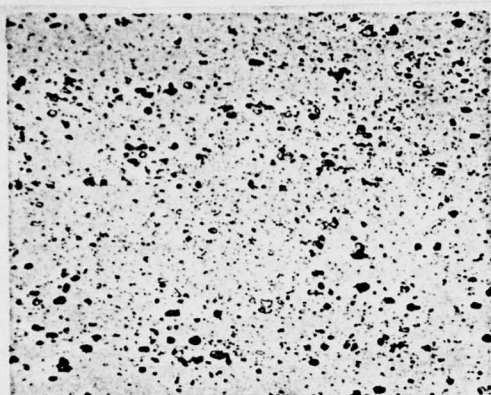


Figure IV-34 210x
Etched in Mixed-Acids Aqueous
Solution



Figure IV-35 100x
Structure of Electropolished
and Anodized Specimen under
Polarized Light

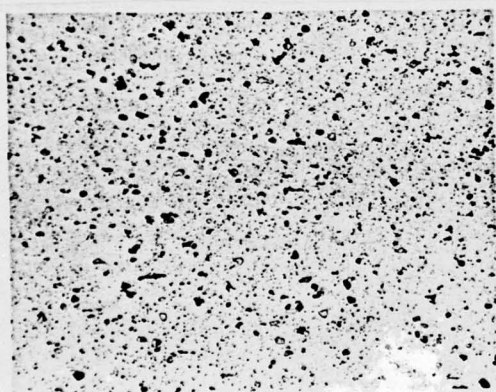


Figure IV-36 210x
Etched in Mixed-Acids Aqueous
Solution



Figure IV-37 100x
Structure of Electropolished
and Anodized Specimen under
Polarized Light

Alloy and Condition LY12M (420°C, 180 min., cooled in
furnace)

Specification 1.0mm cold-rolled sheet

Structural features

Figure IV-34 and Figure IV-35 are longitudinal structures. The compounds still maintain the directionality in arrays. Particles of hardening phases such as $S(CuMgAl_2)$ and $CuAl_2$ are precipitated in large amount from the $\alpha(Al)$ matrix. The sheet has undergone complete recrystallization. The grains are elongated along the extrusion direction. Figure IV-36 and Figure IV-37 are the transverse structures. The compounds are distributed more evenly in this direction than in the longitudinal direction, but do not possess clear directionality. The sheet has undergone complete recrystallization.

4. Structures of Extruded Products

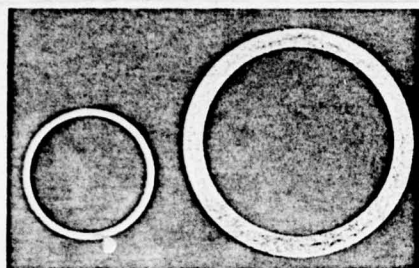


Figure IV-38 1:1
Etched in 18% NaOH Aqueous Solution

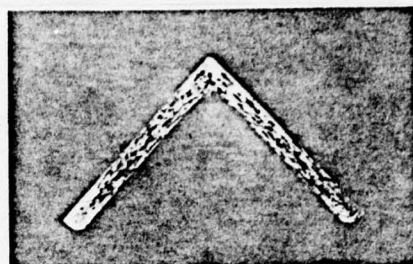


Figure IV-39 1:1
Etched in 18% NaOH Aqueous Solution

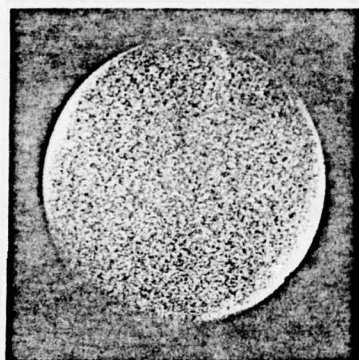


Figure IV-40 1:1
Etched in 18% NaOH Aqueous Solution

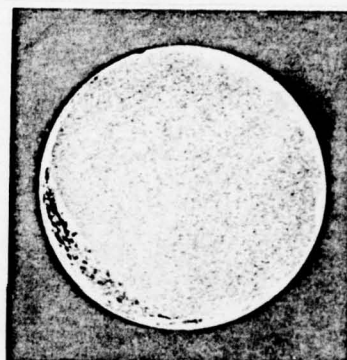


Figure IV-41 1:1
Etched in 18% NaOH Aqueous Solution

Alloy and Condition
Specification

LY12CZ

Figure IV-38 is a $\phi 31 \times 25$ mm cold-spun tube (right), and a $\phi 18 \times 16$ mm cold-drawn tube (left).

Figure IV-39 is a XC118 structural-shape. Figure IV-40 and Figure IV-41 are a $\phi 40$ mm rod.

Structural features

Macrostructures of the tube exhibits fine

grains. Macrostructure of the the structural-shape exhibits uniform recrystallized structure. Front end of the rod (Figure IV-40) exhibits uniform structure; rear end of the rod (Figure IV-41) exhibits a crescent-shaped coarse-grain ring at the edge portion.

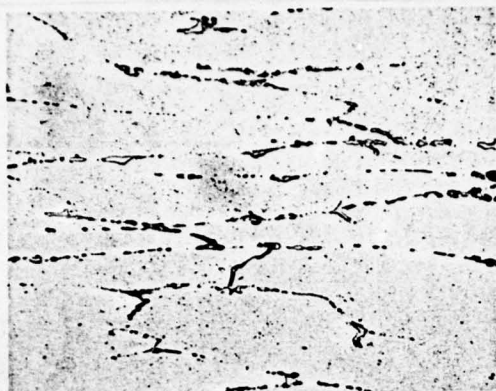


Figure IV-42 210 ×
Etched in Mixed-Acids
Aqueous Solution

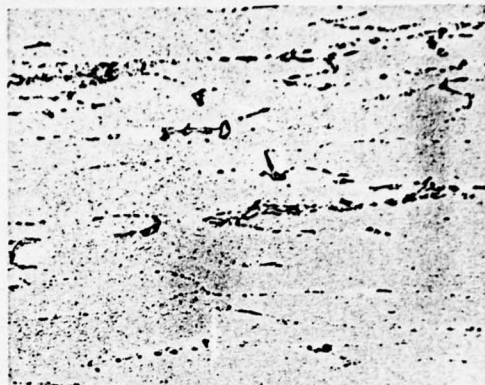


Figure IV-43 210 ×
Etched in Mixed-Acids
Aqueous Solution

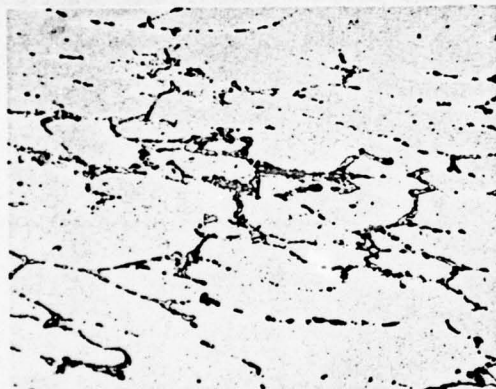


Figure IV-44 210 ×
Etched in Mixed-Acids
Solution

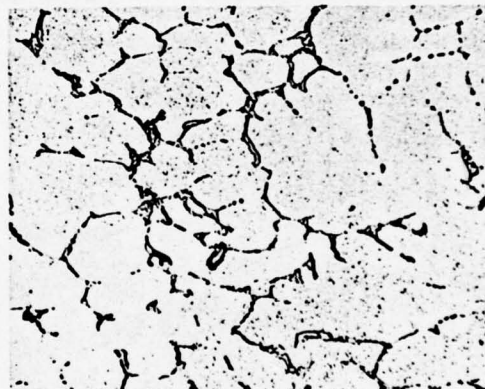


Figure IV-45 210 ×
Etched in Mixed-Acids
Solution



Figure IV-46 210x
Etched in Mixed-Acids Aqueous
Solution

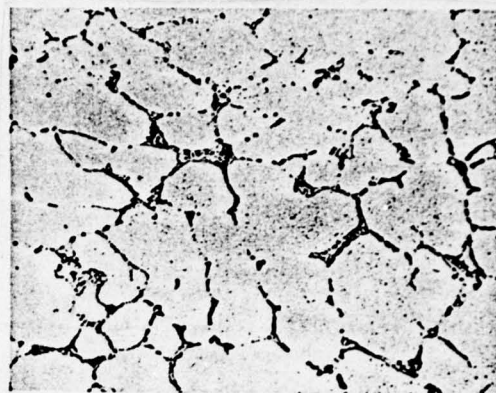


Figure IV-47 210x
Etched in Mixed-Acids Aqueous
Solution

Alloy and Condition LY12R
Specification ϕ 40mm rod

Structural features Figure IV-42, Figure IV-44, and Figure IV-46, are the longitudinal structures of the edge portion, the middle portion, and the central portion, of the front end of the rod respectively. Figure IV-43, Figure IV-45, and Figure IV-47, are the transverse structures of the edge portion, the middle portion, and the central portion of the front end of the rod respectively. The rod still retains a large amount of unbroken cast dendritic network structures. The extent of deformation is greater at the edge portion than at the middle and central portions. The dendritic network is elongated along the

extrusion direction. A large amount of compounds are precipitated from the $\alpha(\text{Al})$ matrix.

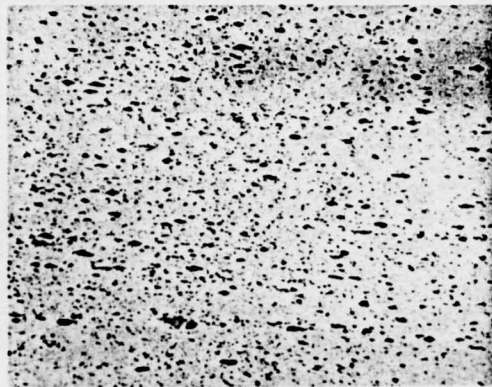


Figure IV-48 210 \times
Etched in Mixed-Acids
Aqueous Solution

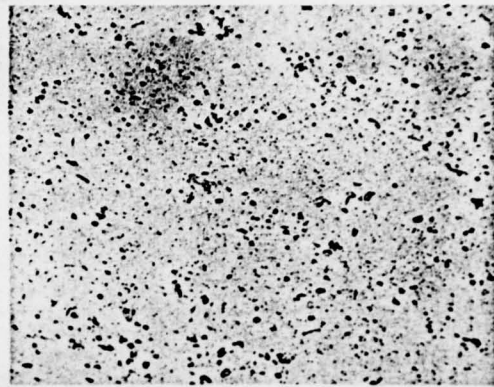


Figure IV-49 210 \times
Etched in Mixed-Acids
Aqueous Solution

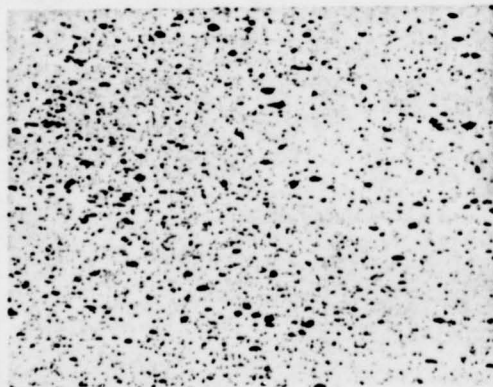


Figure IV-50 210 \times
Etched in Mixed-Acids
Aqueous Solution

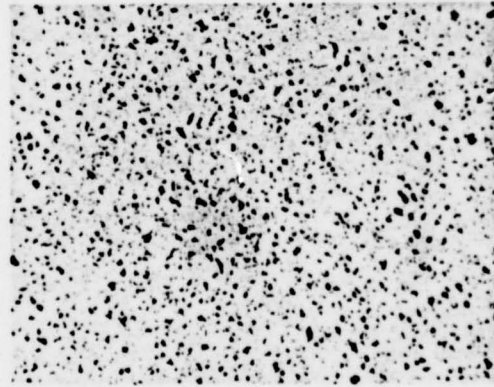


Figure IV-51 210 \times
Etched in Mixed-Acids
Aqueous Solution

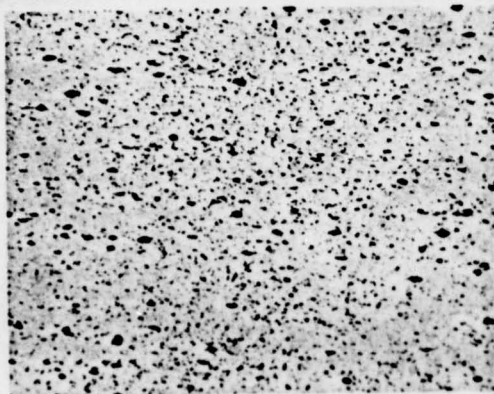


Figure IV-52 210x
Etched in Mixed-Acids Aqueous
Solution

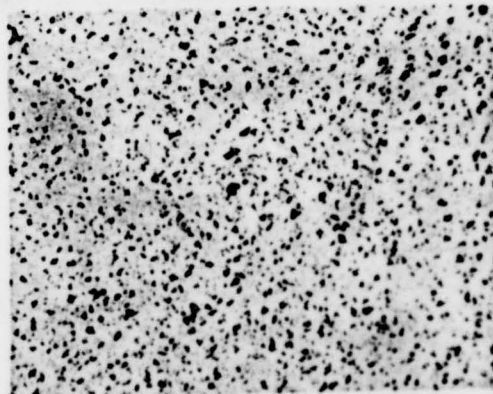


Figure IV-53 210x
Etched in Mixed-Acids Aqueous
Solution

Alloy and Condition

LY12R

Specification

φ40mm rod

Structural features

Figure IV-48, Figure IV-50, and Figure IV-52 are the longitudinal structures of the edge portion, middle portion, and central portion of the rear end of the rod respectively.

Figure IV-49, Figure IV-51, and Figure IV-53 are the transverse structures of the edge portion, the middle portion, and the central portion of the rear end of the rod respectively.

The extent of deformation is greater at the rear end than at the front end.

The cast dendritic network structure is completely broken.

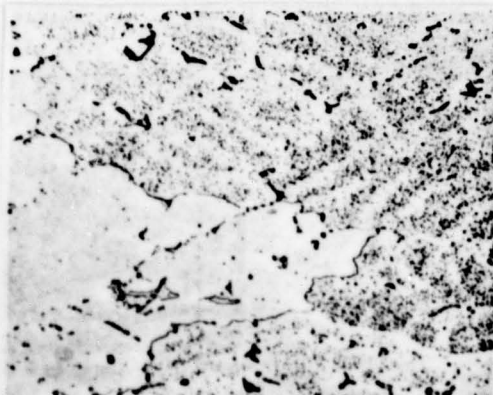


Figure IV-54 210x
Etched in Mixed-Acids
Aqueous Solution

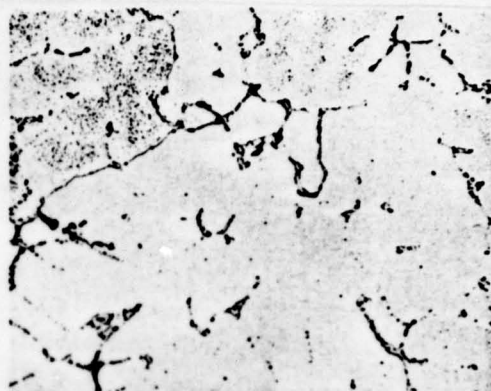


Figure IV-55 210x
Etched in Mixed-Acids
Aqueous Solution

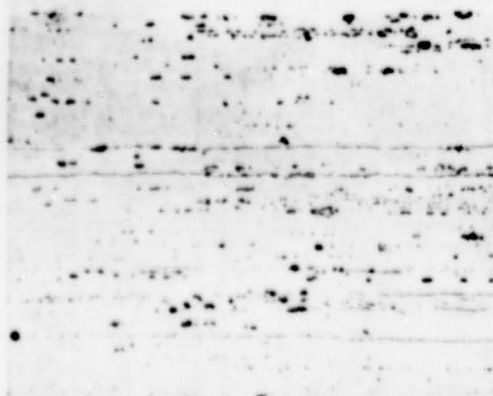


Figure IV-56 210x
Etched in Mixed-Acids
Aqueous Solution

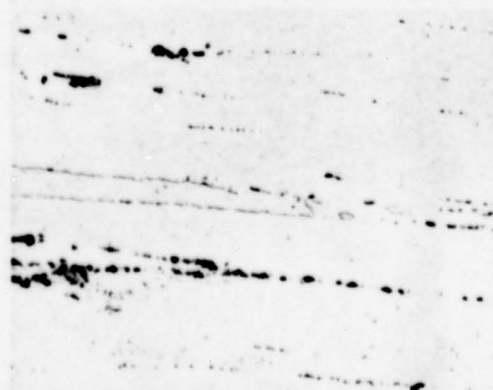


Figure IV-57 210x
Etched in Mixed-Acids
Aqueous Solution

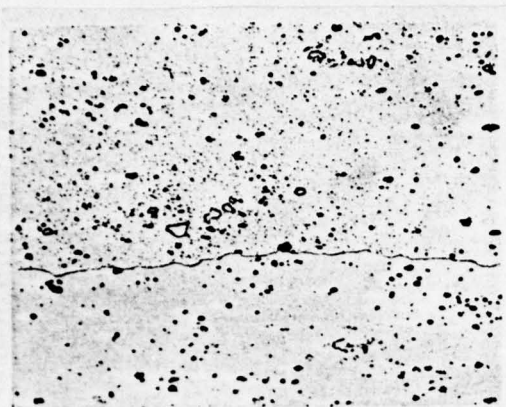


Figure IV-58 210x
Etched in Mixed-Acids Aqueous
Solution

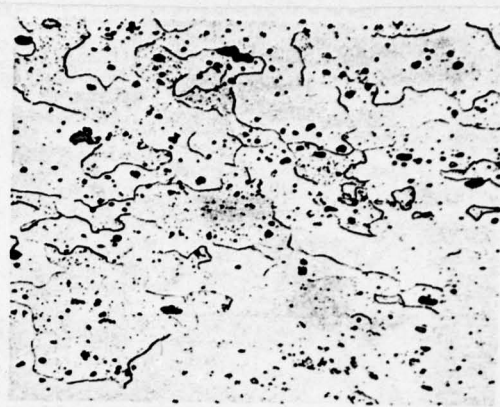


Figure IV-59 210x
Etched in Mixed-Acids Aqueous
Solution

Alloy and Condition
Specification
Structural features

LY12CZ (500°C, 40 min., watercooled)
Ø40mm rod

Figure IV-54 and Figure IV-55 are, respectively, the longitudinal structures of the edge and central portions of the rear end of the rod, which has undergone partial recrystallization. There are still many undissolved compound residues in the central portion.

Figure IV-56 and Figure-57 are the structures of the edge and central portions of the middle section of the rod in the longitudinal direction respectively. The extent of recrystallization here is greater than that at the front end of the rod. Grains are elongated along the extrusion direction.

Figure IV-58 and Figure IV-59 are the longitudinal structures of the edge and central portions of the rear end of the rod respectively. The grains in the coarse-grain region is particularly coarse, but the grains in other regions are fine.

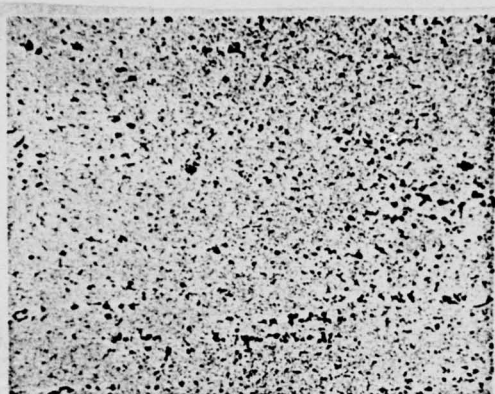


Figure IV-60 210x
Etched in Mixed-Acids Aqueous
Solution

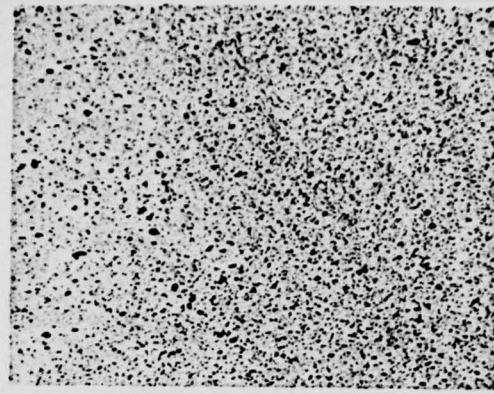


Figure IV-61 210x
Etched in Mixed-Acids Aqueous
Solution

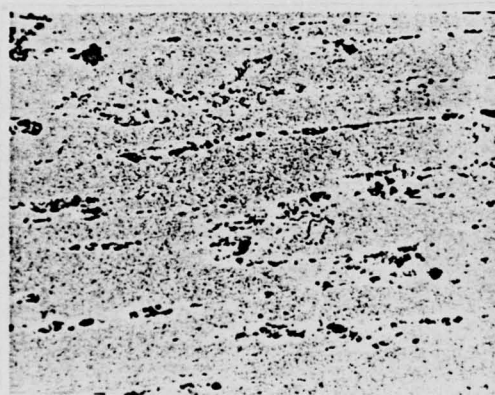


Figure IV-62 210x
Etched in Mixed-Acids Aqueous
Solution

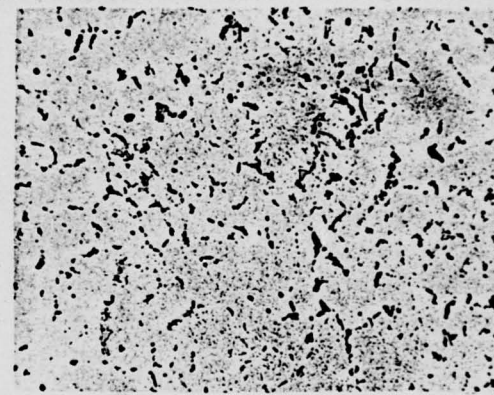


Figure IV-63 210x
Etched in Mixed-Acids Aqueous
Solution

Alloy and Condition	LY12M (420°C, 180 min., cooled in furnace)
Specification	Ø40mm rod
Structural features	Figure IV-60 and Figure IV-62 are the structures of the edge and central

portions of the middle section of the rod in the longitudinal direction respectively.

Figure IV-61 and Figure IV-63 are the transverse structures of the edge and central portions of the middle section of the rod respectively.

Compounds are arranged in arrays along the extrusion direction. There are still a considerable amount of residual compounds in the central portion. Compound particles are precipitated from the $\alpha(\text{Al})$ matrix in a large amount.



Figure IV-64 210x
Etched in Mixed-Acids Aqueous
Solution

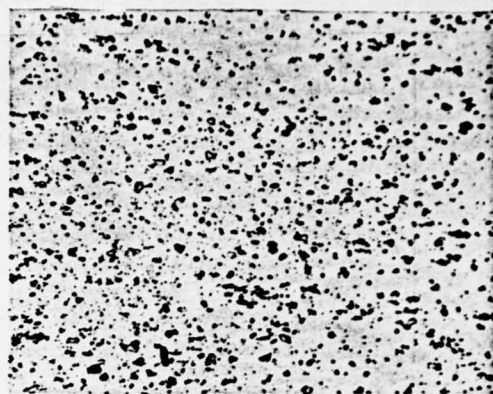


Figure IV-65 210x
Etched in Mixed-Acids Aqueous
Solution

Alloy and Condition
Specification
Structural features

LY12R
Ø68x40mm extruded tube
Figure IV-64 is the longitudinal structure of the central portion of the rear end of the tube. The compounds are broken considerably, and are arranged in arrays along the extrusion direction. Particles are precipitated from the compounds and are dispersed in the α (Al) matrix. Figure IV-65 is the transverse structure of the tube.

AD-A049 264

FOREIGN TECHNOLOGY DIV WRIGHT-PATTERSON AFB OHIO
DEFORMED ALUMINUM ALLOY METALLOGRAPHY.(U)
AUG 77

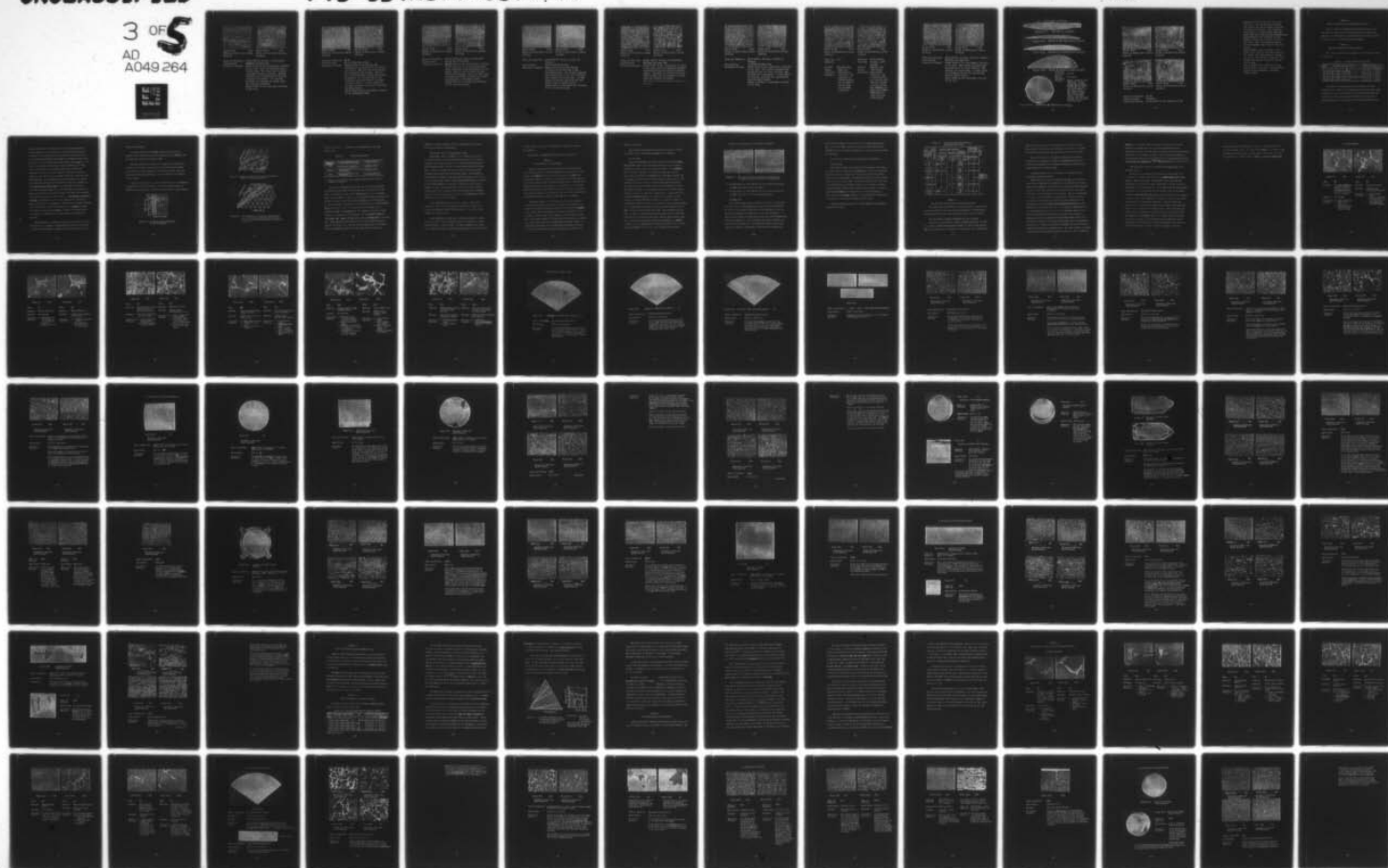
F/G 11/6

UNCLASSIFIED

FTD-ID(RS)T-0577-77

NL

3 OF 5
AD
A049 264



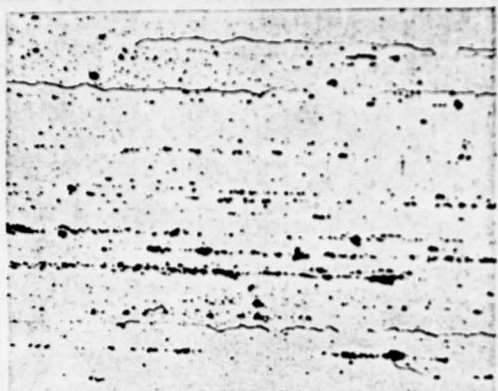


Figure IV-66 210x
Etched in Mixed-Acids Aqueous
Solution

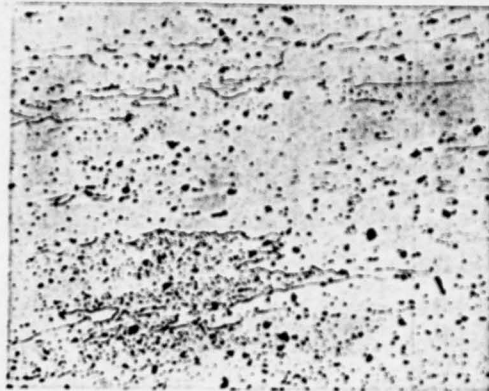


Figure IV-67 210x
Etched in Mixed-Acids Aqueous
Solution

Alloy and Condition
Specification

LY12CZ (500°C, 30 min., water-cooled)
ø68x40mm extruded tube

Structural features

Figure IV-66 is the longitudinal structure of the tube, which has undergone recrystallization. The grains are elongated along the extrusion direction. Soluble compounds have dissolved into the solid solution considerably. The residual compounds are arranged in arrays along the extrusion direction.

Figure IV-67 is the transverse structure of the tube.

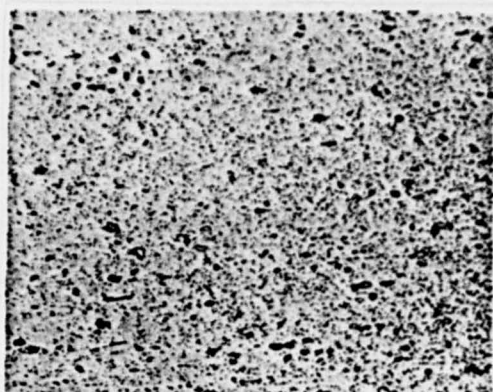


Figure IV-68 210x
Etched in Mixed-Acids Aqueous
Solution

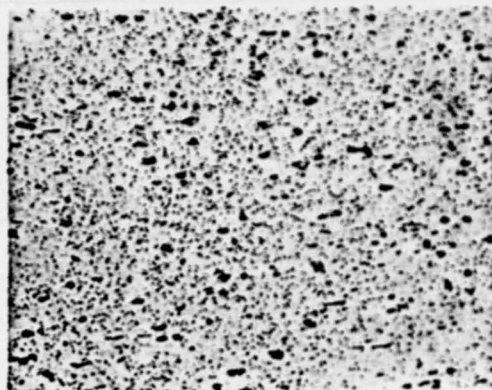


Figure IV-69 210x
Etched in Mixed-Acids Aqueous
Solution

Alloy and Condition

LY12R

Specification

XC-118 Structural-shape

Structural features

Figure IV-68 is the longitudinal structure of the rear end of the structural-shape. The cast dendritic network has completely been broken. Since it is a twice-extruded product, the directionality in the distribution of compounds is weaker than that of an once-extruded product. A large amount of compound particles are precipitated from the α (Al) matrix.

Figure IV-69 is the transverse structure of the structural-shape.

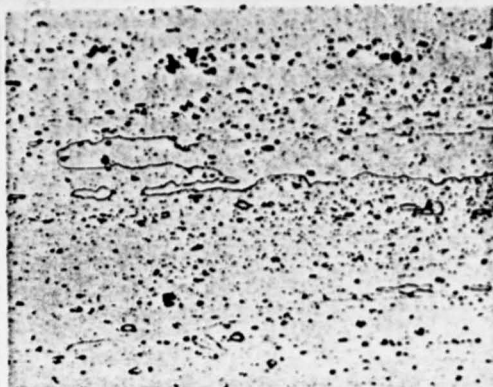


Figure IV-70 210x
Etched in Mixed-Acids Aqueous
Solution

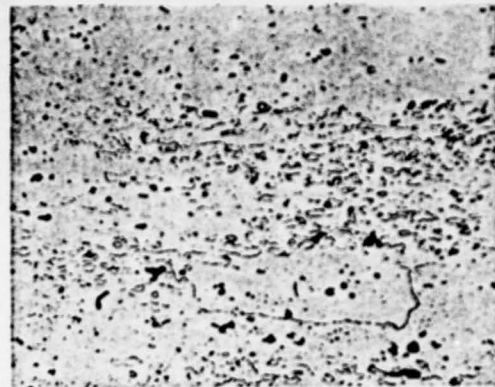


Figure IV-71 210x
Etched in Mixed-Acids Aqueous
Solution

Alloy and Condition	LY12CZ (500°C, 20 min., water-cooled)
Specification	XC-118 Structural-shape
Structural features	<p>Figure IV-70 is the longitudinal structure of the rear end of the structural-shape. After quenching, recrystallization is complete. Grains are elongated along the extrusion direction. There are still some residues of partially soluble and insoluble compounds on the $\alpha(\text{Al})$ matrix.</p> <p>Figure IV-71 is the transverse structure of the structural-shape.</p>

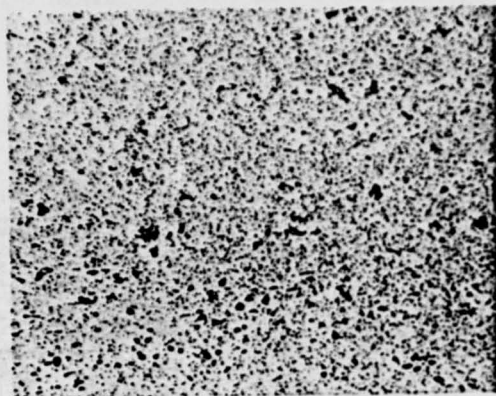


Figure IV-72 210x
Etched in Mixed-Acids Aqueous
Solution

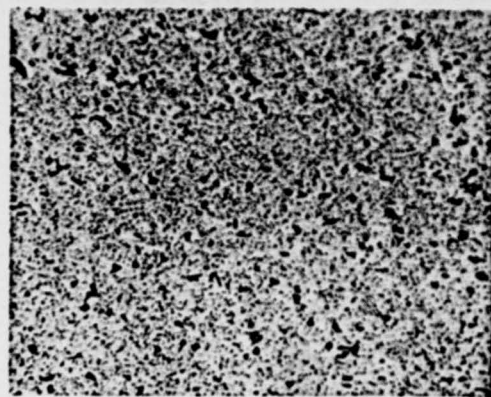


Figure IV-73 210x
Etched in Mixed-Acids Aqueous
Solution

Alloy and Condition	LY12M (420°C, 180 min., cooled in furnace)
Specification	XC-118 Structural-shape
Structural features	Figure IV-72 is the longitudinal structure of the rear end of the structural-shape. The soluble compounds have dissolved into the solid solution. The residues are congregated. A large amount of compound particles are precipitated from the α (Al) matrix. Figure IV-73 is the transverse structure of the structural-shape.

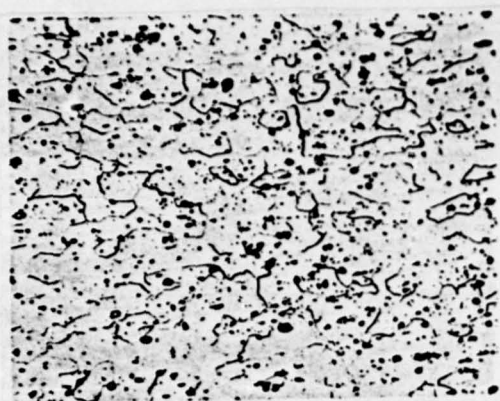


Figure IV-74 210x
Etched in Mixed-Acids Aqueous
Solution

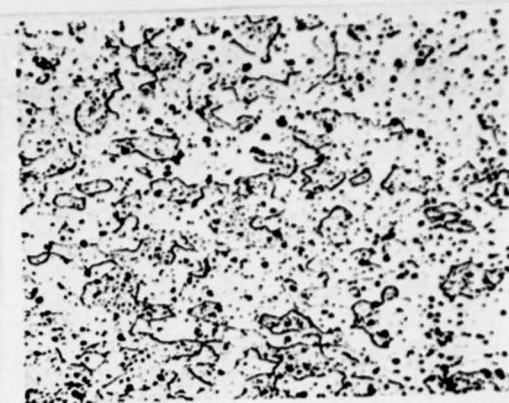


Figure IV-75 210x
Etched in Mixed-Acids Aqueous
Solution

Alloy and Condition
Specification
Structural features

LY12CZ (500°C, 20 min., water-cooled)
φ31x25mm cold-spun tube

Figure IV-74 is the longitudinal structure of the tube, which has undergone complete recrystallization and exhibits equiaxed grains. Compounds are distributed on the α (Al) matrix, and are arranged in arrays along the spinning direction.

Fig. IV-75 is the transverse structure of the tube

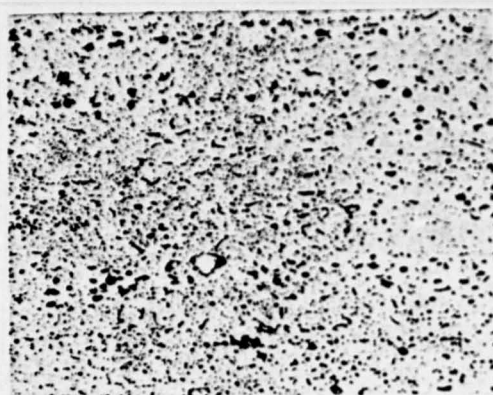


Figure IV-76 210x
Etched in Mixed-Acids Aqueous
Solution

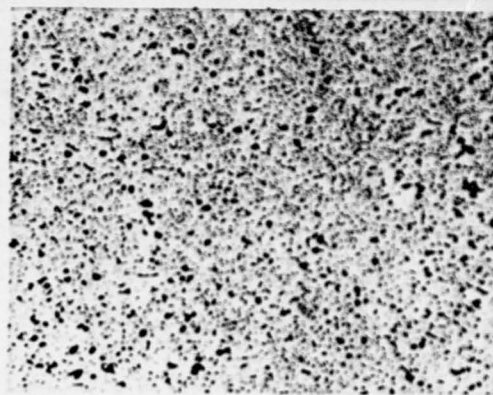


Figure IV-77 210x
Etched in Mixed-Acids Aqueous
Solution

Alloy and Condition	LY12M (420°C, 180 min., cooled in furnace)
Specification	31x25mm cold-spun tube
Structural features	Figure IV-76 is the longitudinal structure of the tube. The soluble compounds have dissolved into the solid solution. The residues are congregated. A large amount of compound particles are precipitated from the α (Al) matrix. Figure IV-77 is the transverse structure of the tube.

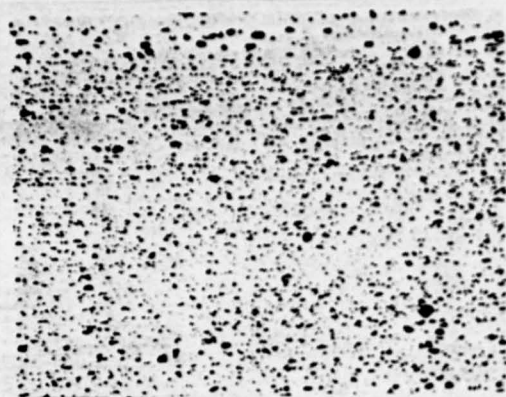


Figure IV-78 210x
Etched in Mixed-Acids Aqueous Solution

Alloy and LY12Y
condition

Specifi- $\phi 18 \times 16$ mm Cold-
cation spun tube
Structural Longitudinal
features structure. The
compounds are
further broken,
and arranged in
arrays along
the spinning
direction.

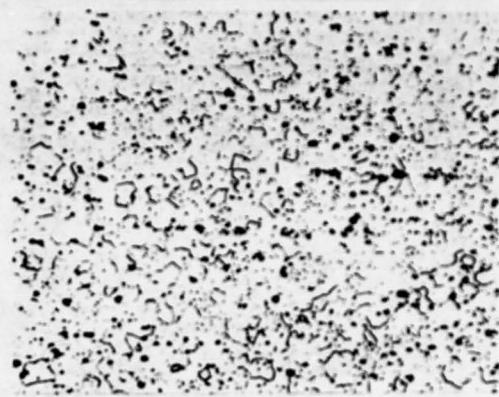


Figure IV-79 210x
Etched in Mixed-Acids Aqueous Solution

Alloy and LY12CZ (500°C,
condition 20 min., water-
cooled)

Specifi- $\phi 18 \times 16$ mm tube
cation (Cold-spun)
Structural Longitudinal
structure. Re-
crystallization
is complete, with
fine and uniform
equiaxed grains.
The $S(\text{CuMgAl}_2)$ &
 CuAl_2 phases dis-
solve into the
solid solution
considerably.

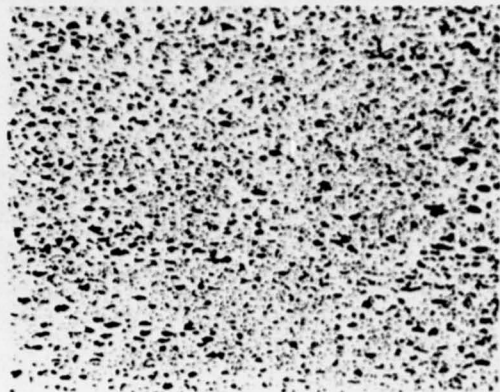


Figure IV-80
Etched in Mixed-Acids Aqueous
Solution

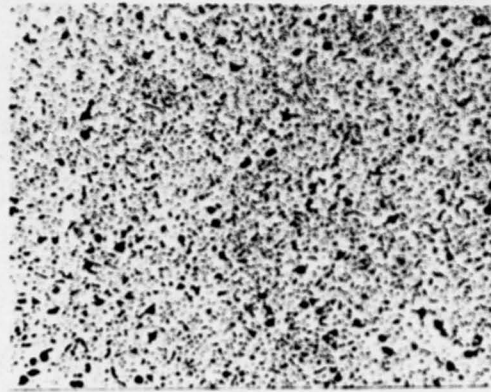


Figure IV-81
Etched in Mixed-Acids Aqueous
Solution

<p>Alloy and Condition</p> <p>Specification</p> <p>Structural features</p>	<p>LY12M (420°C, 180 min., cooled in furnace)</p> <p>Ø18x16mm cold-spun tube</p> <p>Figure IV-80 is the longitudinal structure of the tube. The soluble compounds have dissolved into the solid solution. The residues are congregated. A large amount of compound particles are precipitated from the α(Al) matrix.</p> <p>Figure IV-81 is the transverse structure of the tube.</p>
--	---

5. Structures of Forgings

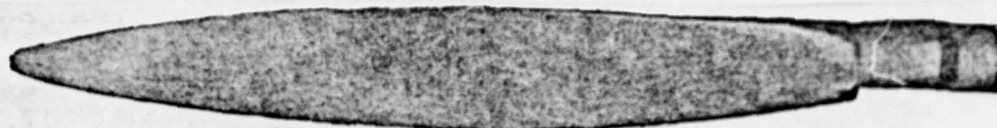


Figure IV-82 Full View of Propeller



Figure IV-83 Etched in 12% NaOH Aqueous Solution



Figure IV-84 Etched in 12% NaOH Aqueous Solution

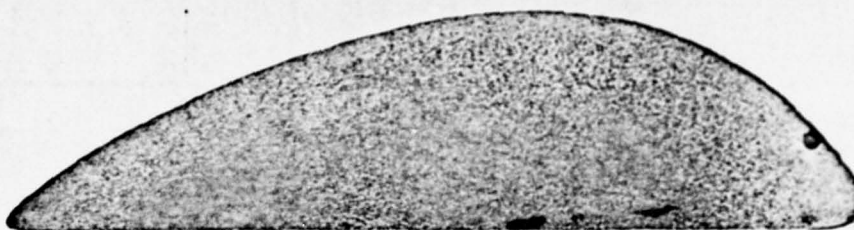


Figure IV-85 Etched in 12% NaOH Aqueous Solution

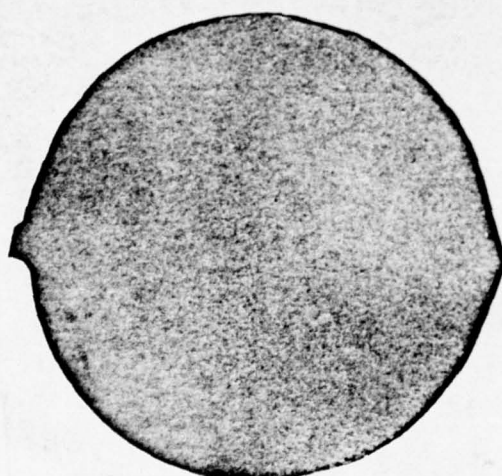


Figure IV-86 Etched in 12% NaOH Aqueous Solution

Alloy and Condition	LY11CZ
Name of Forging	Propeller
Structural Features	

Figure IV-82 is the full view of the propeller. Figures IV-83, IV-84, IV-85, and IV-86 are the macrostructures of the apex region, the middle region, the transitional zone of the base region, and the base region, of the blade respectively.

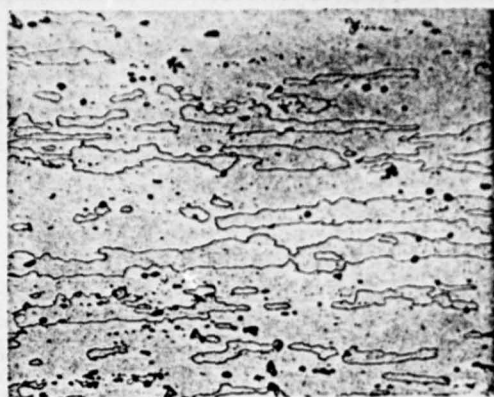


Figure IV-87 210x
Etched in Mixed-Acids Aqueous
Solution

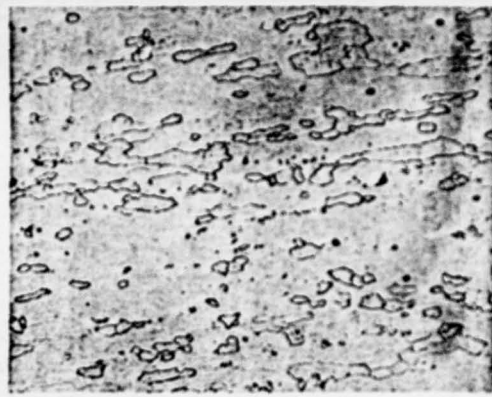


Figure IV-88 210x
Etched in Mixed-Acids Aqueous
Solution

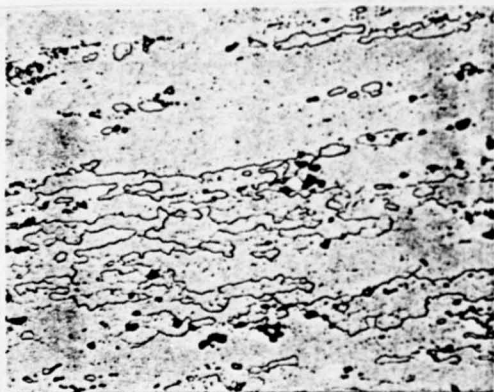


Figure IV-89 210x
Etched in Mixed-Acids Aqueous
Solution

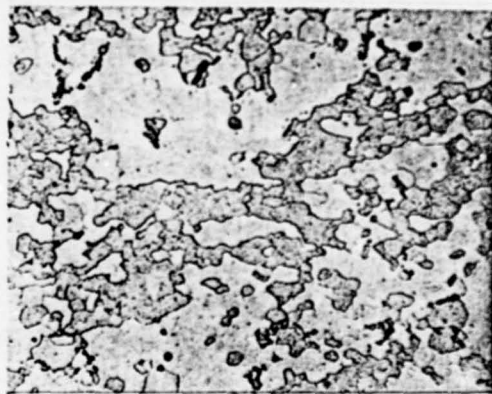


Figure IV-90 210x
Etched in Mixed-Acids Aqueous
Solution

Alloy and Condition	LY11CZ
Name of Forging	Propeller
Structural Features	Figure IV-87 is the structure of the

central portion of the apex region of the blade. The recrystallized grains are coarse, and are elongated along the deformation direction. The compounds are broken to a large extent, and dissolve into the solid solution considerably. Figure IV-88 is the structure of the central portion of the middle region of the blade. The recrystallized grains here are smaller than those at the apex region.

Figure IV-89 is the structure of the transitional zone of the base region of the blade. The recrystallized grains, as well as the extent of compounds being broken, are smaller than those at the apex region.

Figure IV-90 is the structure of the base region of the blade. Recrystallization is not complete. Subgrains still remain.

Chapter 5

Alloy of Aluminum-Magnesium-Silicon-Copper Group

Among the alloys of aluminum-magnesium-silicon-copper group, those which are used often are alloy LD2, LD5, LD6 and LD10. These alloys have good forgeability and they are mainly used to make forged articles, so they are also called forging aluminum.

Section 1

Chemical Composition and Phase Formation

The chemical composition of the alloys of this group can be seen in Table V-1.

Table V-1 Chemical Composition of Alloys

Alloy Brand No.	Principal Constituents (%)						Impurity no more than (%)					
	Cu	Mg	Si	Mn	Ti	Cr	Fe	Ni	Zn	Fe+Ni	Other	total
LD2	0.2~0.6	0.45~0.9	0.5~1.2	或Cr 0.15~0.35	—	—	0.5	—	0.2	—	0.1	0.8
LD5	1.8~2.6	0.4~0.8	0.7~1.2	0.4~0.8	—	—	0.7	0.1	0.3	0.7	0.1	1.1
LD6	1.8~2.6	0.4~0.8	0.7~1.2	0.4~0.8	0.02~0.1	0.01~0.2	0.7	0.1	0.3	0.7	0.1	1.1
LD10	3.9~4.8	0.4~0.8	0.6~1.2	0.4~1.0	—	—	0.7	0.1	0.3	—	0.1	1.2

The alloys of aluminum-magnesium-silicon-copper group are developed on the foundation of aluminum-magnesium-silicon group. Among these alloys, the one which appeared first is 51S (Mg 0.6%, Si. 9%). As early as in 1921, some researcher pointed out that Mg_2Si has a decisive function to the strengthening of alloys of Al-Mg-Si group.

Through examination of the alloys on the diagram of pseudo-binary state of Al-Mg₂Si, and the alloys which contain excessive magnesium or silicon, it is discovered that the effect of age-strengthening of the alloy increases following the quantitative increase of phase Mg₂Si that is in the solid solution when quench heating takes place, and that Mg₂Si is the principal strengthening phase of alloys of this group. It is also discovered through research later that if 51S is not immediately given aging and let it wait for a period of time after quenching, the effectiveness of artificial aging that takes place later will become low. For compensating this kind of loss, on the base of alloy 51S, 0.2-0.6% copper and 0.15-0.35% manganese (or chromium) are added, then comes out LD2 instead. If 1.8-2.6% copper and 0.4-0.8% manganese are added, it will turn to be alloy LD5. When manganese is added, it not only makes the recrystallized grains finer and also uplifts the upper-limit of quenching temperature, and the strength of the alloy is thereby promoted. At the same time, because of the addition of copper, the plasticity of the alloy at hot-working is noticeably improved and the strengthening effect of heat treatment is promoted as well. The addition of copper can also help to control the extrusion effect and to lower the anisotropy of the alloy caused by the addition of manganese.

For eliminating the cylindrical crystal on the ingot of alloy LD5 and preventing the tendency of forming coarse crystal on its products, the alloy is added 0.02-0.1% titanium and 0.01-0.2% chromium, then it

turns to be alloy LD6 .

The copper content in alloy LD10 is much higher, and it is 3.9-4.8% almost as high as that of hard aluminum. It can therefore also be called high strength hard aluminum alloy.

The iron contained in the alloy is 0.2-0.4%. It can prevent the recrystal grains growth when quench heating takes place and increase the strengthening effect. However, if iron content is over 0.8%, there will appear coarse phase $(FeMn)Al_6$, and the plasticity of the alloy is thereby reduced.

Based on the range of its chemical composition and the equilibrium diagram (Figure V-2 and Figure V-3), and through metallographic and microprobe minute analysis, it has been found out that the phase formation

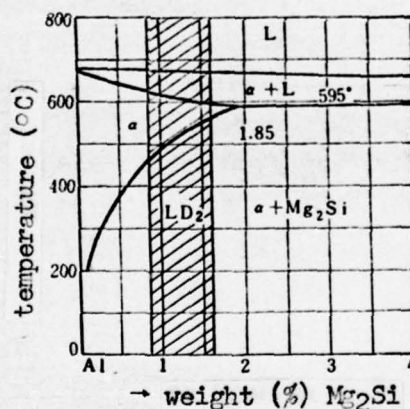


Figure V-I The pseudo binary equilibrium diagram of Al-Mg-Si

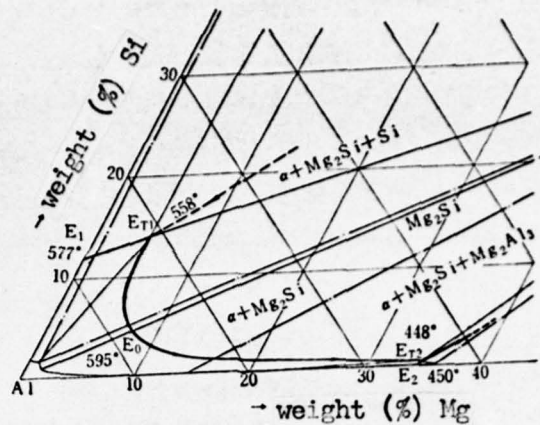


Figure V-2 Dependent aluminum angle part in equilibrium diagram of Al-Mg-Si group alloy

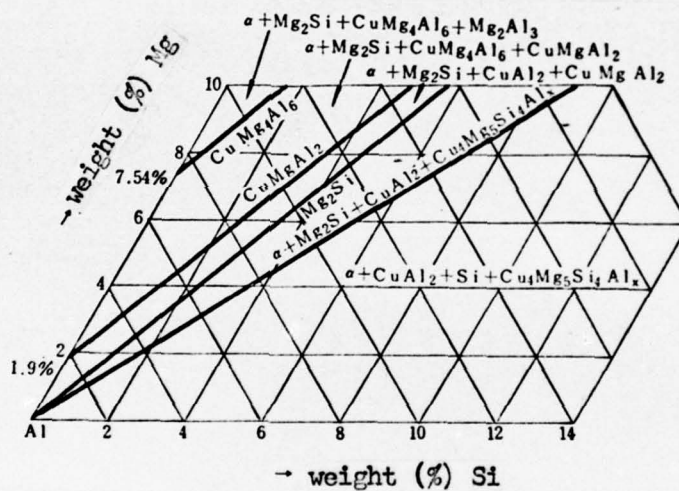


Figure V-3 The distribution of dependent aluminum angle in the region of solid phase which contains 5% Cu in the equilibrium diagram of Al-Mg-Si-Cu group alloy.

of this alloy under condition of gradual cooling is what shown in Table V-2.

Table V-2 Alloy Phase Formation

Brand No. of Alloy	Principal Phase Formation	Impurity Phase
LD2	$\alpha(\text{Al}), \text{Mg}_2\text{Si}, \text{W}(\text{Cu}_4\text{Mg}_5\text{Si}_4\text{Al}_x)$	$(\text{FeMnSi})\text{Al}_6, \text{AlSiFe}$
LD5或LD6	$\alpha(\text{Al}), \text{Mg}_2\text{Si}, \text{W}(\text{Cu}_4\text{Mg}_5\text{Si}_4\text{Al}_x), \text{CuAl}_2$, 少量 $\text{S}(\text{CuMgAl}_2)$	$(\text{FeMnSi})\text{Al}_6, \text{TiAl}_3^*$
LD10	$\alpha(\text{Al}), \text{Mg}_2\text{Si}, \text{S}(\text{CuMgAl}_2), \text{CuAl}_2$, $\text{W}(\text{Cu}_4\text{Mg}_5\text{Si}_4\text{Al}_x)$	$(\text{FeMnSi})\text{Al}_6$ 或 $\text{Mn}_3\text{SiAl}_{12}$

* The appearance of phase TiAl_3 because in alloy LD6 there is an addition of titanium.

Of alloys of Al-Mg-Si-Cu group, when the ratio between magnesium and silicon is 1.73, Mg_2Si will be formed. When the ratio is less than 1.08, it is possible to form a phase $\text{W}(\text{Cu}_4\text{Mg}_5\text{Si}_4\text{Al}_x)$, and the excessive copper will form CuAl_2 . Mg_2Si is a typical chemical compound, of which the combination ratio is 1.73. Phases CuAl_2 , $\text{S}(\text{CuMgAl}_2)$ and $\text{W}(\text{Cu}_4\text{Mg}_5\text{Si}_4\text{Al}_x)$ are metal compounds. According to the available data, in phase $\text{W}(\text{CuMgSiAl})$, Cu: Mg : Si are 4 : 5 : 4, and it contains about 30-40%Al, so its molecular formula is $\text{W}(\text{Cu}_4\text{Mg}_5\text{Si}_4\text{Al}_x)$. The presence of phase W is determined by the condition of crystalization. If the peritectic reaction, from which the phase $\text{W}(\text{Cu}_4\text{Mg}_5\text{Si}_4\text{Al}_x)$ grows can develop fully, there will be $\text{W}(\text{Cu}_4\text{Mg}_5\text{Si}_4\text{Al}_x)$; otherwise, the content of phase $\text{W}(\text{Cu}_4\text{Mg}_5\text{Si}_4\text{Al}_x)$ will be very little, and it may even reach to zero. Phase W is different from phases $\text{S}(\text{CuMgAl}_2)$, CuAl_2 and Mg_2Si . When quench heating is in

process, it can only partially be in the solid solution and takes part in the process of strengthening.

Characteristics of the few principal phases:

Phase Mg_2Si : Bright greyⁱⁿ color and its primary crystal is in the shape of polygon and most of its eutecticum are of the shape of fish-bone. All these can be seen on the segregated swellings and the semicontinuous casting in effective production (Figure V-9 and Figure V-10). But on the normal part of cast ingot it always looks like forked-branches (Figure V-11 through Figure V-14). Before corrosion, usually because polished, it becomes dark blue in color, so it is easy to be recognized. Except that it cannot or can only slightly be corroded in NaOH liquid solution, in mixed acid, 25% HNO_3 and 0.5% HF liquid solution, it can be severely corroded and it can even be completely melted. Mg_2Si which is separated from solid solution $\alpha(Al)$ is in the shape of schists and arranged in a 90° angle with $\alpha(Al)$ solid solution (100) (Figure V-23 and Figure V-24).

Phase $W(Cu_4Mg_5Si_4Al_x)$: Light grey in color, it looks like a skeleton or in the form of congregated chunky crystals. When it is corroded in 25% HNO_3 or 0.5% HF liquid solution, it becomes dark brown (Figure V-5 and Figure V-6).

Phase $(FeMnSi)Al_6$: Bright grey and slightly brighter than phase W, and it is of the shape of skeleton. When it is corroded in 0.5% HF liquid solution, it becomes brown. It is easily confused with phase W. But it cannot be corroded in 25% HNO_3 liquid solution. This characteristic

is often used as a means to differentiate them (Figure V-7 through Figure V-16).

Phases CuAl_2 and $\text{S}(\text{CuMgAl}_2)$: For details, see Chapter 4.

Section 2

Characteristics of Heat Treatment

Alloys of this group have a common strengthening phase Mg_2Si . After quenching, they can have both natural aging and artificial aging. Because the separating of the strengthening phase Mg_2Si under room temperature is slow, the effect of natural aging is not great. And high strengthening effect cannot be achieved without having artificial aging. According to available data, silicon and magnesium in the alloy under artificial aging temperature will first form phases (Mg_2Si and phase W) which contain silicon, and under room temperature, silicon will remain in the super-saturated solid solution $\alpha(\text{Al})$ not easy to separate.

The common weakpoint of these alloys is that after quenching, the period of withholding them under room temperature will lower the effect of the coming artificial aging. This is the so-called retarded effect. Alloy LD2 can demonstrate this effect very clearly. If the withholding period is more than 30 minutes, the strengthening effect will be remarkably reduced. If the period is over 6 hours, the strength of the alloy will fail to meet technological requirement. Even it is alloy LD10, which cannot have the best mechanical property unless it has artificial aging within 3 hours after quenching or wait till 48

hours have passed by.

Some problems which deserve good attention when heat treatment takes place will be respectively discussed in the following.

(1) Alloy LD2

From the pseudo-binary equilibrium diagram of Al-Mg₂Si (Figure V-1), it can be seen that under eutectic temperature, the greatest solubility of strengthening phase Mg₂Si is 1.85%, and the solubility will be reduced following the falling of temperature. When the temperature is at 200°C, the solubility will come down to 0.25%. For this reason, the alloy can have a better strengthening effect in heat treatment. At the same time, the range of quenching temperature of the alloy becomes rather broad. When quenching temperature is higher than 540°C, although the solid solution is full and the strengthening effect of the alloy is improved, but, because of the appearance of the coarse crystalline structure, the strength of the alloy, on the contrary, is brought down (Figure V-4). If the quenching temperature is lower than 500°C, even though it can result in fine crystal structure and the improvement of strength, but because the solid solution is not full, the strengthening effect of the alloy will correspondingly come down. In order to insure the strengthening phase to have a full solid solution and the structure of the alloy does not become coarse, based on the outcomes of experiments and practical production, it appears advisable to have quench heating temperature at $520 \pm 10^\circ\text{C}$, artificial aging at 150-160°C, and the temperature retention is 6-15 hours.

The annealing temperature of alloy LD2 is 380-420°C.

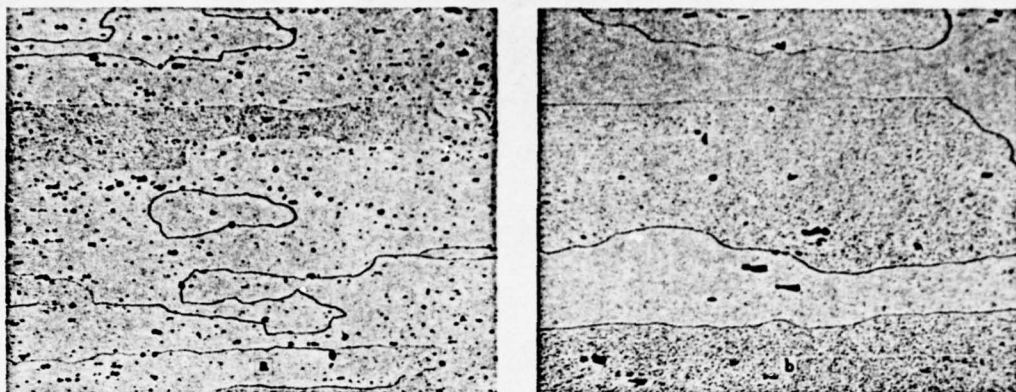


Figure V-4 The effect of different quenching temperature on the size of crystal grains of an alloy LD2 plate

- a - The structure of an alloy LD2 5.0 mm. plate which has quenching at 530°C. The crystal grains are normal.
- b - The structure of an alloy LD2 5.0 mm. plate which has quenching at 560°C. The crystal grains are coarse and large.

(2) Alloy LD5

The principal strengthening phases of this alloy in quench aging are Mg_2Si , $CuAl_2$ and $W(Cu_4Mg_5Si_4Al_x)$, and sometimes phase $S(CuMgAl_2)$ may also come out. Someone believes that alloy LD5 cannot at the same time form phases $CuAl_2$ and $S(CuMgAl_2)$. In our phase analysis of the semicontinuous casting and water cooled ingot, we found only phase $CuAl_2$ and no phase $S(CuMgAl_2)$. When alloy LD5 is heating at 510-520°C, the strengthening phases are all in solid solution. When the temperature goes up over 540°C, the phenomenon of grain growth as occurred with

alloy LD2 can be seen, and the strength of the alloy thereby becomes low. So the best quench heating temperature for alloy LD5 would be 515-525°C. Aging takes place at 155-170°C, and the temperature retention is 4-15 hours.

The annealing temperature for alloy LD5 can be 350-400°C.

(3) Alloy LD10

Alloy LD10 contains great quantity of strengthening phases CuAl_2 and Mg_2Si and only a small amount of $\text{S}(\text{CuMgAl}_2)$. It has high sensitivity to over-burning, so the quench heating temperature for its products cannot be higher than 505°C. Its artificial aging and annealing systems are same as those of alloy LD5. The forged articles of this alloy with large specification and complicated forms, in the process of quenching and sudden cooling, often produce great quenching stress. As a result, curling-ups and cracks are often found on the forged articles. In order to reduce the remnant stress, in the production of various kinds of articles, hot water should be used as cooling agent.

The recrystallization parameter of alloys LD2, LD5 and LD10 will be seen in Table V-3.

Table V-3 The Recrystallization Parameter of
Al-Mg-Si-Cu Group Alloy

Brand No. of Alloy	Variety of Items	Specification (mm.)	Technological Condition						Recrystallization temperature (°C)		Remarks
			Rolling		Extrusion		Annealing Condition		Beginning	Ending	
			T. (°C)	Rate of deformation (%)	T. (°C)	Rate of deformation (%)	S.B.T. or A. F.	Time (min.)			
LD2	Plate	1.0	Room T.	85			Salt bath trough	20	250~255	285~290	
LD2	Plate	4.0	Room T.	50~55			Air furnace	20	250~270	320~350	
LD2	Bar	φ 10			350	98.6	Salt bath trough	20		445~450	Extrusion & recrystallization
LD5	Bar	φ 150			350	87	Salt bath trough	20	380~385	550~555	
LD10	Plate	2.0	Room T.	60			Air furnace	60	250~310	350	

Section 3

The Structure of Cast Ingots and Processed Articles

The general rule of structural changes of cast ingots and processed articles of alloys of this group has been discussed in the Introduction. Here discussions will be on some special features of their structures.

(1) The effect of chemical composition on ingot structure

Because of the complication of their chemical composition, the size of the crystal grains become smaller following the order of LD2, LD5 and LD10. Again because of the difference in composition, their microstructure

shows obvious differences. The network of the dendritic crystal of LD5 and LD10 is thicker than that of LD2, and the network of the former is relatively connected with each other (Figure V-17 through V-32).

Due to the fact that the eutectic structure of alloy LD10 is complicated and the quantity is large, the structure of the crystal grains on its macroscope after corrosion becomes less clear than that of LD2 (Figure V-17 and Figure V-19).

(2) Characteristics of the structure in the welded region of tongue-shaped extruded articles.

XCO51 molds are the main products of alloy LD2. The form of the inner walls of this mold is complicated and the requirement in size is strict, so the mold must be produced by the tongue-shaped mold extrusion method. In metal phase structure, it shows difference in the welded region from articles produced by other methods. Due to the variability of the metal conditions when it is extruded, the normal structure in the welded region displays three different characteristics: (a) the macroscopical structure has the form of jutting bright lines, and its microstructure is coarser than that in the adjacent normal parts; (b) the macroscopical structure has the form of depressed lines, and it is white when viewed from the direction against the light source. Its microstructure is finer than that in the adjacent normal parts, for it is made of a group of fine crystals (Figure V-56); (c) the macroscopical structure in the welded region shows no remarkable difference from other normal parts, nor does the microstructure. The three different structures mentioned above do not destroy structural continuity, and the mechanical

property of the welded region is basically the same as that of the non-welded and normal parts. So they are all qualified and good structure of welding. From this fact, it becomes clear that the production examination of ^a welded region will make an incorrect conclusion if it concentrates only on the characteristics of the macroscopical structure and overlooks the necessity of ^{examining} the microstructure at the same time.

(3) The cutting effect in the coarse crystal-ring region of an extruded article.

The cutting of an extruded article before quenching will affect the size of the recrystallized grains in the coarse crystal-ring region adjacent to cutting section. Figure V-47, for example, shows the macroscopical structure of a testing piece from an extruded article of LD5, which was cut after quenching. Figure V-45 shows the macroscopical structure of the testing piece of that article, which was cut before quenching. From the above two Figures, it can be found out that through the same system of heat treatment, the size of the grains in the coarse crystal region is distinctively different. Figure V-47 shows the real size of the grains in the coarse crystal region; while Figure V-45 shows the grains which are noticeably smaller. This is obviously the result which is affected by the cutting effect. It has been proved by experiments that the affected depth of the cutting effect is related to the way of cutting. If the cutting is made by circular saw, the effect will be the deepest, the next is by band saw. If the cutting is made by manual saw, the effect will be the smallest. Under the

general condition of production, the depth of effect is about 20-30 mm. (Figure V-46). So, if the coarse crystal-ring of the testing piece, which was cut before quenching, is examined, it must first of all cut off 20-30 mm. at the cutting section. before examination takes place.

I. Phase Formation

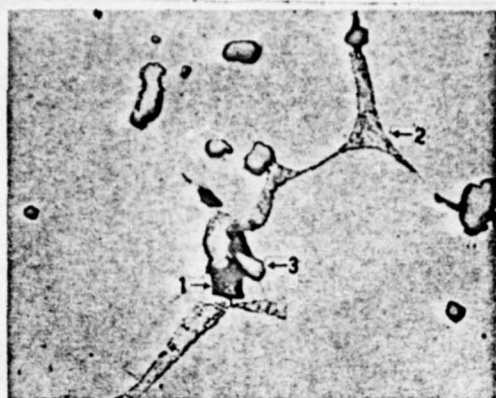


Figure V-5

210x



Figure V-6

210x

Alloy	LD5
Condition	Cast ingot remelting at 600°C, gradually cooled to 580°C, and the temperature is retained for 8 hours, then water cooled.
Corrosion	Not corroded
Features of Structure	1 - Mg_2Si , dark blue; 2 - $\alpha(Al) + CuAl_2$ eutectic 3 - $W(Cu_4Mg_5Si_4Al_x)$ is light grey and chunky in form.

Alloy	LD5
Condition	Same as Figure V-5
Corrosion	25% HNO_3 liquid solution, 5-10 seconds
Features of Structure	1 - Mg_2Si becomes black; 2 - $CuAl_2$ in eutecticum becomes copper red and brown black; 3 - $W(Cu_4Mg_5Si_4Al_x)$ slightly corroded.

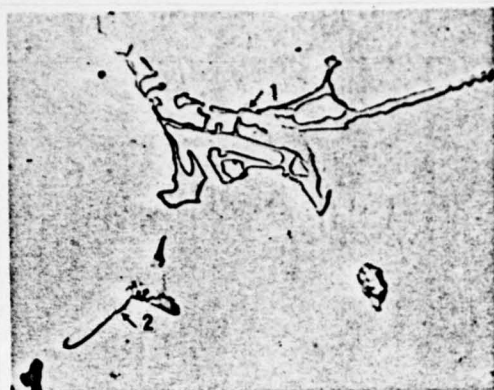


Figure V-7 210x

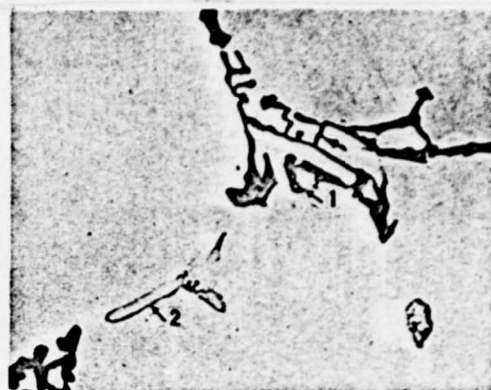


Figure V-8 210x

Alloy	LD5
Condition	Same as Figure V-5
Corrosion	Not corroded
Features of Structure	<p>1 - (FeMnSi)Al₆ is bright grey and in the shape of skeleton</p> <p>2 - CuAl₂, light red</p>

Alloy	LD5
Condition	Same as Figure V-5
Corrosion	0.5%HF liquid solution, 5-10 seconds
Features of Structure	<p>1 - (FeMnSi)Al₆ becomes brown;</p> <p>2 - CuAl₂ cannot be corroded and no change in color.</p>

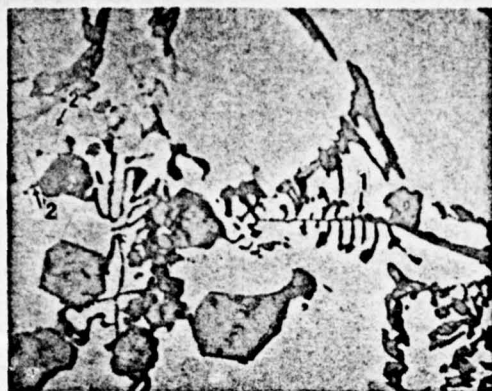


Figure V-9 600x



Figure V-10 210x

Alloy	LD2
Condition	Semicontinuous casting, the position of the segregated swellings
Corrosion	Mixed acid liquid solution, 5-10 seconds
Features of Structure	1 - Mg_2Si corroded and becomes black ; 2 - $(FeMnSi)Al_6$ very slightly corroded.

Alloy	LD2
Condition	Same as Figure V-9
Corrosion	25% HNO_3 liquid solution, 15-20 seconds
Features of Structure	1 - Mg_2Si changed from blue to black; 2 - $(FeMnSi)Al_6$ cannot be corroded, and remains bright grey; 3 - $CuAl_2$ changed from light red to brown black.



Figure V-11

600x

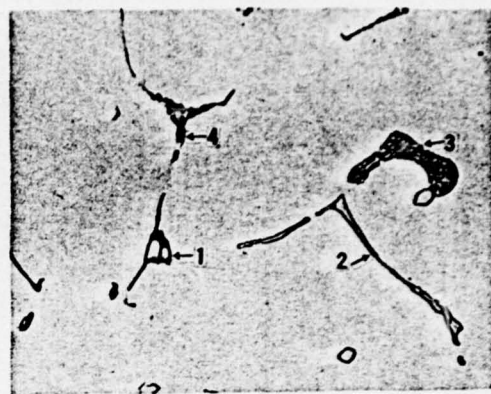


Figure V-12

600x

Alloy	LD2
Condition	Semicontinuous casting, central position
Corrosion	25% HNO_3 liquid solution, 15-20 seconds
Features of Structure	1 - Mg_2Si black in color; 2 - $(\text{FeMnSi})\text{Al}_6$ light grey; 3 - $a(\text{Al}) + \text{Mg}_2\text{Si} + \text{Si}$ eutectic

Alloy	LD5
Condition	Semicontinuous casting, central position
Corrosion	25% HNO_3 liquid solution, 15-20 seconds
Features of Structure	1 - Mg_2Si black in color; 2 - $(\text{FeMnSi})\text{Al}_6$ light grey; 3 - $A(\text{Al}) + \text{Mg}_2\text{Si} +$ CuAl_2 eutectic; 4 - CuAl_2 in eutectic is brown black in color.



Figure V-13

600x



Figure V-14

600x

Alloy	LD10
Condition	Semicontinuous casting, central position
Corrosion	Not corroded
Features of Structure	<p>1 - Mg_2Si dark blue in color and is of a shape of polygon;</p> <p>2 - $CuAl_2$ light red in color;</p> <p>3 - $S(CuMgAl_2)$ grey yellow in color and of a shape of honeycomb;</p> <p>4 - $(FeMnSi)Al_6$ light grey in color and of a shape of skeleton.</p>

Alloy	LD10
Condition	Same as Figure V-13
Corrosion	25% HNO_3 liquid solution, 15-20 seconds
Features of Structure	<p>1 - Mg_2Si becomes black;</p> <p>2 - $CuAl_2$ becomes brown black;</p> <p>3 - phase $S(CuMgAl_2)$ becomes deep black;</p> <p>4 - $(FeMnSi)Al_6$ cannot be corroded.</p>



Figure V15 210x

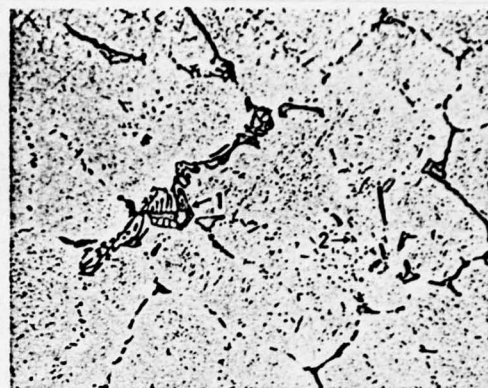


Figure V-16 210x

Alloy	LD10
Condition	Semicontinuous casting, the extreme edge position
Corrosion	Mixed acid liquid solution, 10-15 seconds
Features of Structure	1 - (FeMnSi)Al ₆ light grey; 2 - Mg ₂ Si black in color.

Alloy	LD10
Condition	Cast ingot homogenizing at 490°C for 12 hours, then air cooling
Corrosion	Mixed acid liquid solution, 10-15 seconds
Features of Structure	1 - (FeMnSi)Al ₆ ; 2 - Particles separated from solid solution α(Al).

2. The Structure of Cast Ingots

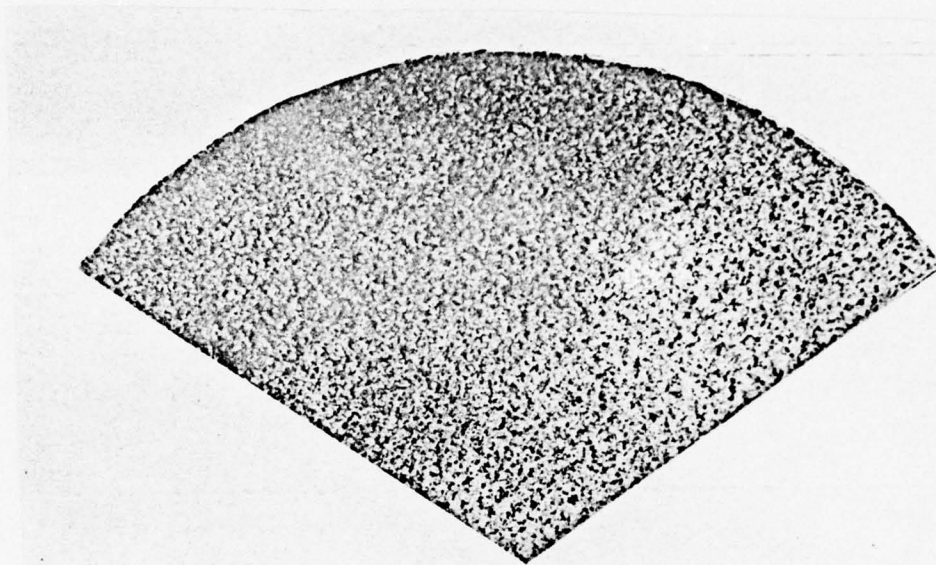


Figure V-17 Corroded in 15%NaOH Liquid Solution 1:3

Alloy and Condition LD2, semicontinuous casting

Specification ϕ 290 mm. round ingot

Features of Structure Transverse macroscopical structure of the ingot, in the edge region, there are fine isometric crystals, but the grains are larger in the middle and central region, and they are larger than those of LD5 and LD10.

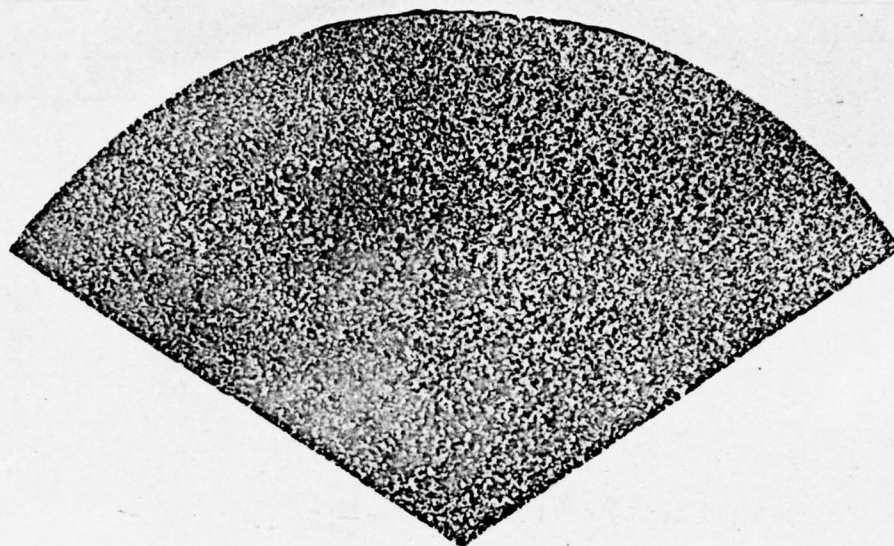


Figure V-18 Corroded in 15%NaOH Liquid Solution 1:3

Alloy and Condition LD5, semicontinuous casting

Specification ϕ 290 mm. round ingot

Features of Structure Transvers macroscopical structure of the ingot, there are segregated swellings on the surface. The edge region is the fine isometric crystal region and the grains in middle and central part are larger. They are smaller than those of LD2.

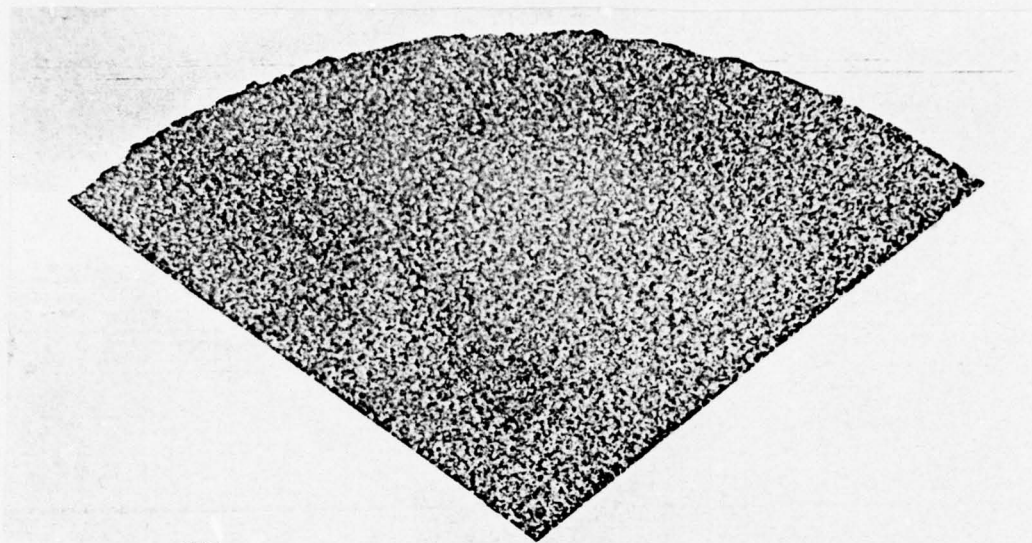


Figure V-19 Corroded in 15% NaOH Liquid Solution 1:3

Alloy and Condition	LD10, semicontinuous casting
Specification	ø 290 mm. round ingot
Features of Structure	Transverse macroscopical structure of the ingot, the crystal grains in the edge region are very small, and the grains are larger in the middle and central part. The crystal grains are smaller and more homogeneous than those of LD5.

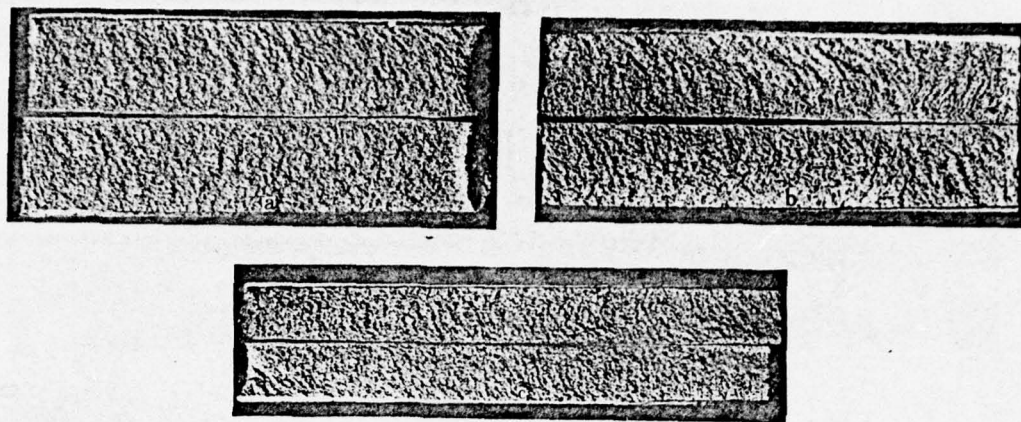


Figure V-20

Alloy and Condition	a - LD2; b - LD5; c - LD10 semicontinuous casting
Specification	Ø 290 mm. round ingot
Features of Structure	Structure of brittle fracture, and the structure is homogeneous and fine.

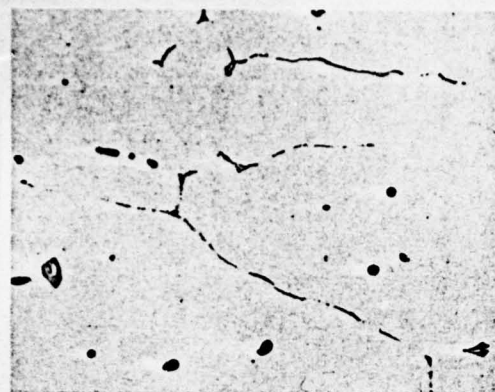


Figure V-21 210x

Corroded in Mixed Acid
Liquid Solution

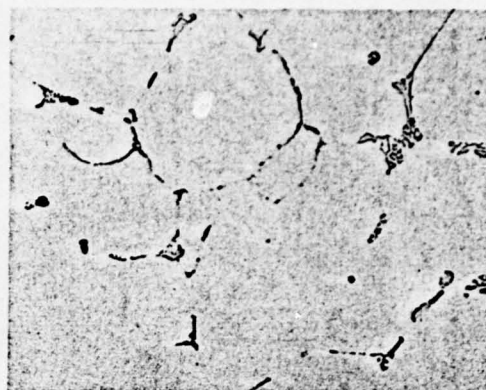


Figure V-22 210x

Corroded in Mixed Acid
Liquid Solution

Alloy and Condition LD2 semicontinuous casting

Specification ϕ 290 mm. round ingot

Features of Structure

Figure V-21 illustrates the structure of the edge part of the ingot. The meshes of the dendritic crystals are coarse but the network is thin.

Figure V-22 illustrates the structure of the central part of the ingot. The meshes of the dendritic crystals are smaller and the network is thicker.

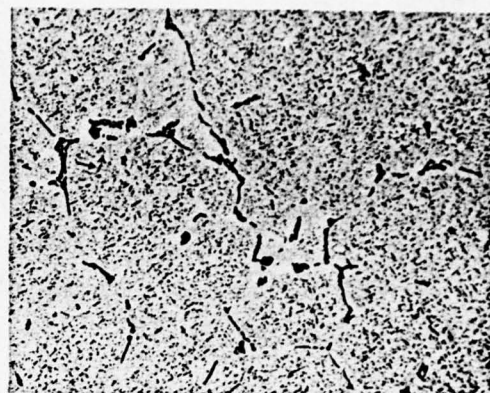
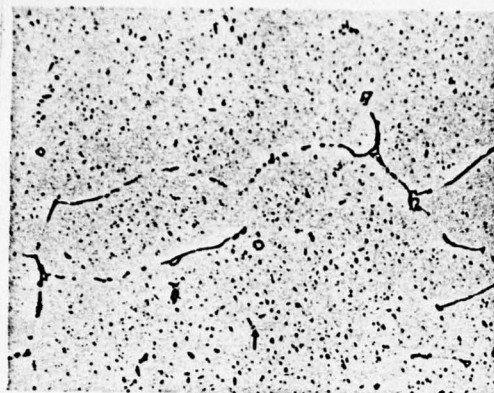


Figure V-23

210x

Figure V-24

210x

Corroded in Mixed Acid
Liquid Solution

Corroded in Mixed Acid
Liquid Solution

Alloy and Condition

LD2 in homogenizing (500°C, staying in homogenizing for 12 hours, then cooled in furnace)

Specification

ø 290 mm. round ingot

Features of
Structure

Figure V-23 illustrates the structure of the edge part of the ingot after homogenization.

Figure V-24 illustrates the structure of the central part of the ingot after homogenization.

On the ingot, after homogenization, there remains the structure of network of the dendritic crystals, and there are also the narrow and long substances separated from Mg_2Si (arrow pointed), and particles separated from phase that contains Mn.

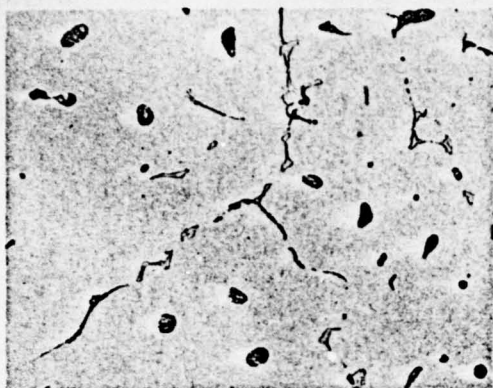


Figure V-25 210x
Corroded in Mixed Acid
Liquid Solution

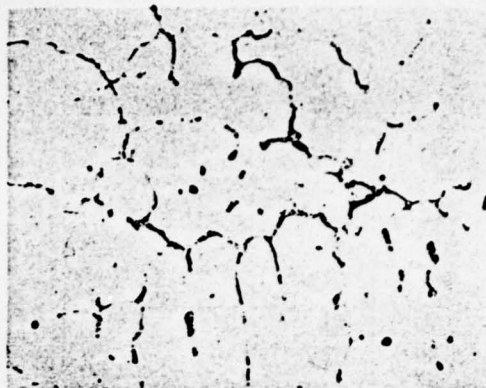


Figure V-26 210x
Corroded in Mixed Acid
Liquid Solution

Alloy and Condition LD5 semicontinuous casting

Specification ϕ 290 mm. round ingot

Features of
Structure

Figure V-25 illustrates the structure of the edge part of the ingot, and the meshes of the dendritic crystals are coarse.

Figure V-26 illustrates the structure of the central part of the ingot, and the meshes of the dendritic crystals are fine.

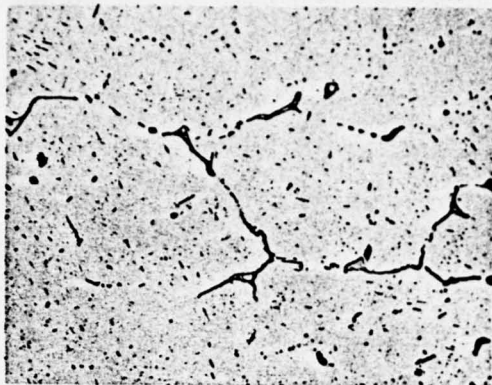


Figure V-27 210x
Corroded in Mixed Acid
Liquid Solution

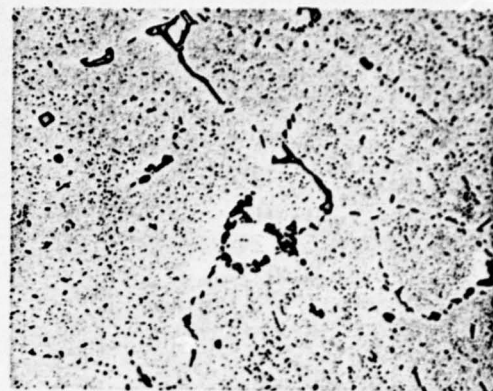


Figure V-28 210x
Corroded in Mixed Acid
Liquid Solution

Alloy and Condition LD5 in the condition of homogenization (530°C, staying in homogenization for 12 hours, then cooled in furnace)

Specification ϕ 290 mm. round ingot

Features of Structure Figure V-27 shows the structure of the edge part of the ingot after homogenization.

Figure V-28 shows the structure of the central part of the ingot after homogenization.

After homogenization, on the ingot remains the network structure of the dendritic crystals, and from the matrices of a(Al) there appears some substance separated from phases Mg_2Si and $CuAl_2$ and particles separated from the phase that contains Mn.

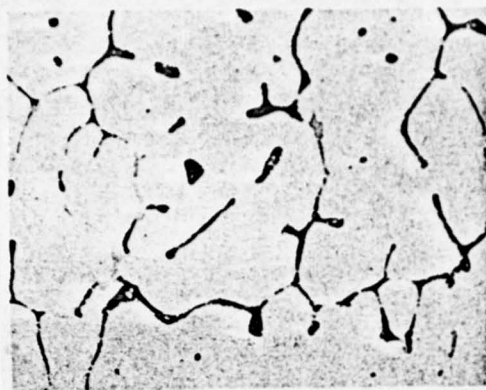


Figure V-29 210x
Corroded in Mixed Acid
Liquid Solution

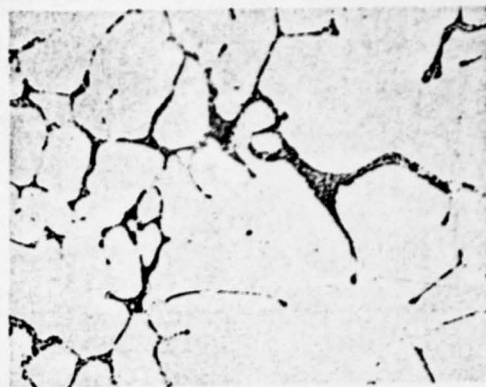


Figure V-30 210x
Corroded in Mixed Acid
Liquid Solution

Alloy and Condition LD10 semicontinuous casting

Specification ϕ 290 mm. round ingot

Features of Structure Figure V-29 shows the structure of the edge part of the ingot, and the meshes of the dendritic crystals are coarse and the network is thin.

Figure V-30 shows the structure of the central part of the ingot, and the meshes of the dendritic crystals are fine but not homogeneous, and the network is thicker than that on the edge part. Due to the fact that the composition of this alloy is more complicated than that of alloy LD2 and LD5, there are many structured substances among the meshes and the network is also thick.

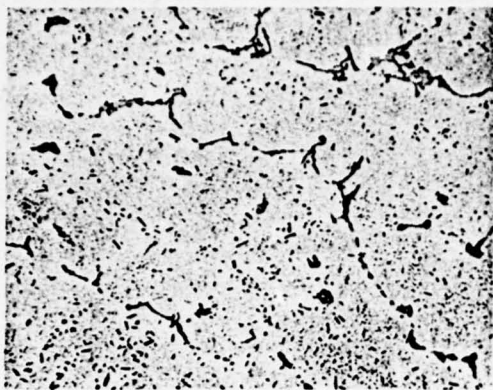


Figure V-31

210x

Corroded in Mixed Acid
Liquid Solution

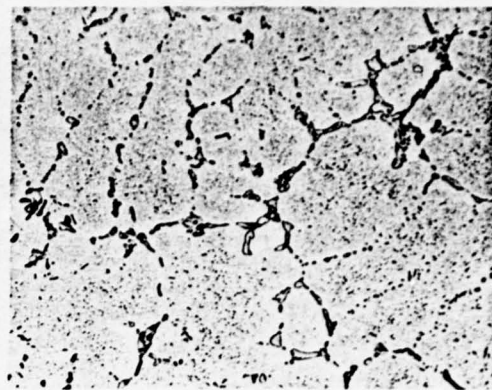


Figure V-32

210x

Corroded in Mixed Acid
Liquid Solution

Alloy and Condition LD10 in the condition of homogenization (490°C, staying in homogenization for 12 hours, then cooled in furnace)

Specification ϕ 290 mm. round ingot

Features of Structure Figure V-31 shows the structure of the edge part of the ingot after homogenization.

Figure V-32 shows the structure of the central part of the ingot after homogenization.

After homogenization, on the ingot remains a part of the network of the dendritic crystals. On the the matrices of a(Al), there is a great quantity of substances separated from phases Mg_2Si , $CuAl_2$ and $S(CuMgAl_2)$ and the particles separated from the phases that contain Mn.

3. The Structure of Extruded Articles

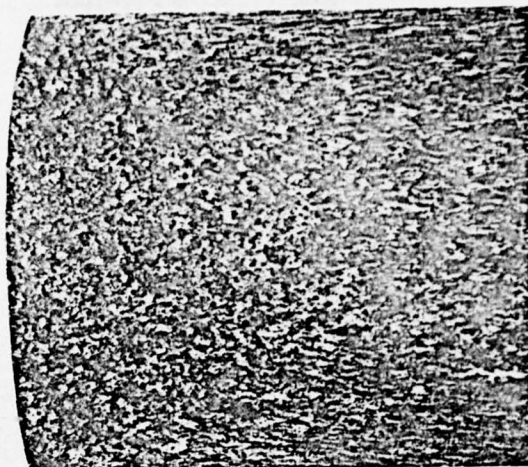


Figure V-33

1:1

Corroded in Mixed Acid
Liquid Solution

Alloy and Condition LD2CS (510°C, 30 minutes, water cooling,
155°C, aging for 15 hours)

Specification ϕ 70 mm. bar

Features of Structure The longitudinal macroscopical structure of the front end of the bar, and on the top there remains the cast-isometric crystal grains which did not deform and the grains are gradually stretched long. On the edge, the deformed fiber structure can be clearly seen.

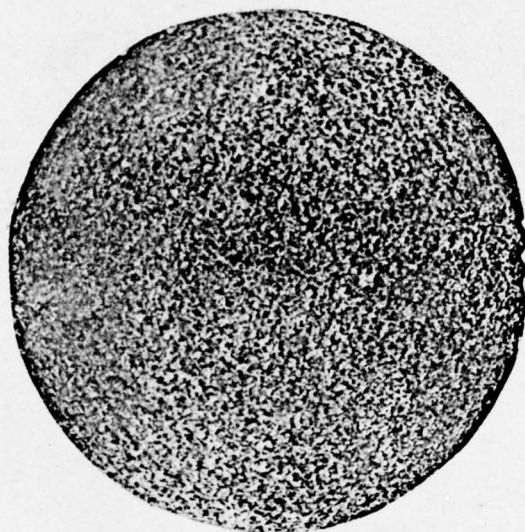


Figure V-34

1:1

Corroded in Mixed Acid
Liquid Solution

Alloy and Condition	LD2CS (510°C, 30 minutes, water cooling, 155°C, aging for 15 hours)
Specification	Ø 70 mm. bar
Features of Structure	The transverse macroscopical structure of the front end of the bar. Except that the crystal grains on the edge region are deformed, in the other region, the appearance of the crystal grains in casting can still be seen.

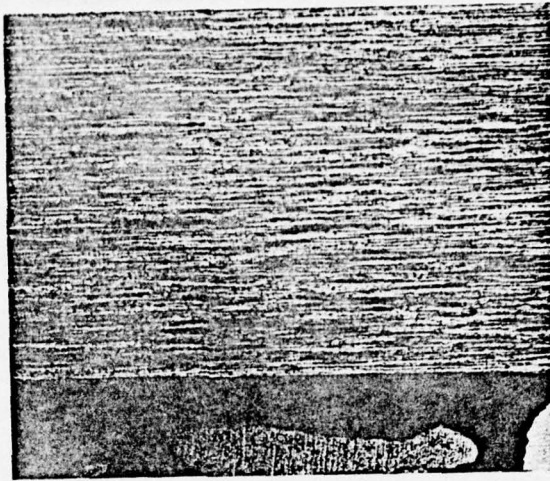


Figure V-35 Corroded in Mixed Acid
Liquid Solution

Alloy and Condition	LD2CS (510°C, 30 minutes, 155°C, aging for 15 hours)
Specification	ø 70 mm. bar
Features of Structure	The longitudinal macroscopical structure of the rear end of the bar. When the bar is extruded, the metal deformation is not even, and the deformation at the rear end is larger than that at the front end. Therefore, on the surface of the rear end appears coarse and large recrystallization region (coarse crystal ring), but on the inner ply, the crystal grains are fine and long like fibers.

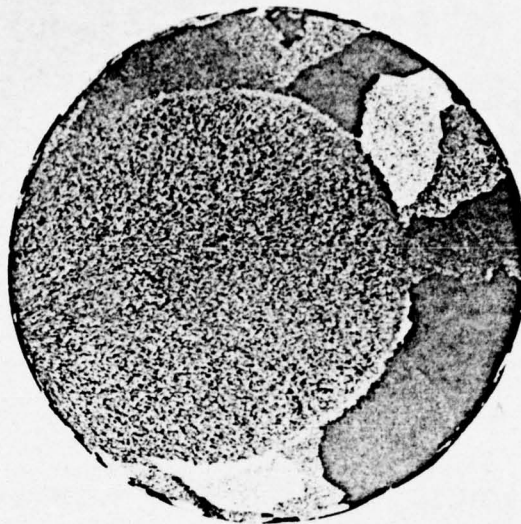


Figure V-36 Corroded in Mixed Acid
Liquid Solution

Alloy and Condition	LD2Cs (510°C, 30 minutes, water cooling, 155°C, aging for 15 hours)
Specification	ø 70 mm. bar
Features of Structure	The transverse macroscopical structure of the rear end of the bar. Because the extruder is multiple holed, the coarse crystal region looks like a crescent.

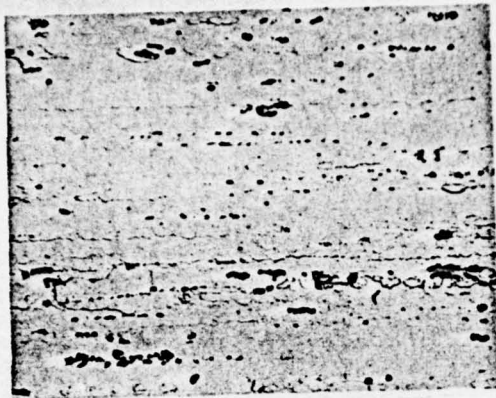


Figure V-37 210x

Corroded in Mixed Acid
Liquid Solution

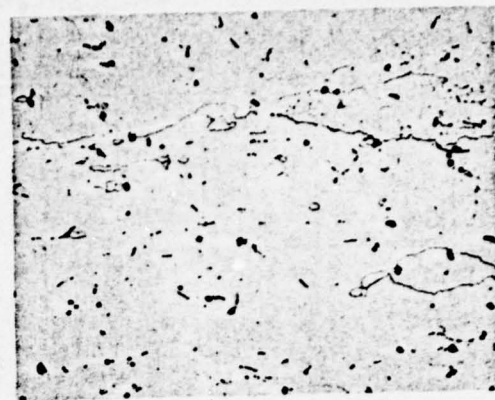


Figure V-38 210x

Corroded in Mixed Acid
Liquid Solution

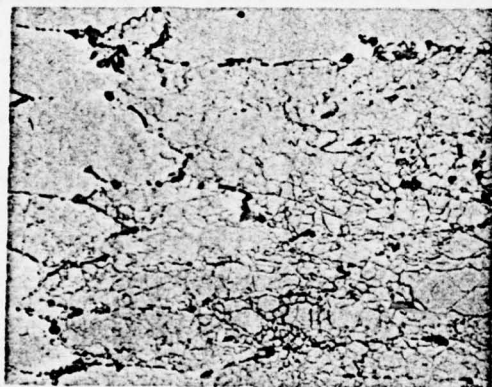


Figure V-39 210x

Corroded in Mixed Acid
Liquid Solution

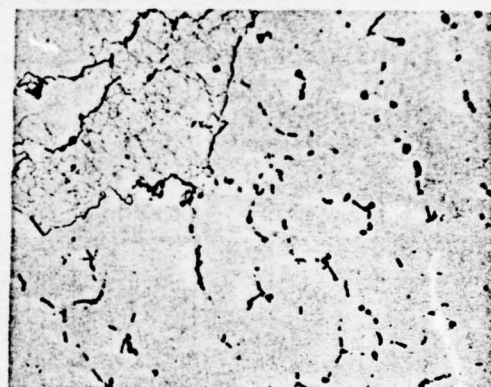


Figure V-40 210x

Corroded in Mixed Acid
Liquid Solution

Alloy and Condition LD2CS

Specification ϕ 70 mm bar

(continued)

Features of
Structure

Figure V-37 shows the longitudinal structure of the edge at the front end of the bar. The chemical compounds are broken and arranged along the extrusion direction, and the alloy has not completely recrystallized. The recrystallized grains stretch along the extrusion direction, and a great number of deformed fiber structures remains.

Figure V-38 shows the transverse structure.

Figure V-39 shows the longitudinal structure of the central part at the front end of the bar. Because the degree of deformation is small, some remnant casting structures can still be seen. Besides some recrystal structures, a number of hypo-crystal grains can be seen.

Figure V-40 shows the transverse structure.

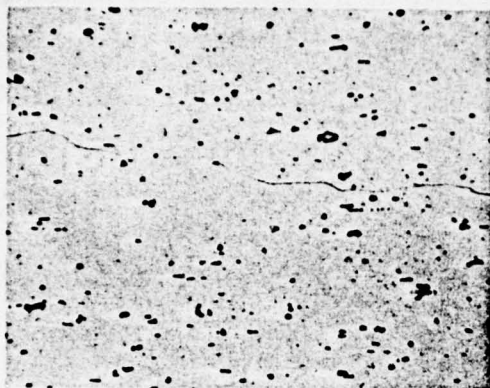


Figure V-41 210x

Corroded in Mixed Acid
Liquid Solution

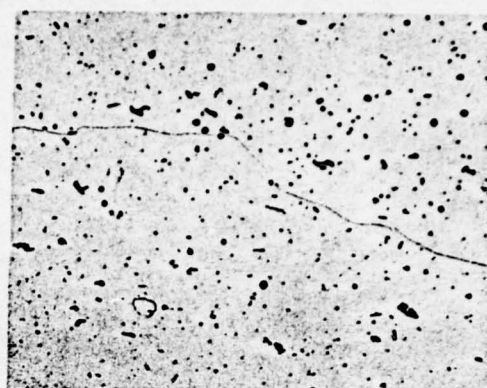


Figure V-42 210x

Corroded in Mixed Acid
Liquid Solution

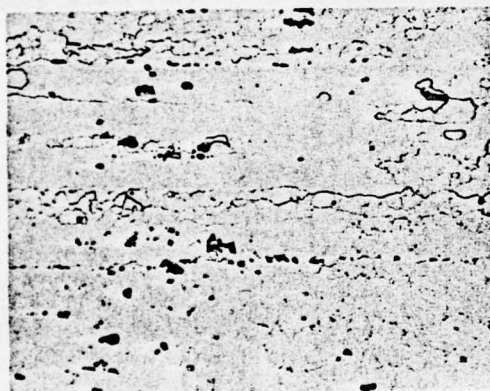


Figure V-43 210x

Corroded in Mixed Acid
Liquid Solution

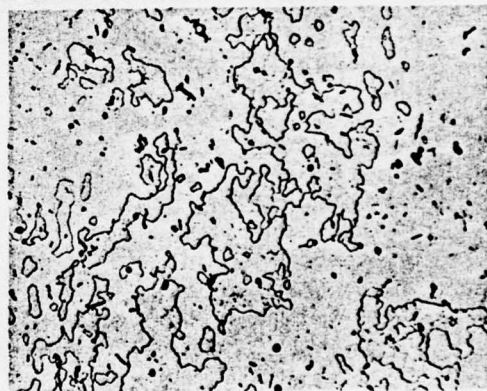


Figure V-44 210x

Corroded in Mixed Acid
Liquid Solution

Alloy and Condition LD2CS

Specification ϕ 70 mm. bar

(continued)

Features of
Structure

Figure V-41 shows the longitudinal structure of the edge region at the rear end of the bar. The chemical compounds are severely broken and scatter on the matrices of $\alpha(\text{Al})$. The alloy has completely recrystallized and the grains are coarse.

Figure V-42 shows the transverse structure.

Figure V-43 shows the longitudinal structure of the central part at the rear end of the bar. The degree of deformation is smaller than that at the central part, but it is larger than that of the central part at the front end. The chemical compounds are therefore broken less severe than those of the edge region, but more severe than those of the central part at the front end. The alloy has not yet completely recrystallized.

Figure V-44 shows the transverse structure.

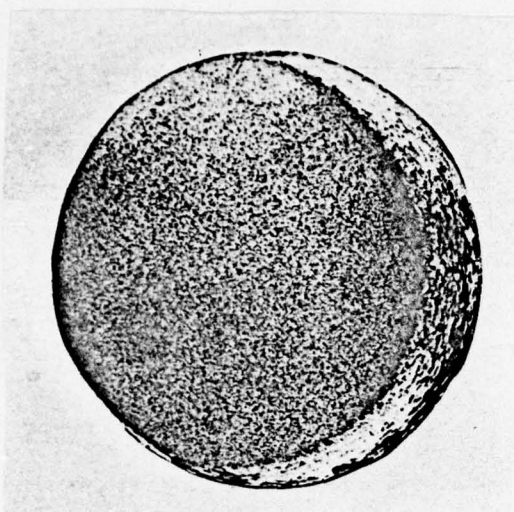


Figure V-45

1:1

Corroded in 30%NaOH Liquid Solution

Alloy and Condition

LD5CS (520°C, 30 minutes, water cooling, 160°C, aging for 8 hours)

Specification ϕ 60 mm. bar

Features of Structure

The transverse macroscopical structure of the rear end of the bar. The testing piece was cut before quenching, so there is cutting effect, the grains in the coarse crystal link are fine and small.

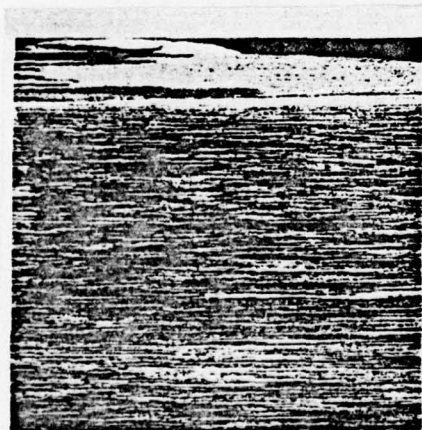


Figure V-46

1:1

Corroded in 30%NaOH Liquid Solution

Alloy and Condition

LD5CS (520°C, 30 minutes, water cooling, 160°C, aging for 8 hours)

Specification ϕ 60 mm. bar

Features of Structure

The longitudinal macroscopical structure of the rear end of the bar. The left end in this Figure corresponds to the transverse structure in Figure V-45, and the right end corresponds to the transverse structure in Figure V-47. It thus can be seen that the depth of the cutting effect on the crystal structure is about 20-30 mm.

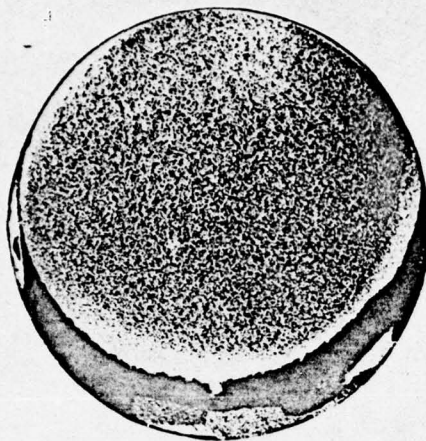


Figure V-47

1:1

Corroded in 30%NaOH Liquid
Solution

Alloy and Condition LD5CS (520°C, 30
minutes, water cooling,
160°C, aging for 8
hours)

Specification ϕ 60 mm. bar

Features of Structure The transverse macro-
scopical structure of
the rear end of the
bar. Because the
testing piece was cut
after quenching,
there is no cutting
effect, and the grains
in the coarse crystal
region are coarse
and large.

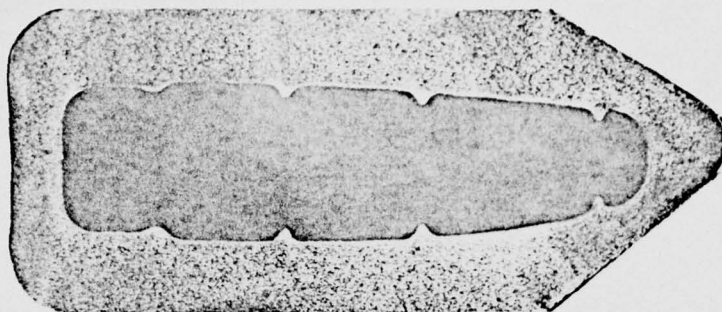


Figure V-48 Corroded in 30%NaOH Liquid Solution

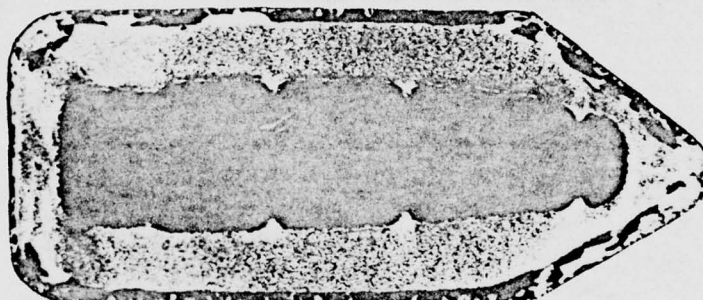


Figure V-49 Corroded in 30%NaOH Liquid Solution

Alloy and Condition LD20S (510°C, 30 minutes, water cooling, 155°C, aging for 15 hours)

Specification XC051 mold

Features of Structure Figure V-48 shows the macrostructure of the front end of the mold.

Figure V-49 shows the macrostructure of the rear end of the mold.

The structure at the front end is homogeneous and fine, and that at the rear end is very not homogeneous. On both inner and outer plys, there are coarse crystal links. The grey-white lines (arrow pointed) in the Figures are the welded regions which are made by a tongue-shaped extruder.

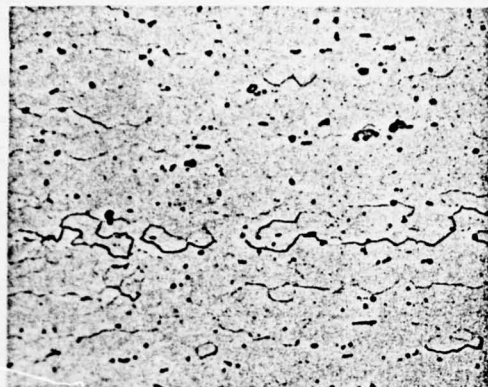


Figure V-50

210x

Corroded in Mixed Acid
Liquid Solution

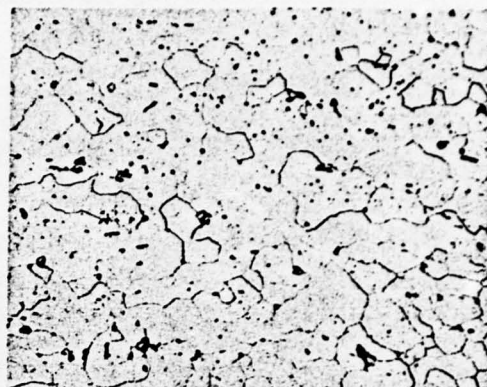


Figure V-51

210x

Corroded in Mixed Acid
Liquid Solution

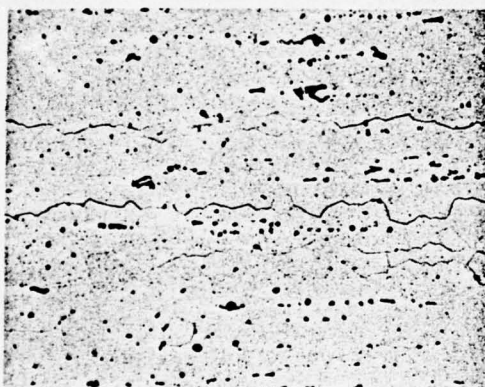


Figure V-52

210x

Corroded in Mixed Acid
Liquid Solution

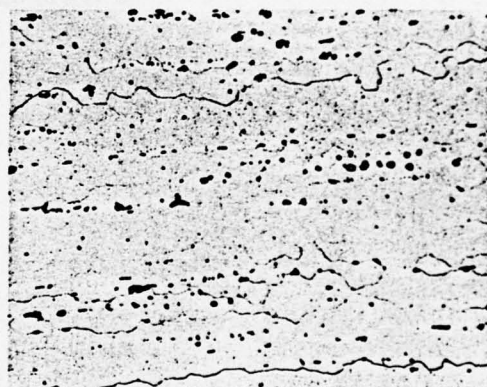


Figure V-53

210x

Corroded in Mixed Acid
Liquid Solution

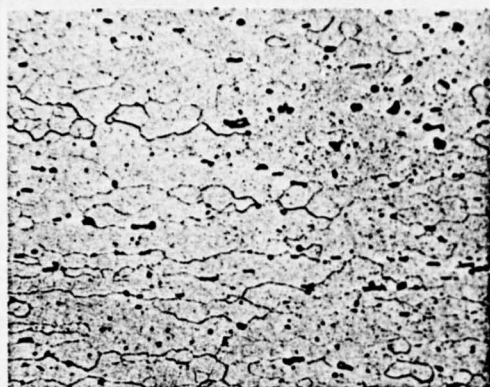


Figure V-54 210x
Corroded in Mixed Acid
Liquid Solution

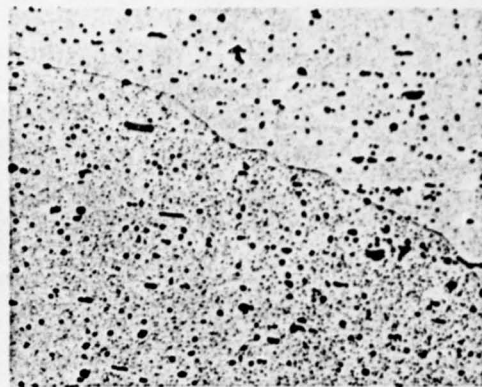


Figure V-55 210x
Corroded in Mixed Acid
Liquid Solution

Alloy and Condition LD2CS

Specification XC051 mold

Features of
Structure

Figure V-50, V-52 and V-54 respectively show the regions of jutting edges on the inner wall at the front end of the mold, and the longitudinal structure in the middle region and the outer wall region. The alloy has already recrystallized, and the grains are relatively homogeneous. The chemical compounds are arranged in lines and those which are on inner wall and outer wall are broken more severely than those in the middle region.

Figure V-51, V-53 and V-55 respectively show the regions of jutting edges on the inner wall at the rear end of the mold, and the longitudinal structure in the middle region and the outer wall region. The outer wall is the structure of the recrystallized coarse grains, and the region of jutting edges on the inner wall and the middle region are the structure of recrystallized fine grains. The chemical compounds are broken much more severely than at the front end, and the directionality of arranging in line is quite strong.

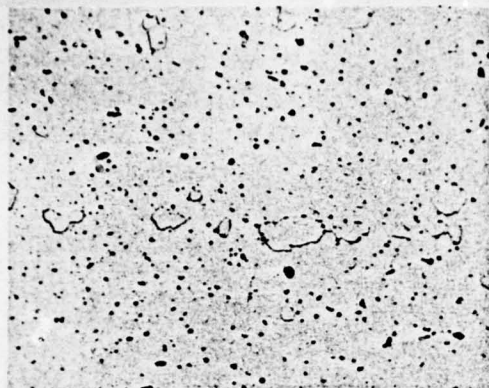


Figure V-56 210x

Corroded in Mixed Acid
Liquid Solution

Alloy and Condition LD2CS

Specification XC051 mold

Features of Structure The Figure shows the transverse structure of the welded regions. There is a group of fine and recrystallized grains. Its corresponding macroscopical structure looks like a depressed groove and also like a white line.

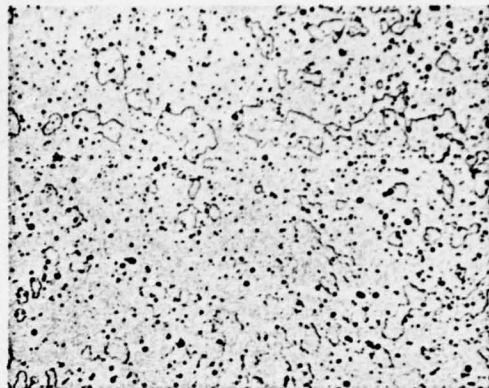


Figure V-57 210x

Corroded in Mixed Acid
Liquid Solution

Alloy and Condition LD2Cs

Specification XC051 mold

Features of Structure The Figure shows the longitudinal structure of the welded regions. The directionality that the chemical compounds here are to arrange themselves in line is rather strong, and among the lines there are fine and small recrystallized grains.

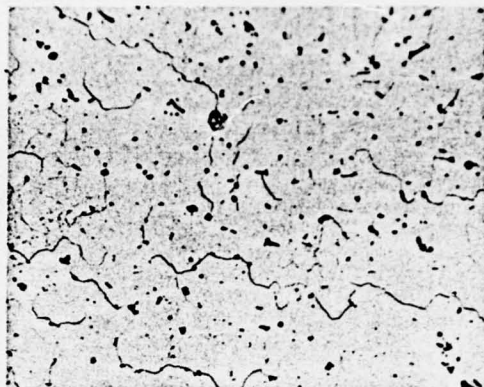


Figure V-58 210x

Corroded in Mixed Acid
Liquid Solution

Alloy and Condition LD2CS

Specification XC051 mold

Features of Structure The Figure shows the transverse structure of the regular part adjacent to the welded region of the mold. Compared with the regions of welded parts, the chemical compounds and the recrystallized grains are all more coarse and larger.

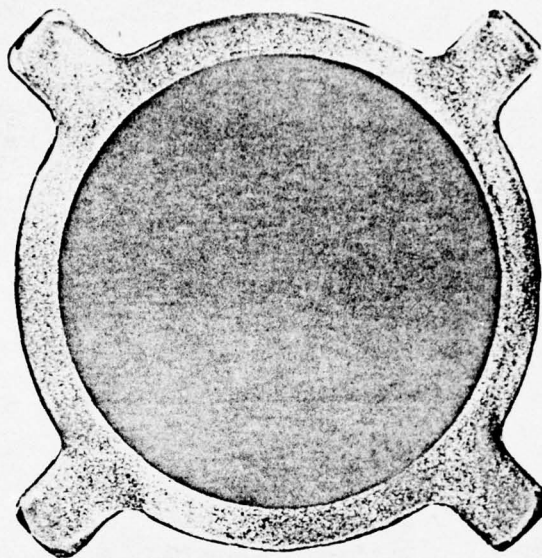


Figure V-59

Corroded in 30%NaOH Liquid
Solution

Alloy and Condition

LD10CS (503 \pm 5°C, 30 minutes, water
cooling, 160°C, aging for 8 hours)

Specification

XCO50 mold

Features of
Structure

The transverse macroscopical structure
of the mold. In the places where there
are the sinew lines there are coarse
crystal rings, and its depth is about
3 mm. From the end of the sinews to
the position of the inner wall, there is
low deformation region which looks like
a triangle.



Figure V-60

210 x

Corroded in Mixed Acid
Liquid Solution

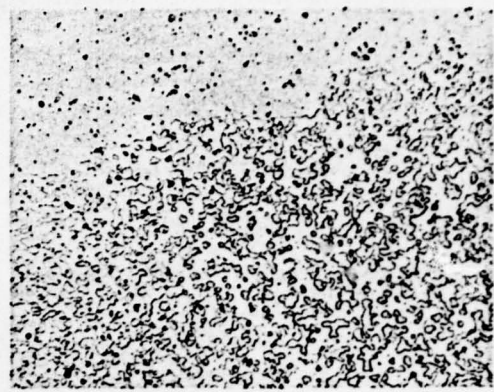


Figure V-61

210 x

Corroded in Mixed Acid
Liquid Solution



Figure V-62

210 x

Corroded in Mixed Acid
Liquid Solution

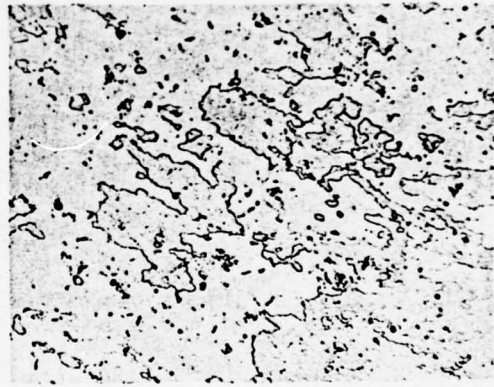


Figure V-63

210 x

Corroded in Mixed Acid
Liquid Solution

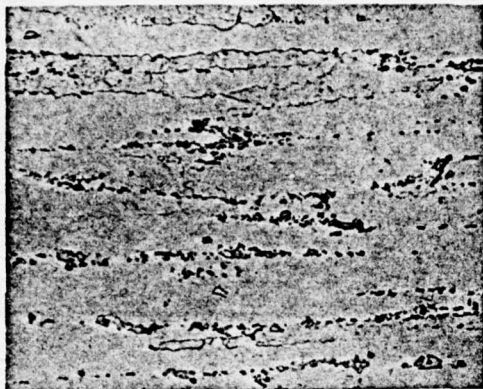


Figure V-64 210x

Corroded in Mixed Acid
Liquid Solution

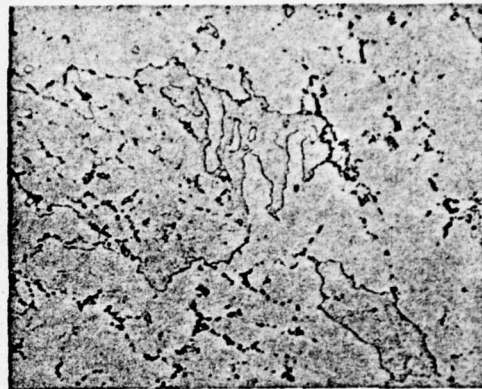


Figure V-65 210x

Corroded in Mixed Acid
Liquid Solution

Alloy and Condition LD10CS

Specification XC050 mold

Features of
Structure

Figure V-60, V-62 and V-64 respectively show the top of the sinews at the rear end of the mold, and the longitudinal structure of the middle part and the inner wall. Alloy has already recrystallized. In the region where deformation is low, the break of the chemical compounds is less severe. The chemical compounds which are among the sinews and on the inner wall are coarse and large, and they are arranged in lines and piles. Those which are on the top of the sinews are fine and small and they are distributed evenly.

Figure V-61, V-63 and V-65 respectively show the top part of the sinews at the rear end of the mold, and the transverse structure of the middle part and the inner wall.

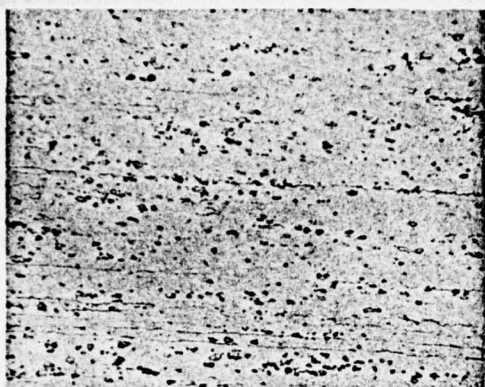


Figure V-66 210x

Corroded in Mixed Acid
Liquid Solution

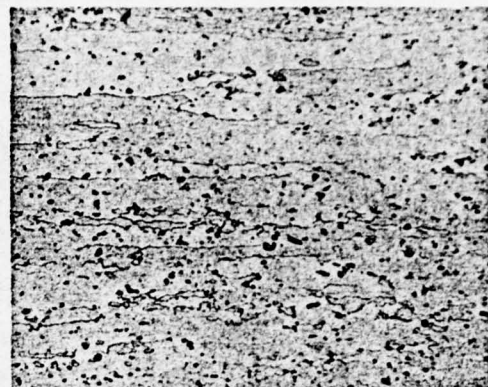


Figure V-67 210x

Corroded in Mixed Acid
Liquid Solution

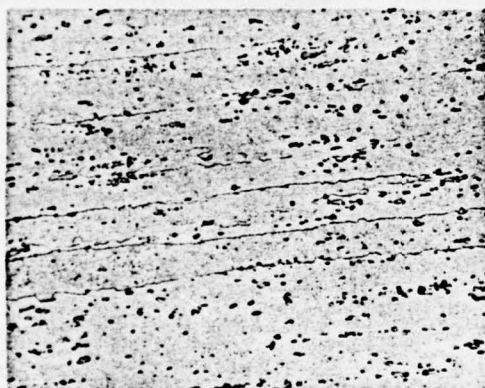


Figure V-68 210x

Corroded in Mixed Acid
Liquid Solution

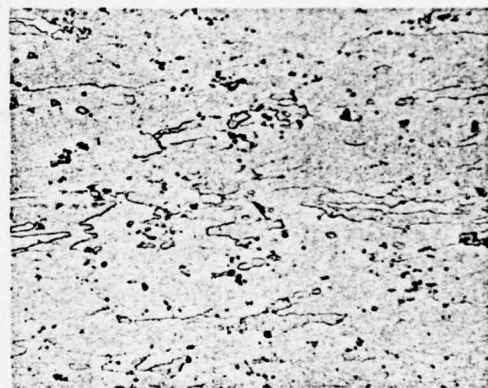


Figure V-69 210x

Corroded in Mixed Acid
Liquid Solution

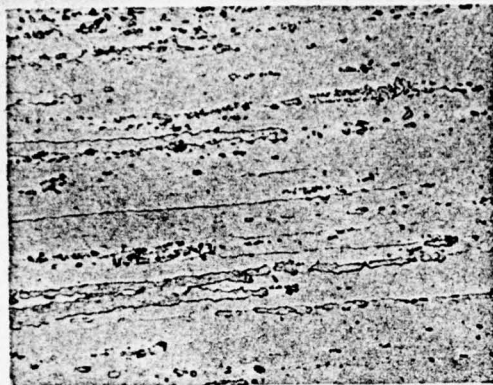


Figure V-70

210x

Corroded in Mixed Acid
Liquid Solution

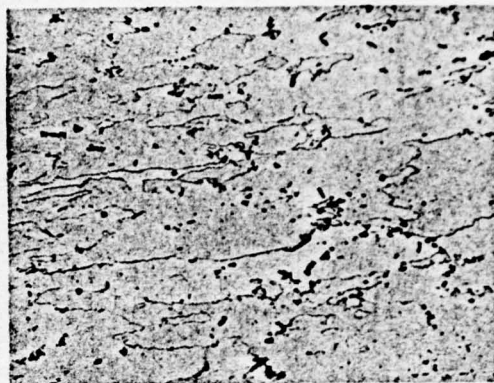


Figure V-71

210x

Corroded in Mixed Acid
Liquid Solution

Alloy and Condition LD10CS

Specification XC050 mold

Features of
Structure

Figure V-66, V-68 and V-70 respectively show the outer wall of the tube wall part at the rear end of the mold, and the longitudinal structure of the middle part and the inner wall. The alloy has already recrystallized and the grains stretch along the direction of the extrusion. Due to the fact that the deformation is greater than that on the same section of the sinew part, the chemical compounds are small and the directionality of arranging them in line along the extrusion direction is quite strong.

Figure V-67, V-69 and V-71 respectively show the outer wall of the tube wall part at the rear end of the mold, and the transverse structure of the middle part and the inner wall.

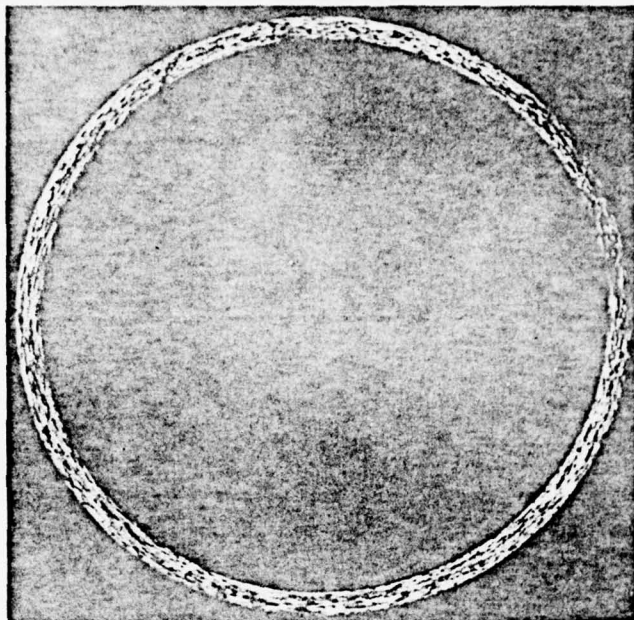


Figure V-72

1:1

Corroded in 30%NaOH
Liquid Solution

Alloy and Condition	LD2CS (510°C, 30 minutes, water cooling, 155°C, aging for 15 hours)
Specification	ø 85 x 77 mm, tube
Features of Structure	The Figure illustrates the transverse macroscopical structure of the tube. On the cross-section the size of the crystal grains is even.

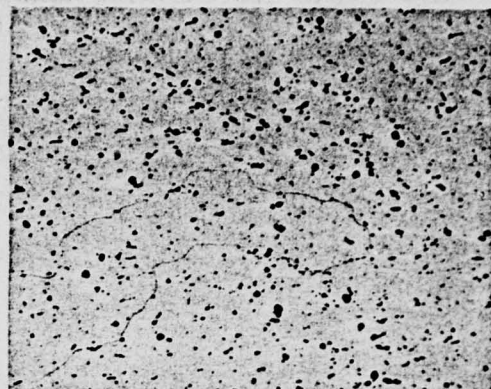
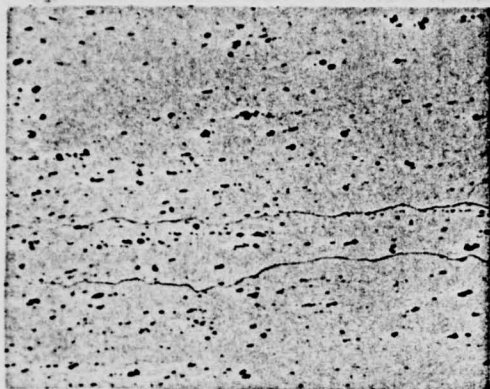


Figure V-73 210x

Figure V-74 210x

Corroded in Mixed Acid
Liquid Solution

Corroded in Mixed Acid
Liquid Solution

Alloy and Condition LD2CS

Specification ϕ 85 x 77 mm. tube

Features of
Structure

Figure V-73 shows the longitudinal structure of the tube. The alloy has completely re-crystallized, and the chemical compounds on the matrices of $\alpha(Al)$ are fine and small and distributed evenly.

Figure V-74 shows its transverse structure.

4. The Structure of Die-forged Articles

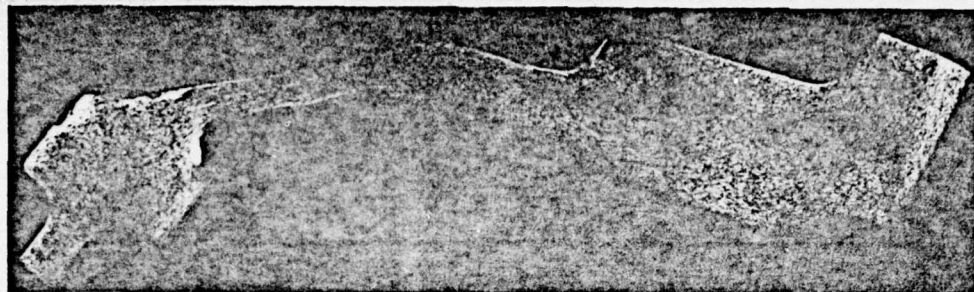


Figure V-75 Corroded in 30%NaOH
Liquid Solution

Alloy and Condition	LD2CS (510°C, 60 minutes, water cooling, 155°C, aging for 15 hours)
Specification	D2 die-forged article
Features of Structure	The Figure shows the macroscopical structure of the lines stretching following a natural flow of the die-forged article. The structure is homogeneous and fine. The stream lines are distributed along the outline of the appearance of the article. In the thin wall part, there are some coarse recrystallized grain structures.



Figure V-76 1:1

Alloy and Condition	LD2CS
Specification	D2 die-forged article
Features of Structure	This Figure illustrates the structure of the transverse fracture in the thin wall part of the die-forged article in Figure V-75.

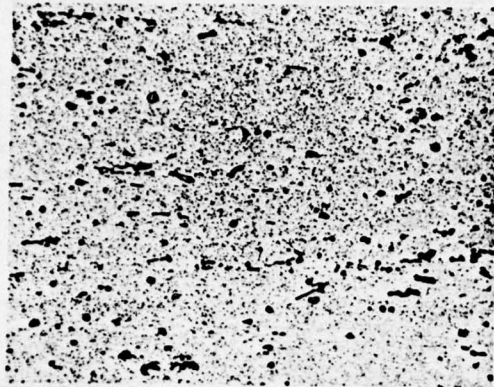


Figure V-77

210x

Corroded in Mixed Acid
Liquid Solution



Figure V-78

210x

Corroded in Mixed Acid
Liquid Solution

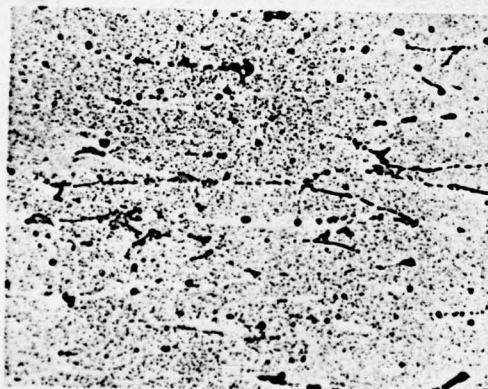


Figure V-79

210x

Corroded in Mixed Acid
Liquid Solution

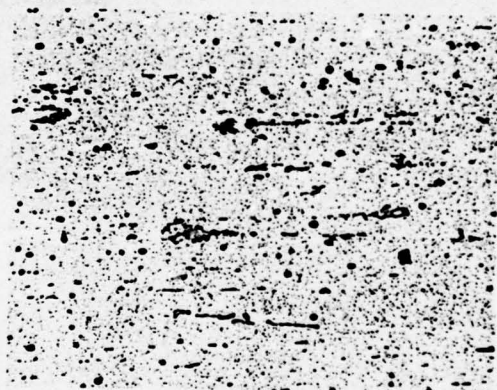


Figure V-80

210x

Corroded in Mixed Acid
Liquid Solution

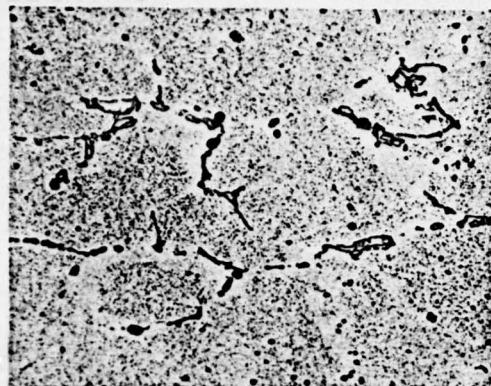


Figure V-81 210x
Corroded in Mixed Acid
Liquid Solution

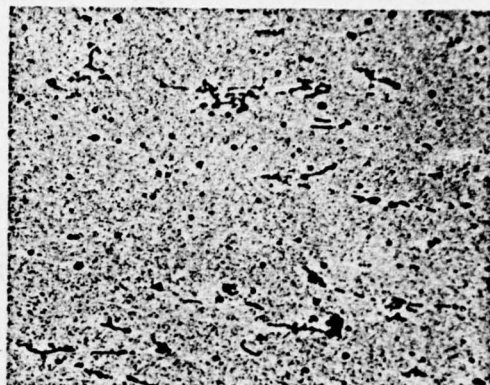


Figure V-82 210x
Corroded in Mixed Acid
Liquid Solution

Alloy and Condition LD2R

Specification D2 die-forged article

Features of
Structure

Figure V-77, V-79 and V-81 respectively show the structure of the outer edge region, the middle region and the inner edge region in the thick wall part of the die-forged article.

Figure V-78, V-80 and V-82 respectively show the structure of the outer edge region, the middle region and the inner edge region in the thin wall part of the die-forged article.

In the thin wall part of the die-forged article, because the degree of deformation is great on the inner edge, the chemical compounds are broken more severely. On the outer edge, the degree of deformation is small, the chemical compounds are broken less severely. The condition of the middle part is in between those two regions.

In the thick wall part of the die-forged article, because the degree of deformation is smaller than that in the thin wall part, the chemical compounds are broken generally less severely. In some places, the outline of the dendritic crystal network can still be seen. And there is a great amount of segregated particles dispersed on the matrices of $\alpha(\text{Al})$ evenly.

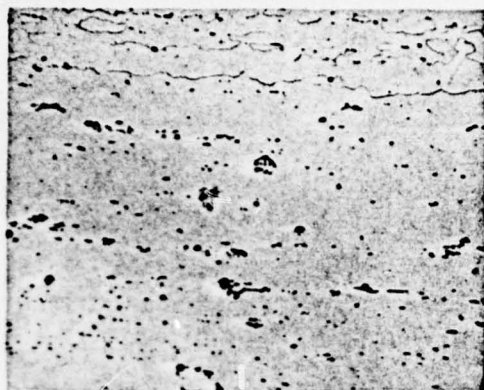


Figure V-83

210x

Corroded in Mixed Acid
Liquid Solution

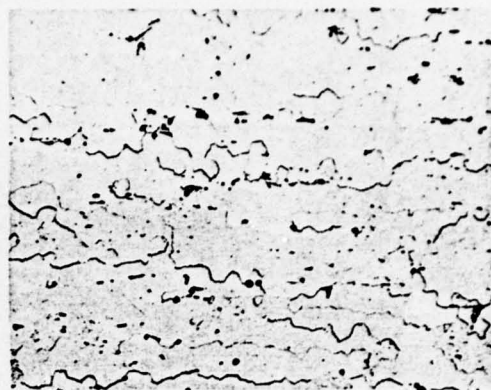


Figure V-84

210x

Corroded in Mixed Acid
Liquid Solution

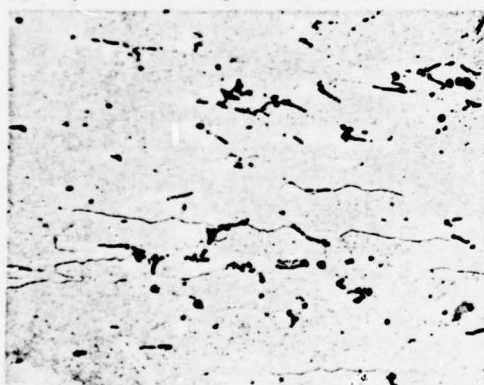


Figure V-85

210x

Corroded in Mixed Acid
Liquid Solution

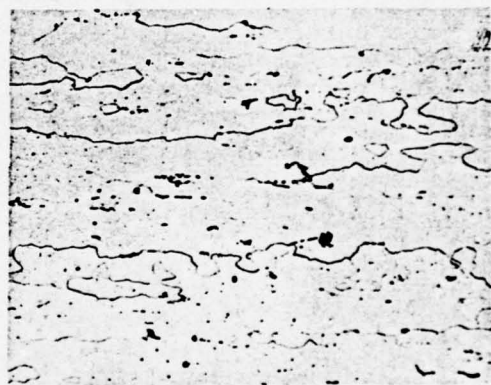


Figure V-86

210x

Corroded in Mixed Acid
Liquid Solution

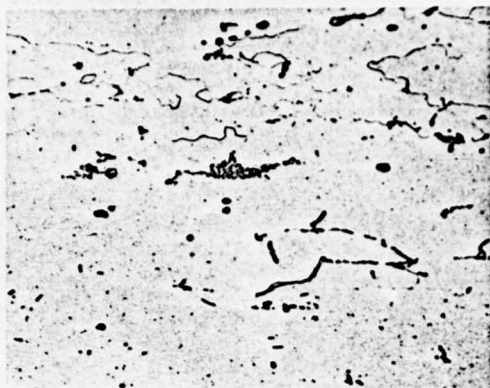


Figure V-87

210x

Corroded in Mixed Acid
Liquid Solution

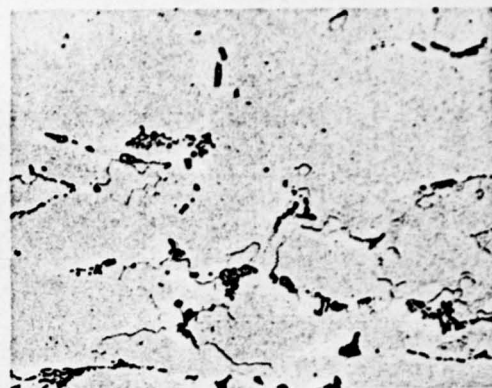


Figure V-88

210x

Corroded in Mixed Acid
Liquid Solution

Alloy and Condition LD2CS

Specification D2 die-forged article

Features of
Structure

Figure V-83, V-85 and V-87 respectively show the structure of the outer edge region and the middle region and the inner edge region in the thin wall part of the die-forged article.

Figure V-84, V-86 and V-88 respectively show the structure of the outer edge region and the middle region and the inner edge region in the thick wall part of the die-forged article.

Compare the chemical compounds and the casting conditions. Because the solid solution is further reduced, alloy has recrystallized and the grains stretch along the deformation direction of the casting.

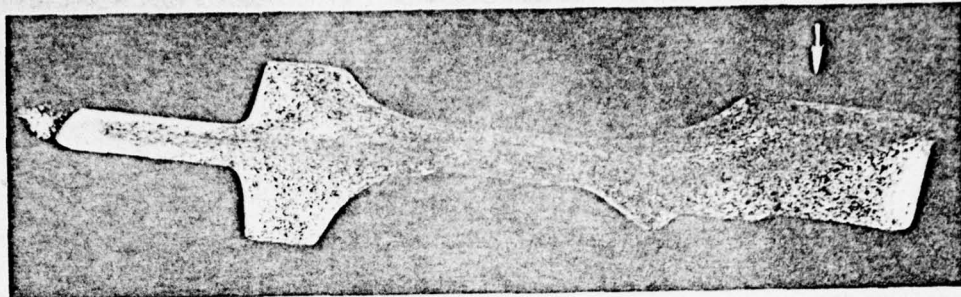


Figure V-89 Corroded in 30%NaOH
Liquid Solution

Alloy and Condition LD5CS (515 \pm 10°C, 60 minutes, water cooling, 160°C, aging for 8 hours)

Specification D3 die-forged article

Features of The Figure shows the radial macroscopical structure, and the steaming lines are fine and flowing along the outline of the mold evenly.

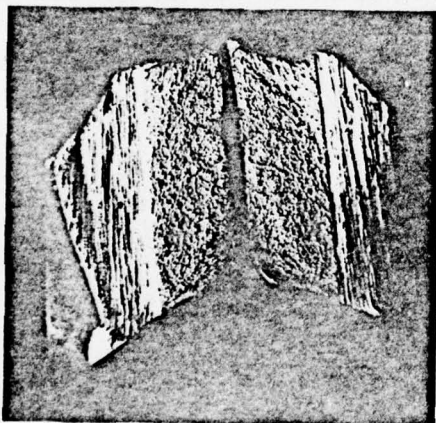


Figure V-90 1:1

Alloy and Condition LD5CS

Specification D3 die-forged article

Features of Structure This Figure shows the structure of the radial fracture in the thick wall part (arrow pointed in Figure V-89), and the structure is fine and homogeneous.

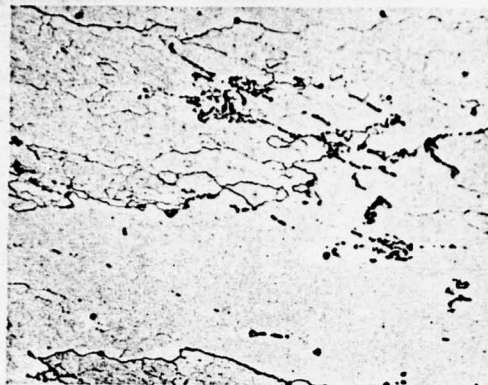


Figure V-91

210x

Corroded in Mixed Acid
Liquid Solution

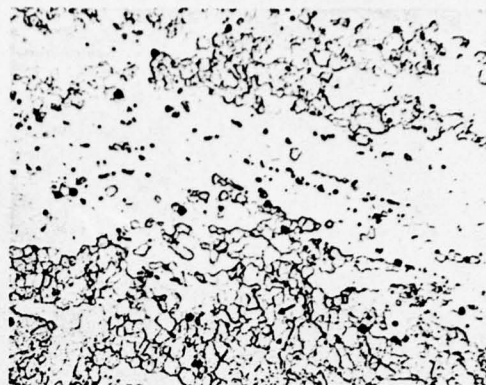


Figure V-92

210x

Corroded in Mixed Acid
Liquid Solution



Figure V-93

210x

Corroded in Mixed Acid
Liquid Solution

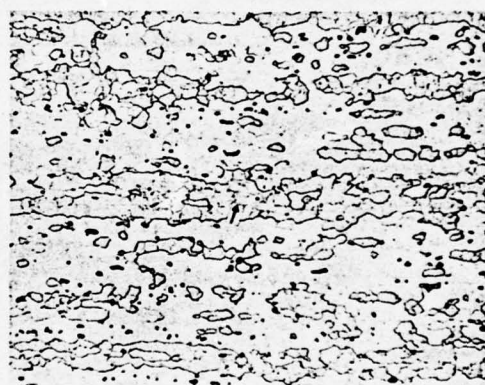


Figure V-94

210x

Corroded in Mixed Acid
Liquid Solution

Alloy and Condition

LD5CS

Specification

D3 die-forged article

Features of
Structure

Figure V-91 and V-93 respectively show the structure of the middle region and the outer edge region in the thick wall part of the die-forged article.

(continued)

Figure V-92 and V-94 respectively show the structure of the middle region and the outer edge region in the thin wall part of the die-forged article.

In the thick wall part of the article, because the degree of deformation at the edge is small and the breaking of chemical compounds is not severe, the remnant casting structure can still be seen. In the middle region, the degree of deformation is great and the amount of the broken chemical compounds is large, the structure is fine and homogeneous.

In the thin wall part of the article, because the degree of deformation is greater than that in the thick wall part and the chemical compounds are broken more thoroughly, no remnant casting structure can be seen. The alloy has not completely recrystallized and on its structure some hypo-crystal grains (arrow pointed) can be seen.

Chapter 6

Alloy of Aluminum-Zinc-Magnesium-Copper Group

Alloys of aluminum-zinc-magnesium-copper group are one kind of aluminum alloy, which has the highest strength under room temperature in production at the present time. Their strength is much higher than that of hard aluminum (LY11 and LY12), so they are usually called super-hard aluminum.

For alloys of this group, the brand marks which are often used include LC3, LC4, LC5 and LC6. They can be processed into plates, bars, wires, pipes and semi-finished forged articles. Mainly, however, they are used to make structure materials. For promoting corrosion resisting capability of the alloy, the surface of its plates is often covered by a layer of aluminum which contains 1%Zn.

Section 1

Chemical Composition and Phase Formation

The chemical composition of alloys of aluminum-zinc-magnesium-copper group can be seen in Table VI-1.

Table VI-1 Chemical Composition of Superhard Aluminum

Brand of Alloy	Principal Constituents (%)						Impurity No. More Than (%)					
	Cu	Mg	Zn	Mn	Cr	Ti	Fe	Si	Mn	Cr	Oth-er	Total*
LC3	1.8~2.4	1.2~1.6	6.0~6.7	—	—	0.02~0.08	0.2	0.2	0.1	0.05	0.1	—
LC4	1.4~2.0	1.8~2.8	5.0~7.0	0.2~0.6	0.1~0.25	—	0.5	0.5	—	—	0.1	1.1
LC5	0.3~1.0	1.2~2.0	7.0~8.0	0.3~0.8	—	—	0.6	0.4	—	—	0.3	—
LC6	2.2~2.8	2.5~3.2	7.6~8.6	0.2~0.5	0.1~0.25	—	0.5	0.3	—	—	0.1	—

*Impurity total

The principal constituents of alloys of this group are zinc, magnesium and copper. In addition, some of the alloys contain manganese, chromium, titanium, zirconium and silver. Zinc and magnesium are the elements that help to strengthen the alloy, and the increase of zinc and magnesium contents can elevate its strength but lower its rolling ability, and also make its stress-corrosion resisting ~~capability~~ poor. But, if a proper amount of copper is added, the mechanical property of the alloy can be promoted and its corrosion resisting ability can also be improved. To the alloy, which contains 6-12% Zn, 1.5-3% Cu is added, its rolling rate and the ^{periodic} strength will be increased, and, at the same time, its stress-corrosion resisting capability can also be improved. But, when the copper content is over 3%, its corrosion resisting ability will become poor.

The addition of manganese and chromium can help to increase strength of the alloy and the effect of aging under fresh quenching, and, at the same time, its stress-corrosion resisting capability can be improved as well.

In the alloys of this group, iron and silicon are harmful impurities. They can form a complicated chemical compound which is hard to dissolve, and this chemical compound will reduce the mechanical property of the extruded articles. Iron can also bring down the shear strength of wires made of alloy LC3 and make their fastening ability poor. Silicon together with the magnesium contained in the alloy form Mg_2Si and reduce the quantity of strengthening phase $MgZn_2$ and $T(Mg_3Zn_3Al_2)$. The strength of the alloy is thereby brought down, so the silicon content should be

controlled at a minimum level. Although the presence of silicon in the alloy is harmful to the strength of shear resistance of wires, but silicon will not affect their fastening ability.

When iron and silicon exist simultaneously, their effect on the quality of the alloy is smaller than that when either of them exists alone. If iron and silicon contents are lower than 0.5%, there will be no effect on the mechanical property of alloy LC4 and LC6. But iron and silicon can reduce the strength of shear resistance of wires made of LC3 and weaken their fastening ability as well.

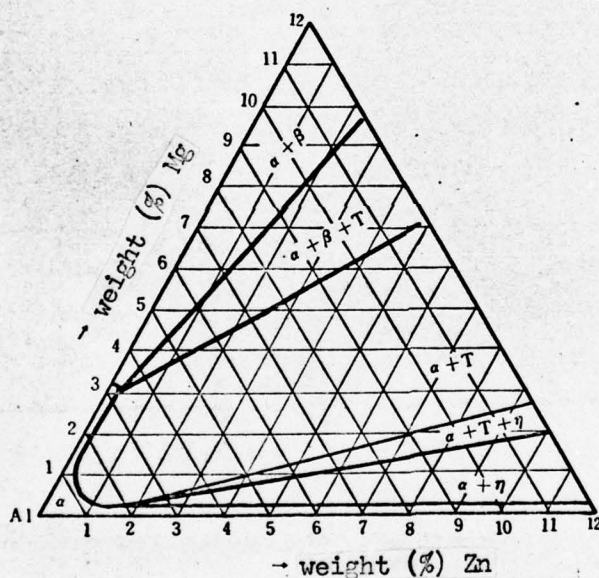


Figure VI-1 The 200°C isothermal section of dependent aluminum angle in the equilibrium diagram of Al-Mg-Zn group alloy

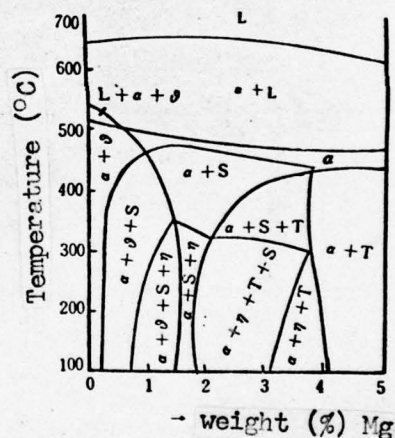


Figure VI-2 The cross section of the variable thermal section of Cu + Mg = 5%, Zn = 6% in the equilibrium diagram of Al-Cu-Mg-Zn group alloy

From Figure VI-1 and Figure VI-2, and the range of the alloy constituents, it can be known that the phases that are formed when alloy LC4 is under the condition of annealing and gradual cooling, are $a(Al)$, $MgZn_2$, $T(AlZnMgCu)$ and $S(CuMgAl_2)$. In addition, there are Mg_2Si , $AlMnFeSi$ and $(FeMn)Al_6$, which are all in small quantity.

In LC4 ingot which is under semicontinuous casting (water cooling), besides $a(Al)$, $T(AlZnMgCu)$ and $S(CuMgAl_2)$, there still are phases Mg_2Si , $AlMnFeSi$ and $(FeMn)Al_6$. These phases all exist on the network of the dendritic crystals.

The binary eutectic $T(AlZnMgCu)$ and $a(Al)$ is of a structure of a 'porous' aggregate. Phase $T(AlZnMgCu)$ is dark grey in color. The eutectic $S(CuMgAl_2)$ and $a(Al)$ looks like a honeycomb (Figure VI-3). Phase $T(AlZnMgCu)$ and $S(CuMgAl_2)$ can all be corroded in mixed acid liquid solution, but the degree of corrosion of $T(AlZnMgCu)$ is smaller than that of $S(CuMgAl_2)$. Phases $AlMnFeSi$ and $(FeMn)Al_6$ are all bright grey in color and they are of the shape of either schists or narrow long pieces. They are easy to be corroded in H_2SO_4 liquid solution. After corrosion, they become black brown (Figure VI-4 and Figure VI-5).

Section 2

Characteristics of Heat Treatment

Quenching and aging: Compared with alloys of Al-Cu-Mg group, the range of quenching temperature of alloys of this group is broader. It

will not affect the strength value of alloys which contain no more than 6% Zn and no more than 3% Mg if the quenching temperature is between 420-480°C. But when the temperature reaches the point higher than 480°C, the corrosion-resisting ability of the alloy will go down. So, under general condition, quenching should take place at 450-480°C.

Pure Al-Mg-Zn alloy has less sensitivity to the speed of quench cooling. But alloys, like LC4 and others because they contain such elements as Cu, Mn and Cr, have greater sensitivity to the speed of quench cooling. So the quench transferring period for these alloys ought to be shortened to the minimum when quenching takes place.

For these alloys when aging takes place, there will be a maximum point on the curve, which indicates relationship between tensile strength and time. If the aging takes place at 120°C, 140°C, 160°C, 180°C and 200°C, there will be two maximum points. Between these two points, on a curve, which indicates relationship between aging temperature and tensile strength, there are two vertexes. The first one appears in between 20-80°C, and the ^{second} one appears in between 120-140°C. If aging (including natural aging) takes place within the temperature range of first vertex, the plasticity of the alloy will be good and its stress-corrosion resisting capability will be not. Materials, which have aging within the temperature range of the second vertex, will have poor extensibility, but their stress-corrosion resisting capability is good, and, at the same time, their periodic strength can also be improved. So the aging temperature for LC4 should be at 120-140°C.

For further improving the stress-corrosion resisting capability of these alloys, the method of step-aging ought to be adopted. A plate of LC4 with thickness of 2.0 mm, for example, takes aging at 120°C for 24 hours, its tensile strength can be as high as 62 kg./mm², and its stress-corrosion-breaking-resistance is 123 hours. If it takes aging at 120°C for 6 hours and repeats it at 160°C for 3 more hours, its tensile strength, as a result, will go down by 2 kg./mm², but its stress-corrosion-breaking-resistance can reach to 525 hours. It is therefore obvious that the adoption of step aging not only raises the stress-corrosion-resistance ability and also shortens the aging period.

Annealing: Of a cold rolled 2.0 mm plate of LC4 (deformation rate is 60%, heating in air furnace and temperature retention is 1.5 hour then cooled under room temperature), the beginning temperature of recrystallization is 300°C and the ending temperature of recrystallization is 370°C. The recrystallization temperature of the extruded articles is higher. A mold with thick wall of 2.0 mm, for example, and its deformation rate is 97.8%, under the same annealing condition, will begin to recrystallize at 400°C, and its ending temperature of recrystallization is 460°C.

Some lesser elements, like manganese, chromium and zirconium, have great effect on the process of recrystallization of alloys. Among these elements, the effect of chromium is the smallest and that of zirconium is the greatest. An alloy plate, for example, which contains 2% Mg and 5% Zn, will begin to recrystallize at 295°C, and end its recrystallization

at 320°C. If 0.05% Zr is added, its ending temperature of recrystallization will become 480°C. So the alloys of this group, under the normal quenching and annealing condition, will have such a structure that on the matrices of the deformable fiber structure appears a small quantity of recrystallized grains. This kind of visible fiber structure has a much higher stress-corrosion resisting capability.

When LC4 is at annealing and cooling in the air, there will be quench effect. Therefore, when it is annealing, the cooling speed is usually no more than 30°C per hour. The annealing temperature of this alloy is 350-420°C. By the cooling speed of no more than 30°C per hour, when it is cooled to 150°C, it must be moved out from the furnace and cooled in the air.

The recrystallized grains of a plate of Al-Zn-Mg alloy, which does not contain such elements as Mn, Cr, Zr, and Ag, will be coarse and isometric crystals. If Mn, Cr, and Zr are added, the grains will become fine and stretch along the direction of main deformation. Especially after Zr is added, this kind of phenomenon is more obvious. The grains stretch very long along the direction of main deformation, and they look like fibers.

Section 3

The Structure of Cast Ingots and Processed Articles

I. Phase Formation

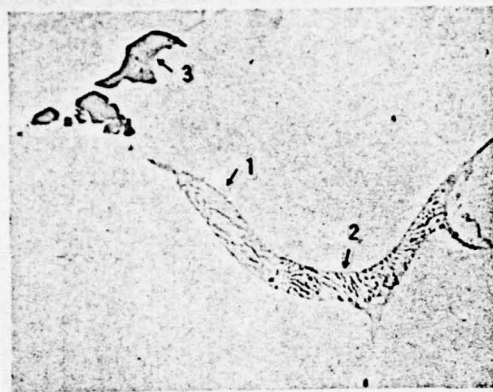


Figure VI-3

210x

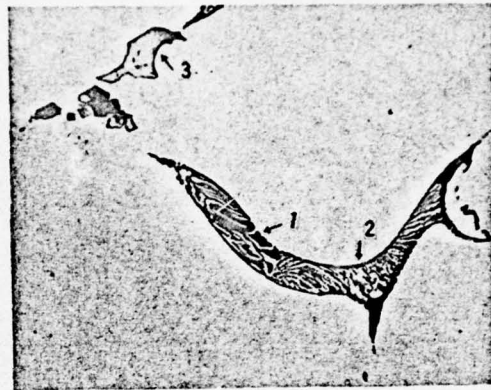


Figure VI-4

210x

Alloy	LC4
Condition	Cast ingot remelting at 700°C and cooled to 650°C, the temperature is retained for 8 hours. Cooled to 400°C, then water quenching.
Corrosion	Not corroded
Features of Structure	1 - T(AlZnMgCu) in eutectic structure; 2 - S(CuMgAl ₂) in eutectic structure; 3 - AlMnFeSi.

Alloy	LC4
Condition	Same as Figure VI-3
Corrosion	20% H ₂ SO ₄ liquid solution
Features of Structure	1 - T(AlZnMgCu) after corroding becomes black; 2 - S(CuMgAl ₂) black in color; 3 - AlMnFeSi brown in color.

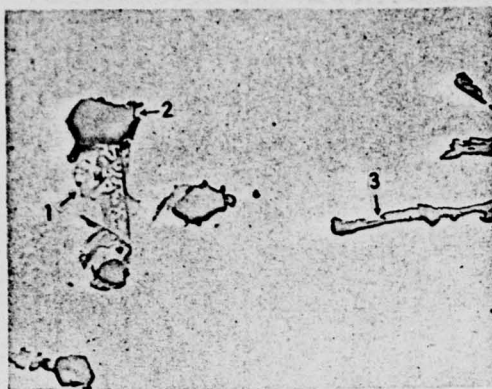


Figure VI-5

210x

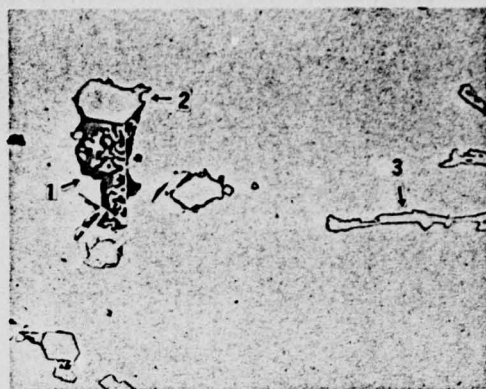


Figure VI-6

210x

Alloy LC4

Condition

Same as Figure VI-3

Corrosion

Not corroded

Features of Structure

- 1 - a(Al) + T(AlZnMgCu) eutectic.
- 2 - AlMnFeSi grey in color;
- 3 - (FeMn)Al₆ grey in color.

Alloy LC4

Condition

Same as VI-3

Corrosion

0.5% HF liquid solution

Features of Structure

- 1 - a(Al) + T(AlZnMgCu) eutectic, phase T is black in color;
- 2 - AlMnFeSi bright brown in color;
- 3 - (FeMn)Al₆ bright brown in color.

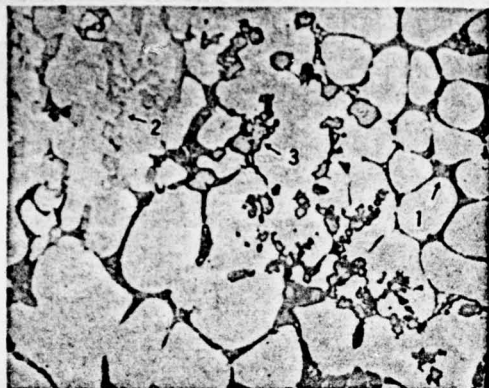


Figure VI-7

210x

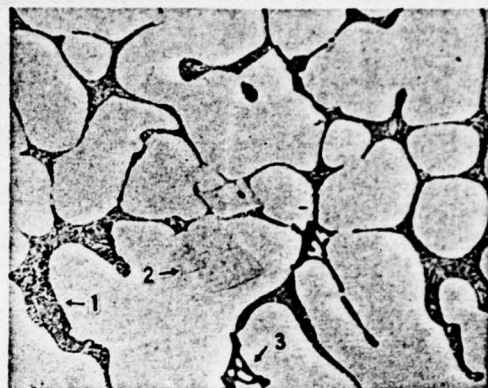


Figure VI-8

300x

Alloy	LC4
Condition	Semicontinuous casting
Corrosion	25% HNO_3 liquid solution
Features of Structure	On the segregated swellings of the cast ingot 1 - $\alpha(\text{Al}) + \text{T}(\text{AlZnMgCu})$ eutectic; 2 - $(\text{FeMn})\text{Al}_6$; 3 - AlMnFeSi .

Alloy	LC4
Condition	Semicontinuous casting
Corrosion	25% HNO_3 liquid solution
Features of Structure	On the segregated swellings of the cast ingot 1 - $\alpha(\text{Al}) + \text{T}(\text{AlZnMgCu})$ eutectic; 2 - $(\text{FeMn})\text{Al}_6$; 3 - $\alpha(\text{Al}) + \text{Mg}_2\text{Si}$ eutectic, Mg_2Si black in color.

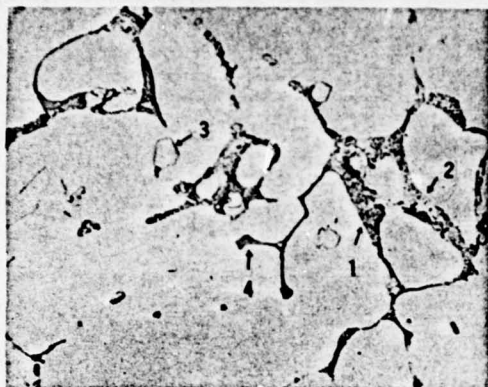


Figure VI-9

250x



Figure VI-10

250x

Alloy	LC4
Condition	Semicontinuous casting
Corrosion	25% HNO_3 liquid solution
Features of Structure	Transverse central part of the cast ingot 1 - Phase S(CuMgAl_2) in eutectic; 2 - Phase T(AlZnMgCu) in eutecticum; 3 - AlMnFeSi ; 4 - Mg_2Si .

Alloy	LC4
Condition	Semicontinuous casting
Corrosion	25% HNO_3 liquid solution
Features of Structure	Transverse central part of the cast ingot 1 - $\alpha(\text{Al} + \text{T}(\text{AlZnMgCu}))$ eutectic; 2 - $\alpha(\text{Al}) + \text{Mg}_2\text{Si}$ eutectic; 3 - AlMnFeSi ; 4 - $(\text{FeMn})\text{Al}_6$.

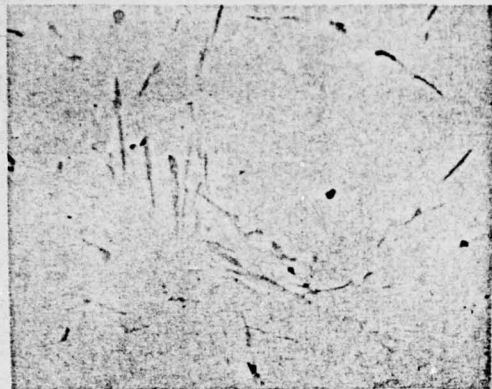


Figure VI-11

210x

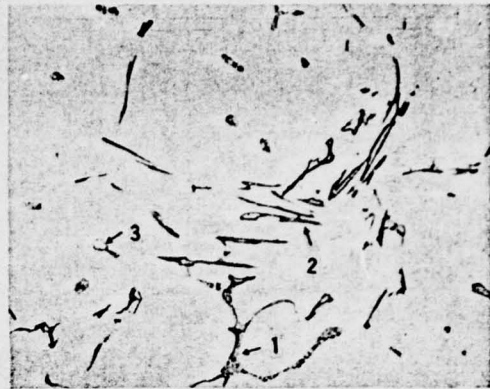


Figure VI-12

210x

Alloy	LC4
Condition	Semicontinuous casting
Corrosion	Not corroded
Features of Structure	the transverse central part of a cast ingot. That which is narrow and long and grey in color is $(FeMn)Al_6$.

Alloy	LC4
Condition	Semicontinuous casting
Corrosion	Mixed acid liquid solution
Features of Structure	The transverse central part of a cast ingot 1 - $a(Al) + T(AlZnMgCu)$ eutectic; 2 - $(FeMn)Al_6$ brown in color; 3 - $AlMnFeSi$.

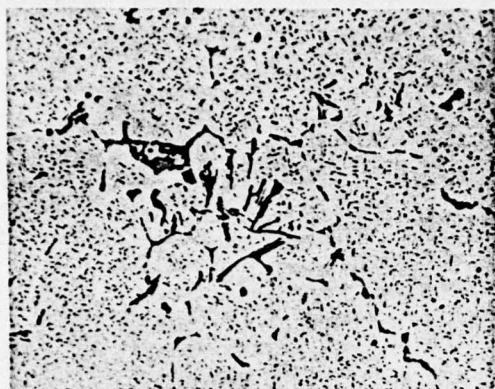


Figure VI-13

210x

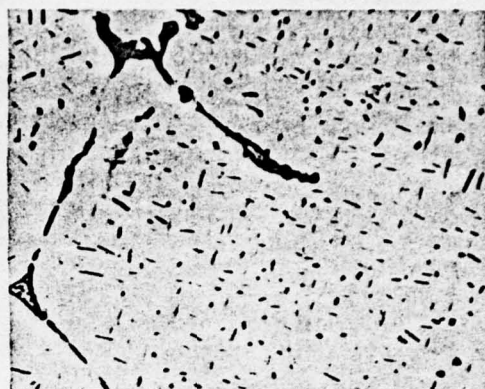


Figure VI-14

630x

Alloy	LC4
Condition	Semicontinuous casting through homogenization treatment at 460°C for 24 hours.
Corrosion	Mixed acid liquid solution
Features of Structure	A great quantity of phase S(CuMgAl ₂), phase T(AlZnMgCu) and phase MgZn ₂ separated from the matrices of a(Al), and particles separated from MnAl ₆ and CrAl ₇ .

Alloy	LC4
Condition	Semicontinuous casting, at 470°C heating for 2 hours, then cooled to 300°C in furnace and retaining the temperature for 8 hours, then cooled to 50°C and taken out of furnace.
Corrosion	Mixed acid liquid solution
Features of Structure	A great quantity of acicular substances separated from the matrices of a(Al). Phase S is black in color, and phase T and MgZn ₂ are deep grey in color.

2. The Structure of Cast Ingots

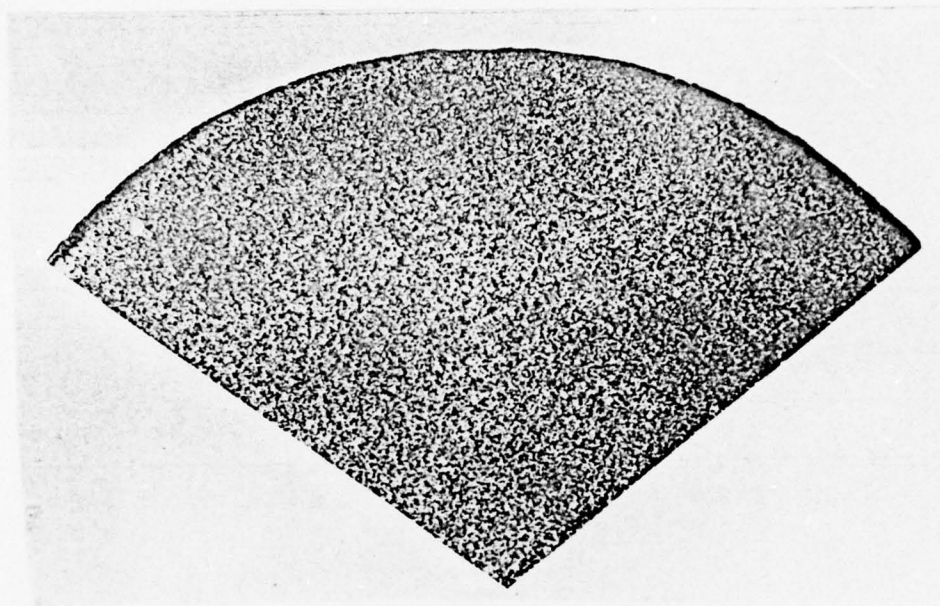


Figure VI-15

Alloy and Condition	LC4, semicontinuous casting
Specification	ϕ 280 mm. round ingot
Corrosion	15%NaOH liquid solution
Features of Structure	The transverse macroscopical structure. At the edge there is a segregated swelling, of which the thickness is 2-3 mm. The crystal grains at the edge are finer than those at the middle and central part.

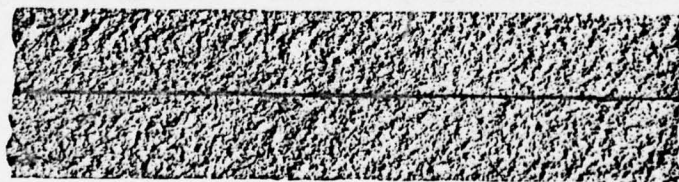


Figure VI-16

Alloy and Condition	LC4, semicontinuous casting
Specification	ϕ 280 MM. round ingot
Features of Structure	Longitudinal fracture structure and the structure is fine and homogeneous.

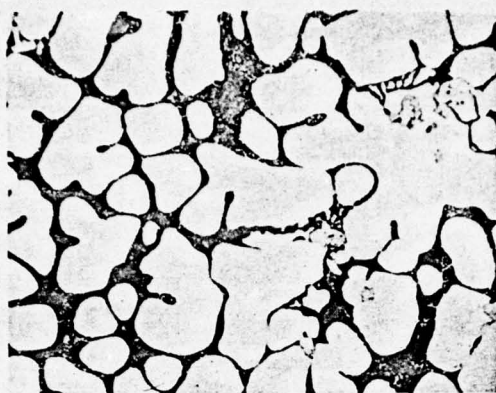


Figure VI-17 210x

Corroded in Mixed Acid
Liquid Solution



Figure VI-18 210x

Corroded in Mixed Acid
Liquid Solution

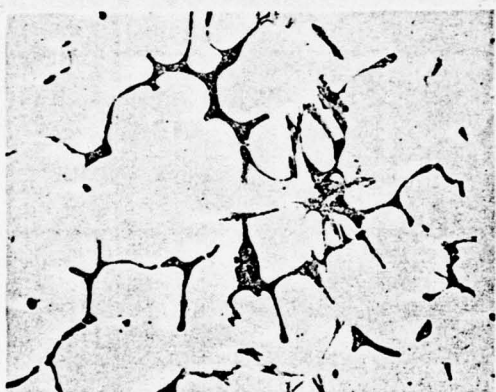


Figure VI-19 210x

Corroded in Mixed Acid
Liquid Solution

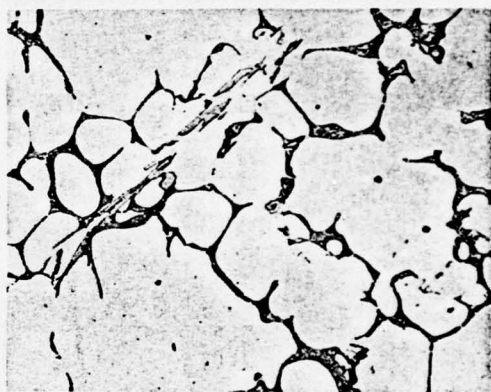


Figure VI-20 210x

Corroded in Mixed Acid
Liquid Solution

Alloy and Condition LC4 , semicontinuous casting

Specification ϕ 280 mm. round ingot

Features of
Structure

Figure VI-17 through Figure VI-20 are the separate illustrations of the structures of the central part, the middle part, the edge part and the transversely segregated (continued)

swellings of the cast ingot. They are all structures of networks of the dendritic crystals. The network on the segregated swellings are thick and aggregated; those at the edge part are thin, and disconnected; and those in the middle and central part are thick and connected.

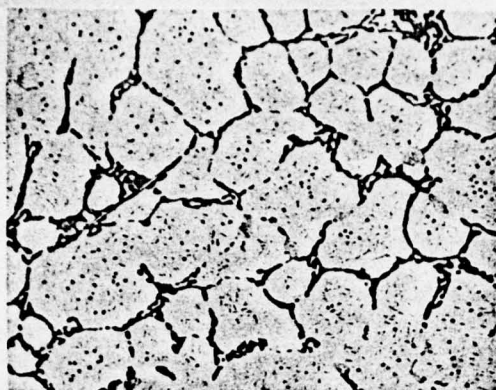


Figure VI-21 210x

Corroded in Mixed Acid
Liquid Solution

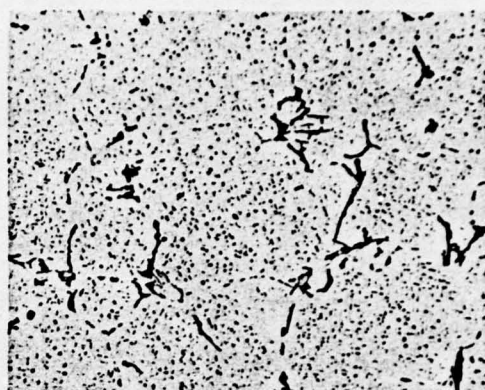


Figure VI-22 210x

Corroded in Mixed Acid
Liquid Solution

Alloy and Condition LC4 semicontinuous casting, through homogenization treatment for 24 hours at 460°C.

Specification ϕ 280 mm. round ingot

Features of
Structure

Figure VI-21 shows the structure of the transverse surface where swellings are segregated. The network of the dendritic crystal is thin and relatively connected. The substances separated from the matrices of $\alpha(\text{Al})$ are particles of the chemical compounds which contain Mn and Cr, and the particles look like many dots. The black narrow and long substances are phase S(CuMgAl_2), and the grey narrow and long substances are phase T(AlZnMgCu) and MgZn_2 .

Figure VI-22 shows the structure of the transverse central part, and most of the dendritic crystals are already in solid solution.



Figure VI-23 40x

The structure of the testing specimen which underwent electrolytic polishing, is under anodic double-filmed polarized light.

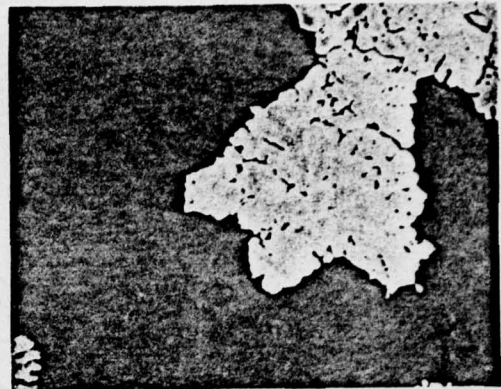


Figure VI-24 40x

The structure of the testing specimen which underwent electrolytic polishing, is under anodic double-filmed polarized light.

Alloy and Condition LC4 semicontinuous casting

Specification ϕ 280 mm. round ingot

Features of Structure Figure VI-23 shows the transverse structure of the edge part of the ingot.

Figure VI-24 shows the transverse structure of the central part of the ingot. The crystal grains at the edge part are finer than those at the central part.

3. The Structure of Plates

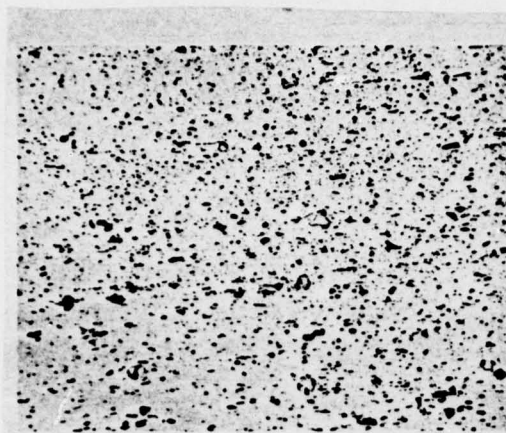


Figure VI-25 210x

Alloy and Condition	LC4R
Specification	Thickness 8.5 mm.
Corrosion	Mixed acid liquid solution
Features of Structure	This Figure shows the longitudinal structure of the central part of a plate. The chemical compounds which are broken arrange themselves along the direction of extrusion, and on the matrices of a(Al) there are separated phase particles.

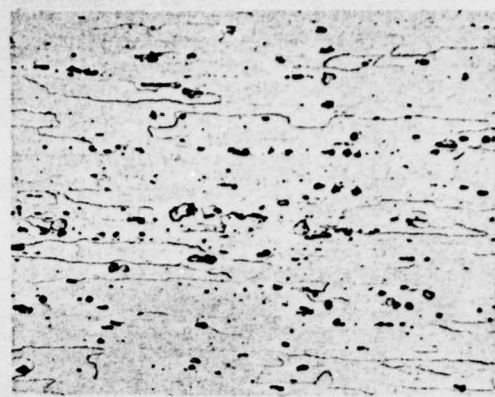


Figure VI-26 210x

Alloy and Condition	LC4CS
Specification	Thickness 8.5 mm.
Corrosion	Mixed acid liquid solution
Features of Structure	This Figure shows the longitudinal structure of the central part of a plate. The alloy has recrystallized and the grains stretch along the direction of extrusion. There are remnant phases S(CuMgAl ₂) and T(Al ZnMgCu), which are not in solid solution, and phase AlMnFeSi which is hard to dissolve.

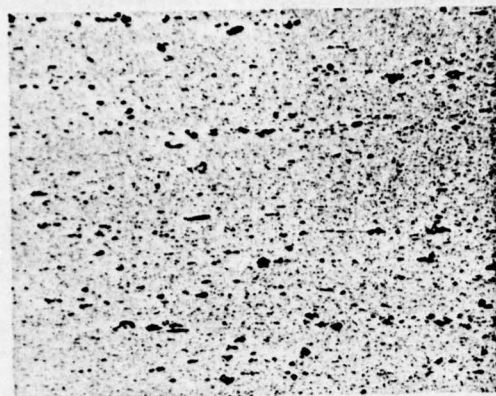


Figure VI-27 210x

Alloy and Condition	LC4Y
Specification	Thickness 4.5 mm.
Corrosion	Mixed acid liquid solution
Features of Structure	This Figure shows the longitudinal structure of the central part of a plate. The chemical compounds are further broken and their directionality of arranging is strong. On the matrices of $\alpha(\text{Al})$ there are many dispersed particles.

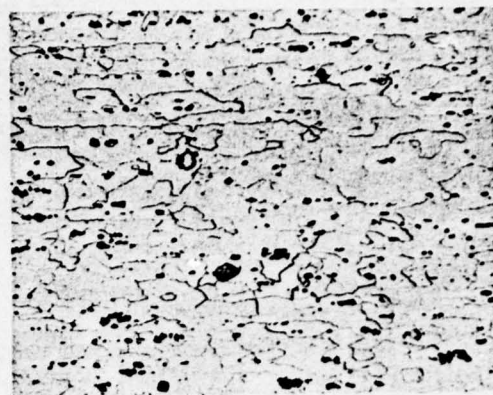


Figure VI-28 210x

Alloy and Condition	LC4Cs
Specification	Thickness 4.5 mm.
Corrosion	Mixed acid liquid solution
Features of Structure	This Figures shows the longitudinal structure of the central part of a plate. The alloy has completely recrystallized. There are remnant phases $\text{S}(\text{Cu MgAl}_2)$ and $\text{T}(\text{AlZnMgCu})$, and the hard-to-dissolve phase AlMnFeSi .

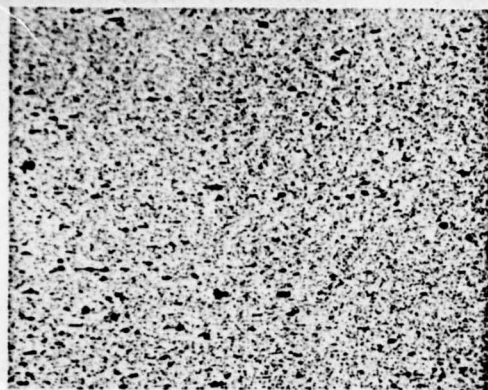


Figure VI-29 210x

Alloy and Condition	LC4M (370°C, temperature retaining for 1.5 hour)
Specification	Thickness 2.0 mm.
Corrosion	Mixed acid liquid solution
Features of Structure	Solid solution $\alpha(\text{Al})$ is decomposed, and phase $\text{S}(\text{CuMgAl}_2)$ and $\text{T}(\text{AlZnMgCu})$ dispersively scatter on the matrices of $\alpha(\text{Al})$.



Figure VI-30 100x

	The testing specimen underwent electrolytic polishing and is under anodic double-filmed light
Alloy and Condition	LC4M (370°C, and temperature retaining for 1.5 hour)
Features of Structure	This Figure shows the palorized light structure of what illustrated in Figure VI-29. The alloy has completely recrystallized.

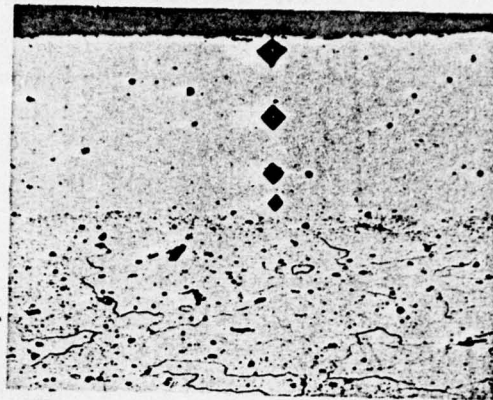


Figure VI-31

210x

Alloy and Condition	LC4Cs
Specification	Thickness 5.0 mm.
Corrosion	Mixed Acid liquid solution
Features of Structure	The bright matrices in the Figure are the aluminum cover, and the thickness is about 0.12 mm. The dark substance underneath it is the body of LC4. From the pattern of distribution of the microhardness of the aluminum cover, it can be known that after heat treatment, the alloy elements diffuse toward the aluminum cover and form a clear phenomenon of concentrated gradients.

4. The Structure of Extruded Articles

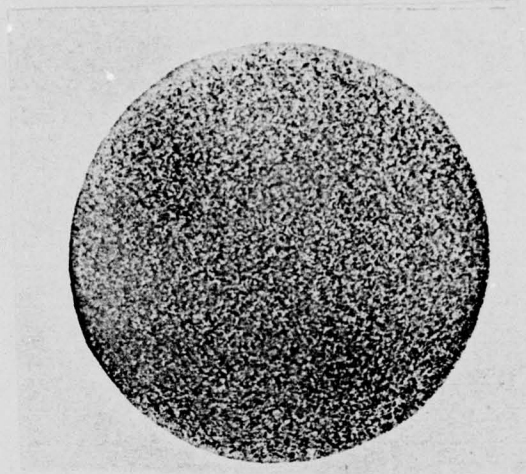


Figure VI-32 Corroded in 25%NaOH
liquid Solution

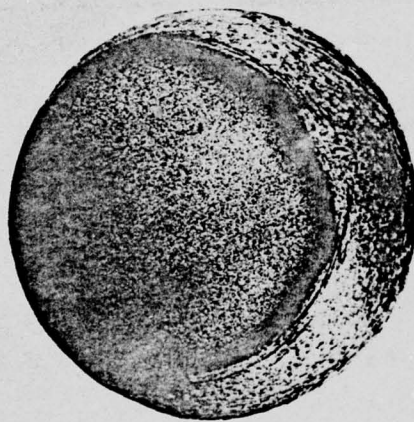


Figure VI-33 Corroded in 25%NaOH
Liquid Solution

Alloy and
Condition

LC4CS

Specification

ø 60 mm. multiple-
holed extruded bar

Features of
Structure

Figure VI-32 shows
the transverse macro-
scopical structure
of the front end of
the bar. The crystal
grains are fine and
homogeneous.

Figure VI-33 shows
the transverse macroscopical structure of the rear end of
the bar. The coarse crystal region looks like a crescent and
the grains in other parts are small and fine.

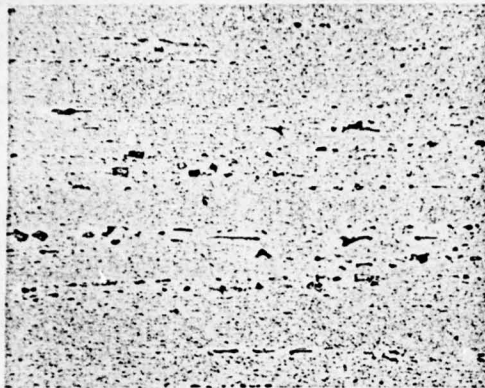


Figure VI-34

210x

Corroded in Mixed Acid
Liquid Solution

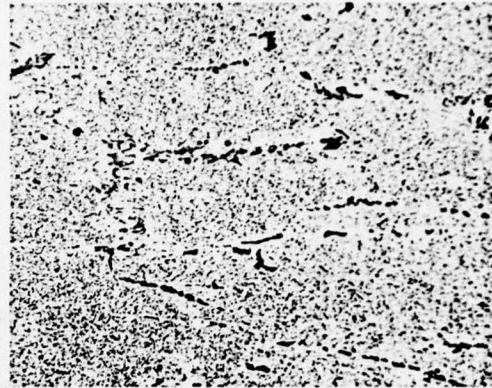


Figure VI-35

210x

Corroded in Mixed Acid
Liquid Solution

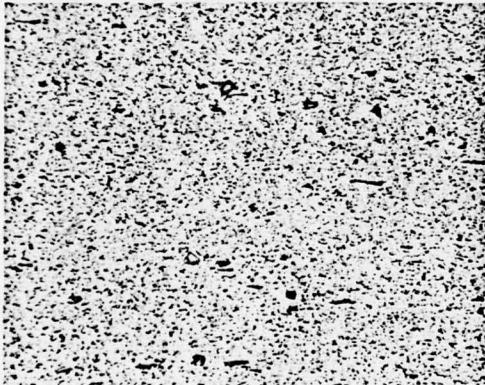


Figure VI-36

210x

Corroded in Mixed Acid
Liquid Solution

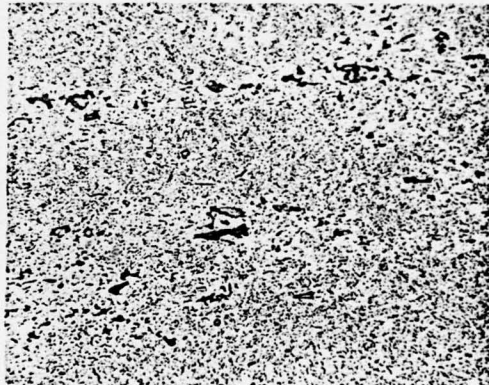


Figure VI-37

210x

Corroded in Mixed Acid
Liquid Solution

Alloy and Condition LC4R

Specification ϕ 60 mm. multiple-holed extruded bar

Features of Structure Figure VI-34 and Figure VI-35 respectively show the longitudinal structure of the central part and the edge part at the front end of the bar. The degree of (continued)

deformation at the central part is smaller than that at the edge part, the remanant casting structure can therefore be seen. From the matrices of $\alpha(\text{Al})$, a great quantity of particles of the soluble phases came out.

Figure VI-36 and Figure VI-37 respectively show the longitudinal structure of the edge part and the central part at the rear end of the bar. The deformation at the rear end is more complete than that at the front end.

AD-A049 264

FOREIGN TECHNOLOGY DIV WRIGHT-PATTERSON AFB OHIO
DEFORMED ALUMINUM ALLOY METALLOGRAPHY. (U)
AUG 77

F/G 11/6

UNCLASSIFIED

FTD-ID(RS)T-0577-77

NL

5 OF 5

AD
A049 264



END

DATE
FILMED

2-78

DDC

Appendix 2 (continued)

(c)

25cc HNO ₃ + 75ccH ₂ O	0.5ccHF + 1.5ccHCl + 2.5cc HNO ₃ + 99.5ccH ₂ O	20ccHCl + 20cc HNO ₃ + 5ccHF + 55ccH ₂ O	10cc H ₃ PO ₄ + 90ccH ₂ O	10g Fe(NO ₃) ₃ + 75ccH ₂ O	micro- hardness H ₅ p	Fusing point °C
slightly corroded	slightly corroded color	slightly corroded color becomes darker	slightly corroded	corroded color becomes dark		870
no	no	no	no	no	510	725
no	very slightly corroded	slightly corroded	slightly corroded	corroded color becomes dark		
color becomes darker	dark, coarse color changes as position changes	color slightly changes dark grey	no	brown	608	
no	no	no	no	no	958	
severely corroded brown	no	no	dark color	dark color	1000	820
brown	slightly corroded	slightly corroded	slightly corroded	slightly corroded		

Appendix 3 The Reference Data of Mechanical Property of

Alloy	Name of Article	Specification (mm)	Condition	Processing Heat Treatment				σ_b	
				Temperature (°C)	Deformation (%)	Temperature (°C)	T. retaining (min)	Longitudinal	Transverse
L2	hot pressed plate	t 10.5	R	400	98			9.53	9.55
L2	hot pressed plate	t 10.5	M	400	98	400	60	7.85	7.94
L2	cpp	t 0.5	Y	room T.	95			18.54	19.24
L2	cpp	t 0.5	M	room T.	95	400	60	8.85	8.26
L4	mold	JX1380-2	R	400				7.51 (thin wall)	7.44 (thick wall)
LD2	ingot	φ 380	ca						18.4
LD2	bar	φ 70	CS	370	92.4	510~540	180	44.8 (front end)	
						155	300	44.2 (rear end)	
LD2	one extruded belt	230 × 90	CS	370~420	86.7	510~540	60	43.63	39.7
						155	300		
LD2	two-extruded mold	AP218	CS	370~420	95.7	510~540	40	35.87	35.83
						155	300		
LD2	forged piece II		R	450~490	80			15.1 (thin wall)	16.1 (thick wall)
LD2	forged piece II		CS	450~490	80	510~540	90	37.1 (thin wall)	
						150~185	720~900	37.5 (tw)	38.0 (tw)
LY12	ingot*	φ 280	ca					23.7	21.4
LY12	ingot		ho			487	720	25.3	18.5
LY12	cpp	t 1.0	Y	room T.	80			28.9	30.3
LY12	cpp	t 1.0	CZ	room T.	80	485~503	18	46.92	46.15
LY12	cpp	t 1.0	M	room T.	80	350~420	60~180	14.38	18.95
LY12	one extruded bar	φ 40	M	320~450	97	380~420	120	22.23	
			CZ			495~500	40	56.52	
LY12	two extruded mold	wt 2.0	M	320~450		380~420	120	21.28	
			CZ			495~500	20	47.30	
LY12	one extruded bar	φ 40	CS	320~450	92.8	500	50	55.8	
						190	360		

* * Casting temperature: 730-715°C, melting temperature 750-700°C;
Casting speed: 55-60 mm/min, water pressure 0.3-1.0 atm;
Crystallization trough: 150mm.

Some Article Made of Deformable Aluminum Alloy

Mechanical Property								HB (kg./mm ²)
(kg./mm ²)		$\sigma_{0.2}$ (kg./mm ²)		δ (%)				
45° height	longi- tudinal	trans- verse	45° height	longi- tudinal	trans- verse	45° height		
8.71	6.44	7.46	6.68	33.27	27.03	29.56	24.2(side) 27.4(middle) 28.4(center) 23.4(surface) 23.0(side) 23.8(middle) 25.9(center) 22.2(surface)	
8.25	4.49	4.55	4.59	41.5	31.7	41.03		
18.92				7.19	4.06	5.26	41.5	
9.35				33.38	35.80	42.02	23.4	
	5 (thin wall)			31.97 (thin wall)			25.9	
	4.5 (thick wall)			35.5 (thick wall)				
		16.9			1.75			
	38.8 (front end)			15.4 (front end)				
	38.3 (rear end)			17.1 (rear end)				
38.45	39.59	35.4	34.65	14.73	13.6	10.5		
	32	32.6		15.2	14.6			
	13.7 (thin wall)			26.4 (thin wall)				
	14.1 (thick wall)			26.6 (thick wall)				
	32.1 (thin wall)			16.1 (thin wall)				
	31.1 (tw)	34.8 (thick wall)		17.8 (tw)	13.9 (thick wall)			
	20.35	18.0		1.94	1.49			
	20.3	15.0		2.85	2.21			
29.08	28.1	29.68	28.11					
45.0	30.78	31.5	30.3	22.24	21.0	23.4		
18.74	11.80	11.68	11.46	20.4	19.36	23.0		
	14.12			16.95				
	41.15			15.52				
	14.25			16.25				
	29.41			21.22				
	48.7			9.32				

Translation note: cpp = cold pressed plate; ca = casting;
t = thickness; ho = homogenization;
tw = thick wall; wt = wall thickness.

Appendix 4 The Representation of Aluminum Alloy Articles

No.	Items	Representation	Example
1	Square Ingot	thickness x width	200 x 1400mm
2	Solid Ingot	diameter (ϕ)	ϕ 800mm
3	Hollow Ingot	outer diameter x inner diameter (ϕ)	ϕ 360 x 210mm
4	Plate	thickness x width x length	200 x 1500 x 4000mm
5	Pipe	outer diameter x inner diameter (ϕ)	ϕ 160 x 152mm
6	Bar	diameter (ϕ)	ϕ 60mm
7	Mold	specially used model No.	XC15-1
8	Wire	diameter (ϕ)	ϕ 2.5mm
9	Foil	thickness x width	0.0075 x 300mm
10	Forged Piece	specially used model No.	K3

Appendix 5 The Symbols of Conditions
of Aluminum Alloy Articles

No.	Names	Symbols
1	annealing	M
2	quenching	C
3	natural aging	Z
4	artificial aging	S
5	quenching + natural aging	CZ
6	quenching + artificial aging	CS
7	hardness	Y
8	3/4 hardness, 1/2 hardness, 1/3 hardness, 1/4 hardness	Y ₁ , Y ₂ , Y ₃ , Y ₄
9	superhardness	T
10	hot rolling, hot extrusion	R
11	good surface	O
12	aluminum free	B
13	quenching natural aging good surface and cold hardening	CZY0

UNCLASSIFIED

SECURITY CLASSIFICATION OF THIS PAGE (When Data Entered)

REPORT DOCUMENTATION PAGE		READ INSTRUCTIONS BEFORE COMPLETING FORM
1. REPORT NUMBER FTD-ID(RS)T-0577-77	2. GOVT ACCESSION NO.	3. RECIPIENT'S CATALOG NUMBER
4. TITLE (and Subtitle) DEFORMED ALUMINUM ALLOY METALLOGRAPHY		5. TYPE OF REPORT & PERIOD COVERED Translation
		6. PERFORMING ORG. REPORT NUMBER
7. AUTHOR(s)		8. CONTRACT OR GRANT NUMBER(s)
9. PERFORMING ORGANIZATION NAME AND ADDRESS Foreign Technology Division Air Force Systems Command U. S. Air Force		10. PROGRAM ELEMENT, PROJECT, TASK AREA & WORK UNIT NUMBERS
11. CONTROLLING OFFICE NAME AND ADDRESS		12. REPORT DATE 1975
		13. NUMBER OF PAGES 387
14. MONITORING AGENCY NAME & ADDRESS (if different from Controlling Office)		15. SECURITY CLASS. (of this report) UNCLASSIFIED
		15a. DECLASSIFICATION/DOWNGRADING SCHEDULE
16. DISTRIBUTION STATEMENT (of this Report) Approved for public release; distribution unlimited.		
17. DISTRIBUTION STATEMENT (of the abstract entered in Block 20, if different from Report)		
18. SUPPLEMENTARY NOTES		
19. KEY WORDS (Continue on reverse side if necessary and identify by block number)		
20. ABSTRACT (Continue on reverse side if necessary and identify by block number) 11		

ACCESSION for	
NTIS	White Section <input checked="" type="checkbox"/>
DDC	Buff Section <input type="checkbox"/>
UNANNOUNCED	<input type="checkbox"/>
JUSTIFICATION	
BY	
DISTRIBUTION/AVAILABILITY CODES	
Dist	SP. GIAL
A	

DD FORM 1 JAN 73 1473

EDITION OF 1 NOV 65 IS OBSOLETE

UNCLASSIFIED

SECURITY CLASSIFICATION OF THIS PAGE (When Data Entered)

REPORT DOCUMENTATION PAGE		READ INSTRUCTIONS BEFORE COMPLETING FORM	
1. REPORT NUMBER	2. REPORT NUMBER	3. REPORT NUMBER	4. REPORT NUMBER
5. TITLE (and Subtitle)	6. AUTHOR(s)		
7. PERFORMING ORGANIZATION NAME AND ADDRESS		8. PERFORMING ORG. REPORT NUMBER	
9. CONTROLLING OFFICE NAME AND ADDRESS		10. CONTRACT OR GRANT NUMBER(s)	
11. MONITORING AGENCY NAME & ADDRESS (if different from Controlling Office)		12. PROGRAM ELEMENT PROJECT, TASK AREA & WORK UNIT NUMBERS	
13. REPORT DATE		14. REPORT DATE	
15. NUMBER OF PAGES		16. SECURITY CLASS. (of this report)	
17. DISTRIBUTION STATEMENT (of this report)		18. DISTRIBUTION STATEMENT (of this report)	
19. SUPPLEMENTARY NOTES		20. KEY WORDS (Continue on reverse side if necessary and identify by block number)	
21. ABSTRACT (Continue on reverse side if necessary and identify by block number)		22. ABSTRACT (Continue on reverse side if necessary and identify by block number)	

Approved for public release; distribution unlimited.

DISTRIBUTION LIST

DISTRIBUTION DIRECT TO RECIPIENT

ORGANIZATION	MICROFICHE	ORGANIZATION	MICROFICHE
A205 DMATC	1	E053 AF/INAKA	1
A210 DMAAC	2	E017 AF/ RDXTR-W	1
B344 DIA/RDS-3C	8	E404 AEDC	1
C043 USAMIIA	1	E408 AFWL	1
C509 BALLISTIC RES LABS	1	E410 ADTC	1
C510 AIR MOBILITY R&D	1	E413 ESD	2
LAB/FIO		FTD	
C513 PICATINNY ARSENAL	1	CCN	1
C535 AVIATION SYS COMD	1	ETID	3
C557 USAIIC	1	NIA/PHS	1
C591 FSTC	5	NICD	5
C619 MIA REDSTONE	1		
D008 NISC	1		
H300 USAICE (USAREUR)	1		
P005 ERDA	1		
P055 CIA/CRS/ADD/SD	1		
NAVORDSTA (50L)	1		
NASA/KSI	1		
AFIT/LD	1		

FTD-ID(RS)T-0577-77